UNIVERSITÀ DEGLI STUDI DI PALERMO

Doctorate: Advances in Modelling, Health-Monitoring, Infrastructures, Geomatics, Geotechnics, Hazards, Engineering Structures, Transportations (AIM HIGHEST)
Department of Engineering
S.S.D. CEAR-06/A

TRANSIENT ANALYSIS OF STOCHASTIC DYNAMIC SYSTEMS BASED ON COMPLEX FRACTIONAL MOMENTS

PH.D. CANDIDATE
LIZHI NIU

Lizhi Niu

THE COORDINATOR OF THE PH.D. PROGRAM
PROF. GIUSEPPE CAMPIONE

SUPERVISORS
PROF. MARIO DI PAOLA
PROF. ANTONINA PIRROTTA
PROF. WEI XU

XXXVII CYCLE
ACADEMIC YEAR 2023/2024

Abstract

Nonlinear dynamic systems are widely used in modern scientific research to model engineering structures, population dynamics, and fuzzy system predictions. However, due to the influence of uncertainties, the transient response probability density, which encapsulates comprehensive statistical information on stochastic dynamic systems, has become a critical tool for deterministic analysis of system evolution. Efficient and accurate construction of transient probability density functions has therefore become a key topic in nonlinear science. Complex fractional moments, constructed using Mellin transform can equivalently describe the probabilistic characteristics of random variables and have shown significant value in accurately reconstructing transient probabilities in stochastic dynamic systems. This thesis establishes and refines the theoretical framework of complex fractional moment, develops efficient transient analysis methods for stochastic dynamic systems under various theoretical models, and explores the influence of inherent parameters on the probabilistic evolution of these systems. The research contributions are outlined as follows:

1. To address the complexity and multi-degree-of-freedom characteristics of engineering structures, the theory of complex fractional moments is extended to Hamiltonian systems. Using the Hamiltonian stochastic averaging principle and considering generalized momentum and displacement, a stochastic differential equation for the Hamiltonian function is established, leading to a diffusion description. A polynomial approximation for implicit functions in the diffusion equation is proposed, and a system of non-homogeneous linear differential equations in the complex space for the related complex fractional moments is derived based on initial and boundary conditions. By employing the ordinary differential equation and the inverse Mellin transform in a probabilistic framework, the transient probability density function is reconstructed. Numerical experiments confirm the feasibility of the complex fractional moments theory in Hamiltonian systems, and validate the accuracy and efficiency of the proposed method. Additionally, the results are used to examine the influence of initial conditions and inherent parameters on the transient response probability density evolution.

2. The complex fractional moment method is refined for stochastic dynamic systems with fractional order derivatives, leading to the development of related stochastic reliability theories. The transient response and first passage evolution of stochastic dynamic systems with fractional order derivatives are explored. Based on generalized harmonic transforms, the fractional-order differential operators are approximated, and the equivalent Fokker-Planck-Kolmogorov equation for stochastic dynamic systems with fractional order derivatives is derived using the amplitude stochastic averaging method. By applying the Mellin transform, a semi-analytical ordinary differential equation about the Fokker-Planck-Kolmogorov equation in the complex domain is derived based on boundary conditions. Additionally, the differential normalization equation for complex fractional moments is established, the equivalent descriptions and

algorithms for reliability functions and first passage times in terms of complex fractional moments are proposed. Simulation results confirm the feasibility of the related theories and analyze the effects of inherent and perturbation parameters on the probabilistic evolution, bifurcation behavior, reliability evolution, and first-passage evolution of the system.

3. To address the singularity in the Mellin transform and the power-law structure of complex fractional moments, the concept of exponential-type of complex fractional moments using the Laplace transform, referred to as the shifted characteristic function, is proposed. A theoretical framework is developed, outlining the existence conditions for shifted characteristic functions, their equivalence with probabilistic characteristics, and a switching equation along the real axis. A novel double-sided Laplace transform is defined, extending the application of the shifted characteristic function to double-sides of the real domain. The shifted characteristic function framework is applied to solve the differential equation and Fokker-Planck-Kolmogorov equation. Numerical experiments validate the feasibility of the shifted characteristic function theory and examine the applicability of the power-law types and exponential types for the drift and diffusion term of stochastic dynamic systems.

4. A framework for generalized complex fractional moment and a related multivariate probabilistic evolution analysis method are established. By introducing multidimensional Mellin transform in probabilistic setting, the concept of generalized complex fractional moment is proposed. Using the existence conditions of multidimensional Mellin transforms in convex domains, an equivalent mapping relationship between generalized complex fractional moments and multidimensional probability density functions in real and complex spaces is established. The equivalence between generalized complex fractional moments and multidimensional characteristic functions is discussed based on the Fourier transform and fractional calculus in multidimensional space. This equivalence is also extended in marginal probability density function. Furthermore, a data-driven method is proposed that combined with generalized complex fractional moments for analyzing the transient behavior of multivariate probability density functions. The proposed theory is validated in two-dimensional space.

5. A novel maximum entropy principle method constrained by complex fractional moments is proposed, which can be applied for reconstructing of approximate probability distribution equations with a limited number of complex fractional moments. By incorporating complex fractional moments with complex parameters into the entropy functional, an extended entropy functional with unknown Lagrange multipliers is constructed, which is utilized for deriving the approximate probability density function. The new method is extended to obtaining transient probability density function in stochastic dynamic systems based on the complex fractional moment equations which is derived from Fokker-Planck-Kolmogorov equation. Numerical simulations verified the effectiveness of the approach.

Key words： Transient response, Complex fractional moments, Hamiltonian systems, Stochastic reliability, Transform, Multivariate, Maximum entropy principle.

Contents

Chapter 1. Introduction

1.1. Historical background

1.1.1 Historical background of stochastic dynamic system

Dynamic systems, mathematical models that describe structural systems over time based on mechanics, are now widely applied across fields such as physics, biology, and sociology. Randomness, a fundamental property of the natural world, plays a crucial role in shaping complex phenomena. Dynamic systems with random perturbations thus provide a closer approximation to the behavior of real-world systems. In dynamic system theory, the focus is typically on invariant factors. For deterministic systems, invariant structures like equilibrium points, limit cycles, and other limiting behaviors can be quantitatively or qualitatively analyzed using dynamic equations [1, 2] . However, in stochastic systems, where trajectories are highly complex and unpredictable, deterministic trajectory analysis is not applicable. Instead, stochastic response, bifurcation, reliability, and most probable trajectories, derived from the statistical properties of stochastic dynamic systems [3-5], offer a powerful framework for describing both local and global dynamics. Based on these insights, a series of researches such as engineering structures, energy harvesters [6, 7], micromechanics [8-10], gene transcription [11-14], oncotherapy [15, 16] under stochastic perturbations are playing a positive and important role in contributing to the development of the objective world.

The stochastic response of dynamic systems focuses on analyzing system behavior under random excitation, including both stable and transient responses, typically represented by statistics, correlation functions, power spectral density, and probability distributions. Such analysis is crucial for enhancing system reliability and optimizing design. At present, the transient response probability density function, which contains the complete statistical information of stochastic dynamic systems, has become the primary focus in studying the stochastic response. The transient response probability density functions of stochastic dynamic systems are governed by the Fokker-Planck-Kolmogorov (FPK) equations, derived from stochastic differential equations. However, only a few specific FPK equations, related to one-dimensional nonlinear systems or multi-degree-of-freedom linear systems, can be solved directly. Current research on generalized stochastic dynamic systems focus mainly on the stable probability characteristics, where the rate of change on the time scale is zero. The transient probability characteristics of the system are typically obtained by solving the FPK equation using numerical or approximate methods. Currently, the methods for obtaining transient probability density functions include Monte Carlo simulation, path integral method [17, 18] , Wiener path integral method [19, 20] , probability density evolution method [21, 22], finite element method [23, 24], finite difference methods [25, 26], and so on. In addition, it has been shown that the transient response PDF of a single-degree-of-freedom nonlinear stochastic

system is expressed as the sum of a set of orthogonal basis functions [27]. However, these methods have some limitations, on the one hand, the existing methods can not balance the efficiency and calculation economy, on the other hand, the calculation accuracy of these methods is insufficient. Therefore, how to obtain the transient response probability characteristics of stochastic dynamic systems efficiently and directly is still the focus in the field of dynamics.

1.1.2 Historical background of complex fractional moment

Observation and statistics have been essential tools for understanding the physical world and shaping social civilization, playing a critical role in the origin of science and continuing to drive disciplinary growth and exploration today. Statistics has been integral to human civilization since ancient times, as reflected in activities such as censuses and land surveys [28, 29]. In 1662, John Graunt [30] a pioneer of modern statistics, analyzed London's population data, introducing the concept of the law of large numbers, which laid the foundation for modern statistics. In 1713, Jakob Bernoulli [31] mathematically formulated probability theory, initiating its systematic study. By the 19th century, Carl Friedrich Gauss's method of least squares [32] as well as Francis Galton's correlation and regression analyses [33, 34] established statistics as a scientific discipline. In the 20th century, Karl Pearson developed the chi-square test and correlation coefficient [35] , forming the basis of modern mathematical statistics. Subsequently, Ronald Fisher's maximum likelihood estimation and analysis of variance [36, 37], Neyman and Pearson's hypothesis testing theory [38, 39], and Wilcoxon's nonparametric statistics [40, 41] gradually refined the theoretical framework of mathematical statistics. Today, the rise of big data, along with advances in system science [42, 43] and artificial intelligence [44] , has accelerated the interdisciplinary application of statistics.

Statistical measures, as direct reflections of observational data, quantify specific attributes of sample data through statistical functions, thereby mapping the objective world into theoretical space. Statistical measures are primary research objects in modern statistics, defined as point estimators of population parameters, possessing properties of unbiasedness, efficiency, and consistency. Based on their applications, statistical measures can be categorized into descriptive and inferential statistics. Descriptive statistics summarize and describe sample features like central tendency, dispersion, and shape, and are applied in fields such as aerospace [45], information sensing [46, 47], biomedical engineering [48, 49], micro-nano mechanics [50, 51], environmental protection [52], and data science [53-55]. Inferential statistics allow for the estimation of population characteristics from samples, addressing uncertainties through methods like parameter estimation, hypothesis testing, and Bayesian analysis, with applications in complex networks, systems science, and structural analysis. Moments, as an important branch of statistical measures, play a significant role in both descriptive and inferential statistics. Consequently, deeper research into moments can expand foundational scientific theories, advance industrial scientific systems, and contribute to human progress.

Since the *k*-th order moments are the coefficient of Taylor expansion of the characteristic functions which are used to describe sample distributions, early research on moments in data or probability distributions mainly focused on integer forms, i.e., $\left\{E\left[X^j\right], j\in\mathbb{Z}^+\right\}$. However, studies on the Hausdorff moment problem in Hilbert space [56, 57] revealed that, for a linear operator $A: L^2_{[0,1]}\to l^2$, the unboundedness of A^{-1} causes ill-condition moment problems when mapping the function $f(x)$ in $L^2_{[0,1]}$ space to its integer moment sequence $\left\{E\left[X^j\right], j\in\mathbb{Z}^+\right\}\in l^2$ by A. Additionally, reconstructing functions can be distorted by weak perturbations in integer moments, namely $\left\{E\left[X^j\right]+\varepsilon_j, j\in\mathbb{Z}^+\right\}$, where $\sum\varepsilon_j^2$ is arbitrarily small. Fractional moments $\left\{E\left[X^\alpha\right], \alpha\in\mathbb{R}\right\}$ effectively address this issue. In subsequent research, fractional moments combined with the maximum entropy principle have advanced in reconstructing probability distributions. However, the maximum entropy method with fractional moments does not establish a direct link with the probability density function or characteristic function. For special cases like α-stable random variables, the probability density function of which exists only under specific conditions (Gaussian distribution when $\alpha=2$, Cauchy distribution when $\alpha=1$, Levy distribution when $\alpha=0.5$), Generally, the probabilistic characteristics are described by the characteristic function for $0<\alpha<2$, and moments do not exist for $\alpha>2$. This limitation renders the maximum entropy method based on fractional moments unsuitable for reconstructing the probabilistic characteristics of α-stable random variables.

Fractional calculus is considered a generalized operation of calculus [58-61] . It provides a tool for describing long-memory or hereditary effects and plays an important role in studying diffusion, turbulence, fractals, and more. Therefore, it is widely applied in control theory [62], life sciences [63, 64] , geological sciences [65, 66], and other fields. Some kinds of fractional calculus, such as Riemann-Liouville, Riesz, and Caputo fractional derivatives, have increasingly perfected their theoretical frameworks and integrated with other theories. For example, the Riesz fractional integral at is equivalent to the Mellin transform, probabilistically, this forms the complex fractional moment (CFM) $E\left[X^{\gamma-1}\right]=\int_0^\infty p_X(x)x^{\gamma-1}\mathrm{d}x$, where $\gamma\in\mathbb{C}$ and $\gamma=\rho+i\eta$. Different from integer and fractional moments, CFM comply with Mellin transform rules, and when the real part of variable γ, namely ρ, is within the Fundamental Strips (FS), the Mellin transform of the probability density function $p_X(x)$ i.e., the CFM $E\left[X^{\gamma-1}\right]$ exists and is reversible in the Mellin transform sense. This means CFMs are entirely equivalent to probability density and characteristic functions. Since the inverse transform process along the imaginary axis η with fixed real part ρ, CFMs are suitable for reconstructing the probabilistic characteristics of bounded-moment random variables including

α-stable random variables. Additionally, due to the connection between Mellin transforms and Riesz fractional integrals, CFMs can be analyzed using fractional calculus theory. Thus, serving as a bridge between probability theory, integral transform theory, and fractional calculus, CFMs possess significant research value and vast development and application potential.

In summary, the equivalence between CFMs and probability characteristic shows immense research potential in expanding stochastic dynamic system theory. On the other hand, there is substantial development for transient probability analysis in stochastic dynamic systems. Therefore, the deep integration of complex fractional moments and transient analysis of stochastic dynamic systems will significantly promote the development of both fields and the broader scientific community.

1.2. Research Status

1.2.1 Research status of transient analysis of stochastic dynamic system

Current research on stochastic dynamic systems focuses primarily on steady-state responses. However, due to the influence of initial conditions, inherent parameters, and perturbation parameters, systems may suffer damage before reaching a steady state if their response exceeds reliability thresholds. Therefore, understanding and analyzing the transient response probability density of stochastic dynamic systems has attracted many researchers. The transient response probability density of stochastic systems has been explored. Ghanem and Spanos [67] summarized and discussed the application of spectral stochastic finite element methods to uncertainty response problems from a numerical computation perspective. Roberts and Spanos [68] analyzed statistical and equivalent linearization methods in addressing issues related to stochastic vibrations, including probability theory, stochastic vibrations, and stochastic responses. Kougioumtzoglou [19, 20] and Ghanem [69] discussed the application of the Wiener path integral method and stochastic Galerkin expansions in the stochastic response problems of nonlinear systems. Jin et al. [70-72], using data-driven methods, determined the maximum Lyapunov exponent and reliability function of the system from discrete data, exploring the stochastic reliability and first passage time problems in stochastic systems. Chen and Qian [73-75] applied radial basis function neural networks to analyze the transient and non-steady-state stochastic responses of stochastic collision systems and multi-potential well energy harvesters. Lyu, Chen, and Li [21, 76, 77] explored the probabilistic response of noise-excited nonlinear systems using probability density evolution equations, and analyzed the vulnerability of engineering structures to earthquakes [22]. Soize [78] derived probabilistic models using entropy optimization principles to construct the transient response of mechanical systems under impulsive loading. Liu and Zhu [79] utilized the stochastic averaging method to study the

transient stochastic response of quasi-integrable Hamiltonian systems. Yue and Xu [80, 81] investigated the transient response of self-sustained oscillators under harmonic and bounded noise excitation using the generalized cell mapping method, analyzing the P-bifurcation phenomena and the advantages of the method.

1.2.2 Research status of complex fractional moment

Research on CFMs originated with Mario Di Paola and his cooperators, who applied fractional calculus to study the probabilistic characteristics of random variables [82, 83]. In 2012, they first proposed the concept of CFMs based on Riesz fractional integrals [84], establishing a equivalence between CFMs, probability density functions, and characteristic functions. The theory of CFMs has provided valuable insights for probabilistic analysis and has been applied to reconstruct transient probabilistic characteristics in stochastic dynamic systems. Jin and Di Paola et al. [85, 86] were the first derived the transform equation for CFMs, enabling their transfer on the real axis. This work laid the foundation for solving the FPK equation through associated ordinary differential equations governing CFMs. They subsequently applied this method to nonlinear stochastic dynamic systems, solving the FPK equation and validating the method's efficiency and accuracy. Xie et al. [87] incorporated vibro-impact factors into traditional nonlinear systems and employed equivalent vibro-impact transform methods to analyze the application of CFMs in stochastic impact systems, and examined the effects of collision coefficients on the system. Di Matteo and Pirrotta et al. [88, 89] extended the application of CFMs to nonlinear systems excited by non-Gaussian white noise, solving the Kolmogorov-Feller equation with high accuracy and efficiency. Alotta et al. [90, 91] combined Fourier and Mellin transforms to derive solutions for fractional FPK equations (Einstein-Smoluchowski equation) using CFMs, and obtaining approximate analytical solutions for fractional FPK equations driven by α-stable white noise. Butera et al. [92] directly applied the Mellin transform to Riesz fractional differential equations, addressing truncation errors and convergence issues arisen by using the Laplace transform to solve fractional differential equations involving the Mittag-Leffler function. Subsequently, Di Paola summarized the theory and applications of the CFMs method [93]. Recognizing that CFMs are defined in the positive real domain, Dai et al. [94] proposed an improved method based on spatial partitioning, extending the application of CFMs from the positive real domain to the entire real domain. Niu et al. [95] applied the CFMs method to time-delay scenarios and extended its application to the transient analysis of nonlinear systems under colored noise excitation [96]. Itoh et al. utilized CFMs to analyze nonlinear systems under combined Gaussian white noise and Poisson white noise excitation [97], nonlinear rigid systems [98], and systems with fractional differential terms [99]. These studies validated the accuracy of CFMs and expanded their application domains.

Additionally, the theoretical framework and applications of CFMs based on Mellin transforms are continually expanding. Cottone and Di Paola utilized Mellin transform to extend

spectral moments based on power spectral density [100, 101] to fractional spectral moments [102]. They discovered that any stationary Gaussian process with a known power spectral density can be equivalently represented by its associated fractional spectral moments and Riesz fractional integrals [103]. This methodology was applied to the simulation of multivariable wind fields [104] and parameter identification in environmental vibration tests [105]. Paolo Pinnola developed a new method for describing correlation functions using complex spectral moments based on power spectral density [106], providing a probabilistic description of the steady-state response of linear fractional oscillators under Gaussian white noise excitation. Di Paola and colleagues used Mellin transform properties in fractional calculus to propose a wavelet analysis method applicable to arbitrary functions [107], detailing its application to CFMs in earthquake engineering [108]. Alotta and others applied complex spectral moments to the comprehensively describe normal multivariable random vector processes [109].

In summary, there are several key issues in the study of CFMs combined with the transient response probability of stochastic dynamic systems:

1. The application of CFMs to the reconstruction of transient probability in various stochastic dynamic systems has significant potential for further development. Currently, complex fractional moments are defined by using Mellin integral transforms, focusing on power-type moment. This has limited their application primarily to Langevin systems with polynomial structures. However, their suitability and effectiveness in transient analysis of other systems, such as Hamiltonian systems, remain insufficiently investigated.

2. The potential equivalence concepts of complex fractional moments have not been fully explored. While the equivalence between CFMs and probability density functions or characteristic functions allows for efficient reconstruction of the probabilistic characteristics of stochastic dynamic systems, these characteristics can not fully describe the system. For addressing issues like damage analysis, concepts such as reliability functions and first passage time are often more relevant. The equivalence between CFMs and these concepts has not been established, highlighting the need for further research to understand other evolutionary characteristics of systems using CFMs.

3. The theoretical framework of CFMs remains incomplete. Currently, this framework is based on the one-dimensional Mellin transform of functions. Expanding this framework to encompass higher-dimensional or exponential structures for complex fractional moments would be significant for the development of the field of stochastic dynamic systems.

1.3. Preliminaries

1.3.1 Wiener process and Gaussian white noise

Wiener process, also named as Brownian motion, is defined as a real stochastic process with continuous time in mathematics, which was initially used to describe the continuous and irregular motion of pollen particles in a liquid. The mathematical definition of the Wiener process is as follows [110, 111]:

Definition 1.1: Let $(\Omega, \mathfrak{B}, P)$ be a complete probability space, $\{\mathfrak{F}_t; t \in [0,T]\}$ be a system increasing with time t on the $\sigma-$ subalgebra of $\mathfrak{B}$, and $\{X_t; t \in [0,T]\}$ be a stochastic process on $(\Omega, \mathfrak{B}, P)$. $(X_t, \mathfrak{F}_t, P)$ can be called a Wiener process if:

1) The sample path of X_t is time-continuous and $X_0 = 0$.

2) For $t \geq s$, $t, s \in [0,T]$, $E[X_t | \mathfrak{F}_t] = X_s$ holds by measure, where $E[\bullet|\bullet]$ denotes the conditional expectation with respect to measure P.

3) For $t \geq s$, $t, s \in [0,T]$, $E[(X_t - X_s)_2 | \mathfrak{F}_t] = t - s$ holds by measure.

Usually, the Wiener process is expressed as $W(t)$.

Definition 1.2: Denote by $\xi(t)$ the Gaussian white noise which is the formal derivative of the Wiener process, i.e. $\xi(t) = \mathrm{d}W(t)/\mathrm{d}t$, and satisfies:

1) $E[\xi(t)] = 0$.

2) $E[\xi(t)\xi(s)] = \sigma^2 \delta(t-s)$, $t \geq s$, where $\delta(\bullet)$ is a Dirac function.

3) $\xi(t) \sim N(0, \sigma^2)$ holds at any moment *t*.

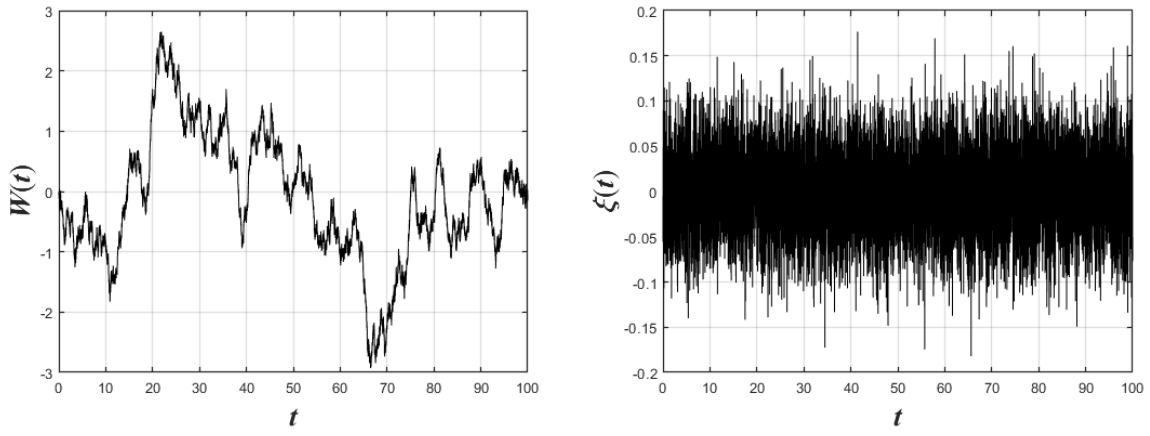

(a) (b)

Figure 1-1 (a): Wiener process; (b): Gaussian white noise. $\sigma = 0.1$.

1.3.2 Fractional calculus

Fractional Calculus is an extension of calculus that extends the traditional integer order derivatives and integrals to any real or complex order, and its creation makes it possible to model and analyze more complex phenomena. Here we introduce the definitions and properties of several common fractional-order differentials and fractional-order integrals.

Definition 1.3: Denote by $\left({}^{RL}I_{\pm}^{\alpha} f\right)(x)$ the Riemann-Liouville (RL) type fractional order integral, which is described by the following definition:

$$\left(I_{\pm}^{\alpha} f\right)(x)=\frac{1}{\Gamma(\gamma)}\int_0^{\infty}\xi^{\gamma-1} f\left(x\pm\xi\right)\mathrm{d}\xi, \tag{1-1}$$

where $\Gamma(\bullet)$ is the Euler gamma function.

Definition 1.4: The RL fractional-order differential arises based on the definition of RL integral, which, denoted $\left({}^{RL}D^{\alpha} f\right)(x)$, can be described in the following form

$$\left(D_{\pm}^{\alpha} f\right)(x)=\frac{(\pm 1)^n}{\Gamma(n-\alpha)}\frac{\mathrm{d}^n}{\mathrm{d}x^n}\int_0^{\infty} s^{n-\alpha-1} f\left(x\mp\xi\right)\mathrm{d}\xi;\quad n-1<\alpha<n. \tag{1-2}$$

Definition 1.5: Denote by $\left({}^{C}D^{\alpha} f\right)(x)$ the Caputo type fractional order differential, which is described by the following definition:

$$\left(D_{C}^{\alpha} f\right)(x)=\frac{1}{\Gamma(n-\alpha)}\int_0^{t}(x-\xi)^{-\alpha+n-1}\, f^{(n)}(\xi)\mathrm{d}\xi. \tag{1-3}$$

Definition 1.6: Denote by $\left({}^{R}I^{\alpha} f\right)(x)$ the Riesz fractional order integral, which is defined as follows:

$$\left(I_{R}^{\alpha} f\right)(x)=\frac{1}{2\Gamma(\gamma)\cos(\gamma\pi/2)}\int_{-\infty}^{\infty}|x-\xi|^{\alpha-1}\, f\left(\xi\right)\mathrm{d}\xi. \tag{1-4}$$

Property 1.1: The RL fractional order integral (1-1) has the following properties in the Fourier domain:

$$\mathcal{F}\left\{\left(I_{\pm}^{\alpha} f\right)(x);\theta\right\}=(\mp i\theta)^{-\alpha}\,\mathcal{F}\left\{f\left(x\right);\theta\right\}, \tag{1-5}$$

where

$$(\mp i\theta)^{-\alpha}=\left[\cos(\alpha\pi/2)\pm i\,\mathrm{sign}(\theta)\sin(\alpha\pi/2)\right]|\theta|^{-\alpha}. \tag{1-6}$$

Property 1.2: Caputo type fractional order derivative can be related to Riemann-Liouville (RL) fractional order derivative and the associated equation can be described as:

$$\left(D_C^{\alpha} f\right)(x)=\left(D_{\pm}^{\alpha}\right)\left[f(x)-\sum_{k=0}^{m-1}\frac{x^k}{k!}\right] f^{(k)}(0). \tag{1-7}$$

Property 1.3: The Riesz-type fractional order integral Fourier transform can be expressed as

$$\mathcal{F}\left\{\left(I_R^{\alpha} f\right)(x);\theta\right\}=|\theta|^{-\alpha}\,\mathcal{F}\left\{ f(x);\theta\right\}. \tag{1-8}$$

1.3.3 Reliability function and first passage time

The reliability function and the time of first crossing of a stochastic dynamic system are usually used to describe the time that occurs when a critical physical quantity of the system exceeds a safety boundary, typically through the probability density function or moments of the system.

Definition 1.7: Consider a one-dimensional diffusion process and denote by $p(x,t\,|\,x_0,t_0)$ its transfer probability density function and $R(t,t_0,x_0)$ its reliability function, then $R(t,t_0,x_0)$ can be expressed in the following form:

$$R(t,t_0,x_0)=\int_{x_l}^{x_c} p(x,t\,|\,x_0,t_0)\,\mathrm{d}x. \tag{1-9}$$

Here x_l and x_c are absorbing boundaries, so the transfer probability density is nonconservative on the interval $[x_l,x_c]$.

Usually the reliability function is obtained by dominating the backward Kolmogorov equation for the transition probability density function $p(x,t\,|\,x_0,t_0)$ on the interval $[x_l,x_c]$, i.e.:

$$\frac{\partial R(t,t_0,x_0)}{\partial t_0}+m(x_0)\frac{\partial R(t,t_0,x_0)}{\partial x_0}+\frac{1}{2}\sigma^2(x_0)\frac{\partial^2 R(t,t_0,x_0)}{\partial x_0^2}=0. \tag{1-10}$$

Let $\tau=t-t_0$, Eq. (1-10) can be rewritten as:

$$-\frac{\partial R(\tau,x_0)}{\partial \tau}+m(x_0)\frac{\partial R(\tau,x_0)}{\partial x_0}+\frac{1}{2}\sigma^2(x_0)\frac{\partial^2 R(\tau,x_0)}{\partial x_0^2}=0, \tag{1-11}$$

Its initial and boundary conditions can be written in the following form:

$$R(\tau,x_0)\big|_{\tau=0}=1,\ x_l\le x_0\le x_c,\ \ R(\tau,x_0)\big|_{x_0=x_c}=0. \tag{1-12}$$

And the probability density function of the first crossing time is generally written as

$$p_T(\tau,x_0)=\frac{\partial F_T(\tau,x_0)}{\partial \tau}=-\frac{\partial R(\tau,x_0)}{\partial \tau}. \tag{1-13}$$

Figure 1-2 shows the schematic of the first crossing time and reliability function of the system,

respectively.

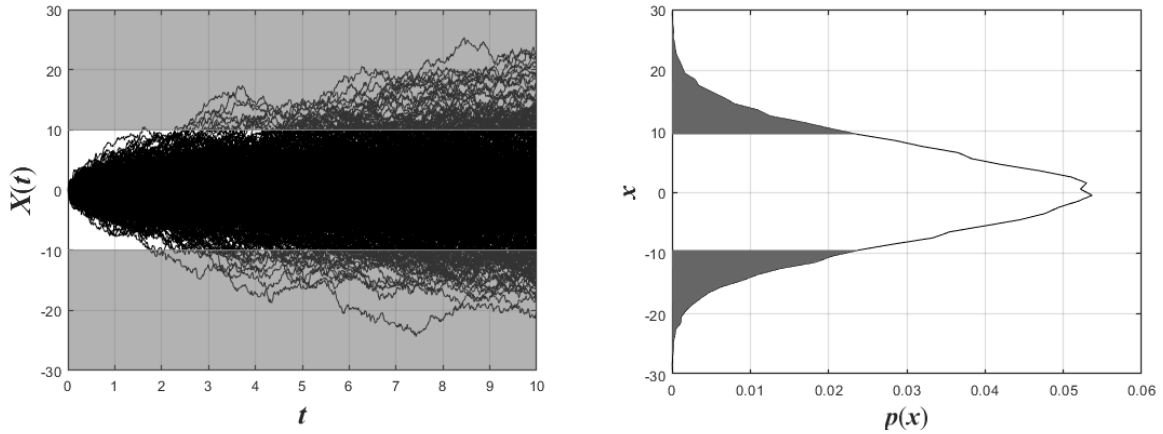

(a) (b)

Figure 1-2 (a): Schematic of first crossing time; (b): Schematic of reliability function. $x \in [-10,10]$.

1.3.4 Integral transforms and their properties

Integral transforms enable the conversion of functions between different domains using integral operators. This approach facilitates efficient analysis and processing of functions, enhancing computational efficiency and providing deeper insights into system behavior. Here we introduce several common integral transforms.

Definition 1.8 (Laplace Transform): Suppose that $f(x)$ is a real function defined on the interval $[0,\infty]$. By denoting its Laplace transform as $f^{\mathcal{L}}(s)$, the expression is given below:

$$\mathcal{L}\{f(x);s\} = f^{\mathcal{L}}(s) = \int_0^{\infty} e^{-sx} f(x)\mathrm{d}x; \quad s = \beta - i\theta, \tag{1-14}$$

where $\mathcal{L}\{\bullet\}$ denotes the Laplace operator. Functions $f(x)$ and $f^{\mathcal{L}}(s)$ are called Laplace transform pairs, which implies that one of them can be reconstructed by doing a Laplace transform or an inverse Laplace transform on the other. For Eq.(1-14) , the condition for the existence of $f^{\mathcal{L}}(s)$ is that there exists a constant $c \in \mathbb{R}^+$ such that

$$\int_0^{\infty} \left| f(x) \right| e^{-cx}\mathrm{d}x < \infty. \tag{1-15}$$

The constant c satisfying equations (1-15) usually has a minimum value $c_{\min}$ and $(c_{\min},\infty)$ is called the Fundamental Strip (FS) of the Laplace transform. If β belongs to the FS, then the inverse transform of $f^{\mathcal{L}}(s)$ exists and $f(x)$ can be reconstructed by the following equations

$$f(x) = \mathcal{L}^{-1}\{f^{\mathcal{L}}(s);x\} = \frac{1}{2\pi}\int_{-\infty}^{\infty} f^{\mathcal{L}}(s)e^{sx}\mathrm{d}\theta = \frac{e^{\beta x}}{2\pi}\int_{-\infty}^{\infty} f^{\mathcal{L}}(s)e^{-i\theta x}\mathrm{d}\theta. \tag{1-16}$$

Observing Eq. (1-16), we can see that the above integral proceeds along the imaginary axis while the real part β remains constant. The properties of Laplace transform are shown below:

Property 1.4: If the functions $f(x)$ and $g(x)$ are both one-sided and $f(x)*g(x)$ denotes the Laplace transform of the product of the two functions, then:

$$f(x)*g(x)=\int_0^x f(x-\bar{x})g(\bar{x})\mathrm{d}\bar{x};\ \mathcal{L}\{f(x)*g(x);s\}=f^{\mathcal{L}}(s)g^{\mathcal{L}}(s). \tag{1-17}$$

Property 1.5: Given $f^{(n)}(x)=\mathrm{d}^n f(x)/\mathrm{d}x^n$, then

$$\mathcal{L}\left\{f^{(n)}(x);s\right\}=s^n f^{\mathcal{L}}(s)-\sum_{k=1}^{n-1}s^k f^{(n-k-1)}(0);\ n=0,1,... \tag{1-18}$$

$$\mathcal{L}\left\{{}_0^cD_x^\alpha\left(f(x)\right);s\right\}=s^\alpha f^{\mathcal{L}}(s)-\sum_{k=1}^{n-1}s^{\alpha-k-1}f^{(k)}(0);\ n-1<\alpha\le n \tag{1-19}$$

where ${}_0^cD_x^\alpha$ denotes Caputo type fractional order differentiation. Furthermore, the differentiation with respect to the variable s satisfies the following equation

$$(-1)^n\frac{\mathrm{d}^n}{\mathrm{d}s^n}f^{\mathcal{L}}(s)=\mathcal{L}\left\{x^n f(x);s\right\}, \tag{1-20}$$

$$\int_s^\infty f^{\mathcal{L}}(\tau)\mathrm{d}\tau=\mathcal{L}\left\{x^{-1}f(x);s\right\}. \tag{1-21}$$

Property 1.6: Shift of Laplace Transforms

$$\mathcal{L}\left\{e^{s_0x}f(x);s\right\}=f^{\mathcal{L}}(s-s_0); \tag{1-22}$$

$$\mathcal{L}\left\{f(ax);s\right\}=\frac{1}{a}\mathcal{L}\left\{f(x);\frac{s}{a}\right\}=\frac{1}{a}f^{\mathcal{L}}\left(\frac{s}{a}\right);\ (a>0) \tag{1-23}$$

Definition 1.9 (Fourier transform): Assuming that $f(x)$ is integrable which defined on the real number field and forms a Fourier transform pair with a bilateral Fourier transform function $f^{\bar{\mathcal{F}}}(\theta)$, its Fourier transform and inverse Fourier transform are defined as follows:

$$\bar{\mathcal{F}}\left\{f(x);\theta\right\}=f^{\bar{\mathcal{F}}}(\theta)=\int_{-\infty}^{\infty}e^{i\theta x}f(x)\mathrm{d}x, \tag{1-24}$$

$$\bar{\mathcal{F}}^{-1}\left\{f^{\bar{\mathcal{F}}}(\theta);x\right\}=f(x)=\frac{1}{2\pi}\int_{-\infty}^{\infty}e^{-i\theta x}f^{\bar{\mathcal{F}}}(\theta)\mathrm{d}\theta, \tag{1-25}$$

where $\bar{\mathcal{F}}\{\bullet\}$ is the double-sided Fourier transform operator. According to Eqs. (1-24), (1-25), (1-14) and (1-16), it can be found that the Fourier transform agrees with the Laplace transform when $\beta=0$. When $s_0=\beta$, according to eq.(1-22) , we can find that the

$$\mathcal{L}\left\{e^{\beta x}f\left(x\right);s\right\}=\mathcal{L}\left\{f\left(x\right);s-\beta=-i\theta\right\}=\int_0^\infty f\left(x\right)e^{i\theta x}\mathrm{d}x=f^{\mathcal{F}}\left(\theta\right). \tag{1-26}$$

$f^{\mathcal{F}}\left(\theta\right)$ is a one-sided Fourier transform function defined on $\left[0,\infty\right)$. According to Eq. (1-26), the properties of the Laplace transform are still valid in the Fourier transform case.

Definition 1.10 (Mellin transform): Suppose that $f\left(x\right)$ is a real function defined on $\left[0,\infty\right)$ and $f^{\mathcal{M}}\left(\gamma\right)=M_f\left(\gamma-1\right)$ is a Mellin transform function of a function $f\left(x\right)$, then

$$f^{\mathcal{M}}\left(\gamma\right)=M_f\left(\gamma-1\right)=\mathcal{M}\left\{f\left(x\right);\gamma\right\}=\int_0^\infty f\left(x\right)x^{\gamma-1}\mathrm{d}x \tag{1-27}$$

where $\gamma=\rho+i\eta$, i is imaginary units. The existence condition for the Mellin transform is $\rho\in\left(-p,-q\right)$, where p and q are the orders of the function $f\left(x\right)$ at $x=0$ and $x=\infty$, respectively, i.e.

$$\lim_{x\to0}f\left(x\right)=\mathcal{O}\left(x^p\right),\ \ \lim_{x\to\infty}f\left(x\right)=\mathcal{O}\left(x^q\right). \tag{1-28}$$

Example for $f\left(x\right)=\left(1+x\right)^{-1}$, then $\lim_{x\to0}\left(1+x\right)^{-1}=1=\mathcal{O}\left(x^0\right)$, $\lim_{x\to\infty}f\left(x\right)=x^{-1}=\mathcal{O}\left(x^{-1}\right)$, then the Mellin transform of the function $\left(1+x\right)^{-1}$ exists when $\rho\in\left(0,1\right)$.

If the Mellin transform of a function exists, then the inverse of Eq. (1-27) exist, namely

$$f\left(x\right)=M_f^{-1}\left(\gamma-1\right)=\mathcal{M}^{-1}\left\{M_f\left(\gamma-1\right);x\right\}=\frac{1}{2\pi}\int_{-\infty}^{\infty}M_f\left(\gamma-1\right)x^{-\gamma}\mathrm{d}\eta. \tag{1-29}$$

Considering Eq. (1-4) the Mellin transform function $M_f\left(\gamma-1\right)$ is equivalent in the fractional order integral sense to the expression of the Riesz fractional order integral when $x=0$, i.e.

$$2\Gamma\left(\gamma\right)\cos\left(\gamma\pi/2\right)\left({}^{R}I^{\gamma}f\right)\left(0\right)=M_f\left(\gamma-1\right) \tag{1-30}$$

Property 1.7: Shift of Mellin Transform

$$\mathcal{M}\left\{x^{v}f\left(x\right);\gamma\right\}=f^{\mathcal{M}}\left(\gamma+v\right) \tag{1-31}$$

$$\mathcal{M}\left\{x^{-1}f\left(x^{-1}\right);\gamma\right\}=f^{\mathcal{M}}\left(1-\gamma\right) \tag{1-32}$$

Property 1.8: Derivatives of Mellin Transform

$$\mathcal{M}\left\{f^{(n)}\left(x\right);\gamma\right\}=\left(-1\right)^n\frac{\Gamma\left(\gamma\right)}{\Gamma\left(\gamma-n\right)}f^{\mathcal{M}}\left(\gamma-n\right) \tag{1-33}$$

$$\mathcal{M}\left\{xf'\left(x\right);\gamma\right\}=-\gamma f^{\mathcal{M}}\left(\gamma\right) \tag{1-34}$$

1.4. Framework

This thesis focuses on the generalized extension of complex fractional moments in the transient analysis of stochastic dynamic systems. By considering the theoretical frameworks including evolution analysis, system configuration, and dimension space, the theoretical framework of complex fractional moments in a probabilistic sense is established. Related concepts of complex fractional moments is proposed and applied in generalized cases to achieve efficient transient response analysis of stochastic dynamic systems. The research framework of this thesis is illustrated in Figure 1-3, and the specific work is organized as follows:

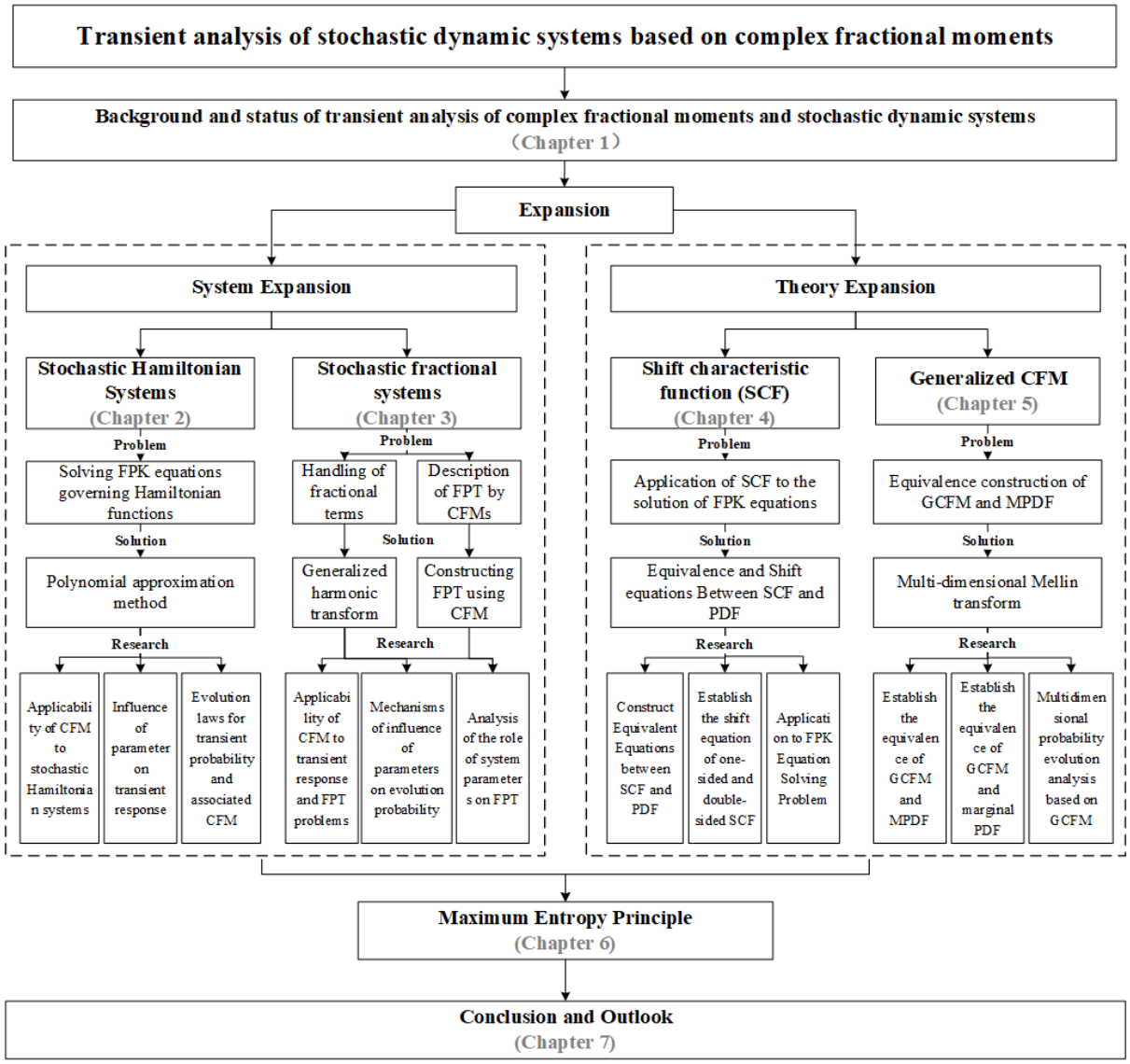

Figure 1-3 Thesis architecture diagram.

Chapter 1 introduces the background, significance, and current state of research on CFM and transient analysis of stochastic dynamic systems. It also defines and explains some concepts, such as Wiener processes, various types of fractional calculus, integral transforms, and concepts

related to stochastic reliability.

Chapter 2 extends the application of CFMs to stochastic Hamiltonian systems. It derives the CFM equations based on the Hamiltonian function and proposes a polynomial approximation method for implicit functions in Hamiltonian diffusion equations. The chapter discusses the applicability of the CFM method in Hamiltonian systems and investigates the effects of polynomial approximation parameters, system parameters, perturbation parameters, and initial conditions on the system behavior and the accuracy of the CFM method.

Chapter 3 focuses on stochastic systems with Caputo-type fractional-order terms, studying the transient analysis and stochastic reliability of CFMs in fractional-order scenarios. It derives the associated CFM differential equations, achieves differential normalization of CFMs, and establishes equivalent descriptions among CFMs, reliability functions, and first passage times.

Chapter 4 introduces an exponential configuration of CFMs based on the Laplace transform, known as the shifted characteristic function, and establishes its equivalence with the probability density function. By exploiting the orthogonal properties of complex exponential functions, a switching equation for the shifted characteristic function along the real axis is derived, later extending to bilateral cases. This chapter proposes the application of shifted characteristic functions in solving FPK equations, analyzing their applicability in terms of computational accuracy and efficiency, and discussing the distinct applicable scenarios of CFMs and shifted characteristic functions.

Chapter 5 introduces generalized CFMs in multidimensional contexts. Using the concept of multidimensional Mellin transforms, it constructs the equivalence between generalized CFMs, multidimensional probability density functions, and multidimensional characteristic functions in the positive real domain, extending it to the entire real domain. This chapter establishes a direct connection between generalized CFMs and marginal PDFs across the entire real domain and proposes a data-driven method for constructing multidimensional evolving probability densities.

Chapter 6 proposes the MEP under CFM constraint, which can be used to approximate the PDF based on the known CFMs. By introducing Lagrange multiplier, the CFMs constraint equation of extended entropy function is derived, and the probability distribution of random variable is approximated by finding the optimal parameter. In addition, the method is extended to the transient PDF of stochastic dynamic systems by deriving the moment equation.

Chapter 7 summarizes the research presented in this thesis, outlines its innovative contributions, and provides a plan and outlook for the future development of CFM theory based on the completed work.

Chapter 2. Transient analysis of complex fractional moments under stochastic Hamiltonian systems

2.1. Introduction

With the rapid development of engineering technologies in fields such as aerospace engineering, robotic arms, and space-deformable structures, the accuracy in describing the physical world has greatly improved. However, this progress has also led to increasingly complex mechanical models with higher degrees of freedom for analyzing engineering structures. For such problems, classical mechanics models become less effective as the degrees of freedom increase. In the field of analytical mechanics, due to the difficulty in solving partial differential equations, efficiently analyzing multi-degree-of-freedom systems remains a significant challenge.

The Hamiltonian system offers significant advantages in addressing such issues by constructing equations of motion for generalized displacement and momentum from an energy perspective, making it widely applicable to multi-degree-of-freedom mechanical problems. Currently, research on Hamiltonian systems has become widespread, including the development of the symplectic Runge-Kutta algorithm for infinite-horizon linear quadratic differential games [112], symplectic integration algorithms for separable Hamiltonian functions [113], and an unconventional Hamiltonian variational principle in phase space for the dynamics of honeycomb sandwich plates [114] . Additionally, Oz H [115, 116] has made outstanding contributions in applying Hamilton's principle to derive general solutions for control problems and dynamic system algebraic equations.

However, systems are inevitably subject to internal or external noise, making traditional dynamic evolution analysis methods based on system trajectories unsuitable. Analyzing systems from a probabilistic evolution perspective often proves more effective. Numerous scholars have studied stochastic Hamiltonian systems [117]. Jia developed a stochastic averaging method for quasi-integrable Hamiltonian systems under Gaussian white noise and Poisson white noise excitation [118] , using perturbation methods to solve the associated FPK equation and analyze the system's probabilistic evolution. Deng proposed a stochastic averaging method for quasi-integrable Hamiltonian systems under fractional Gaussian noise excitation [119], analyzing the system's characteristics and the impact of parameters from the perspectives of steady-state probability and mean value. Gan studied the reliability function and first passage time for quasi-integrable Hamiltonian systems und er Gaussian white noise excitation [120].

Nevertheless, the transient response probability analysis of stochastic Hamiltonian systems is still primarily based on traditional numerical or semi-analytical methods, and improving the accuracy and computational efficiency of these results remains a significant challenge in the field of stochastic dynamics. To address these issues, this chapter explores the

advantages of complex fractional moments in reconstructing transient probabilities in stochastic dynamic systems, extends the theory and its application of CFM to Hamiltonian systems, and analyze the transient probabilistic evolution mechanism of stochastic Hamiltonian systems. Section 2.2 introduces the stochastic averaging method under Hamiltonian systems and derives the governing FPK equation for the Hamiltonian. Section 2.3 applies the Mellin transform to derive inhomogeneous linear system of equations for the associated CFMs, and Section 2.4 proposes a polynomial approximation method for Hamiltonian systems. Numerical experiments validate the applicability of the complex fractional moment method in stochastic Hamiltonian systems.

2.2. Stochastic average method for stochastic Hamiltonian systems

For engineering problems, a stochastic Hamiltonian system with n degrees of freedom can typically be described in the following form:

$$\begin{aligned}&\dot{Q}_j = \frac{\partial H'}{\partial P_j},\\ &\dot{P}_j = -\frac{\partial H'}{\partial Q_j} - \varepsilon\sum_{k=1}^{n} c_{jk}\frac{\partial H'}{\partial P_k} + \varepsilon^{\frac{1}{2}}\sum_{l=1}^{m} g_{jl}W_l(t),\ j=1,2,...,n.\end{aligned} \tag{2-1}$$

Here, c_{jk} represents the damping coefficient, $W_l(t)$ represents Gaussian white noise, Q_j represents the generalized displacement, P_j represents the generalized momentum, ε is a small parameter, and g_{jl} is a function of the generalized displacement and momentum. Considering the case of weak damping and weak excitation, Eq. (2-1) can be expressed as a quasi-nonintegrable Hamiltonian system. In this section, we consider Eq. (2-1) in the Stratonovich form, which can be represented by the following stochastic differential equation:

$$\begin{aligned}&\mathrm{d}Q_j = \frac{\partial H'}{\partial P_j}\mathrm{d}t,\\ &\mathrm{d}P_j = -\left(\frac{\partial H'}{\partial Q_j} + \varepsilon\sum_{k=1}^{n} c_{jk}\frac{\partial H'}{\partial P_k}\right)\mathrm{d}t + \varepsilon^{\frac{1}{2}}\sum_{l=1}^{m} g_{jl}\mathrm{d}B_l(t),\end{aligned} \tag{2-2}$$

where $B_l(t)$ represent the wiener process. By introducing Wong-Zakai correction term, Eq. (2-2) can be transferred into the following equation:

$$\begin{aligned}&\mathrm{d}Q_j = \frac{\partial H'}{\partial P_j}\mathrm{d}t,\\ &\mathrm{d}P_j = -\left(\frac{\partial H'}{\partial Q_j} + \varepsilon\sum_{k=1}^{n} c_{jk}\frac{\partial H'}{\partial P_k} + \varepsilon\pi\sum_{k=1}^{n}\sum_{l,s=1}^{m} K_{js}g_{ks}\frac{\partial g_{jl}}{\partial P_k}\right)\mathrm{d}t + \varepsilon^{\frac{1}{2}}\sum_{l=1}^{m} g_{jl}\mathrm{d}B_l(t),\\ &j=1,2,...,n.\end{aligned} \tag{2-3}$$

Due to the influence of the correction term in Eq. (2-3) on the system's restoring force

and damping force, we decompose it into a restoring force part and a damping force part. According to the formulation of Eq. (2-3), the restoring force part arising from the decomposition of the Wong-Zakai correction term is combined with $-\partial H'/\partial Q_j$, resulting in a new restoring force term denoted as $-\partial H/\partial Q_j$, where $H=H(Q,P)$ is the modified Hamiltonian function. Similarly, the damping force part from the decomposition of the Wong-Zakai correction term is combined with $-\sum_{k=1}^{n} c_{jk}\partial H'/\partial P_k$, resulting in a new damping force term denoted as $-\sum_{k=1}^{n} m_{jk}\partial H/\partial P_k$, where $m_{jk}=m_{jk}(Q,P)$ is the new coefficient matrix. At this point, Eq. (2-3) can be transformed into the following equation:

$$\begin{aligned} \mathrm{d}Q_j &= \frac{\partial H}{\partial P_j}\mathrm{d}t, \\ \mathrm{d}P_j &= -\left(\frac{\partial H}{\partial Q_j}+\varepsilon\sum_{k=1}^{n} m_{jk}\frac{\partial H}{\partial P_k}\right)\mathrm{d}t+\varepsilon^{\frac{1}{2}}\sum_{l=1}^{m} g_{jl}\mathrm{d}B_l(t),\ j=1,2,...,n. \end{aligned} \tag{2-4}$$

Eq. (2-4) represents a fully non-integrable quasi-Hamiltonian system, where H is the Hamiltonian function. According to the Itô derivative rule, the differential equation governing the Hamiltonian function can be expressed as:

$$\mathrm{d}H=\sum_{j=1}^{n}\frac{\partial H}{\partial Q_j}\mathrm{d}Q_j+\sum_{j=1}^{n}\frac{\partial H}{\partial P_j}\mathrm{d}P_j+\frac{1}{2}\sum_{j.k=1}^{n}\frac{\partial^2 H}{\partial P_j\partial P_k}(\mathrm{d}P_j)(\mathrm{d}P_k),\ j=1,2,...,n. \tag{2-5}$$

Substituting Eq. (2-4) into Eq. (2-5), and the Itô differential equation governing the Hamilton function $H(t)$ can be obtained as follow:

$$\begin{aligned} \mathrm{d}H=&\varepsilon\left(-\sum_{j,k=1}^{n} m_{jk}\frac{\partial H}{\partial P_j}\frac{\partial H}{\partial P_k}+\sum_{j.k=1}^{n}\sum_{l.s=1}^{m}\pi K_{ls}g_{jl}g_{ks}\frac{\partial^2 H}{\partial P_j\partial P_k}\right)\mathrm{d}t \\ &+\varepsilon^{\frac{1}{2}}\sum_{j=1}^{n}\sum_{l=1}^{m} g_{jl}\frac{\partial H}{\partial P_j}\mathrm{d}B_l(t)+O\left(\mathrm{d}t^{\frac{3}{2}}\right). \end{aligned} \tag{2-6}$$

Neglecting the high-order term in Eq. (2-6), and approximating the Hamiltonian function $H(t)$ with a Markov process, the Hamiltonian function $H(t)$ is governed by the following Itô stochastic differential equation:

$$\mathrm{d}H=m(H)\mathrm{d}t+\sigma(H)\mathrm{d}B(t), \tag{2-7}$$

where

$$m(H)=\varepsilon\left(-\sum_{j,k=1}^{n} m_{jk}\frac{\partial H}{\partial P_j}\frac{\partial H}{\partial P_k}+\sum_{j.k=1}^{n}\sum_{l.s=1}^{m} D_{ls}g_{jl}g_{ks}\frac{\partial^2 H}{\partial P_j\partial P_k}\right),$$

$$\sigma^2(H)=2\varepsilon\sum_{j,k=1}^{n}\sum_{l,s=1}^{m}D_{ls}g_{jl}g_{ks}\frac{\partial H}{\partial P_j}\frac{\partial H}{\partial P_k}.$$

According to the ergodicity of Markov processes, by introducing stochastic averaging and time averaging, the drift and diffusion terms in Eq. (2-7) can be expressed as:

$$\bar{m}(H)=\varepsilon\left\langle-\sum_{j,k=1}^{n}m_{jk}\frac{\partial H}{\partial P_j}\frac{\partial H}{\partial P_k}+\sum_{j.k=1}^{n}\sum_{l.s=1}^{m}D_{ls}g_{jl}g_{ks}\frac{\partial^2 H}{\partial P_j\partial P_k}\right\rangle_t, \tag{2-8}$$

$$\bar{\sigma}^2(H)=2\varepsilon\left\langle\sum_{j,k=1}^{n}\sum_{l,s=1}^{m}D_{ls}g_{jl}g_{ks}\frac{\partial H}{\partial P_j}\frac{\partial H}{\partial P_k}\right\rangle_t. \tag{2-9}$$

Here, $\langle\bullet\rangle_t$ denotes the time average. It is noteworthy that non-integrable Hamiltonian systems exhibit ergodicity on the n-dimensional constant energy surface. Therefore, we can replace the time average with the spatial average over the fast variable $Q_1,Q_2,...,Q_n,P_2,...P_n$, that is:

$$\langle F\rangle_t=\frac{1}{T(H)}\int_\Omega F\left(\frac{\partial H}{\partial p_1}\right)^{-1}\mathrm{d}q_1\mathrm{d}q_2\cdots\mathrm{d}q_n\mathrm{d}p_2\cdots\mathrm{d}p_n, \tag{2-10}$$

$T(H)$ denotes the quasi-periodic average for the quasi-Hamiltonian system (2-4), which can be expressed as:

$$T(H)=\int_\Omega\left(\frac{\partial H}{\partial p_1}\right)^{-1}\mathrm{d}q_1\mathrm{d}q_2\cdots\mathrm{d}q_n\mathrm{d}p_2\cdots\mathrm{d}p_n. \tag{2-11}$$

Here, the integration domain Ω is defined as:

$$\Omega:\ H(q_1,q_2,\cdots q_n,p_1=0,p_2\cdots p_n)\le H. \tag{2-12}$$

In general, the drift term $\bar{m}(H)$ and the diffusion coefficient $\bar{\sigma}^2(H)$ of a Hamiltonian system can be expressed or expanded as polynomials, that is:

$$\bar{m}(H)=\sum_{j=-1}^{l_1}a_jH^j,\quad \bar{\sigma}^2(H)=\sum_{j=0}^{l_2}b_jH^j, \tag{2-13}$$

where a_j and b_j are the polynomial coefficients. At this point, the FPK equation associated with the Itô equation (2-7) can be expressed as:

$$\frac{\partial p(H,t)}{\partial t}=-\frac{\partial}{\partial H}\left[\bar{m}(H)\,p(H,t)\right]+\frac{1}{2}\frac{\partial^2}{\partial H^2}\left(\bar{\sigma}^2(H)\,p(H,t)\right), \tag{2-14}$$

where $p(H,t)$ is the probability density function governing the Hamiltonian function. The initial condition for Eq. (2-14) is:

$$p(H,0)=p(H_0).$$

Here, we assume $p(H_0)$ is Dirac function $\delta(H-H_0)$, and the boundary conditions of Eq. (2-14) are:

$$\lim_{H\to 0} p(H,t)<\infty,\ \lim_{H\to\infty} p(H,t)=0,\ \lim_{H\to\infty}\frac{\partial p(H,t)}{\partial H}\to 0. \tag{2-15}$$

2.3. Application of complex fractional moments method to stochastic Hamiltonian systems

The CFM method utilizes the Mellin transform to convert the FPK equation in the real domain into an ordinary differential equation in the complex domain. Subsequently, by combining normalization techniques and the inverse Mellin transform, the transient PDF of stochastic dynamic system at any given time can be reconstructed. For Eq. (2-14), we multiply both sides of the equation by $H^{\gamma-1}$ and then integrate the resulting equation over the interval $(0,\infty)$. At this point, equation (2-14) can be expressed as:

$$\begin{aligned}\frac{\int_0^\infty \partial p(H,t)H^{\gamma-1}\mathrm{d}H}{\partial t}&=-\int_0^\infty\frac{\partial}{\partial H}\left[\bar{m}(H)\,p(H,t)\right]H^{\gamma-1}\mathrm{d}H\\&\quad+\frac{1}{2}\int_0^\infty\frac{\partial^2}{\partial H^2}\left(\bar{\sigma}^2(H)\,p(H,t)\right)H^{\gamma-1}\mathrm{d}H,\end{aligned} \tag{2-16}$$

where $\gamma=\rho+i\eta$, i is the imaginary unit. Applying the method of integration by parts, Eq. (2-16) can be transformed into the following form:

$$\begin{aligned}\frac{\partial M_p^H(\gamma-1,t)}{\partial t}&=-\left[\bar{m}(H)H^{\gamma-1}p(H,t)\right]\Big|_0^\infty+(\gamma-1)\int_0^\infty\bar{m}(H)H^{\gamma-2}p(H,t)\mathrm{d}H\\&\quad+\frac{1}{2}\left\{\frac{\partial}{\partial H}\left[\bar{\sigma}^2(H)\,p(H,t)H^{\gamma-1}\right]\right\}\Big|_0^\infty-\frac{1}{2}(\gamma-1)H^{\gamma-2}\bar{\sigma}^2(H)\,p(H,t)\Big|_0^\infty\\&\quad+\frac{1}{2}(\gamma-1)(\gamma-2)\int_0^\infty\bar{\sigma}^2(H)H^{\gamma-3}p(H,t)\mathrm{d}H,\end{aligned} \tag{2-17}$$

where

$$M_p^H(\gamma-1,t)=\int_0^\infty p(H,t)H^{\gamma-1}\mathrm{d}H. \tag{2-18}$$

Eq. (2-18) represents the Mellin transform, $M_p^H(\gamma-1,t)$ denotes the Hamiltonian complex fractional moment. According to the definition of the Mellin transform, for a function $f(x)$, when ρ belongs to the interval $(-p,-q)$, Eq. (2-18) has an inverse transform, where

$$f(x)=\begin{cases}\mathcal{O}\left(x^{p}\right), & x\to 0,\\ \mathcal{O}\left(x^{q}\right), & x\to\infty.\end{cases}$$

$(-p,-q)$ is referred to as Fundamental Strip (FS). The inverse Mellin transform of Eq. (2-18) can be expressed as:

$$p(H,t)=\frac{1}{2\pi i}\int_{\rho-i\infty}^{\rho+i\infty}M_p^H(\gamma-1,t)H^{-\gamma}\mathrm{d}\gamma=\frac{1}{2\pi}\int_{-\infty}^{\infty}M_p^H(\gamma-1,t)H^{-\gamma}\mathrm{d}\eta. \tag{2-19}$$

And the discretized form of Eq.(2-19) is:

$$p(H,t)\approx\frac{\Delta\eta}{2\pi}\sum_{k=-m}^{m}M_p^H(\gamma_k-1,t)H^{-\gamma_k}, \tag{2-20}$$

where $m\Delta\eta$ is the truncation value and $\Delta\eta$ is the truncation step size. Based on the properties of the FPK equation, its boundary conditions can be expressed in the following form:

$$\lim_{H\to 0}p(H,t)\to\mathcal{O}\left(H^{0}\right),\quad\lim_{H\to\infty}p(H,t)\to 0,\quad\lim_{H\to\infty}\frac{\partial p(H,t)}{\partial H}\to 0. \tag{2-21}$$

Substituting the boundary conditions (2-21) into Eq. (2-17), the non-integral terms on the right-hand side of Eq. (2-17) can be ignored. Considering Eq. (2-13), Eq. (2-17) can then be expressed as:

$$\begin{aligned}\frac{\mathrm{d}M_p^H(\gamma-1,t)}{\mathrm{d}t}&=(\gamma-1)\sum_{j=-1}^{l_1}a_i\int_0^{\infty}H^{\gamma+j-2}p(H,t)\mathrm{d}H\\&\quad+\frac{1}{2}(\gamma-1)(\gamma-2)\sum_{j=0}^{l_2}b_i\int_0^{\infty}H^{\gamma+j-3}p(H,t)\mathrm{d}H.\end{aligned} \tag{2-22}$$

According to Eq. (2-18), Eq. (2-22) can be expressed as:

$$\begin{aligned}\frac{\mathrm{d}M_p^H(\gamma-1,t)}{\mathrm{d}t}&=(\gamma-1)\sum_{j=-1}^{l_1}a_iM_p^H(\gamma+j-2,t)\\&\quad+\frac{1}{2}(\gamma-1)(\gamma-2)\sum_{j=0}^{l_2}b_iM_p^H(\gamma+j-3,t).\end{aligned} \tag{2-23}$$

Since $M_p^H(\gamma-1,t)$, $M_p^H(\gamma+j-2,t)$ and $M_p^H(\gamma+j-3,t)$ are all present within Eq. (2-23), According to the literature [85, 121], we introduce a normalization coefficient to unify the variables, which is:

$$C_{ks}(\Delta\rho)=\int_{-\pi/\Delta\eta}^{\pi/\Delta\eta}e^{-\Delta\rho-i(k-s)\Delta\eta\xi}\mathrm{d}\xi. \tag{2-24}$$

Utilizing the normalization coefficient, we can achieve the transformation of the Hamiltonian complex fractional moment along the real axis, that is:

$$M_p^H\left(\gamma_s^{(1)}-1,t\right)=\frac{\Delta\eta}{2\pi}\sum_{k=-m}^{m}M_p^H\left(\gamma_k^{(2)}-1,t\right)C_{ks}\left(\Delta\rho\right), \tag{2-25}$$

where $\rho^{(2)}=\rho^{(1)}+\Delta\rho$. Using Eq. (2-25), $M_p^H\left(\gamma_s+j-2,t\right)$ and $M_p^H\left(\gamma_s+j-3,t\right)$ can be equivalently represented as $M_p^H\left(\gamma_k-1,t\right)$ However, due to the high dimensionality of the equation system or unreasonable step size selection during computation, Eq. (2-23) is prone to divergence in calculations. To avoid this issue, according to Eq. (2-20), when $\Delta\eta$ is sufficiently small, its integral over the interval $\left[\exp\left(-\pi/\Delta\eta\right),\exp\left(\pi/\Delta\eta\right)\right]$ is approximately 1, that is:

$$\int_{e^{-\frac{\pi}{\Delta\eta}}}^{e^{\frac{\pi}{\Delta\eta}}}p\left(H,t\right)\mathrm{d}H\approx\sum_{k=-m}^{m}\int_{e^{-\frac{\pi}{\Delta\eta}}}^{e^{\frac{\pi}{\Delta\eta}}}\frac{\Delta\eta}{2\pi}M_p^H\left(\gamma_k-1,t\right)H^{-\gamma_k}\mathrm{d}H\approx 1, \tag{2-26}$$

where $-m\le k\le m$. By substituting Eq. (2-25) and Eq. (2-26) into Eq. (2-23) we obtain a set of $2m$ ordinary differential equations (ODEs). Solving this ODEs, and combining it with the inverse Mellin transform (2-20), allows for the reconstruction of the probabilistic characteristics of the stochastic Hamiltonian system.

2.4. Numerical simulation

In this section, we consider the system as follows:

$$\begin{aligned}\ddot{X}_1+\left(\beta_0+\beta\left(X_1^2+X_2^2\right)\right)\dot{X}_1+g_1\left(X_1,X_2\right)&=\xi_1+X_1\xi_2,\\ \ddot{X}_2+\left(\beta_0+\beta\left(X_1^2+X_2^2\right)\right)\dot{X}_2+g_2\left(X_1,X_2\right)&=\xi_1+X_2\xi_2,\end{aligned} \tag{2-27}$$

where $\xi_l,l=1,2$ is an uncorrelated Gaussian white noise with noise intensity D_l. g_l is a polynomial in X_l and $\dot{X}_l$, and β_0,β are system parameters. Here we set:

$$\begin{aligned}g_1\left(X_1,X_2\right)&=\omega_1^2X_1+\lambda\omega_1^2\left(\omega_1^2X_1^2+\omega_2^2X_2^2\right)X_1,\\ g_2\left(X_1,X_2\right)&=\omega_2^2X_2+\lambda\omega_2^2\left(\omega_1^2X_1^2+\omega_2^2X_2^2\right)X_2.\end{aligned} \tag{2-28}$$

Let $Q_l=X_l,P_l=\dot{X}_l\left(l=1,2\right)$, Eq.(2-27) can be expressed as:

$$\begin{aligned}\dot{Q}_l&=P_l,\\ \dot{P}_l&=-\left(\beta_0+\beta\left(Q_1^2+Q_2^2\right)\right)P_l-g_l\left(Q_1,Q_2\right)+\xi_1+Q_l\xi_2,\end{aligned} \tag{2-29}$$

The Hamiltonian function associated with system (2-29) can be described as:

$$H\left(Q,P\right)=\frac{1}{2}\sum_{i=1}^{2}P_i^2+U\left(Q_1,Q_2\right), \tag{2-30}$$

where

$$U\left(Q_1,Q_2\right)=\frac{1}{2}\left(\omega_1^2Q_1^2+\omega_2^2Q_2^2\right)+\frac{1}{4}\lambda\left(\omega_1^2Q_1^2+\omega_2^2Q_2^2\right)^2. \tag{2-31}$$

According to Eq. (2-7)-(2-12), the Itô differential equation governing the Hamiltonian function can be described as:

$$\mathrm{d}H\left(t\right)=\bar{m}\left(H\right)\mathrm{d}t+\bar{\sigma}\left(H\right)\mathrm{d}B\left(t\right), \tag{2-32}$$

Where $\bar{m}\left(H\right)$ and $\bar{\sigma}\left(H\right)$ are drift term and diffusion term, satisfying:

$$\bar{m}\left(H\right)=\frac{1}{T\left(H\right)}\int_{\Omega}\left[-\sum_{i=1}^{2}\left(\beta_0+\beta\left(Q_1^2+Q_2^2\right)\right)P_i^2+\sum_{j=1}^{2}\left(D_1+Q_j^2D_2\right)\right]\cdot\frac{1}{P_1}\mathrm{d}Q_1\mathrm{d}Q_2\mathrm{d}P_2, \tag{2-33}$$

$$\bar{\sigma}^2\left(H\right)=\frac{1}{T\left(H\right)}\int_{\Omega}\left[2D_1+D_2Q_1^2P_1^2+D_2Q_2^2P_2^2\right]\frac{1}{P_1}\mathrm{d}Q_1\mathrm{d}Q_2\mathrm{d}P_2, \tag{2-34}$$

where

$$T\left(H\right)=\int_{\Omega}\frac{1}{P_1}\mathrm{d}Q_1\mathrm{d}Q_2\mathrm{d}P_2. \tag{2-35}$$

The integration domain Ω satisfies $\Omega=\left\{\left(Q_1,Q_2,P_1,P_2\right)\middle|H\left(Q_1,Q_2,0,P_2\right)\le H\right\}$. To facilitate the solution of Eq. (2-33) to (2-35), we introduce the following transform:

$$x=\frac{R}{\omega_1}\cos\theta,\ y=\frac{R}{\omega_2}\sin\theta, \tag{2-36}$$

hence, the drift term and diffusion term can be expressed as:

$$\bar{m}\left(H\right)=2D_1-2\beta_0\left(H-\frac{1}{4}R-\frac{\lambda}{12}R^2\right)-\frac{1}{2}\beta\left(\frac{1}{\omega_1^2}+\frac{1}{\omega_2^2}\right)\left(H-\frac{1}{3}R-\frac{\lambda}{8}R^2\right)R+\frac{1}{4}\left(\frac{1}{\omega_1^2}+\frac{1}{\omega_2^2}\right)D_2R, \tag{2-37}$$

$$\bar{\sigma}^2\left(H\right)=4D_1\left(H-\frac{1}{4}R-\frac{\lambda}{12}R^2\right)+\frac{1}{2}D_2\left(\frac{1}{\omega_1^2}+\frac{1}{\omega_2^2}\right)\left(H-\frac{1}{3}R-\frac{\lambda}{8}R^2\right)R, \tag{2-38}$$

where R is the solution of the following equation:

$$\lambda^2R^2+2\lambda R=4\lambda H. \tag{2-39}$$

Substituting Eq. (2-39) into Eq. (2-37) and (2-38), we can obtain:

$$\bar{m}\left(H\right)=s_1+s_2R+s_3H+s_4HR, \tag{2-40}$$

$$\bar{\sigma}^2\left(H\right)=s_5R+s_6H+s_7HR. \tag{2-41}$$

The coefficient of (2-40) and (2-41) are:

$$
\begin{aligned}
&s_1 = 2D_1,\\
&s_2 = \frac{\beta_0}{6} + \frac{D_2}{4}\left(\frac{1}{\omega_1^2}+\frac{1}{\omega_2^2}\right) - \frac{\beta}{12\lambda}\left(\frac{1}{\omega_1^2}+\frac{1}{\omega_2^2}\right),\\
&s_3 = \frac{\beta}{6\lambda}\left(\frac{1}{\omega_1^2}+\frac{1}{\omega_2^2}\right) - \frac{4\beta_0}{3}, s_4 = -\frac{\beta}{4}\left(\frac{1}{\omega_1^2}+\frac{1}{\omega_2^2}\right),\\
&s_5 = \left(\frac{D_2}{12\lambda}\left(\frac{1}{\omega_1^2}+\frac{1}{\omega_2^2}\right) - \frac{D_1}{3}\right),\\
&s_6 = \left(\frac{8D_1}{3} - \frac{D_2}{6\lambda}\left(\frac{1}{\omega_1^2}+\frac{1}{\omega_2^2}\right)\right),\\
&s_7 = \frac{D_2}{4}\left(\frac{1}{\omega_1^2}+\frac{1}{\omega_2^2}\right).
\end{aligned}
\tag{2-42}
$$

Since Eq. (2-39) is in implicit form, to facilitate its solution, we propose an approximate transformation method. Considering the variable λ when it is sufficiently large, we have:

$$
R = \frac{1}{\lambda}\left(\sqrt{1+4\lambda H}-1\right) \approx \frac{2}{\sqrt{\lambda}} H^{\frac{1}{2}} - \frac{1}{\lambda}. \tag{2-43}
$$

Substituting Eq. (2-43) into Eq. (2-40) and (2-41), the new expression of (2-40) and (2-41) are:

$$
\bar{m}(H) = \left(s_1 - \frac{s_2}{\lambda}\right) + \left(\frac{2s_2}{\sqrt{\lambda}}\right) H^{\frac{1}{2}} + \left(s_3 - \frac{s_4}{\lambda}\right) H + \frac{2s_4}{\sqrt{\lambda}} H^{\frac{3}{2}}, \tag{2-44}
$$

$$
\bar{\sigma}^2(H) = -\frac{s_5}{\lambda} + \frac{2s_5}{\sqrt{\lambda}} H^{\frac{1}{2}} + \left(s_6 - \frac{s_7}{\lambda}\right) H + \frac{2s_7}{\sqrt{\lambda}} H^{\frac{3}{2}}. \tag{2-45}
$$

And the related FPK equation is:

$$
\frac{\partial p(H,t)}{\partial t} = -\frac{\partial}{\partial H}\left[\bar{m}(H)\, p(H,t)\right] + \frac{1}{2}\frac{\partial^2}{\partial H^2}\left(\bar{\sigma}^2(H)\, p(H,t)\right). \tag{2-46}
$$

Applying Eqs. (2-16) to (2-26), the Hamiltonian CFM differential equation can be obtained as follows:

$$
\begin{aligned}
\frac{\mathrm{d}M_p^H(\gamma-1,t)}{\mathrm{d}t} &= L_1 M_p^H(\gamma-1,t) + L_2 M_p^H\left(\gamma-\frac{1}{2},t\right) + L_3 M_p^H\left(\gamma-\frac{3}{2},t\right)\\
&\quad + L_4 M_p^H(\gamma-2,t) + L_5 M_p^H\left(\gamma-\frac{5}{2},t\right) + L_6 M_p^H(\gamma-3,t),
\end{aligned}
\tag{2-47}
$$

where

$$
\begin{aligned}
&L_1=(\gamma-1)\left(s_3-\frac{1}{\lambda}s_4\right), L_2=(\gamma-1)\frac{2}{\sqrt{\lambda}}s_4,\\
&L_3=(\gamma-1)\left(\frac{2}{\sqrt{\lambda}}s_2\right)+(\gamma-1)(\gamma-2)\left(\frac{s_7}{\sqrt{\lambda}}\right),\\
&L_4=(\gamma-1)\left(s_1-\frac{1}{\lambda}s_2\right)+\frac{1}{2}(\gamma-1)(\gamma-2)\left(s_6-\frac{s_7}{\lambda}\right),\\
&L_5=\frac{1}{2}(\gamma-1)(\gamma-2)\left(\frac{2s_5}{\sqrt{\lambda}}\right),\\
&L_6=\frac{1}{2}(\gamma-1)(\gamma-2)\left(-\frac{s_5}{\lambda}\right),
\end{aligned}
\tag{2-48}
$$

Using the above equation, we can obtain a semi-analytical solution for the transient probability density function of system (2-27).

In this section, the parameters are selected as Table 2-1:

Table 2-1 Parameters

Parameters	Values	Parameters	Values
β_0	-0.015	β	0.05
λ	10	D_1	0.01
D_2	0.1	ω_1	1
ω_2	2	ρ	2.1
m	120	$\Delta\eta$	0.3

The trajectory and phase diagrams of system (2-27) are shown in Figure 2-1. According to the results, it is observed that the two sets of generalized coordinates converge to a stable point and a stable limit cycle, respectively. Figure 2-2 presents the potential function of the system. From the figure, it can be seen that the system has a minimum potential energy at the point $(0,0)$.

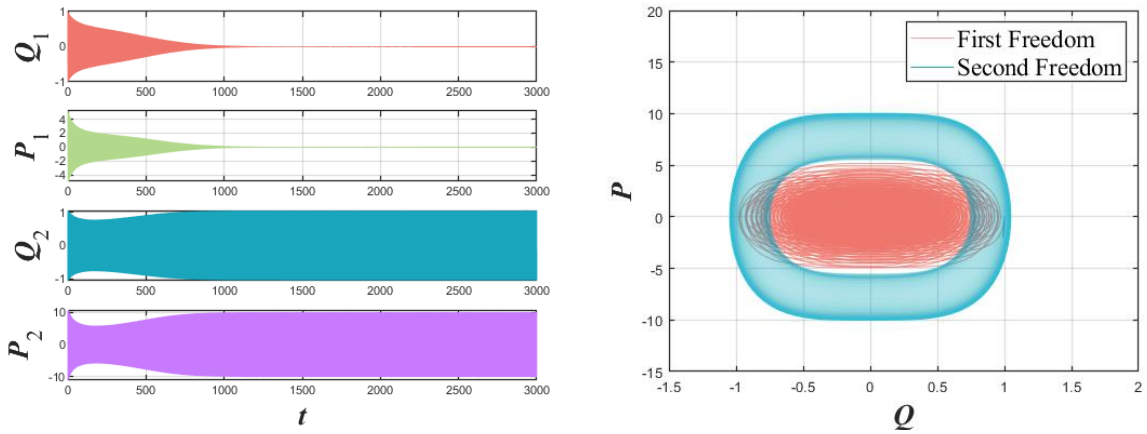

(a) (b)

Figure 2-1 (a) Trajectory. (b) Phase diagram

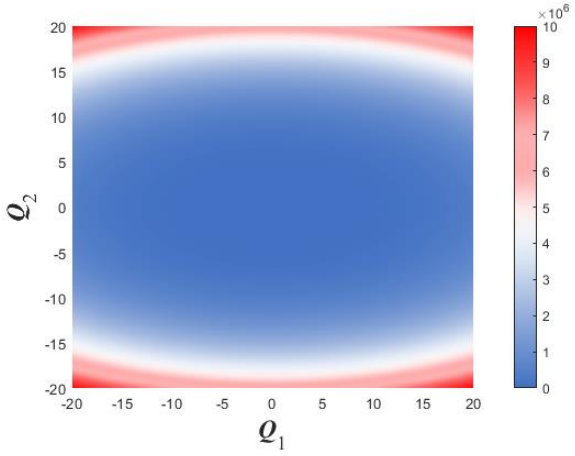

Figure 2-2 Potential function

$$Ae(t)=\frac{1}{N}\sum_{i=1}^{N}\left|p_{CFM}\left(H_i,t\right)-p_{MCS}\left(H_i,t\right)\right| \tag{2-49}$$

To quantify the accuracy of the CFM method and observe the trend of its error, we introduce the average error $Ae(t)$, as expressed in equation (2-49). Figure 2-3 shows the influence of truncation values m on the $Ae(t)$ when $t=5,10,20$. The results indicate that when $m\geq 10$, the average error is nearly zero. However, when the truncation value m fixed, increasing the time necessitates a higher truncation value m to maintain accuracy.

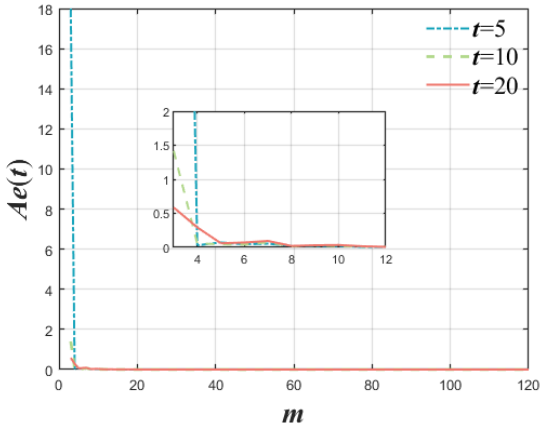

Figure 2-3 The average error of the CFM method

Figure 2-4 shows the real and imaginary parts of the CFM of system (2-27) when $t=10,20,30,40$. Figure 2-5 (a) illustrates the evolution of the system's transient probability density function with time, where the lines represent results obtained using the CFM method and the scatter points represent results from Monte Carlo simulations. Figure 2-5(b) displays the joint Hamiltonian transient probability density function, where the lines indicate the peak positions of the transient probability density function at different times. The results indicate that the CFM method effectively reconstructs the evolutionary probabilistic characteristics of the stochastic Hamiltonian system. Additionally, the CFM method can compute the system's probabilistic characteristics at $t=40$ within 3 seconds, while the Monte Carlo method requires over 500 seconds for the same calculation under identical conditions. Moreover, the results obtained using the CFM method exhibit greater continuity compared to those from the Monte Carlo method. From the perspective of the system itself, the peak value of the transient probability characteristics of system (2-27) decreases as time progresses, while the position of the probability peak increases over time.

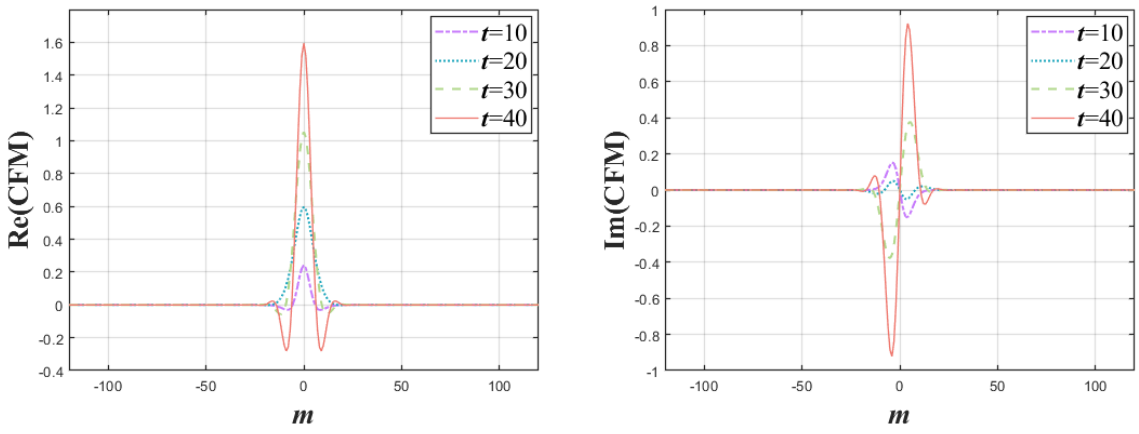

(a) (b)

Figure 2-4 The (a) real part and (b) imaginary part of CFM when $t=10,20,30,40$

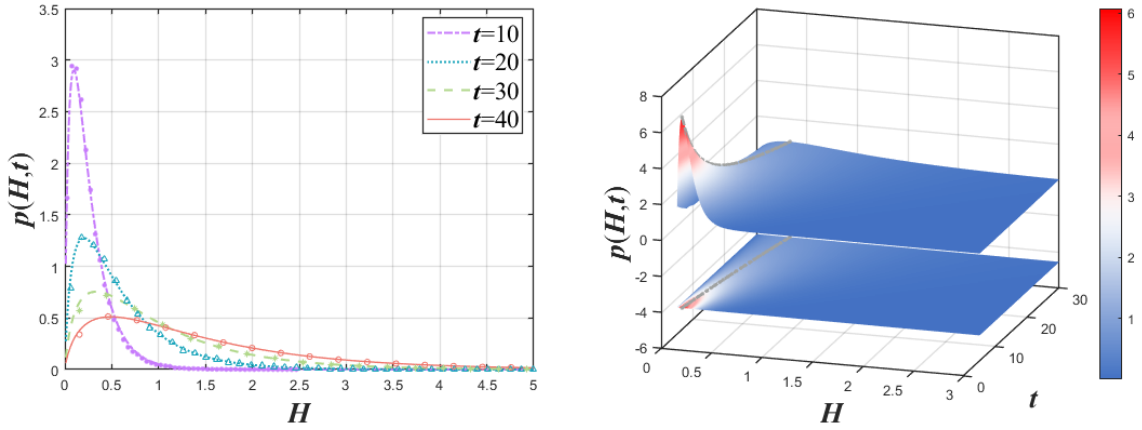

Figure 2-5 (a) The transient PDF with different t, where the line is results by CFM method, the dot is the results by Monte-Carlo method; (b) The distribution map of the peak of transient PDF

Figure 2-6 (a) illustrates the impact of parameter β_0 on the system's transient PDF. The lines represent results obtained from the CFM method, while the points are derived from Monte Carlo simulations. The results show that an increase in parameter β_0 reduces the peak of the transient PDF, indicating an enhanced diffusion effect in the system. Figure 2-6 (b) displays the distribution of the peak values of the PDF in the phase space (t,β_0). It is evident that increases in both time t and parameter β_0 lead to greater system diffusion.

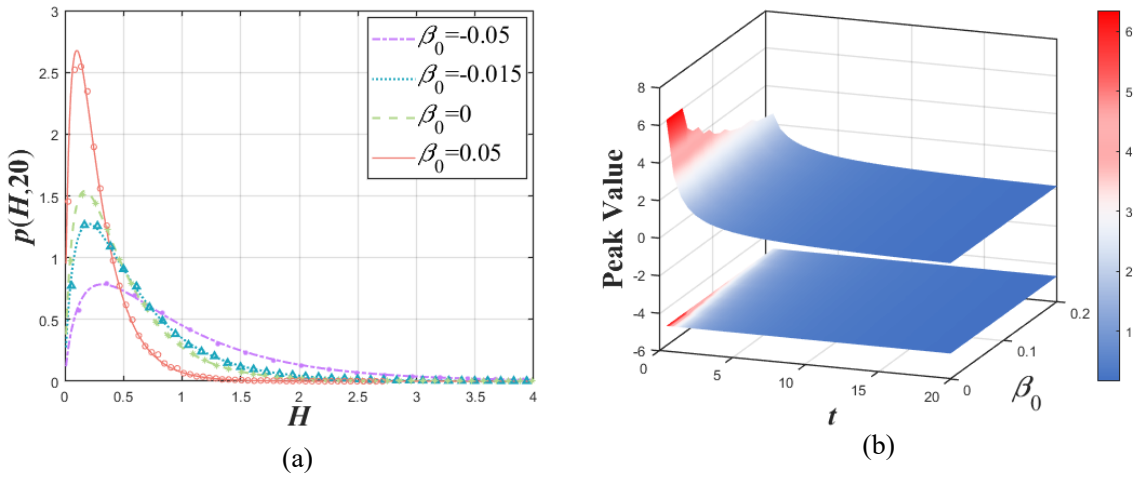

Figure 2-6 (a) The transient response PDF with different β_0 when $t=20$. (b) The peak value of transient PDF in the parameter space (t,γ)

Figures 2-7 (a-b) show the variation in the transient PDF of a Hamiltonian system at time $t=20$ with respect to additive noise intensity D_1 and multiplicative noise intensity D_2. The results indicate that increases in both external and parametric excitation reduce the peak value of the transient PDF. Figure 2-8 illustrates the distribution of the peak values of the transient

PDF in the parameter space (D_1, D_2). The results show that increases in both D_1 and D_2 enhance the system's diffusion trend.

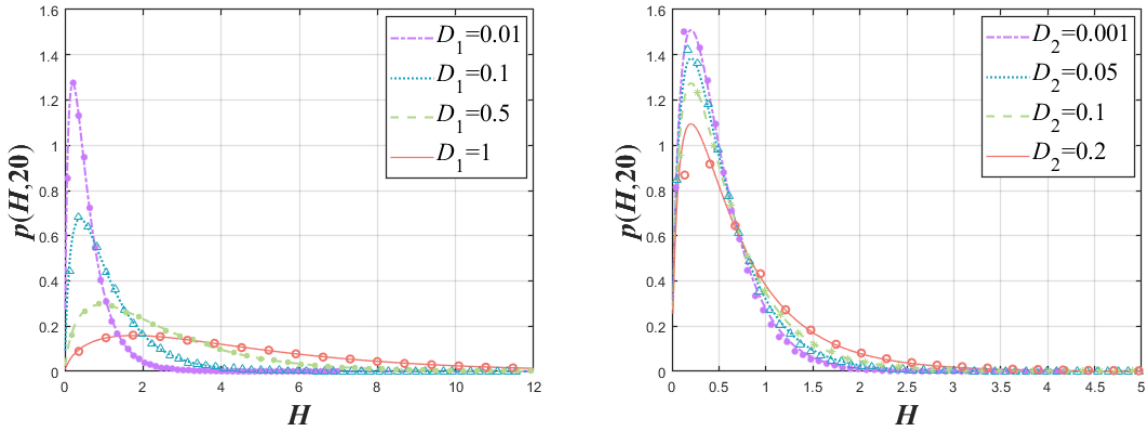

Figure 2-7 The transient response PDF with different noise intensity when $t = 20$. (a) D_1; (b) D_2

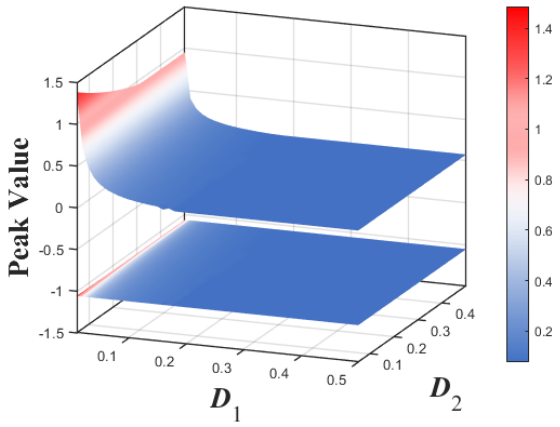

Figure 2-8 The peak value of transient PDF in the parameter space (D_1, D_2) when $t = 20$

This chapter proposes an approximate transformation method suitable for Hamiltonian systems, which effective for large λ. To examine the influence of λ on the accuracy of CFM method, Figure 2-9 (a) shows the transient PDFs for different system parameters λ. Figure 2-9 (b) illustrates the change in average error at $t = 5$ and $t = 20$ when $\lambda \in [7, 30]$. The results indicate that changes in parameter λ consistently have a minimal and stable impact on the outcomes at different times.

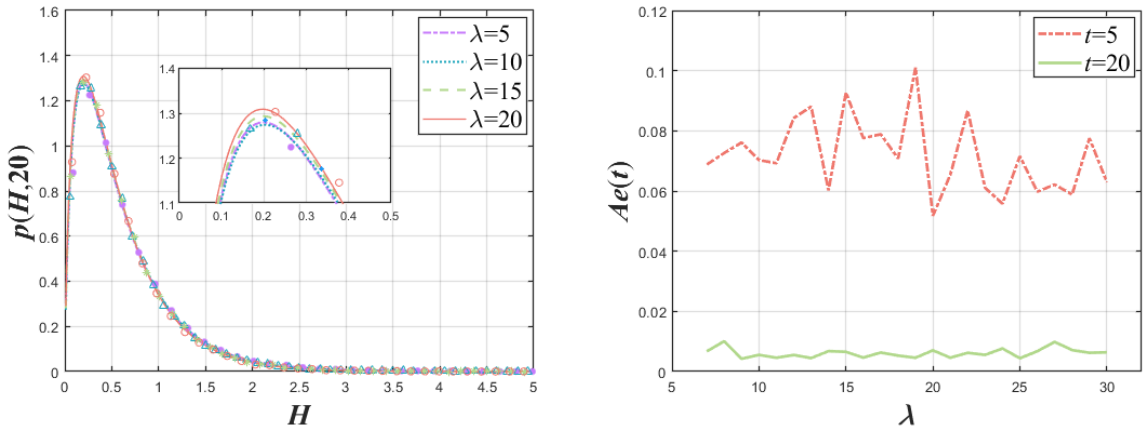

(a) (b)

Figure 2-9 (a) The influence of λ on transient PDF of system; (b) Average error of the CFM method with λ when $t=5$ and $t=20$

Additionally, we examined the impact of initial values on the accuracy of CFM method in Hamiltonian systems and its effect on probability evolution. Using the initial value parameters shown in Table 2-2, Figure 2-10 depicts the distribution of the transient PDF at $t=10$. The results indicate that the accuracy of the CFM method which applied to stochastic Hamiltonian systems is not sensitive to initial values. However, from the system's perspective, increasing the initial values significantly reduces the peak of the transient probability density function, promoting diffusion behavior in stochastic Hamiltonian systems.

Table 2-2 Initial value

Q_1	Q_2	P_1	P_2	H
0	0	0	0	**0**
0.5	0	0	0	**0.2813**
1	0	0	0	**3**
1	0.5	1	1	**12**

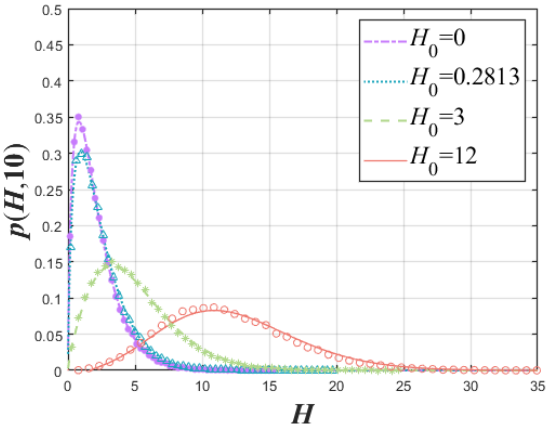

Figure 2-10 Transient response with different initial value when $t=10$

2.5. Conclusion

This chapter evaluates the applicability of the complex fractional moment method in stochastic Hamiltonian systems excited by additive and multiplicative Gaussian white noise. It investigates the effects of time and parameter variations on the system using results obtained from the complex fractional moment method. First, the Hamiltonian stochastic averaging method is used to derive a one-dimensional Hamiltonian Itô stochastic differential equation and the corresponding FPK equation. Subsequently, the Mellin transform is applied to derive ODEs for the complex fractional moments, leading to a set of $2m$ ODEs through variable normalization. By solving these equations numerically and applying the inverse Mellin transform, a semi-analytical solution for the transient probability density function of the system at various times is reconstructed. The numerical results indicate that the complex fractional moment method is applicable to stochastic Hamiltonian systems, including cases where drift and diffusion terms are non-integer polynomials. The method demonstrates both high accuracy and computational efficiency in stochastic Hamiltonian systems. Additionally, this chapter explores the influence of parameter changes on the system's transient probability characteristics, showing the increases in time, noise intensity, and initial values enhance system diffusion. Finally, a polynomial approximation method for the Hamiltonian system is proposed and its effectiveness is validated through numerical analysis under different values and times.

Chapter 3. Analysis of probabilistic evolution and first passage based on complex fractional moments in stochastic dynamic systems with fractional order differential operators

3.1. Introduction

Due to the superiority of fractional calculus in describing problems such as electrochemistry [122], porous media materials [123], turbulence [124], and biological characteristics [125], and it has garnered increasing attention from scholars. Currently, combining fractional calculus with the stochastic dynamic systems has become a new research hotspot, with many scholars attempting to study such systems. Examples include the stochastic response problem of self-excited systems with fractional derivative and the bifurcation behavior of oscillators under noise [126, 127]. Chen et al. studied the stable response of a Duffing oscillator with fractional derivatives under Gaussian white noise excitation [128] and extended fractional derivative terms to Hamiltonian systems [129] . Sun et al. examined the stochastic P-bifurcation of stochastic nonlinear systems using fractional derivatives [130], providing critical conditions for parameter-induced stochastic bifurcations based on changes in the extremum of the probability density function. Zhang et al. analyzed the stochastic bifurcation of a double-rhythmic system with fractional damping under different noise excitations for multi-attractor energy harvesters [4]. However, research on stochastic dynamic systems with fractional derivatives has largely focuses on stable situations, with little exploration of the probabilistic evolution of such systems.

So far, efficiently and accurately obtaining the transient response probability density function for stochastic dynamic systems remains a significant challenge. Some methods, such as the Galerkin method, finite element method, finite difference method, path integral method, Wiener path integral method, and radial basis function neural network method, can provide numerical or semi-analytical solutions for the transient probability density function of stochastic dynamic systems. However, their computational efficiency can still be improved. The stochastic variable transform method [131, 132] has been shown to solve the first probability density function of stochastic homogeneous linear second-order complex differential equations. Since the transient response probability density function contains complete statistical information of the stochastic dynamic system, developing an efficient and accurate method for this purpose remains crucial, particularly for extended applications like system reliability.

To address this issue, this chapter examines the probabilistic evolution and first passage problems of dynamic systems with Caputo-type fractional derivative terms under additive and multiplicative Gaussian white noise based on the complex fractional moment method. Section 3.2 introduces the generalized harmonic transform method to equivalently replace fractional terms and derives the system's FPK equation using the stochastic averaging method. Section

3.3 applies the complex fractional moment method to obtain a semi-analytical solution for the FPK equation. Section 3.4 establishes the equivalent description of the system's complex fractional moments with the reliability function and first passage time. In Section 3.5, numerical experiments analyze the influence of system parameters on probabilistic evolution and verify the effectiveness of the stochastic reliability theory based on complex fractional moments. Finally, Section 3.6 summarizes the findings of this chapter.

3.2. Equivalent expression and stochastic average of stochastic systems with fractional differential terms

In this section, we consider stochastic dynamic systems with Caputo-type fractional derivatives. The equation of motion is described as follows:

$$\ddot{X}+\mu D_C^{\alpha}\left(X\right)+\beta f\left(X,\dot{X}\right)\dot{X}+\omega_0^2 X=\sum_{k=1}^{n} g_k\left(X,\dot{X}\right)\xi_k\left(t\right), \tag{3-1}$$

where $D_C^{\alpha}\left(\bullet\right),0<\alpha<1$ represents the Caputo-type fractional derivatives operator, $f\left(x,\dot{x}\right)$ and $g_k\left(x,\dot{x}\right)$ are polynomial with respect to x and $\dot{x}$, and $\xi_k\left(t\right)$ are Gaussian white noise, and satisfied:

$$\begin{aligned} &E\left[\xi_k\left(t\right)\right]=0,\\ &E\left[\xi_k\left(t\right)\xi_k\left(t+\tau\right)\right]=2D_k\delta\left(\tau\right),\\ &E\left[\xi_k\left(t\right)\xi_j\left(t+\tau\right)\right]=0,k\neq j. \end{aligned} \tag{3-2}$$

Where D_k represent the intensity of noise. In the case of weak damping and weak excitation, the Eq. (3-1) can be regarded as the system with a family of quasi-periodic solutions according to its the quasi-conservative property. According to the generalized harmonic function, the solution of the system (3-1) can be assumed as follow:

$$x\left(t\right)=A\left(t\right)\cos\Phi\left(t\right),\dot{x}\left(t\right)=-A\left(t\right)\omega_0\sin\Phi\left(t\right),\Phi\left(t\right)=\omega_0 t+\theta\left(t\right), \tag{3-3}$$

where $A\left(t\right)$ and $\Phi\left(t\right)$ represent the amplitude process and the phase process, respectively. and the fractional differential term of a system is not only related to the damping force, but also to the restoring force. Therefore, the Caputo fractional derivative term is expressed in the following format:

$$D_C^{\alpha}\left(x\right)=C\left(\alpha\right)\dot{x}\left(t\right)+K\left(\alpha\right)x\left(t\right). \tag{3-4}$$

To obtain the analytic expression of $C\left(\alpha\right)$ and $K\left(\alpha\right)$, we introduce the following formulae:

$$\begin{aligned}\lim_{T\to\infty}\int_0^T \frac{\sin(\omega_0 t)}{t^\alpha}\mathrm{d}t &= \omega_0^{\alpha-1}\Gamma(1-\alpha)\cos\frac{\alpha\pi}{2},\\ \lim_{T\to\infty}\int_0^T \frac{\cos(\omega_0 t)}{t^\alpha}\mathrm{d}t &= \omega_0^{\alpha-1}\Gamma(1-\alpha)\sin\frac{\alpha\pi}{2},\end{aligned} \tag{3-5}$$

and $C(\alpha)$ can be obtained as follow:

$$\begin{aligned}C(\alpha) &= -\frac{1}{\pi A\omega_0}\int_0^{2\pi}\left[C(\alpha)\left(-A(t)\omega_0\sin\Phi\right)+K(\alpha)A(t)\cos\Phi(t)\right]\sin\Phi\mathrm{d}\Phi\\ &= -\frac{1}{\pi A\omega_0}\int_0^{2\pi}\left[C(\alpha)\dot{x}(t)+K(\alpha)x(t)\right]\sin\Phi\mathrm{d}\Phi\\ &= -\frac{1}{\pi A\omega_0}\int_0^{2\pi}D_C^\alpha\left(A\cos\Phi\right)\sin\Phi\mathrm{d}\Phi\\ &= -\frac{1}{\pi A\omega_0}\lim_{T\to\infty}\frac{1}{T}\int_0^T D_C^\alpha\left(A\cos(\omega_0 t+\theta)\right)\sin(\omega_0 t+\theta)\mathrm{d}t\\ &= \frac{2}{\Gamma(1-\alpha)}\lim_{T\to\infty}\frac{1}{T}\int_0^T\left\{\left[\int_0^t\left\{\frac{\sin(\omega_0 u+\theta)}{(t-u)^\alpha}\right\}du\right]\sin(\omega_0 t+\theta)\right\}\mathrm{d}t.\end{aligned} \tag{3-6}$$

Let $s=t-u$, and Eq. (3-6) can be rewritten as:

$$\begin{aligned}C(\alpha) &= \frac{2}{\Gamma(1-\alpha)}\lim_{T\to\infty}\frac{1}{T}\int_0^T\left\{\left[\int_0^t\left\{\frac{\sin(\omega_0 t+\theta-\omega_0 s)}{s^\alpha}\right\}ds\right]\sin(\omega_0 t+\theta)\right\}\mathrm{d}t\\ &= \frac{2}{\Gamma(1-\alpha)}\lim_{T\to\infty}\frac{1}{T}\int_0^T\left\{\left[\int_0^t\left\{\frac{\cos(\omega_0 s)}{s^\alpha}\right\}ds\right]\sin(\omega_0 t+\theta)\sin(\omega_0 t+\theta)\right\}\mathrm{d}t\\ &\quad -\frac{2}{\Gamma(1-\alpha)}\lim_{T\to\infty}\frac{1}{T}\int_0^T\left\{\left[\int_0^t\left\{\frac{\sin(\omega_0 s)}{s^\alpha}\right\}ds\right]\cos(\omega_0 t+\theta)\sin(\omega_0 t+\theta)\right\}\mathrm{d}t,\end{aligned} \tag{3-7}$$

Appling Eq. (3-5), one can obtain:

$$C(\alpha)=\omega_0^{\alpha-1}\sin(\alpha\pi/2). \tag{3-8}$$

After the similar procedure, the $K(\alpha)$ can be obtained as follow:

$$K(\alpha)=\frac{1}{\pi\omega_0}\int_0^{2\pi}D_C^\alpha\left(A\cos\Phi\right)\cos\Phi\mathrm{d}\Phi=\omega_0^\alpha\cos\frac{\alpha\pi}{2}. \tag{3-9}$$

Substituting Eq.(3-8) and Eq.(3-9) into Eq. (3-4), we can obtain the equation as follow:

$$D_C^\alpha(X)=\omega_0^{\alpha-1}\sin\frac{\alpha\pi}{2}\dot{X}(t)+\omega_0^\alpha\cos\frac{\alpha\pi}{2}X(t). \tag{3-10}$$

Substituting Eq.(3-10) into Eq. (3-1), one can obtain the equivalent equation without fractional derivative:

$$\ddot{X}+\left[\mu C(\alpha)+\beta f(x,\dot{x})\right]\dot{X}+\omega^2 X=\sum_{k=1}^{n} g_i(X,\dot{X})\xi_k(t), 0<\alpha<1, \tag{3-11}$$

where $\omega^2=\mu K(\alpha)+\omega_0^2$ The above method approximates the non-Markov system (3-1) with a Markov system (3-11). Utilizing Eqs. (3-1) and (3-3), we can obtain:

$$\dot{A}(t)=\frac{\sin\Phi}{\omega}\left\{\left[\mu C(\alpha)+\beta f(x,\dot{x})\right]\dot{x}-\sum_{k=1}^{n} g_k(x,\dot{x})\xi_k(t)\right\}, \tag{3-12}$$

$$\dot{\theta}(t)=\frac{\cos\Phi}{A\omega}\left\{\left[\mu C(\alpha)+\beta f(x,\dot{x})\right]\dot{x}-\sum_{k=1}^{n} g_k(x,\dot{x})\xi_k(t)\right\}. \tag{3-13}$$

Let $g_{1k}(x,\dot{x})=\frac{\sin\Phi}{\omega}g_k(x,\dot{x})$, $g_{2k}(x,\dot{x})=\frac{\cos\Phi}{A\omega}g_k(x,\dot{x})$, and applying the stochastic averaging method, the fast variables of the system are eliminated, the Itô stochastic differential equation governing the slow variable amplitude process can be expressed as:

$$\mathrm{d}A=\bar{m}(A)\mathrm{d}t+\bar{\sigma}(A)\mathrm{d}B(t), \tag{3-14}$$

where

$$\bar{m}(A)=\left\langle\frac{\sin\Phi}{\omega}\left[\mu C(\alpha)+\beta f(x,\dot{x})\right]\dot{x}+\frac{1}{2}\sum_{l=1}^{2}\sum_{r,s=1}^{n} R_{rs}(h)\frac{\partial g_{1r}(A,t)}{\partial x_l}g_{ls}(A,t+h)\right\rangle_t, \tag{3-15}$$

$$\bar{\sigma}^2(A)=\left\langle\sum_{r,s=1}^{n} R_{rs}(h)g_{1r}(A,t)g_{1s}(A,t+h)\right\rangle_t, \tag{3-16}$$

where $R_{rs}(h)$ are the correlation functions of two Gaussian white noises, and

$$\langle f\rangle_t=\lim_{T\to\infty}\frac{1}{T}\int_0^T f\ \mathrm{d}t=\frac{1}{2\pi}\int_0^{2\pi} f\ \mathrm{d}\Phi, \tag{3-17}$$

Usually, the drift term $\bar{m}(A)$ and the diffusion term $\bar{\sigma}^2(A)$ are the polynomial functions of A, satisfy

$$\bar{m}(A)=\sum_{j=-1}^{l_1} c_{1j}A^j,\quad \bar{\sigma}^2(A)=\sum_{j=0}^{l_2} c_{2j}A^j, \tag{3-18}$$

where c_{1j},c_{2j} are the polynomial coefficients. The FPK equation of system (3-11) can be expressed as：

$$\frac{\partial p_A(a,t)}{\partial t}=-\frac{\partial}{\partial a}\left[\bar{m}(a)p_A(a,t)\right]+\frac{1}{2}\frac{\partial^2}{\partial a^2}\left[\bar{\sigma}^2(a)p_A(a,t)\right], \tag{3-19}$$

where $p_A(a,t)$ is transient PDF, and the initial condition is $p_A(a,t)=p_A(a_0)$, where

$$p_A(a_0)=\delta(a-a_0), \tag{3-20}$$

$\delta(a-a_0)$ is Dirac-Delta function. The boundary conditions of Eq. (3-19) are

$$\lim_{a\to 0} p_A(a,t)<\infty,\ \lim_{a\to\infty} p_A(a,t)\to 0,\ \lim_{a\to\infty}\partial p_A(a,t)/\partial a\to 0. \tag{3-21}$$

3.3. Application of complex fractional moment method

The CFM method is a semi-analytic method based on Mellin transform and the FPK equation to obtain the PDF of the system transient response. According to the definition of CFM, we denote the CFM of PDF $p_A(a)$ in probability sense by $\mathcal{M}\{p_A(a);\gamma\}$ as:

$$\mathcal{M}\{p_A(a);\gamma\}=M_p(\gamma-1)=\int_0^\infty p_A(a)a^{\gamma-1}\mathrm{d}a=E\left[A^{\gamma-1}\right], \tag{3-22}$$

where $\gamma=\rho+i\eta$, i represents the imaginary unit. The existence of the inverse of Eq. (3-22) is that the real part of γ belongs to FS, namely $\rho\in(-p,-q)$, where

$$p_A(a)=\mathcal{O}(a^p),a\to 0;\ \ p_A(a)=\mathcal{O}(a^q),a\to\infty, \tag{3-23}$$

which is introduced in section 1.3.4. If the inverse Mellin transform exist, then we have

$$p_A(a)=\frac{1}{2\pi}\int_{-\infty}^{\infty}\mathcal{M}\{p_A(a);\gamma\}a^{-\gamma}\mathrm{d}\eta. \tag{3-24}$$

According to CFM method, and substituting Eq. (3-18) and Eq. (3-22) into Eq. (3-19), we can obtain the following equation:

$$\begin{aligned}\frac{\mathrm{d}M_p(\gamma-1,t)}{\mathrm{d}t}&=(\gamma-1)\sum_{j=-1}^{l_1}c_{1j}M_p(\gamma-2+j,t)\\&\quad+\frac{1}{2}(\gamma-1)(\gamma-2)\sum_{j=0}^{l_2}c_{2j}M_p(\gamma-3+j,t).\end{aligned} \tag{3-25}$$

Due to the existence of multiple variables in Eq. (3-25), it cannot be solved directly. Here we introduce the normalized equation,

$$M_p(\gamma_0-1,t)=\frac{2\pi/\Delta\eta-\sum_{\substack{j=-m\\j\neq 0}}^{m}\left(\frac{\mathrm{e}^{-\frac{\pi}{\Delta\eta}(\gamma_j-1)}-\mathrm{e}^{\frac{\pi}{\Delta\eta}(\gamma_j-1)}}{-\gamma_j+1}\right)M_p(\gamma_j-1,t)}{\left(\exp\left(-\frac{\pi}{\Delta\eta}(\gamma_0-1)\right)-\exp\left(\frac{\pi}{\Delta\eta}(\gamma_0-1)\right)\right)/(-\gamma_0+1)}, \tag{3-26}$$

and the normalization condition,

$$M_p(\gamma_s^{(1)}-1,t)=\frac{\Delta\eta}{2\pi}\sum_{j=-m}^{m}M_p(\gamma_s^{(2)}-1,t)C_{js}(\Delta\rho), \tag{3-27}$$

where

$$C_{js}\left(\Delta\rho\right)=\frac{2\pi}{\Delta\eta}\frac{\sin\left[\pi\left(j-s\right)-i\pi\Delta\rho/\Delta\eta\right]}{\pi\left(j-s\right)-i\pi\Delta\rho/\Delta\eta}. \tag{3-28}$$

According to Eqs. (3-24)-(3-28), the semi-analytical solution of Eq. (3-19) can be obtained as follow:

$$\frac{\mathrm{d}M_p\left(\gamma-1,t\right)}{\mathrm{d}t}=A_0M_p\left(\gamma-1,t\right)+B_0, \tag{3-29}$$

where A_0 is a matrix with $2m\times2m$ elements, B_0 is a vector with $2m\times1$ elements.

3.4. Reliable function and first passage time

In this section, we propose a new method to obtain the first passage time based on the definition of fractional moments. According to the definition of fractional moments and the description in Section 1.3.3, we substitute Eq. (3-24) into Eq. (1-9), then

$$\begin{aligned}R_{a_l}^{a_c}\left(t,a\right)&=\int_{a_l}^{a_c}p_A\left(a,t\right)\mathrm{d}a=\int_{a_l}^{a_c}\frac{1}{2\pi}\int_{-\infty}^{\infty}M_p\left(\gamma-1,t\right)a^{-\gamma}\mathrm{d}\eta\mathrm{d}a\\&=\frac{1}{2\pi}\int_{-\infty}^{\infty}M_p\left(\gamma-1,t\right)\left(\int_{a_l}^{a_c}a^{-\gamma}\mathrm{d}a\right)\mathrm{d}\eta=\frac{1}{2\pi}\int_{-\infty}^{\infty}M_p\left(\gamma-1,t\right)F\left(1-\gamma,a\right)\mathrm{d}\eta,\end{aligned} \tag{3-30}$$

where $\left[a_l,a_c\right]$ is the integral domain, and

$$F\left(1-\gamma,a\right)=\int_{a_l}^{a_c}a^{-\gamma}\mathrm{d}a=\frac{1}{1-\gamma}a^{1-\gamma}\Big|_{a_l}^{a_c}. \tag{3-31}$$

Therefore, the discretization equation of Eq. (3-30) can be expressed as

$$R_{a_l}^{a_c}\left(t,a\right)=\frac{\Delta\eta}{2\pi}\sum_{k=-m}^{m}M_p\left(\gamma_k-1,t\right)F\left(1-\gamma_k,a\right). \tag{3-32}$$

According to the definition of first passage time, we have

$$p_T\left(t,a\right)=-\frac{\partial R_{a_l}^{a_c}\left(t,a\right)}{\partial t}. \tag{3-33}$$

Based on Eq. (3-30), Eq. (3-33) can be rewritten as:

$$p_T\left(t,a\right)=-\frac{1}{2\pi}\frac{\partial\int_{-\infty}^{\infty}M_p\left(\gamma-1,t\right)F\left(1-\gamma,a\right)\mathrm{d}\eta}{\partial t}, \tag{3-34}$$

thus

$$p_T\left(t,a\right)=-\frac{1}{2\pi}\int_{-\infty}^{\infty}\dot{M}_p\left(\gamma-1,t\right)F\left(1-\gamma,a\right)\mathrm{d}\eta. \tag{3-35}$$

where

$$\dot{M}_p\left(\gamma-1,t\right)=A_0M_p\left(\gamma-1,t\right)+B_0. \tag{3-36}$$

The discretization form of Eq. (3-35) can be expressed as

$$p_T(t,a) = -\frac{\Delta\eta}{2\pi}\sum_{k=-m}^{m}\dot{M}_p(\gamma-1,t)F(1-\gamma_k,a). \tag{3-37}$$

or

$$p_T(t,a) = -\frac{\Delta\eta}{2\pi}\sum_{k=-m}^{m}\left(A_0 M_p(\gamma-1,t)+B_0\right)F(1-\gamma_k,a). \tag{3-38}$$

Since $M_p(\gamma_0-1,t)$ are represented as a linear combination of $M_p(\gamma_j-1,t)$, here, we introduce the normalization expression of the derivatives of CFM. According to Eq. (3-26), By differentiating both sides of the equation with respect to t, we obtain

$$\dot{M}_p(\gamma_0-1,t) = -\frac{\sum_{\substack{j=-m\\ j\neq 0}}^{m}\left(\frac{\mathrm{e}^{-\frac{\pi}{\Delta\eta}(\gamma_j-1)}-\mathrm{e}^{\frac{\pi}{\Delta\eta}(\gamma_j-1)}}{-\gamma_j+1}\right)\dot{M}_p(\gamma_j-1,t)}{\left(\exp\left(-\frac{\pi}{\Delta\eta}(\gamma_0-1)\right)-\exp\left(\frac{\pi}{\Delta\eta}(\gamma_0-1)\right)\right)/(-\gamma_0+1)}, \tag{3-39}$$

Substitute Eq. (3-39) into Eq. (3-38), $p_T(t,a)$ can be obtained quickly and directly.

3.5. Numerical simulation

Usually, the dynamic system is subjected to internal and external noise excitation, where additive noise and multiplicative noise are used to describe these two types of noise, respectively. The research shows that when additive and multiplicative noises exist in the system simultaneously, the system may lead to asymmetric or skewed non-Gaussian probability distribution. In addition, the exist of multiplicative noise can cause more complex dynamics in the phase space of the system. Thus, considering the following system:

$$\ddot{X}+\mu D_C^{\alpha}X+\beta\left(1+b_1X^2+b_2X^4\right)\dot{X}+\omega_0^2X = c_1\eta_1(t)+c_2X\eta_2(t), \tag{3-40}$$

where $0<\alpha<1$, and the fractional term is the Caputo-type fractional derivative introduced in section 1.3.4, which is defined as:

$$\left(D_C^{\alpha}X\right)(t) = \frac{1}{\Gamma(1-\alpha)}\int_0^t\frac{\dot{X}(s)}{(t-s)^{\alpha}}\mathrm{d}s. \tag{3-41}$$

According to Eq. (3-10), Eq.(3-40) can be written as:

$$\begin{aligned}\ddot{X}+\left[\mu\omega_0^{\alpha-1}\sin\frac{\alpha\pi}{2}+\beta\left(1+b_1X^2+b_2X^4\right)\right]\dot{X}+\left(\mu\omega_0^{\alpha}\cos\frac{\alpha\pi}{2}+\omega_0^2\right)X \\ = c_1\eta_1(t)+c_2X\eta_2(t).\end{aligned} \tag{3-42}$$

Here, Eq. (3-42) can be rewritten as follows:

$$\ddot{X}+\left[\beta_1+\beta b_1 X^2+\beta b_2 X^4\right]\dot{X}+\omega^2 X=c_1\eta_1(t)+c_2 X\eta_2(t), \tag{3-43}$$

where $\beta_1=\mu\omega_0^{\alpha-1}\sin\frac{\alpha\pi}{2}+\beta$, and $\omega^2=\mu\omega_0^{\alpha}\cos\frac{\alpha\pi}{2}+\omega_0^2$. Utilizing Eqs. (3-12)-(3-18), the drift term and diffusion coefficient can be expressed as:

$$\bar{m}(A)=\frac{c_1^2 D_1}{2A\omega^2}+\left(\frac{3D_2c_2^2}{8\omega^2}-\frac{\beta_1}{2}\right)A-\frac{b_1\beta A^3}{8}-\frac{b_2\beta A^5}{16}, \tag{3-44}$$

$$\bar{\sigma}^2(A)=\frac{c_1^2 D_1}{\omega^2}+\frac{c_2^2 D_2}{4\omega^2}A^2. \tag{3-45}$$

3.5.1 Error analysis

Table 3-1 System parameters

Parameters	Values	Parameters	Values
ρ	4.1	m	120
$\Delta\eta$	0.5	μ	-0.01
α	0.9	β	0.05
ω_0	1	b_1	0.1
b_2	0.1	D_1	0.01
D_2	0.1	c_1, c_2	1

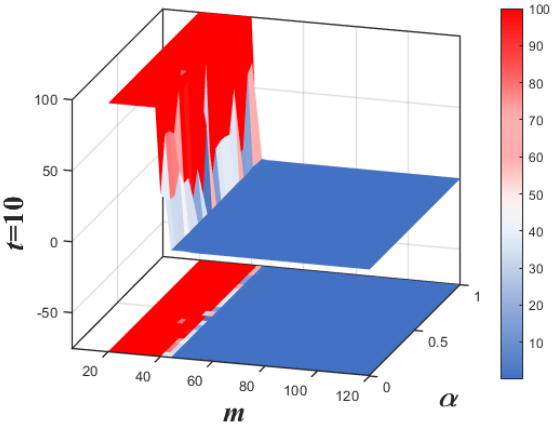

(a)

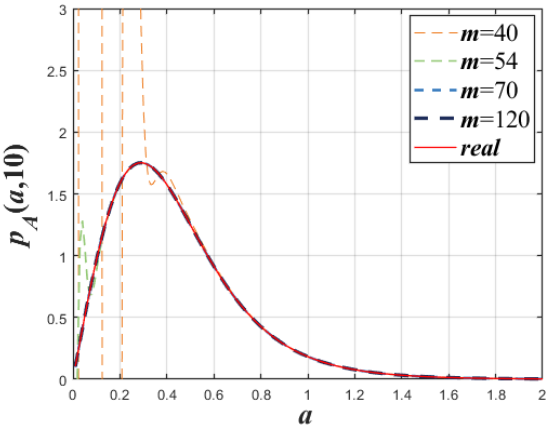

(b)

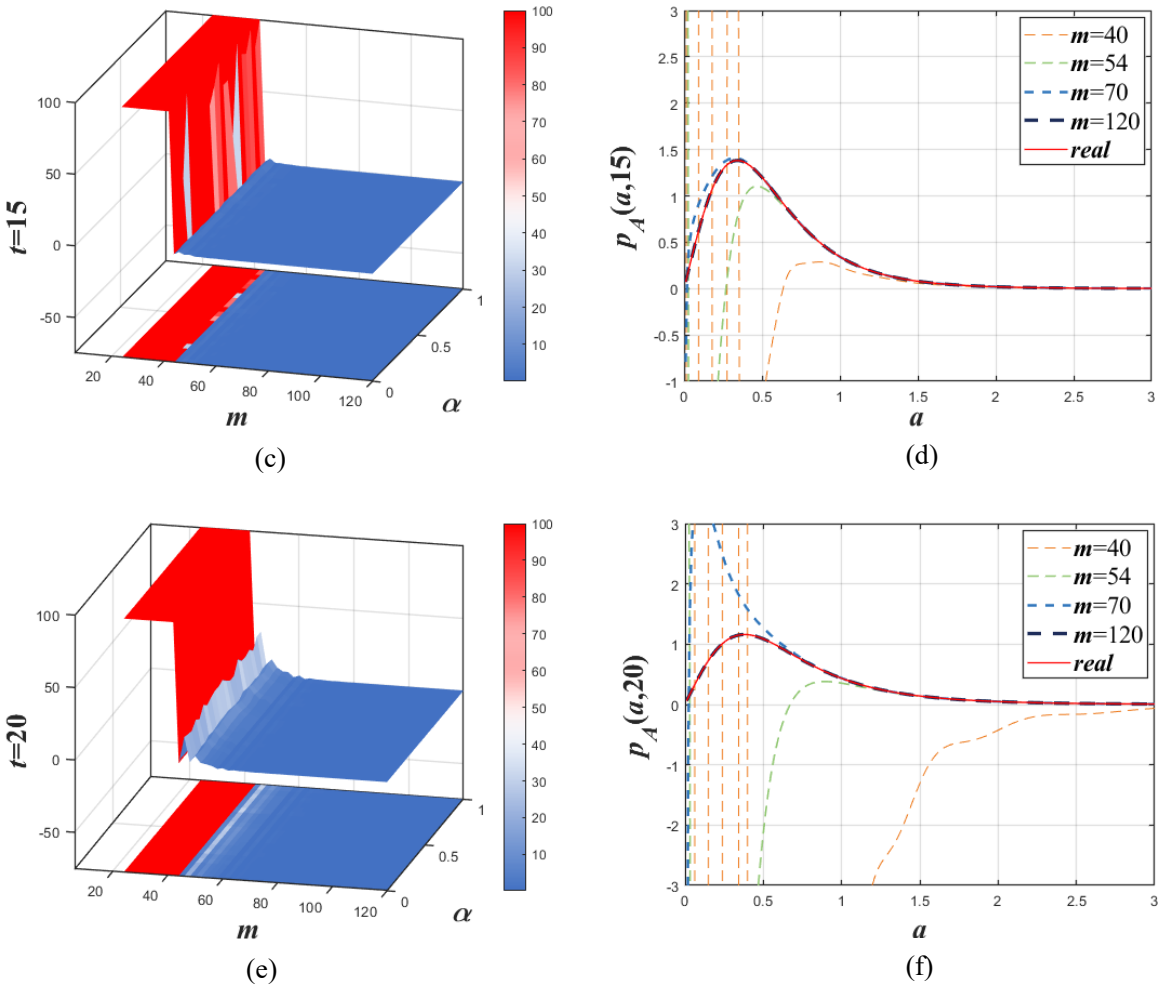

Figure 3-1 The average error of CFM method with the cutoff value m and fractional order α. The distribution map when (a) $t=10$; (c) $t=15$; (e) $t=20$. The PDF obtained by CFM method with different cutoff value when (b) $t=10$; (d) $t=15$; (f) $t=20$ when $\alpha=0.5$

In this section, we use the system parameters listed in Table 3-1. Figures 3-1 (a)(c)(e) show the trends of average error in the CFM method with respect to time t, truncation value m, and fractional order α, where the z-axis represents the error magnitude. The definition of average error in this section is the same as in Eq. (2-49) in Chapter 2. As illustrated in Figure 3-1, when $m<26$, the CFM method is not applicable for solving the transient response PDF of system (3-40). The results also indicate that the fractional order α has an insignificant impact on the probability evolution of system (3-40). Figures 3-1 (b), (d), and (f) depict the transient probability characteristics obtained under different truncation values and time conditions. The results indicate that the error of the CFM method decreases with increasing truncation values, while the required truncation value for accuracy increases with time.

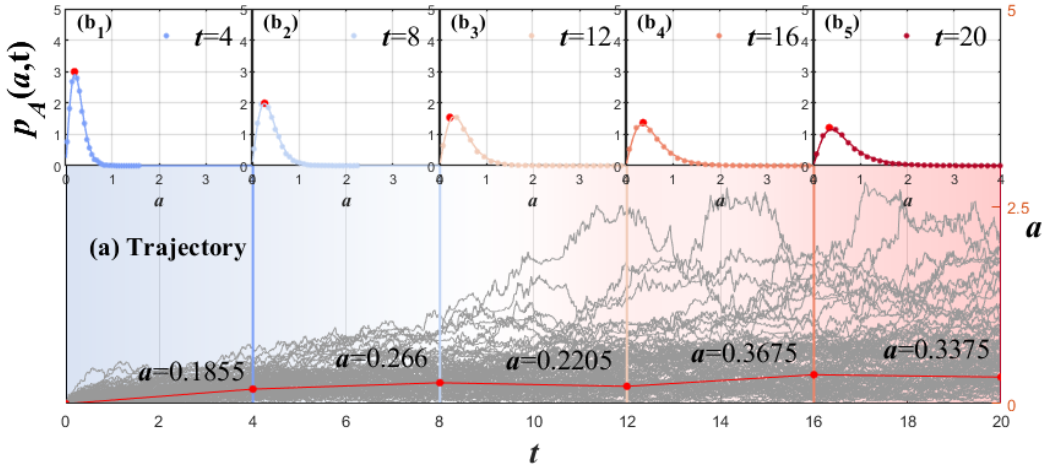

Figure 3-2 (a) The trajectory of system amplitude; (b_1-b_5) The PDF when $t = 4,8,12,16,20$

Figure 3-2 (a) illustrates the evolution of the amplitude of system (3-40), with red dots marking the peak positions of the transient probability characteristics at different times. Figures 3-2 (b_1-b_5) present the transient PDF of the system when $t = 4,8,12,16,20$, where the lines represent results obtained using CFM method and the scatter points correspond to Monte Carlo Simulation results. A stepwise algorithm was used to handle the fractional differential terms in the system. The results demonstrate that the CFM method accurately captures the transient response PDF at different times. Moreover, the CFM method is computationally efficient, with computation times for the results at different times remaining within 3 seconds. Furthermore, from the system's perspective, an increase in time reduces the peak of the transient probability characteristics.

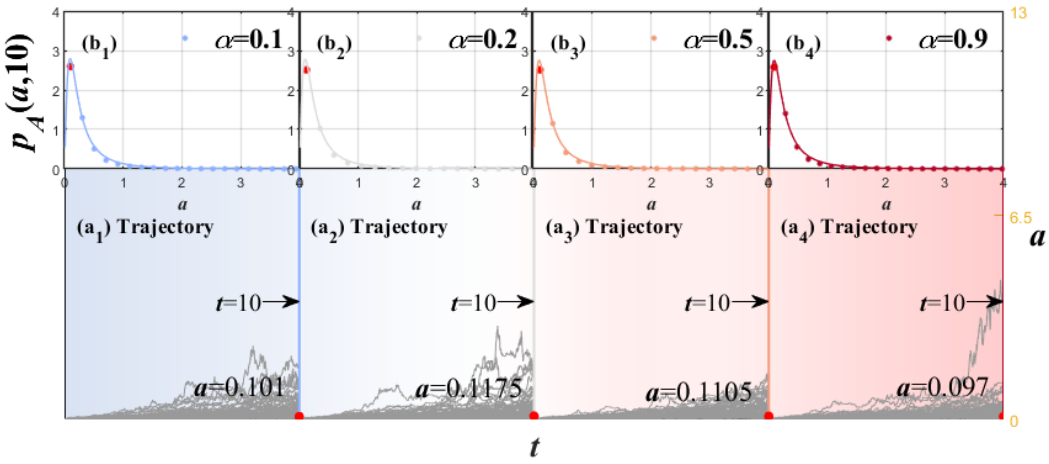

Figure 3-3 (a_1-a_4) The trajectory of system amplitude; (b_1-b_4) The PDF when $t = 10$ and $\alpha = 0.1,0.2,0.5,0.9$

Figure 3-3 (a_1-a_4) display the trajectories of amplitude of the system (3-40) with different

α when $t=10$, in which the red points are the positions of the probability peaks when $\alpha=0.1,0.2,0.5,0.9$. Figure 3-3 (b_1-b_4) are the amplitude PDF with different α when $t=10$. According to the pictures, the CFM method remains high computational efficiency when α changed. In addition, the change of α has no obvious effect on the evolution of the system.

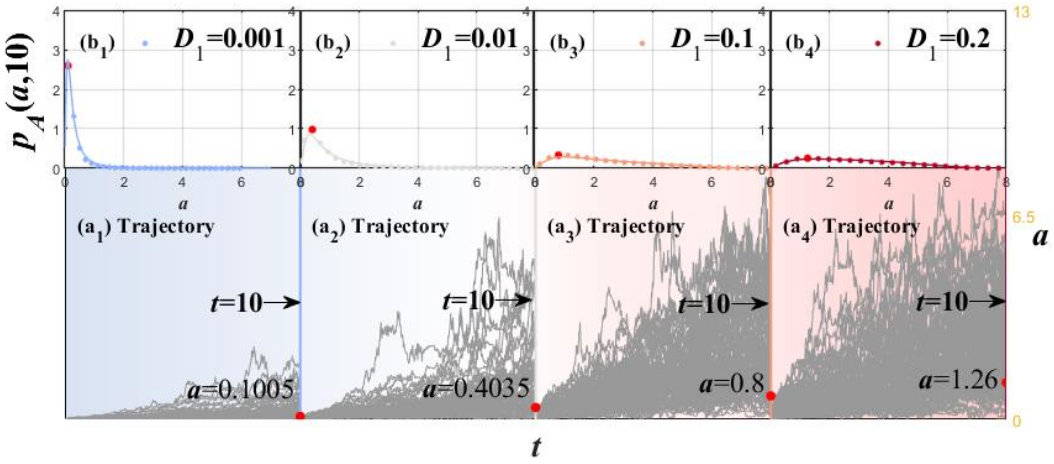

Figure 3-4 (a_1-a_4) The trajectory of system amplitude; (b_1-b_4) The PDF when $t=10$ and $D_1=0.001,0.01,0.1,0.2$

Figure 3-4 (a_1-a_4) exhibit the amplitude trajectories of the system (3-40) when $D_1=0.001$ and $0.01,0.1,0.2$, in which the red points are the positions of the probability peaks. Figure 3-4 (b_1-b_4) are amplitude PDFs with different noise intensities D_1. According to the results, the CFM method can still maintain high computational accuracy for different noise intensities D_1. In addition, the increase of the noise intensity D_1 will reduce the peak value of the transient PDF of the system, and the position of the peak appears to move to a larger amplitude.

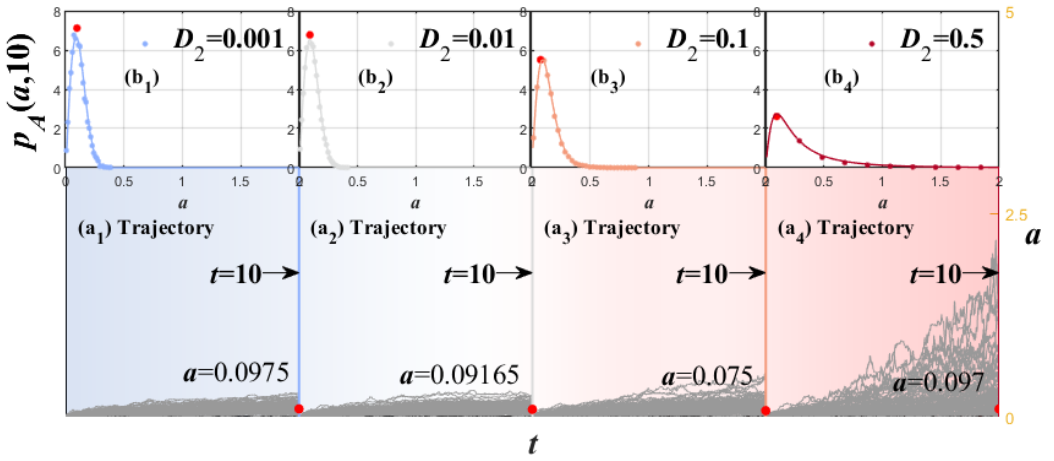

Figure 3-5 (a_1-a_4) The trajectory of system amplitude with D_2; (b_1-b_4) The PDF when $t=10$ and $D_2=0.001,0.01,0.1,0.5$

Figure 3-5 (a_1-a_4) display the amplitude trajectories of the system (3-40) under different

noise intensities D_2, in which the red points are the positions of probability peaks when $t=10$. Figure 3-5 (b_1-b_4) are the transient PDF when $t=10$. From Figure 3-5, the change of D_2 will not affect the accuracy of the CFM method. In addition, the increase of noise intensity D_2 will decrease the transient amplitude PDF of the system peak, but the location of the peaks does not change significantly.

3.5.2 Probability evolution analysis

Currently, research on the steady-state probability density functions of stochastic dynamic systems is relatively advanced within the field of stochastic dynamics. The influence of system parameters on the evolution of steady-state probability densities, such as the mechanisms driving stochastic P-bifurcation, is well understood. However, there has been limited discussion regarding the probabilistic evolution characteristics during stochastic bifurcation. This section aims to analyze this issue. Based on Eqs. (3-44) and (3-45), we can derive the system's FPK equation. Let $\partial p(a,t)/\partial t=0$, then the stationary PDF can be obtained as follows:

$$p_A(a)=4\omega^2 aN\left(4c_1^2D_1+c_2^2D_2a^2\right)^{P_1}e^{P_2}, \tag{3-46}$$

where

$$\begin{aligned} P_1&=-\frac{2\omega^2\left(c_2^4D_2^2\beta_1+2c_1^4b_2\beta D_1^2-D_1D_2b_1\beta c_1^2c_2^3\right)}{c_2^6D_2^3},\\ P_2&=-\frac{\beta\omega^2a^2\left(c_2^2b_2D_2a^2+4c_2^2b_1D_2-8c_1^2b_2D_1\right)}{8c_2^4D_2^2}, \end{aligned} \tag{3-47}$$

and N is the normalization constant. Based on Eq.(3-46), let $\partial p(a)/\partial a=0$, then we can obtain:

$$b_2\beta\omega^2a^6+2b_1\beta\omega^2a^4+\left(8\beta_1\omega^2-2c_2^2D_2\right)a^2-8c_1^2D_1=0. \tag{3-48}$$

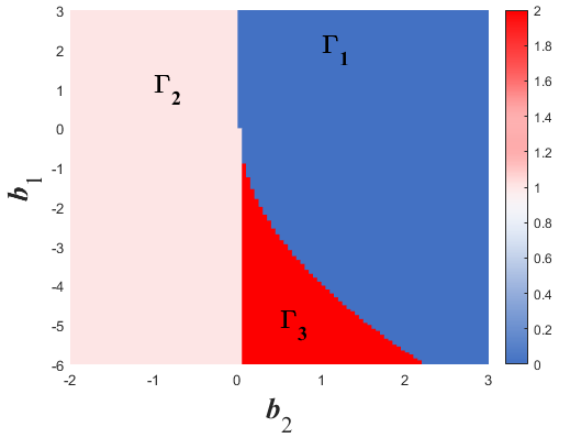

Figure 3-6 Stationary bifurcation diagram of system

Figure 3-6 presents the bifurcation diagram in the parameter space (b_1, b_2), where Γ_1, Γ_2 and Γ_3 denote that Eq. (3-48) has zero, one and two positive real roots, respectively. According to the bifurcation diagram, the parameters used in the following analysis are shown in Table 3-2.

Table 3-2 System parameters

Parameters	Values	Parameters	Values
ρ	4.1	m	200
$\Delta\eta$	0.48	μ	0.05
α	0.5	β	0.05
ω_0	1	b_1	0.5
b_2	-0.015	D_1	0.1
D_2	2	c_1, c_2	1

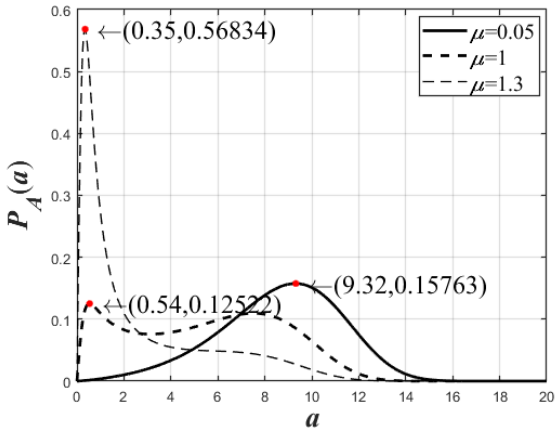

(a)

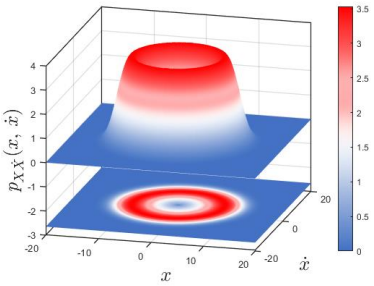

(b)

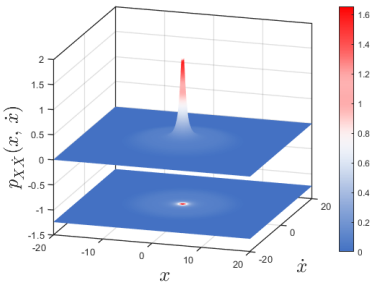

(c)

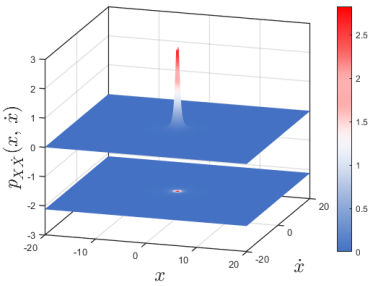

(d)

Figure 3-7 (a) Stationary PDF of system with different μ; (b-d) Joint PDF when $\mu = 0.05, 1, 1.3$

Figure 3-7 (a) shows the stable PDF of system (3-40), with the red dot indicating the coordinate of the peak of stable PDF. Figure 3-7 (b-d) display the joint PDF of displacement and velocity for different parameter values. The results indicate that as μ changes, both the number and shape of the peak in the stable PDF of system (3-40) change. Additionally, the

joint probability distribution of the system transitions between unimodal and bimodal, indicating the occurrence of stochastic P-bifurcation.

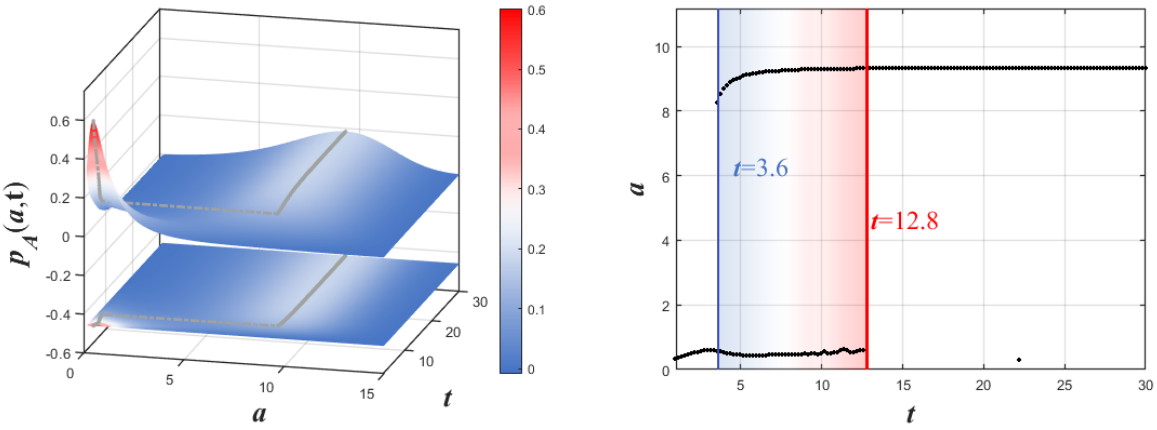

(a) (b)

Figure 3-8 (a) Joint transient PDF； (b) Diagram of peak coordinate

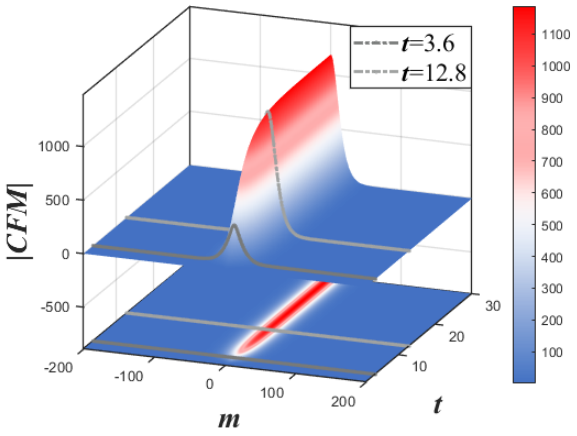

Figure 3-9 The diagram of modulus of joint CFM

The joint amplitude PDF of amplitude and time is shown in Figure 3-8 (a), where the gray line is the peak position of the PDF. Figure 3-8 (b) presents the diagram of peak position associated with Figure 3-8 (a). In this part, we define the left, middle, and right part of Figure 3-8 (b) as the first, second, and third stages, respectively. From the diagram, the transient PDF located in first stage is characterized by single peak with small values. The transient PDF evolves into double peaks in the second stage when $t=3.6$, then transfer to the third stage when $t=12.8$, where the transient PDF is characterized by single peak with large values. Figure 3-9 presents the modulus of joint CFM of m and time, which correspond to Figure 3-8. From Figure 3-9, the modulus of CFM of the system enters the “surge region” and “plateau region” when $t=3.6$ and $t=12.8$, respectively.

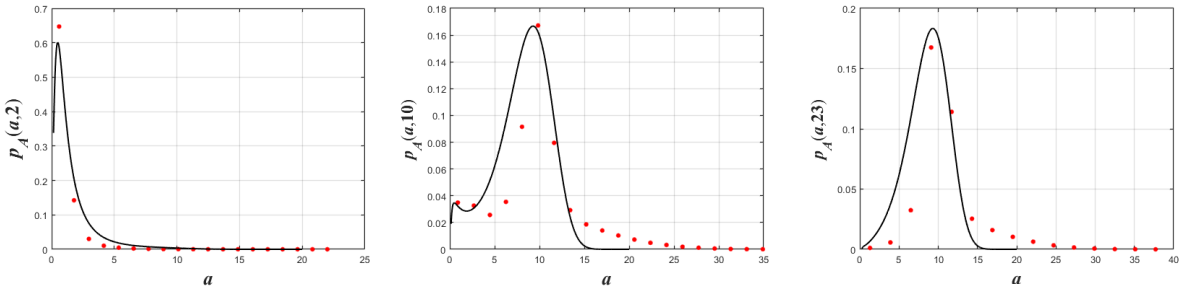

(a) (b) (c)

Figure 3-10 The transient amplitude PDF for different time. (a) $t=2$; (b) $t=10$; (c) $t=23$

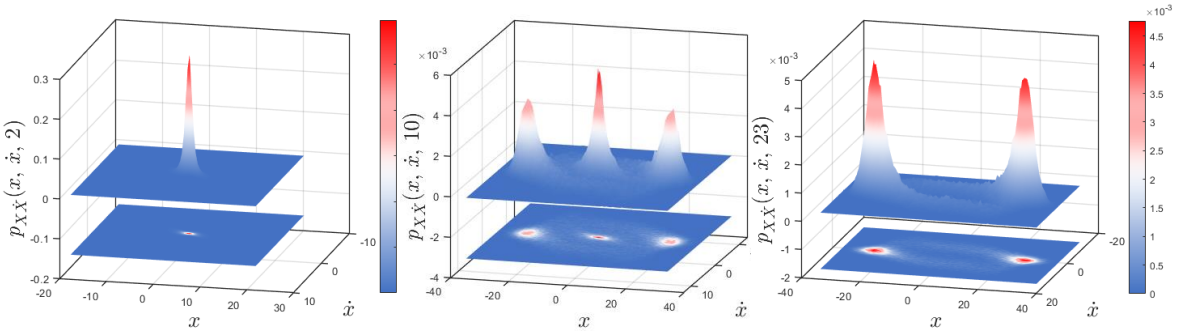

(a) (b) (c)

Figure 3-11 Joint PDF of displacement and velocity when (a) $t=2$; (b) $t=10$; (c) $t=23$

The transient PDF of the system when $t=2,10,23$ is shown in Figure 3-10 (a-c), in which the lines are the results obtained by the CFM method, and the scattered points are the results obtained by the MCS method. According to the results, the error of the CFM method increases slightly, but it can accurately describe the state of the transient PDF. Figure 3-11 (a-c) are the joint transient PDF of displacement and velocity. The joint PDF of the system appears “one peak”, “three peaks”, and “two peaks” in three stages, respectively.

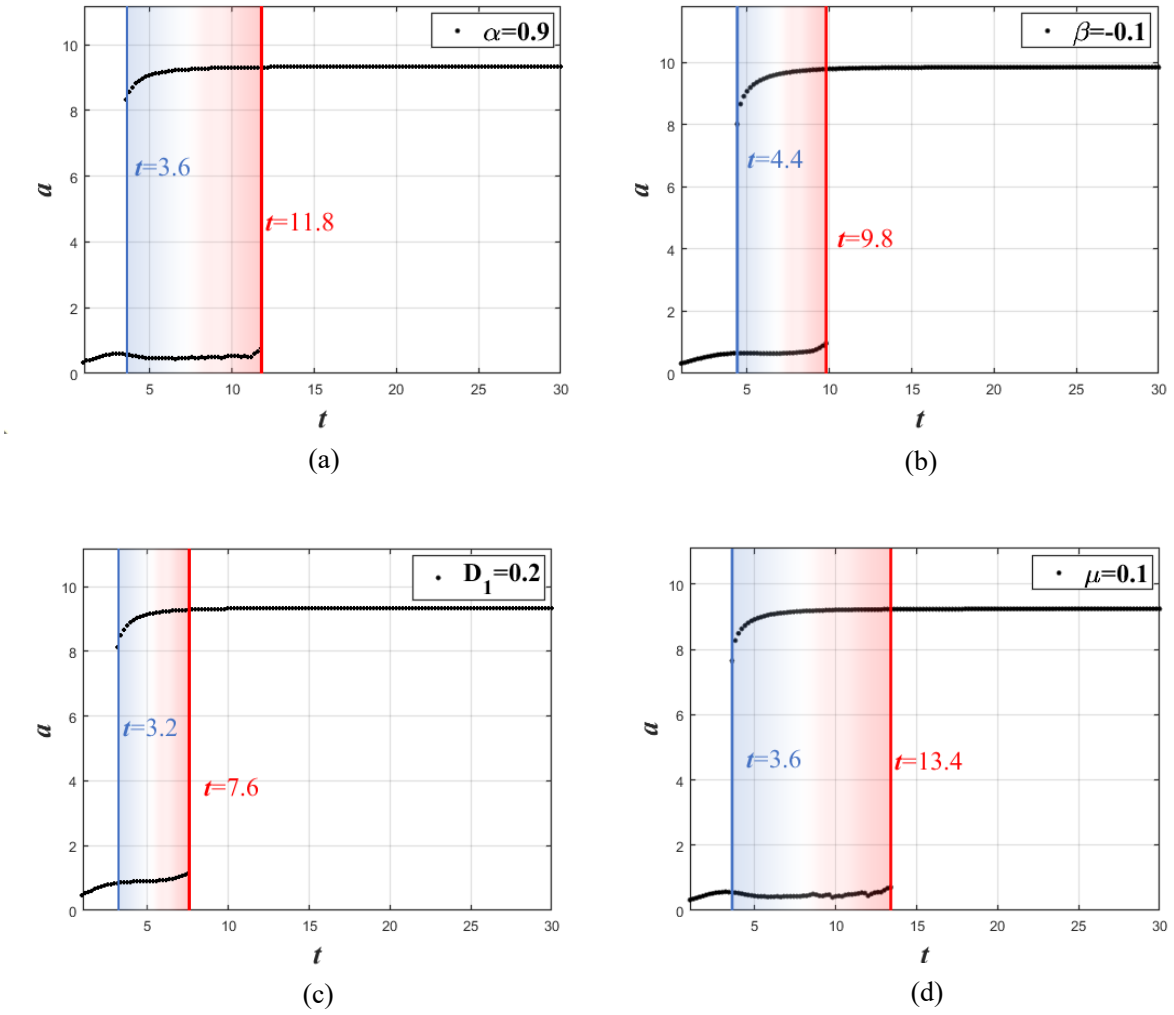

Figure 3-12 Distribution of peak for different parameters. (a) $\alpha = 0.9$; (b) $\beta = -0.1$; (c) $D_1 = 0.2$; (d) $\mu = 0.1$

The influence on the evolution of transient PDF when the system parameters change is shown in Figure 3-12 (a-d). Compared to Figure 3-8 (b), the increase of α has little effect on the evolution from the first stage to the second stage, but it will accelerate the evolution from the second stage to the third stage, which means that the second stage of evolution will be shorter. Furthermore, the decrease of β will extend the evolution time from first stage to second stage and accelerate the evolution from second stage to third stage. In addition, the increase of the noise intensity D_1 will accelerate the probability evolution, the evolution time of the first and second stages will be shortened. Besides, the increase of μ will delay the evolution time of the system probability from the second stage to the third stage, but the evolution time in the first stage has not changed, which means that the time the probability evolution stays in the second stage increases.

3.5.3 Reliability function and first passage analysis

In this section, we mainly consider the first passage time of stochastic dynamic system. Here, the system parameters are selected as follows:

Table 3-3 System parameters

Parameters	Values	Parameters	Values
ρ	4.1	m	120
$\Delta\eta$	0.5	μ	-0.01
α	0.5	β	0.05
ω_0	1	b_1	0.1
b_2	0.1	D_1	0.01
D_2	0.1	c_1, c_2	1
A_l	0.1	A_c	0.8

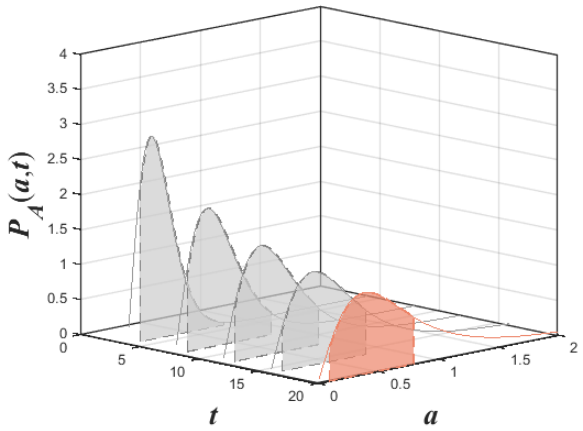

Figure 3-13 Schematic diagram of reliability function

According to the definition of the reliability function, the reliability function is the probability that the system is between $[A_l, A_c]$ when time is t. The schematic diagram of reliability function is shown in Figure 3-13, where the line is the PDF of the system when $t = 4, 8, 12, 16, 20$, and the shaded area is the range of the reliability function. According to the novel method proposed in this chapter, the reliability function and the first passage time of the system can be obtained by Eq. (3-30) and Eq. (3-39).

Parameter of α

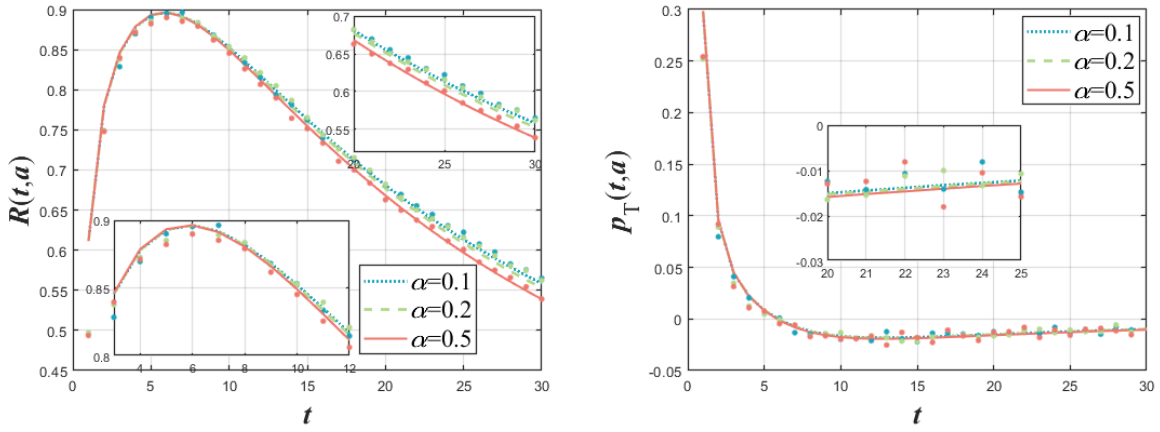

(a) (b)

Figure 3-14 The diagram of (a) Reliability function; (b) FPT with different α

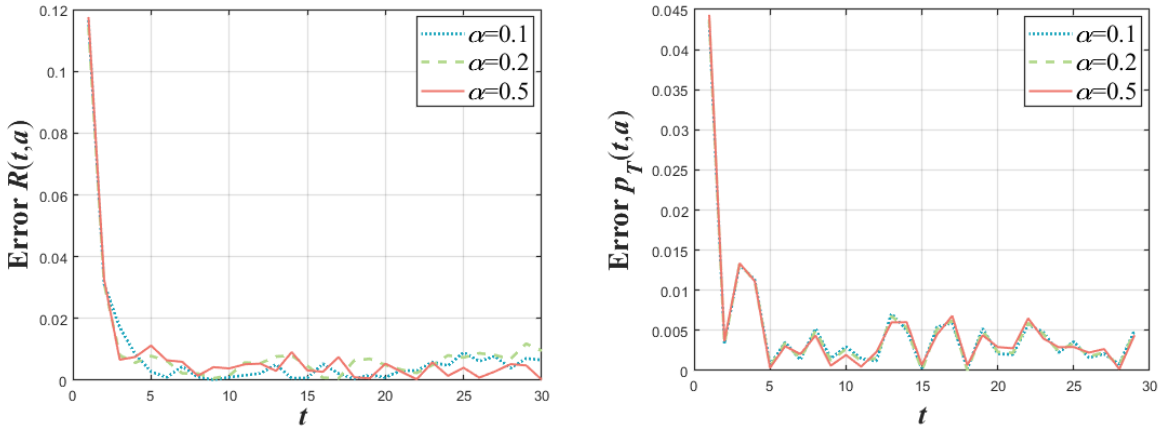

(a) (b)

Figure 3-15 (a) Average error of reliability function. (b) Average error of FPT. with α

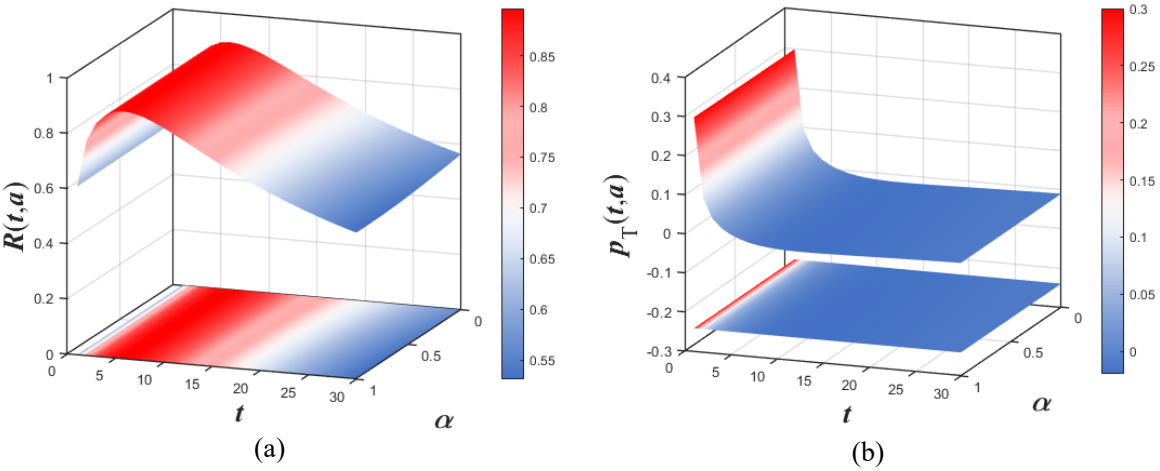

(a) (b)

Figure 3-16 (a) Joint distribution of reliability function in (t,α); (b) Joint distribution of FPT in (t,α)

Figure 3-14 shows the reliability function and first passage time of the system under different α, where the line represent the results obtained by the novel method, and the scatter represent the results obtained by MCS method. Figure 3-15 presents the average error of the novel method. Compared to MCS method, the novel method has high accuracy, and greatly improve the calculation speed in the process of calculation. In addition, the increase of α reduce the reliability in the tail. Figure 3-16 displays the joint distribution diagram of the reliability function and the FPT with time and α.

Parameter of D_1

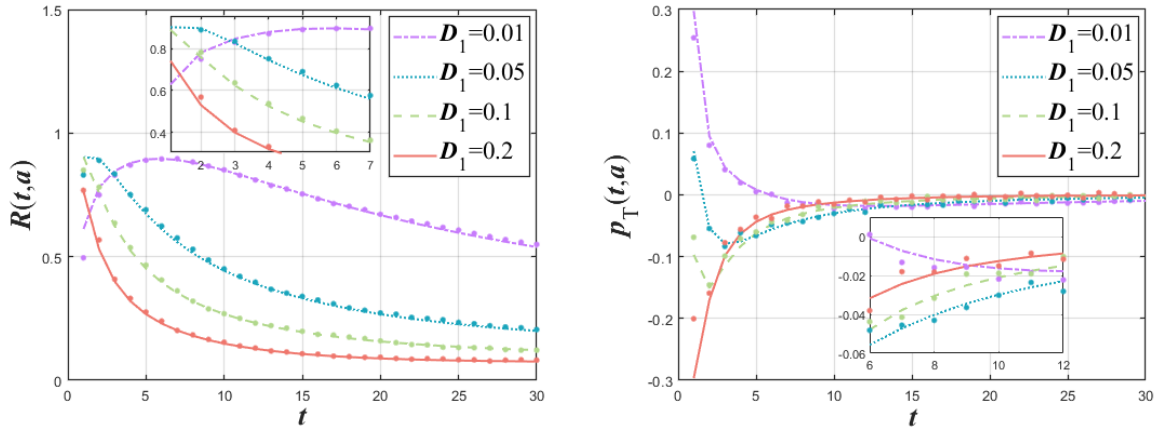

(a) (b)

Figure 3-17 The diagram of (a) Reliability function; (b) FPT with different D_1

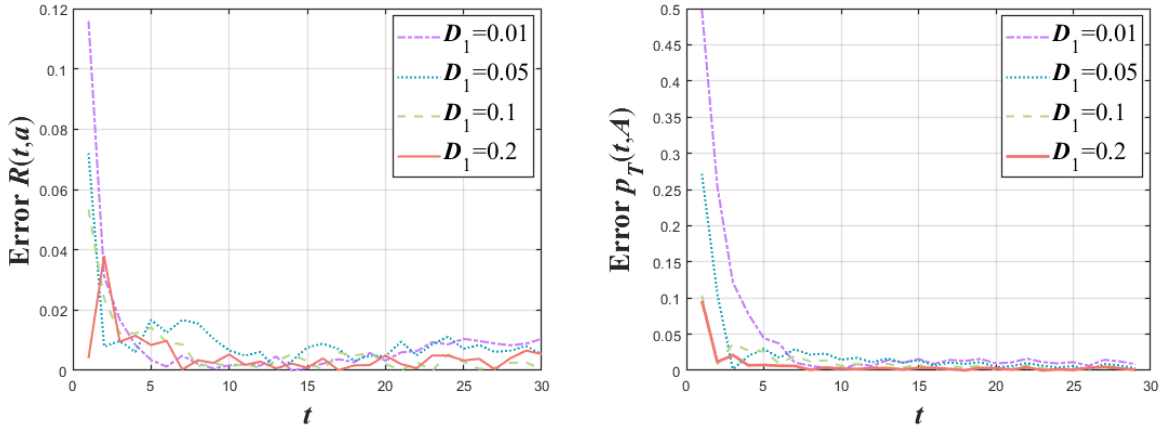

(a) (b)

Figure 3-18 Average error of (a) Reliability function; (b) FPT with different D_1

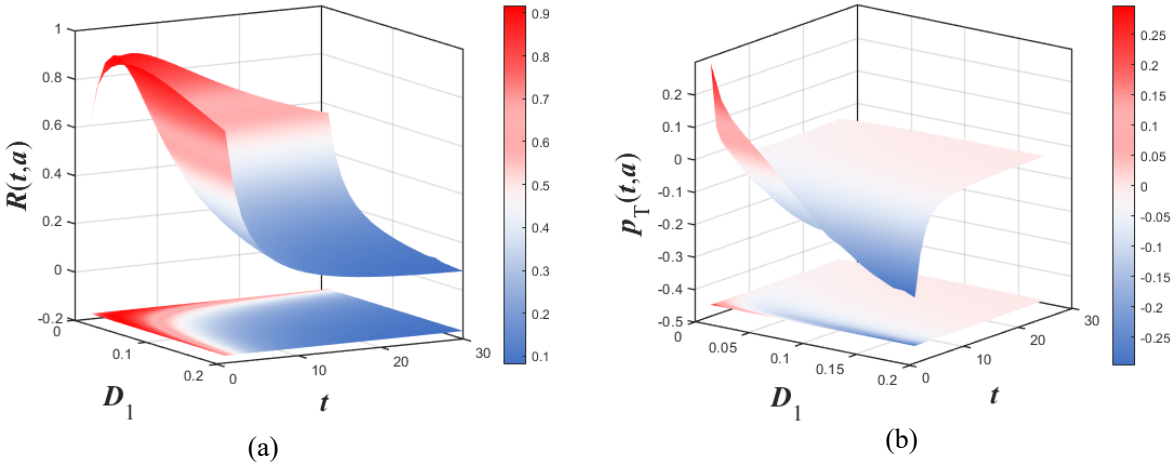

(a) (b)

Figure 3-19 (a) Joint distribution of reliability function in (t, D_1); (b) Joint distribution of FPT in (t, D_1)

Figure 3-17 shows the diagram of reliability function and FPT when the noise intensity D_1 change, and Figure 3-18 displays the average error of CFM method. It can be seen from the pictures that the novel method has high accuracy for different D_1 in calculating the reliability function and the FPT. In addition, the increase of D_1, will obviously change the reliability function and the FPT of the system, which will increase the value of reliability function. Figure 3-19 exhibits the joint distribution diagram of the reliability function and the FPT of noise intensity D_1 and t.

Parameter of μ

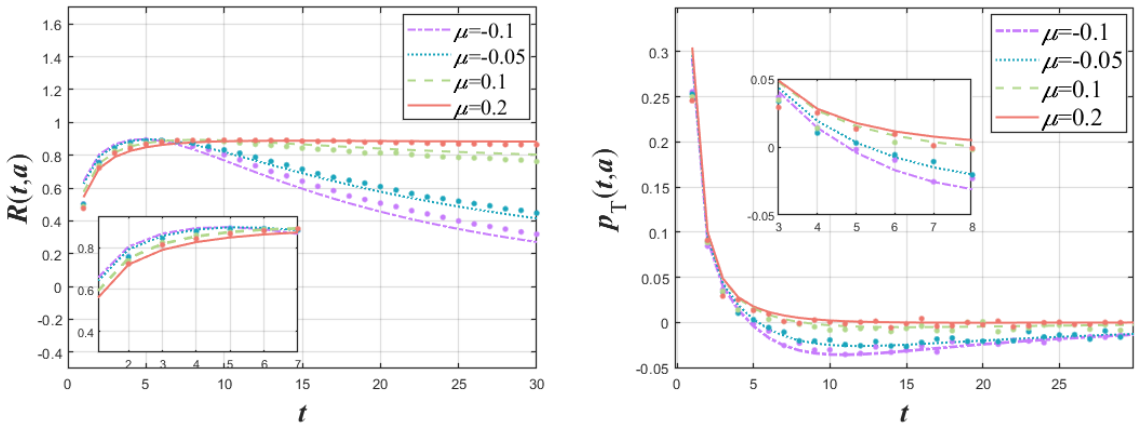

(a) (b)

Figure 3-20 The diagram of (a) Reliability function; (b) FPT with different μ

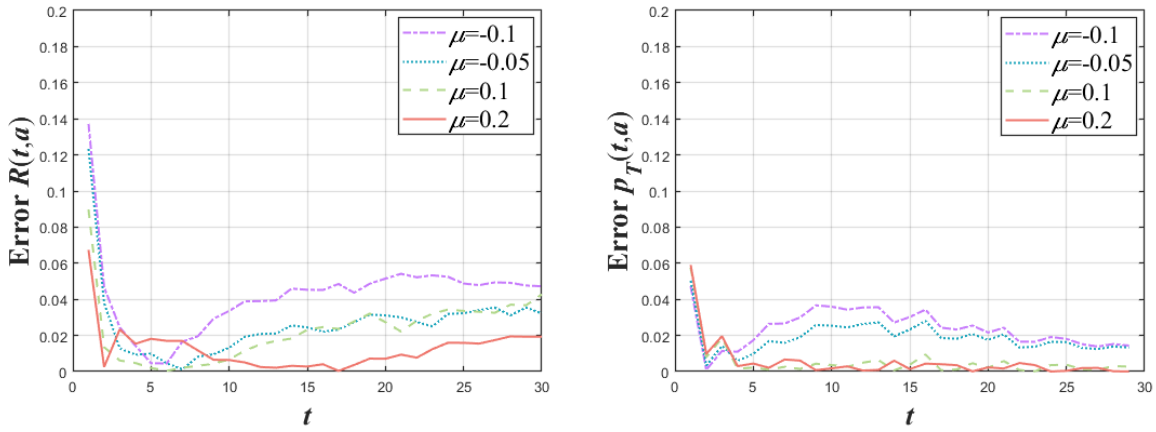

(a) (b)

Figure 3-21 Average error of (a) Reliability function; (b) FPT with different μ

Figure 3-20 presents the reliability function and the FPT of the system under different values of parameter μ, where the lines represent results obtained by novel method, and the scatter is the results obtained by MCS method. Figure 3-21 illustrates the average error of the novel method. According to the pictures, the novel method can accurately solve reliability function and the FPT under different μ. In addition, the results exhibit that the increase of μ will increase the results of the reliability function and the FPT when t is large. Figure 3-22 shows the joint distribution diagram of the reliability function and the FPT of μ and t.

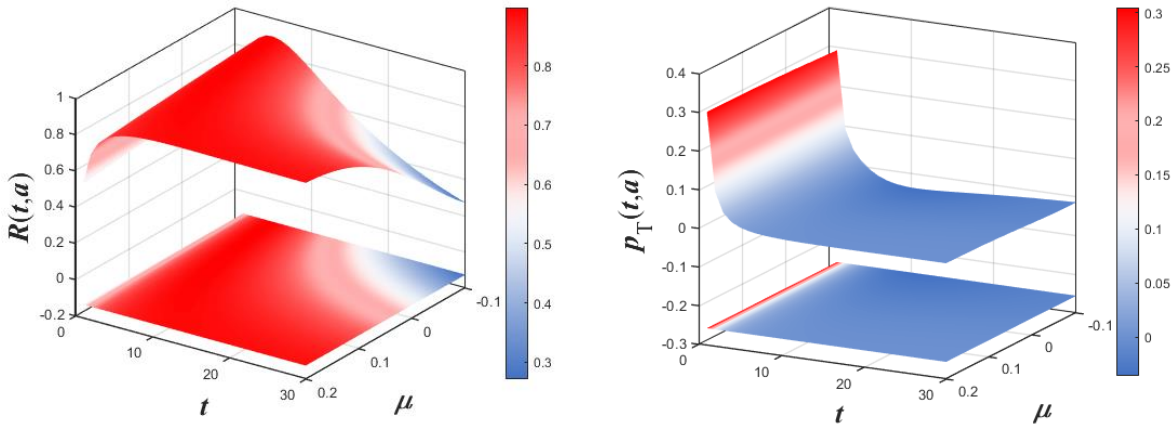

(a) (b)

Figure 3-22 (a) Joint distribution of reliability function in (t,μ); (b) Joint distribution of FPT in (t,μ)

3.6. Conclusion

This chapter examines the applicability of the complex fractional moment method for stochastic dynamic systems with Caputo-type fractional derivatives under additive and multiplicative Gaussian white noise excitation, focusing on their probabilistic evolution characteristics and reliability. Using the stochastic averaging method, we derived the stochastic

Itô differential equation governing the slow variable amplitude process of the system, as well as the FPK equation governing the system's transient probability density. The complex fractional moment method was introduced to obtain a semi-analytical solution for this equation. Compared to traditional methods based on data statistics for obtaining probabilistic characteristics, the complex fractional moment method maintains computational accuracy across different scenarios and significantly improves computational efficiency. Furthermore, based on the results obtained through the complex fractional moment method, this chapter discusses the evolution process of the transient amplitude response probability density function and the joint transient probability density function, as well as the effects mechanisms of time growth and system parameter changes. Additionally, for the first time, the mechanisms through fractional orders, noise intensity, and system parameters influence the transient probability density during stochastic P-bifurcation in steady-state scenarios were discussed. Moreover, a new method is proposed based on complex fractional moments to obtain the reliability function and first passage time, equivalence between the reliability function, first passage time, and complex fractional moments is established. Numerical simulations demonstrate that the proposed method offers both high accuracy and computational efficiency. The results indicate that the fractional order has a minimal impact on the reliability function and first passage time, while variations in noise intensity and system parameters significantly affect the system's reliability function and first passage time.

Chapter 4. Laplacian generalization and application of complex fractional moments

4.1. Introduction

The Probability Density function (PDF), or equivalently its Fourier Transform (FT), known as the Characteristic Function (CF), fully characterize the Random Variables within a probabilistic framework. In various fields, including physics, biomechanics, heat transportation, the governing differential equations are typically nonlinear and incorporate stochastic inputs such as Normal, Poisson, α-stable white noises. The evolution of the PDF is described by the associated Fokker-Planck-Kolmogorov (FPK) equation. As regards, numerous methods, both approximate and exact, exist for determining the PDF of the response process. Additionally, techniques such as the path integral method, based on the Chapman-Kolmogorov equation, are explored in [133-135]. This approach is particularly effective for systems driven by Gaussian or Poisson white noise, especially in addressing the barrier problem [82, 136, 137]. To address the loss of Markovianity in response processes involving fractional derivatives, recent literature has proposed the Wiener path integration method.

One notable drawback of the path integral method is its time-consuming nature, particularly when dealing with distributions that exhibit heavy tails, such as the α-stable distribution [138, 139]. Another significant limitation arises when random phenomena are derived from experimental data or Monte Carlo simulations; methods relying on integer moments or moments of the form $E\left[X^{\rho_J}\right]$ with $\rho_J \in \mathbb{R}^+$ prove inadequate for accurately reconstructing the PDF [140, 141]. Solutions to the Fokker-Planck equation that utilize Taylor expansion of the CF in terms of integer moments or cumulants often yield unsatisfactory results for nonlinear systems. This is because the governing equations involve an infinite hierarchy of differential equations, and truncating the Taylor expansion of the CF produces divergent CF values, and consequently the PDF may not be reconstructed by the expansion of the CF. Additionally, methods based on Maximum Entropy Principle in terms of integer moments or fractional moments work well only for some distributions of the PDF.

Further, the reconstruction of the PDF with a limited amount of information is not applicable to all probability distributions. This is because all available information is evaluated in real domain, and for α-stable distribution $\left(0<\alpha<2\right)$, moments of order $E\left[X^{\rho_J}\right]$ exist only for $\rho_J=\alpha$, meaning that the moment greater than two does not exist. To address these challenges, recently studies propose a method for reconstructing the PDF (or equivalently, the CF), based on the evaluation of Complex Fractional Moments of the type $E\left[X^{\gamma-1}\right]$, $\gamma=\rho+i\eta$. These CFMs are basically the Mellin Transform (MT) of the PDF. If ρ is properly

selected, the inverse MT returns the PDF as a Fourier series in logarithmic scale of the domain x of the PDF. Using this concept, numerous publications for solving various problems are available.

Drawing from this experience, we recognize that working in the complex domain can effectively reconstruct the PDF using integral transforms. However, these transforms come with distinct applications and limitations; for instance, the Mellin transform has a singularity at $x=0$. To extend the theoretical framework for reconstructing the PDF invoking complex quantities, a method based on Laplace transform is discussed in detail and compared with the method based on the MT. It is shown that the presented method leads to work with moments of the form $E\left[\exp\left(-sX\right)\right]$, where $s=\beta-i\theta$. These moments, derived from the Laplace transform, generate the so called, Shifted Characteristic Function (SCF), as the presence of β corresponds to the shift property of the Laplace transform. Utilizing these complex quantities, the PDF can also be reconstructed.

Furthermore, a new definition of double-sided LT is introduced, remaining valid for PDF reconstruction. The solutions to the Fokker-Planck-Kolmogorov (FPK) equations for the double-sided PDF are presented. To demonstrate the versatility of the Laplace transform method, examples illustrating solutions for classical differential equations, fractional differential equations, and FPK equations are included. Lastly, a comparison between the Laplace and Mellin transform methods is provided. In the latter, a refined definition of the inverse Mellin transform is proposed to address the singularity issue at $x=0$, which has been a concern in previous studies.

4.2. Discretization of the inverse LT for the Probability Density Function

First of all, representing the generic function $f\left(x\right)$ in Eq. (1-14) as $p_X\left(x\right)$, namely the PDF of the RV X with domain $x\geq 0$, the FT of $p_X\left(x\right)$ is, by definition, the Characteristic Function (CF) labeled as $\phi_X\left(\theta\right)$, which is given by:

$$\begin{aligned}\phi_X\left(\theta\right)&=E\left[e^{i\theta X}\right]=\int_0^\infty e^{i\theta x}p_X\left(x\right)\mathrm{d}x=p_X^{\mathcal{F}}\left(\theta\right)\\&=\int_0^\infty\cos\left(\theta x\right)p_X\left(x\right)\mathrm{d}x+i\int_0^\infty\sin\left(\theta x\right)p_X\left(x\right)\mathrm{d}x=A_{p_X}^{\mathcal{F}}\left(\theta\right)+iB_{p_X}^{\mathcal{F}}\left(\theta\right),\end{aligned}\tag{4-1}$$

where $E\left[\bullet\right]$ represents the mean value of the RV, $A_{p_X}^{\mathcal{F}}\left(\theta\right)$ and $B_{p_X}^{\mathcal{F}}\left(\theta\right)$ are the real and the imaginary part of $\phi_X\left(\theta\right)$, respectively.

The cosine transform ($A_{p_X}^{\mathcal{F}}\left(\theta\right)$) and the sine transform ($B_{p_X}^{\mathcal{F}}\left(\theta\right)$) are even and odd function with respect to θ, respectively. Moreover $B_{p_X}^{\mathcal{F}}\left(\theta\right)$ is the Hilbert transform of $A_{p_X}^{\mathcal{F}}\left(\theta\right)$, namely

$$B_{p_X}^{\mathcal{F}}(\theta)=\frac{1}{\pi}\mathcal{P}\int_{-\infty}^{\infty}A_{p_X}^{\mathcal{F}}(\bar{\theta})\left|\theta-\bar{\theta}\right|^{-1}\mathrm{d}\bar{\theta}=\hat{A}_{p_X}^{\mathcal{F}}(\theta),\tag{4-2}$$

where the symbol $\mathcal{P}$ in Eq. (4-2) stands for Cauchy Principle Value (PV) of the integral in parenthesis, and the superimposed $\wedge$ stands for the Hilbert transform operator.

On the other hand, since

$$\int_0^{\infty}e^{-\beta x}p_X(x)e^{i\theta x}\mathrm{d}x=\mathcal{F}\left\{e^{-\beta x}p_X(x);\theta\right\}=\mathcal{L}\left\{p_X(x);s\right\},\tag{4-3}$$

the LT of the one-sided PDF may be considered as a *Shifted Characteristic Function* (SCF), namely

$$\mathcal{L}\left\{p_X(x);s\right\}=\phi_X^S(\beta-i\theta)=\int_0^{\infty}e^{-\beta x}p_X(x)e^{i\theta x}\mathrm{d}x=\mathcal{F}\left\{e^{-\beta x}p_X(x);\theta\right\}=E\left[e^{-sX}\right].\tag{4-4}$$

Where the apex S in the CF means *shifted*.

The inverse LT, according to Eq. (1-16), returns $p_X(x)$ in the form

$$p_X(x)=\frac{1}{2\pi}\int_{-\infty}^{\infty}E\left[e^{-sX}\right]e^{-sx}\mathrm{d}\theta.\tag{4-5}$$

Let

$$\phi_X^S(\beta)=A_{p_X}^{\mathcal{L}}(s)+iB_{p_X}^{\mathcal{L}}(s)=\int_0^{\infty}e^{-\beta x}p_X(x)\cos(\theta x)\mathrm{d}x+i\int_0^{\infty}e^{-\beta x}p_X(x)\sin(\theta x)\mathrm{d}x,\tag{4-6}$$

where $B_{p_X}^{\mathcal{L}}(s)=A_{p_X}^{\mathcal{L}}(s)$. The discretized form of Eq. (4-5), obtained by dividing the θ axis in small intervals $\Delta\theta$ of equal length, can be expressed as:

$$p_X(x)\cong\frac{1}{2b}\sum_{k=-\infty}^{\infty}\mathcal{L}\left\{p_X(x);s_k\right\}e^{s_kx},\tag{4-7}$$

where $b=\pi/\Delta\theta$, $s_k=\beta+ik\pi/b$. By taking into account $A_{p_X}^{\mathcal{L}}(\beta+i\theta)=A_{p_X}^{\mathcal{L}}(\beta-i\theta)$ and $B_{p_X}^{\mathcal{L}}(\beta+i\theta)=-B_{p_X}^{\mathcal{L}}(\beta-i\theta)$, Eq. (4-7) may be rewritten as:

$$p_X(x)\simeq\frac{e^{\beta x}}{2b}\left[A_{p_X}^{\mathcal{L}}(\beta)+2\sum_{k=1}^{m}\left(A_{p_X}^{\mathcal{L}}(s_k)\cos\left(\frac{k\pi}{b}x\right)+B_{p_X}^{\mathcal{L}}(s_k)\sin\left(\frac{k\pi}{b}x\right)\right)\right],\tag{4-8}$$

where m is the cut-off value in the domain θ. In passing we observe the significance of the first term that is $A_{p_X}^{\mathcal{L}}(\beta)=E\left[\exp(-\beta X)\right]$, it follows that the higher β, the larger the shift of SCF is. The coefficient can be expressed as:

$$
\begin{aligned}
A_{p_X}^{\mathcal{L}}(\beta) &= \int_0^{2b} p_X(x) e^{-\beta x} \mathrm{d}x = E\left[e^{-\beta X}\right], \\
A_{p_X}^{\mathcal{L}}(s_k) &= \int_0^{2b} p_X(x) e^{-\beta x} \cos\left(\frac{k\pi}{b}x\right) \mathrm{d}x = E\left[e^{-\beta X}\cos\left(\frac{k\pi}{b}X\right)\right], \\
B_{p_X}^{\mathcal{L}}(s_k) &= \int_0^{2b} p_X(x) e^{-\beta x} \sin\left(\frac{k\pi}{b}x\right) \mathrm{d}x = E\left[e^{-\beta X}\sin\left(\frac{k\pi}{b}X\right)\right].
\end{aligned}
\tag{4-9}
$$

From Eq. (4-9), we observe that only in the limit as $\Delta\theta \to 0\,(b \to \infty)$, for $\beta = 0$, the total area of the PDF is unitary. This observation is useful for properly selected $\Delta\theta$ and the corresponding b to ensure an accurate representation of the PDF in discretized form.

As previously stated the very relevant aspect in the inverse Laplace transform in Eq. (4-5) is that the integral is performed along the imaginary axis θ while β remain constant, this implies that the existence of statistical moments of the form $E\left[\exp\left(-\beta X\right)\right]$ guarantee the existence of $E\left[\exp\left(-\left(\beta - i\theta\right)X\right)\right]$ for every value of θ.

In many engineering problems, the governing Fokker Planck equations involves derivative of the PDF, along with products of the PDF by some non-linear functions of the form $\sum_{j=1}^{n} \partial\left[\exp\left(-\alpha_j x\right) p_X(x)\right] / \partial x$. This results in the corresponding SCF being evaluated in different values of β. Consequently, such equations may not be solvable in Laplace domain. To solve these problems by using the representation of the PDF in terms $A_{p_X}^{\mathcal{L}}(s_k)$, $B_{p_X}^{\mathcal{L}}(s_k)$, we need to address the following problem: Is it possible finding $A_{p_X}^{\mathcal{L}}(s_k + \Delta\beta)$ and $B_{p_X}^{\mathcal{L}}(s_k + \Delta\beta)$ if $A_{p_X}^{\mathcal{L}}(s_k)$, $B_{p_X}^{\mathcal{L}}(s_k)$ are known? In order to solve this crucial issue, we observe that $p_X(x)$ in Eq. (4-8) is independent on β, provided that β belongs to the FS of the LT, it follows that from Eq. (4-8), we can write

$$
\begin{aligned}
&A_{p_X}^{\mathcal{L}}(\beta + \Delta\beta) + 2\sum_{k=1}^{m}\left(A_{p_X}^{\mathcal{L}}(s_k + \Delta\beta)\cos\left(\frac{k\pi}{b}x\right) + B_{p_X}^{\mathcal{L}}(s_k + \Delta\beta)\sin\left(\frac{k\pi}{b}x\right)\right) \\
&= e^{-\Delta\beta x}\left[A_{p_X}^{\mathcal{L}}(\beta) + 2\sum_{k=1}^{m}\left(A_{p_X}^{\mathcal{L}}(s_k)\cos\left(\frac{k\pi}{b}x\right) + B_{p_X}^{\mathcal{L}}(s_k)\sin\left(\frac{k\pi}{b}x\right)\right)\right],
\end{aligned}
\tag{4-10}
$$

by multiplying both sides of Eq. (4-10) by $\cos\left(\frac{J\pi x}{b}\right)\mathrm{d}x$, $J = 1, 2, ..., m$ and $\sin\left(\frac{J\pi x}{b}\right)\mathrm{d}x$, and integrating in the range $[0, 2b]$, due to the orthogonality conditions of the trigonometric function in $[a, a + 2b]$, we get:

$$\begin{aligned} A_{p_X}^{\mathcal{L}}\left(s_J+\Delta\beta\right)&=\frac{1}{2b}A_{p_X}^{\mathcal{L}}\left(\beta\right)a_{0J}+\frac{1}{b}\sum_{k=1}^{m}\left[A_{p_X}^{\mathcal{L}}\left(s_k\right)a_{Jk}+B_{p_X}^{\mathcal{L}}\left(s_k\right)c_{Jk}\right],\\ B_{p_X}^{\mathcal{L}}\left(s_J+\Delta\beta\right)&=\frac{1}{2b}A_{p_X}^{\mathcal{L}}\left(\beta\right)b_{0J}+\frac{1}{b}\sum_{k=1}^{m}\left[A_{p_X}^{\mathcal{L}}\left(s_k\right)c_{kJ}+B_{p_X}^{\mathcal{L}}\left(s_k\right)b_{Jk}\right], \end{aligned} \tag{4-11}$$

where

$$\begin{aligned} &a_{0J}=\int_0^{2b}e^{-\Delta\beta x}\cos\left(\frac{J\pi}{b}x\right)\mathrm{d}x=b^2\Delta\beta r_J,\\ &b_{0J}=\int_0^{2b}e^{-\Delta\beta x}\sin\left(\frac{J\pi}{b}x\right)\mathrm{d}x=bJ\pi r_J,\\ &a_{Jk}=\int_0^{2b}e^{-\Delta\beta x}\cos\left(\frac{J\pi}{b}x\right)\cos\left(\frac{k\pi}{b}x\right)\mathrm{d}x=\frac{b^2\Delta\beta}{2}\left(t_{Jk}+s_{Jk}\right),\\ &b_{Jk}=\int_0^{2b}e^{-\Delta\beta x}\sin\left(\frac{J\pi}{b}x\right)\sin\left(\frac{k\pi}{b}x\right)\mathrm{d}x=\frac{b^2\Delta\beta}{2}\left(t_{Jk}-s_{Jk}\right),\\ &c_{Jk}=\int_0^{2b}e^{-\Delta\beta x}\cos\left(\frac{J\pi}{b}x\right)\sin\left(\frac{k\pi}{b}x\right)\mathrm{d}x=\frac{b\pi}{2}\left(\left(J+k\right)s_{Jk}-\left(J-k\right)t_{Jk}\right),\\ &t_{Jk}=\frac{1-e^{-2b\Delta\beta}}{b^2\Delta\beta^2+\left(J-k\right)^2\pi^2},\ s_{Jk}=\frac{1-e^{-2b\Delta\beta}}{b^2\Delta\beta^2+\left(J+k\right)^2\pi^2},r_J=\frac{1-e^{-2b\Delta\beta}}{J^2\pi^2+b^2\Delta\beta^2},\\ &J,k=1,2,...,m,\ \ \Delta\beta\neq 0. \end{aligned} \tag{4-12}$$

Eq.(4-12) constitute a set of $2m+1$ linear algebra equations that can be expressed in matrix form as:

$$\mathbf{a}_p^{\mathcal{L}}\left(s+\Delta\beta\right)=\frac{1}{2b}\mathbf{D}^{\mathcal{L}}\mathbf{a}_p^{\mathcal{L}}\left(s\right);\ \ s=\beta-i\theta,\ \ \Delta\beta\neq 0, \tag{4-13}$$

$$\mathbf{D}^{\mathcal{L}}=\begin{pmatrix} a_{00} & \boldsymbol{a}_{0J}^{\mathrm{T}} & \boldsymbol{b}_{0J}^{\mathrm{T}}\\ \boldsymbol{a}_{0J} & 2\mathbf{A} & 2\mathbf{C}\\ \boldsymbol{b}_{0J} & 2\mathbf{C}^{\mathrm{T}} & 2\mathbf{B}\end{pmatrix};\ \mathbf{a}_p^{\mathcal{L}}\left(s\right)=\begin{pmatrix} A_{p_X}^{\mathcal{L}}\left(\beta\right)\\ \boldsymbol{A}_{p_X}^{\mathcal{L}}\left(s_k\right)\\ \boldsymbol{B}_{p_X}^{\mathcal{L}}\left(s_k\right)\end{pmatrix};\ \mathbf{a}_p^{\mathcal{L}}\left(s+\Delta\beta\right)=\begin{pmatrix} A_{p_X}^{\mathcal{L}}\left(\beta+\Delta\beta\right)\\ \boldsymbol{A}_{p_X}^{\mathcal{L}}\left(s_k+\Delta\beta\right)\\ \boldsymbol{B}_{p_X}^{\mathcal{L}}\left(s_k+\Delta\beta\right)\end{pmatrix}. \tag{4-14}$$

Here, $\mathbf{a}_p^{\mathcal{L}}\left(\boldsymbol{s}+\Delta\beta\right)$ and $\mathbf{a}_p^{\mathcal{L}}\left(\boldsymbol{s}\right)$ are vectors with $2m+1$ components. In the matrix $\mathbf{D}^{\mathcal{L}}$, the first row of the $\left(2m+1\right)\times\left(2m+1\right)$ matrix $\mathbf{D}^{\mathcal{L}}$ contains a_{00}, $\boldsymbol{a}_{0J}^{\mathrm{T}}\left(J=0,...,m\right)$ and $\boldsymbol{b}_{0J}^{\mathrm{T}}\left(J=1,2,...,m\right)$, the symmetric matrix $\mathbf{A}$ is a $m\times m$ matrix, where J,k element is a_{Jk}, the matrix $\mathbf{B}$ is a $m\times m$ symmetric matrix where J,k element are b_{Jk}. Moreover the matrix $\mathbf{C}$ is a $m\times m$ matrix where J,k element is c_{Jk}. If $\Delta\beta=0$, then $\mathbf{D}^{\mathcal{L}}$ is $2b\mathbf{I}_{2m+1}$, being $\mathbf{I}_{2m+1}$ the $\left(2m+1\right)\times\left(2m+1\right)$ identity matrix. By means of Eq. (4-13), the vector $\mathbf{a}_p^{\mathcal{L}}\left(s+\Delta\beta\right)$ is constructed by knowing $\mathbf{a}_p^{\mathcal{L}}\left(s\right)$, Eqs. (4-10)-(4-14) remain valid provided β and $\beta+\Delta\beta$ belong to the FS of the Laplace transform. From Eq. (4-13), we realize that if we

select $\beta = 0$, the vector $\mathbf{a}_p^{\mathcal{L}}(s)$ becomes the corresponding Fourier vector, and the matrix $\mathbf{D}^{\mathcal{L}}$ reverts to the corresponding $\mathbf{D}^{\mathcal{F}}$.

4.3. Generalization for double-sided PDF

The probability density function of a RV is generally not one-sided. In this case, we need to adapt the concepts used in the previous sections to the double-sided case. First of all, noticing that the Laplace Transform applies to one sided function and is widely used for solving differential equation with assigned initial conditions in zero. It follows that in probabilistic setting for double-sided PDF, we need to generalize LT in the domain x defined in $-\infty < x < \infty$, leading to the definition of the double-sided LT.

In some textbooks [142, 143] and in the tables of transform, the double-sided Laplace transform, labeled as $\bar{f}^{\mathcal{L}}(s)$, and its inverse are defined as

$$\begin{aligned} f^{\bar{\mathcal{L}}}(s) &= \bar{\mathcal{L}}\{f(x);s\} = \int_{-\infty}^{\infty} e^{-sx} f(x)\mathrm{d}x \\ &= \int_0^{\infty} \left(f(x)e^{-\beta x} \right) e^{i\theta x}\mathrm{d}x + \int_0^{\infty} \left(f(-x)e^{\beta x} \right) e^{-i\theta x}\mathrm{d}x; \\ f(x) &= \frac{1}{2\pi}\int_{\theta=-\infty}^{\infty} e^{sx} f^{\bar{\mathcal{L}}}(s)\mathrm{d}\theta. \end{aligned} \tag{4-15}$$

From the definition Eq. (4-15), we realize that the double sided LT is the summation of two one-sided LT terms, one in the negative range ($x < 0$), and the other one in the positive range $x > 0$. This definition is valid in the integral form, provided that the FS of the LT is properly selected. However, taking into account that $\lim_{x\to\infty} f(-x)e^{\beta x}$, for large value of β, the reconstructed function may be divergent. Such an example, let

$$f(x) = \exp(-\nu|x|)(\nu > 0), \tag{4-16}$$

in this case, the one-sided LT of $f(x)U(x)$ in Eq. (4-15) has a FS in the range $0 \le \beta < \infty$, while for $f(x)U(-x)$, the integral converges for $0 \le \beta < \nu$. It follows that the FS for $f(x) = \exp(-\nu|x|)$ is $0 \le \beta < \nu$. In any cases, also by selecting β into the FS, the inverse LT by using Eq. (4-15) returns $f(x)$ in the whole domain, but produces inaccurate results in the corresponding discretized form when $\beta \neq 0$.

In order to overcome this drawback, we propose a new definition of the double-sided LT in the form

$$\begin{aligned} p_X^{\bar{\mathcal{L}}}(s) &= \bar{\mathcal{L}}\{p_X(x);s\} = \int_{-\infty}^{\infty} e^{-(\beta - i\theta\,\mathrm{sign}(x))|x|} p_X(x)\mathrm{d}x \\ &= \int_{-\infty}^{\infty} e^{-\beta|x|} p_X(x) e^{i\theta x}\mathrm{d}x = \bar{\mathcal{F}}\left\{e^{-\beta|x|} p_X(x);\theta\right\}; \end{aligned} \tag{4-17}$$

And then its inverse reconstructed by the double-sided PDF is given as:

$$p_X(x)=\frac{1}{2\pi}\int_{\theta=-\infty}^{\infty}\overline{p}_X^{\mathcal{L}}(s)e^{\beta|x|}e^{-i\theta x}\mathrm{d}\theta=\frac{e^{\beta|x|}}{2\pi}\int_{\theta=-\infty}^{\infty}p_X^{\bar{\mathcal{L}}}(s)e^{-i\theta x}\mathrm{d}\theta. \tag{4-18}$$

With this definition, the aforementioned problem disappear because the $p_X(x)U(x)$ and $p_X(x)U(-x)$ are both multiplied by $\exp(-\beta|x|)$, thus $p_X(x)$ and $p_X(-x)$ are weighted in the same manner. Such an example for the non-symmetric case $p_X(x)=\frac{\nu}{2}\exp(-\nu|x-\mu|)$, the double-sided LT evaluated by Eq. (4-15), is given

$$p_X^{\bar{\mathcal{L}}}(s)=\frac{\nu}{2}\int_{-\infty}^{\infty}e^{-\nu|x-\mu|}e^{-\beta|x|}e^{i\theta x}\mathrm{d}x=\begin{cases}\dfrac{\nu\beta e^{\mu\nu}}{|s|^2+2i\theta\nu-\nu^2}-\dfrac{\nu^2e^{\mu s}}{s^2-\nu^2};s=\beta+i\theta,\mu<0;\\ \dfrac{\nu\beta e^{-\mu\nu}}{|s|^2-2i\theta\nu-\nu^2}-\dfrac{\nu^2e^{-\mu s}}{s^2-\nu^2};s=\beta-i\theta,\mu>0.\end{cases} \tag{4-19}$$

The corresponding $p_X^{\bar{\mathcal{L}}}(s)$ for $\beta=0$ is

$$p_X^{\bar{\mathcal{F}}}(\theta)=\nu^2e^{i\mu\theta}/\left(\theta^2+\nu^2\right). \tag{4-20}$$

The derivative of the double-sided LT, by using Eq. (4-17) instead of the classical definition is given as

$$\bar{\mathcal{L}}\left\{\frac{\mathrm{d}^n}{\mathrm{d}x^n}p_X(x);s\right\}=\int_{-\infty}^{\infty}\frac{\mathrm{d}^n\left[p_X(x)\right]}{\mathrm{d}x^n}e^{-\beta|x|+i\theta x}\mathrm{d}x=(-\bar{s})^n\,p_X^{\bar{\mathcal{L}}}(\bar{s});\ \ \bar{s}=\beta\mathrm{sign}(x)-i\theta. \tag{4-21}$$

The discretized form of Eq. (4-18), taking into account that $A_p^{\bar{\mathcal{L}}}(s)$ and $B_p^{\bar{\mathcal{L}}}(s)$ are symmetric and antisymmetric with respect to θ, respectively, is given as:

$$\begin{aligned}p_X(x)&\cong\frac{e^{\beta|x|}}{2b}\sum_{k=-m}^{m}\bar{\mathcal{L}}\left\{p_X(x);s\right\}e^{-i\theta_k x}\\&=\frac{e^{\beta|x|}}{2b}\left[A_p^{\bar{\mathcal{L}}}(\beta)+2\sum_{k=1}^{m}\left(A_p^{\bar{\mathcal{L}}}(s_k)\cos\left(\frac{k\pi}{b}x\right)+B_p^{\bar{\mathcal{L}}}(s_k)\sin\left(\frac{k\pi}{b}x\right)\right)\right],\end{aligned} \tag{4-22}$$

where $\Delta\theta$ is the step-size of discretization in θ domain.

For symmetric PDF ($p_X(x)=p_X(-x)$), the imaginary part of Eq. (4-17) is zero, while the real part is the LT of $2p_X(x)U(x)$ (one-sided). This implies that the PDF can be reconstructed by using the inverse Laplace Transform ($\mathcal{L}\left\{p_X(x);s\right\}$) by assuming for $p_X(x)=p_X(x)U(x)$, and the PDF in the negative x domain obeys to the symmetry condition. For $\beta=0$, Eq. (4-17) coalesces with the classical definition of the FT when

$p_X(x)$ defined in the range $(-\infty,\infty)$. Therefore, Eq. (4-22) remain valid by substituting $\beta=0$ into Eq. (4-17) and evaluating $A_{p_X}^{\mathcal{F}}(s_k)$ and $B_{p_X}^{\mathcal{F}}(s_k)$ in Eq. (4-22). However, the trigonometric Fourier series exhibit the aliasing effect, when reconstructing the PDF by using Eq. (4-22) for $\beta>0$. It follows that $p_X(x)$ reconstructed by using Eq. (4-22) has to be multiplied by a window function $U(x+b)-U(x-b)$ in range $[-b,b]$.

From Eq. (4-15) and Eq. (4-22), we realize that with a limited values of quantities $A_p^{\bar{\mathcal{L}}}(s_k)$ and $B_p^{\bar{\mathcal{L}}}(s_k)$, we may reconstruct the PDF. In the practical applications, the PDF is often unknown, but the realization of a RV or from the data coming from Monte-Carlo simulations are available. Constructing the PDF from such data can be challenging, as it requires a large number of samples. In contrast, evaluating moments of the form $E\left[\exp\left(-\left(\beta-i\theta\,\mathrm{sign}(X)\right)|X|\right)\right]$ is straightforward using the generic formula, which is also valid in complex domain, namely

$$E\left[\exp\left(-\bar{s}\,|X|\right)\right]=\frac{1}{N}\sum_{k=1}^{N}\exp\left(-\bar{s}\left|X^{(k)}\right|\right) \tag{4-23}$$

where N is the number of samples, and $X^{(k)}$ is the k-th realization of the RV X.

In Figure 4-1, the double-sided LT of PDF

$$p_X(x)=\frac{\nu}{2}\exp\left(-\nu|x-\mu|\right) \tag{4-24}$$

is plotted for for $\beta=0.1$ and 0.35. The Shifted CF is plotted according to the double-sided LT according to Eq. (4-19). The discretized version, evaluated by Eq. (4-22) is contrasted with the exact PDF, the parameter selected for $\Delta\theta=0.2$, and $m=78$.

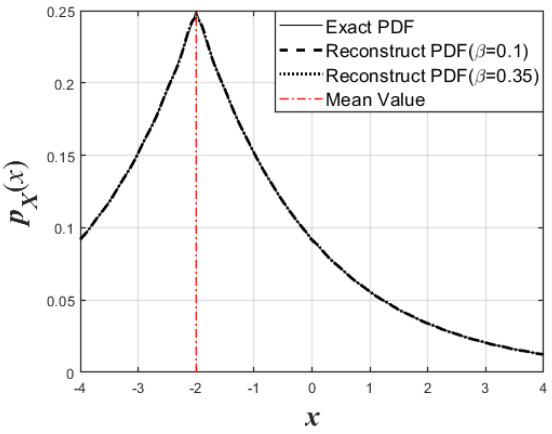

(a)

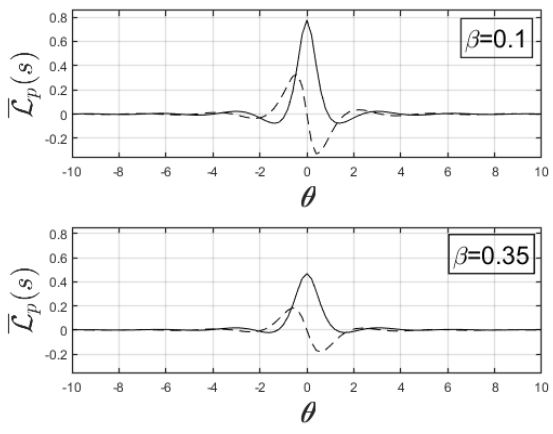

(b)

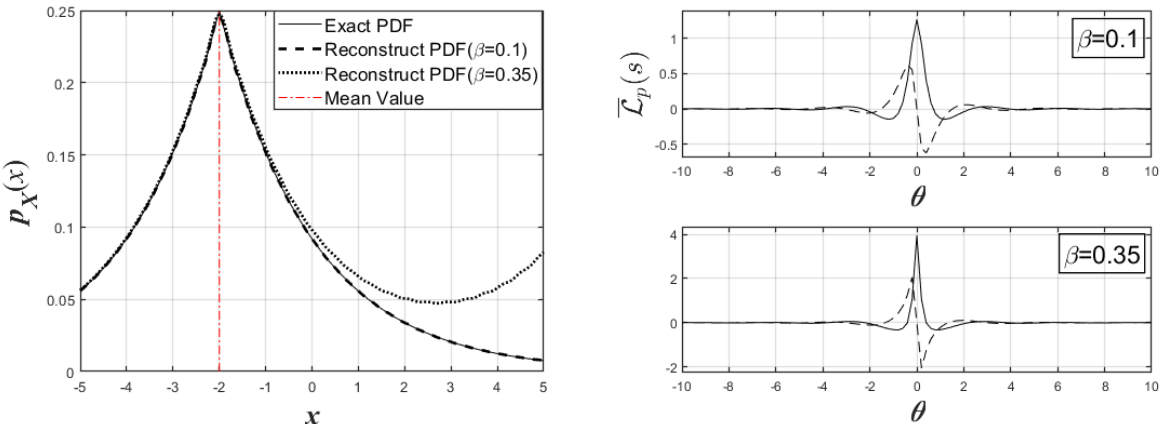

(c) (d)

Figure 4-1 $b=\pi/\Delta\theta=15.7$, $\nu=0.5$, $\Delta\theta=0.2$, $m=78$, and $m\Delta\theta\simeq b$.(a) The continuous line plot by the exact PDF, dashed line and dotted line reconstructed by Eq. (4-22) with $\beta=0.1,0.35$, respectively; (b) SCF of Eq. (4-19) for different values of β, the continuous line represent the real part, the dashed line represent the imaginary part; (c) The continuous line plot by the exact PDF, dashed line and dotted line reconstructed by Eq. with $\beta=0.1,0.35$, respectively; (d) SCF of Eq. (4-15) for different values of β, the continuous line represent the real part, the dashed line represent the imaginary part

In Figure 4-1, the difference appeared in Figure 4-1(c) between the exact PDF and that reconstructed PDF by means of the double-sided definition given in Eq. (4-15) can be avoided by the new definition (4-19) with the same parameters.

From the results of this section on the SCF method for reconstructing the PDF with a limited number of information, some conclusions may be withdrawn:

1) For one-sided PDF, both Fourier and Laplace operators are able to reconstruct the PDF of a RV or a stochastic process.
2) For double-sided distribution, the FT may be used without any problem, as all PDFs are Fourier transformable. However, for the SCF, the double-sided definition given in Eq. (4-17) must be applied.
3) Since in Eq. (4-22), the PDF is reconstructed in the discretized form over the range $-b\le x\le b$ in a classical Fourier series of orthogonal trigonometric function, the PDF remains valid only in the interval $[-b,b]$, which has to be considered zero outside the interval due to the aliasing effects. These effect persist in both FT and LT methods, also the double-sided definition of $\overline{\mathcal{L}}$ and $\overline{\mathcal{F}}$ is used in Eq. (4-22) as it is shown in Figure 4-2.
4) A close inspection of the double sided LT in Eq. (4-17) and (4-18) reveals that the SCF exhibits a smooth trend, which means that $\Delta\theta$ may be selected without needing to be excessively small. Conversely, for $\beta\neq 0$, Eq. (4-15) does not work well for two main reasons: a) The SCF exhibits a more pronounced oscillatory trend compared to the SCF evaluated in Eq. (4-22), leading to that $\Delta\theta$ has to be selected smaller; b) If the order

$\beta \geq \nu$, the PDF reconstructed by Eq. (4-15) is inaccurate when the discretized equation is used.

5) If the RV X is characterized by the CF rather than the PDF, as in the case of α-stable RVs, the Fourier or the Laplace transform method can be directly applied to the real and imaginary parts of CF.
6) The SCF method is useful for solving the fractional differential equations with variable coefficients expressed in exponential form.

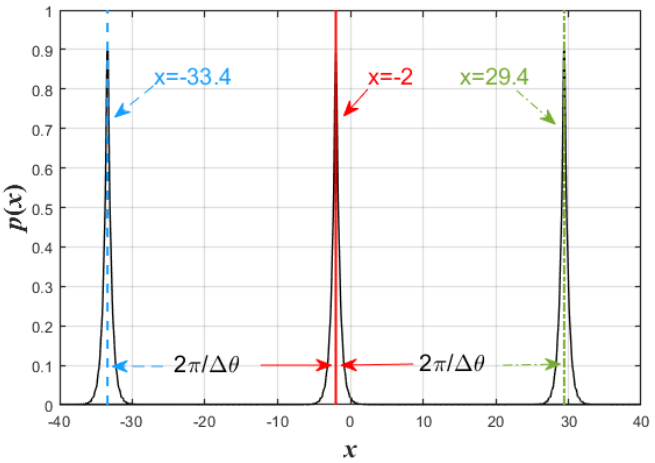

Figure 4-2 The aliasing problem with $\beta = 0$, $\nu = 2$, $\Delta\theta = 0.2$, $m = 78$, $b = \pi / \Delta\theta = 15.7$

4.4. Application of SCF method in solving FPK equation

This section presents two different applications of one-sided and double-sided LT. The first involves using the LT for solving deterministic differential equation (both classical and fractional) with time-dependent coefficients, while the second focuses on solving the Fokker-Planck-Kolmogorov (FPK) equation.

4.4.1 One-sided

Let us now show the simple example in which the PDF is ruled by a FPK equation defined in the range $[0,\infty)$. The equation of motion of the one-degree-of-freedom oscillator enforced by the multiplicative noise is given as:

$$\begin{cases} \ddot{X} + c_1 \dot{X} + \omega^2 X = e_1 X \xi(t) \\ X(0) = X_0, \quad \dot{X}(0) = \dot{X}_0 \end{cases} \tag{4-25}$$

where X and $\dot{X}$ are the abbreviation of $X(t)$ and $\dot{X}(t)$ represent the displacement and velocity of the system, respectively. ω is the frequency, and $\xi(t)$ is a zero mean normal white noise process fully characterized in probabilistic setting by its correlation function given as:

$$R_\xi(t_1,t_2) = E\left[\xi(t_1)\xi(t_2)\right] = q(t_1)\delta(t_2 - t_1) = q(t_2)\delta(t_2 - t_1). \tag{4-26}$$

Where $E[\bullet]$ is the mathematical expectation, is the strength of the white noise. If $\xi(t)$ is stationary, then $R_\xi(t_1,t_2)=R_\xi(t_2-t_1)=q\delta(t_2-t_1)$.

With the weak excitation and weak damping, assuming the Wong-Zakai correction term produces no additional force, Eq. (4-25) has the quasi-periodic solutions due to it is the quasi-conservative system, which means that we can express the $X(t)$ and $\dot{X}(t)$ as follow:

$$X(t)=A(t)\cos(\Theta(t)),\ \dot{X}(t)=-A(t)\omega\sin(\Theta(t)), \tag{4-27}$$

where $A(t)$ is the amplitude process and $\Theta=\omega t+\theta(t)$ is the phase process. Substituting Eq. (4-27)into (4-25), and applying the stochastic averaging technique, one can obtain the Itô stochastic differential equation

$$\begin{cases} \mathrm{d}A(t)=m(A(t))\mathrm{d}t+\sigma(A(t))\mathrm{d}W(t), \\ A(0)=A_0, \end{cases} \tag{4-28}$$

where $W(t)$ is the Winner process defined in section 1.3.1, $A(0)=A_0$ is the initial condition, which is a RV with assigned PDF. $m(A(t))$ and $\sigma(A(t))$ is the drift term and diffusion term, respectively, which are expresses as

$$\begin{aligned} m(A)&=z_1A, \\ \sigma^2(A)&=z_2^2A^2. \end{aligned} \tag{4-29}$$

Where $z_1=\frac{3e_1^2q}{8\omega^2}-\frac{c_1}{2}$, $z_2^2=\frac{e_1^2q}{4\omega^2}$. The FPK associated to eq.(4-28) is given as:

$$\begin{cases} \dfrac{\partial p_A(a,t)}{\partial t}=-\dfrac{\partial\left[m(a)\,p_A(a,t)\right]}{\partial a}+\dfrac{1}{2}\dfrac{\partial^2\left[\sigma^2(a)\,p_A(a,t)\right]}{\partial a^2}, \\ p_A(a,0)=p_{A_0}(a) \end{cases} \tag{4-30}$$

where $p_A(a,t)$ is the PDF of the slowly varying process $A(t)$ and $p_{A_0}(a)$ is the corresponding assigned initial condition of the amplitude $A(t)$ at $t=0$. By assuming that at each time t, we multiply Eq. (4-30) with e^{-sa}, and integrate from 0 to Infinity, then we have:

$$\begin{aligned} \frac{\partial\mathcal{L}_{p_A}(s,t)}{\partial t}=&-\left[m(a)\,p_A(a,t)e^{-sa}\right]_0^\infty-s\int_0^\infty m(a)\,p_A(a,t)e^{-sa}\mathrm{d}a \\ &+\left[\frac{1}{2}\frac{\partial\sigma^2(a)\,p_A(a,t)}{\partial a}e^{-sa}\right]_0^\infty+\frac{1}{2}s\left[\sigma^2(a)\,p_A(a,t)e^{-sa}\right]_0^\infty \\ &+\frac{1}{2}s^2\int_0^\infty\sigma^2(a)\,p_A(a,t)e^{-sa}\mathrm{d}a, \end{aligned} \tag{4-31}$$

where

$$\mathcal{L}_{p_A}(s,t)=\int_0^{\infty}e^{-sa}p_A(a,t)\mathrm{d}a \tag{4-32}$$

is the SCF in t. Considering the initial condition, the first, third and fourth term in the right side of eq (4-31) can be vanished, applying eq.(4-29) , we can rewritten eq. (4-31) as:

$$\frac{\mathrm{d}\mathcal{L}_{p_A}(s,t)}{\mathrm{d}t}=-s\left(\frac{3e_1^2q}{8\omega^2}-\frac{c_1}{2}\right)\int_0^{\infty}ap_A(a,t)e^{-sa}\mathrm{d}a+\frac{s^2e_1^2q}{8\omega^2}\int_0^{\infty}a^2p_A(a,t)e^{-sa}\mathrm{d}a. \tag{4-33}$$

According to the property of Laplace transform, Eq. (4-33) can be rewritten as:

$$\frac{\partial\mathcal{L}_{p_A}(s,t)}{\partial t}=s\left(\frac{3e_1^2q}{8\omega^2}-\frac{c_1}{2}\right)\mathcal{L}'_{p_A}(s,t)+\frac{s^2e_1^2q}{8\omega^2}\mathcal{L}''_{p_A}(s,t). \tag{4-34}$$

$\mathcal{L}'_{p_A}(s,t)$ and $\mathcal{L}''_{p_A}(s,t)$ means the first and second order derivative of $\mathcal{L}_{p_A}(s,t)$ with s. Applying the differential methods, the discretized form of eq.(4-34) can be rewritten as：

$$\begin{aligned}\frac{\mathrm{d}\mathcal{L}_{p_A}(s_k,t)}{\mathrm{d}t}=&\left(\frac{3e_1^2qs_k}{8\omega^2\Delta s}-\frac{c_1s_k}{2\Delta s}+\frac{e_1^2qs_k^2}{8\omega^2(\Delta s)^2}\right)\mathcal{L}_{p_A}(s_{k+1},t)\\&-\left(\frac{2e_1^2qs_k^2}{8\omega^2(\Delta s)^2}+\frac{3e_1^2qs_k}{8\omega^2\Delta s}-\frac{c_1s_k}{2\Delta s}\right)\mathcal{L}_{p_A}(s_k,t)+\frac{e_1^2qs_k^2}{8\omega^2(\Delta s)^2}\mathcal{L}_{p_A}(s_{k-1},t)\end{aligned} \tag{4-35}$$

Noticed that the solution of Eq. (4-35) may be divergent during the calculation because at each new time instant, we introduce the following equation from Eq. (4-7) according to the information that the total area of the PDF is 1, then we have

$$\frac{1}{2b}\sum_{k=-m}^{m}\mathcal{L}_{p_A}\{s_k,t\}\int_0^{2b}e^{s_kx}\mathrm{d}x=1 \tag{4-36}$$

Which also means

$$\mathcal{L}_{p_A}\{s_0,t\}=\frac{1}{c_0}\left(2b-\sum_{\substack{k=-m\\k\neq0}}^{m}\mathcal{L}_{p_A}\{s_k,t\}c_k\right). \tag{4-37}$$

Where $c_k=\left(e^{2bs_k}-1\right)/s_k$. It worth noticed that $c_0=2b$ if $\beta=0$. Eqs. (4-35) and (4-37) give a set of $2m$ ordinary differential equations, where $s=-m,...,-1,1,...m$. Here, we select the parameter of system as $c_1=-0.05$, $e_1=1$, $\omega=1$, $q=0.01$, and the initial condition is $p_X(x,0)=\delta(a-1)$, of which the SCF is $\mathcal{L}_{p_A}(s,0)=\exp(-s)$.

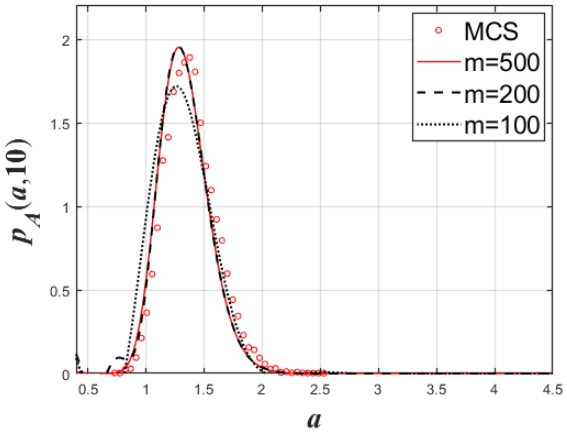

Figure 4-3 The reconstructed PDF when $t=10$ with different cut-off value m

The result with different cut-off value m when $t=10$ by LT method and Monte-Carlo Simulation is plotted in Figure 4-3. on which we choose the parameter as $\beta=0$, $\Delta\theta=0.1$. From the pictures, we may observe that with the increase of m, the accuracy is increase. The calculation time is 0.8s, 3.3s, and 20s when $m=100,200$ and 500. Figure 4-4 (a) and (b) displays the evolution of real part and imaginary part of SCF when $t\in[0,10]$, where the black dotted line is plotted in $m=0$.

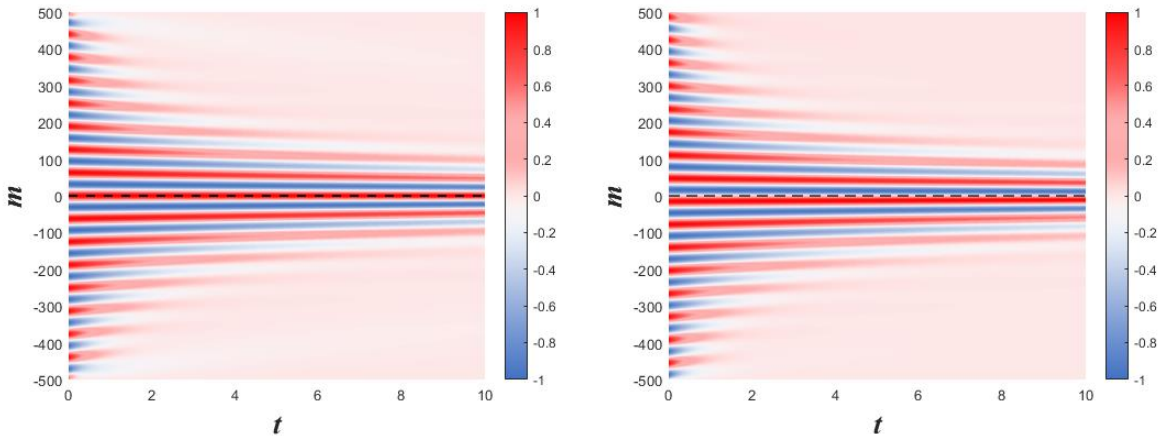

(a) (b)

Figure 4-4 (a) The real part of SCF and (b) The imaginary part of SCF when $t\in[0,10]$. The black dotted line is drawn when $m=0$

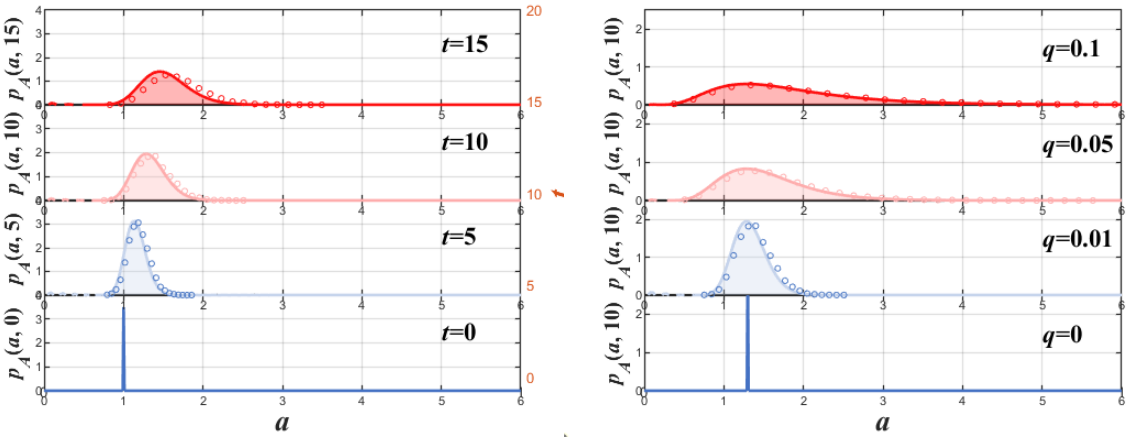

(a) (b)

Figure 4-5 $m=500$. (a) The reconstructed PDF when $t=5,10,15$; (b) The reconstructed PDF when $q=0.01,0.05,0.1$ and $t=10$

Figure 4-5 exhibits the reconstructed PDF with the change of time t and the intensity of noise q, where the line is obtained from LT method, and the dot is obtained from Mont Carlo Simulation. The results verified the accuracy of LT method in solving FPK equation.

4.4.2 Double-sided

Let the stochastic differential equation be given in the form

$$\begin{cases} \dot{X}(t)=f\left(X(t)\right)+\xi(t), \\ X(0)=X_0, \end{cases} \tag{4-38}$$

where $\xi(t)$ is a zero-mean normal white noise as mentioned in Eq. (4-25). X_0 is a RV with assigned PDF $p_{X_0}(x)=p_{X_0}(x,0)$. In Eq. (4-38), $f\left(X(t)\right)$ is a nonlinear function of the stochastic process $X(t)$. The FPK equation, ruling the evolution of the PDF of the stochastic process $X(t)$ is given as:

$$\begin{cases} \dfrac{\partial}{\partial t}p_X(x,t)=-\dfrac{\partial}{\partial x}\left[f(x,t)\,p_X(x,t)\right]+\dfrac{q}{2}\dfrac{\partial^2\left[p_X(x,t)\right]}{\partial x^2} \\ p_X(x,0)=p_{X_0}(x) \qquad \text{(Assigned)} \end{cases}. \tag{4-39}$$

To consider a generalized situation, in this application, we assume that $p_X(x,0)=\delta(x-a)$, $a>0$ and $f(x)=a\left(e^{-vx}+e^{vx}\right)+c$. In this case, the $p_X(x,t)$ is not symmetric, and thus the double-sided LT can be applied. By making the Laplace transform of both members of Eq. (4-39), according to Eq. (4-17), and applying double-sided Laplace transform to Eq. (4-39), we can obtain:

$$\begin{cases} \dfrac{\mathrm{d}}{\mathrm{d}t}\bar{\mathcal{L}}_{p_X}(s)=\int_{-\infty}^{\infty} f(x)\,p_X(x)\left(-\beta\,\mathrm{sign}(x)+i\theta\right)e^{-\beta|x|+i\theta x}\mathrm{d}x \\ \qquad\qquad +\dfrac{q}{2}\int_{-\infty}^{\infty} p_X(x)\left(-\beta\,\mathrm{sign}(x)+i\theta\right)^2 e^{-\beta|x|+i\theta x}\mathrm{d}x \quad , \\ \bar{\mathcal{L}}_{p_X}\left\{p_{X_0}(x),s\right\}=\bar{\mathcal{L}}_{p_X}\left\{\delta(x-a_0);s\right\}=e^{-a_0 s}; \end{cases} \tag{4-40}$$

the Laplace transform can be transferred along the real axis. To simplify the calculation, we suppose $\beta=0$, then Eq. (4-40) can also be rewritten as:

$$\begin{cases} \dfrac{\mathrm{d}}{\mathrm{d}t}\phi_p(\theta,t)=ia\theta\phi_p(\theta+\nu,t)+ia\theta\phi_p(\theta-\nu,t)+\left(ic\theta-\dfrac{q}{2}\theta^2\right)\phi_p(\theta,t), \\ \phi_p\{\theta,0\}=\bar{\mathcal{F}}_p\left\{\delta(x-a_0);\theta\right\}; \end{cases} \tag{4-41}$$

where $\phi_p(\theta,t)$ is the double-sided Fourier transform of PDF, namely the Characteristic function, and

$$\begin{aligned} \phi_p(\theta+\nu,t)&=\int_{-\infty}^{\infty} e^{-\nu x+i\theta x}p_X(x,t)\mathrm{d}x; \\ \phi_p(\theta-\nu,t)&=\int_{-\infty}^{\infty} e^{\nu x+i\theta x}p_X(x,t)\mathrm{d}x. \end{aligned} \tag{4-42}$$

The SCF can be translated along the real axis, which means that the $\phi_p(\theta_J+\nu,t)$ can be expressed as a set of $2m+1$ $\phi_p(\theta_k,t)$ according to Eq. (4-11), where $k=-m,...,m$. To prevent divergence in the results, we introduce the normalization condition, which is

$$\int_{-b}^{b} p_X(x,t)\mathrm{d}x\cong\frac{1}{2b}\int_{-b}^{b}\left(\phi_p(\theta_0,t)+\sum_{\substack{k=-m\\k\neq 0}}^{m}\phi_p(\theta_k,t)e^{-i\theta_k x}\right)\mathrm{d}x\cong 1, \tag{4-43}$$

namely

$$\phi_p(\theta_0,t)=1+\frac{1}{2b}\sum_{\substack{k=-m\\k\neq 0}}^{m}\phi_p(\theta_k,t)\frac{e^{-i\theta_k b}-e^{i\theta_k b}}{i\theta_k}. \tag{4-44}$$

Substitute Eq. (4-42)-(4-44) into (4-41), we can obtain a set of $2m$ ODEs, where $J=-m,...,-1,1,...,m$. Solving the ODEs, and we can reconstruct the double-sided PDF over time t. In this case, we select $a=-0.1$, $c=0.3$, $\nu=0.1$, $q=0.01$, $m=120$, and $\Delta\theta=0.2$. And the initial condition is $\phi_p(\theta,0)=e^{ia_0\theta}$, $a_0=0$, and the transient PDF can be reconstructed as follow.

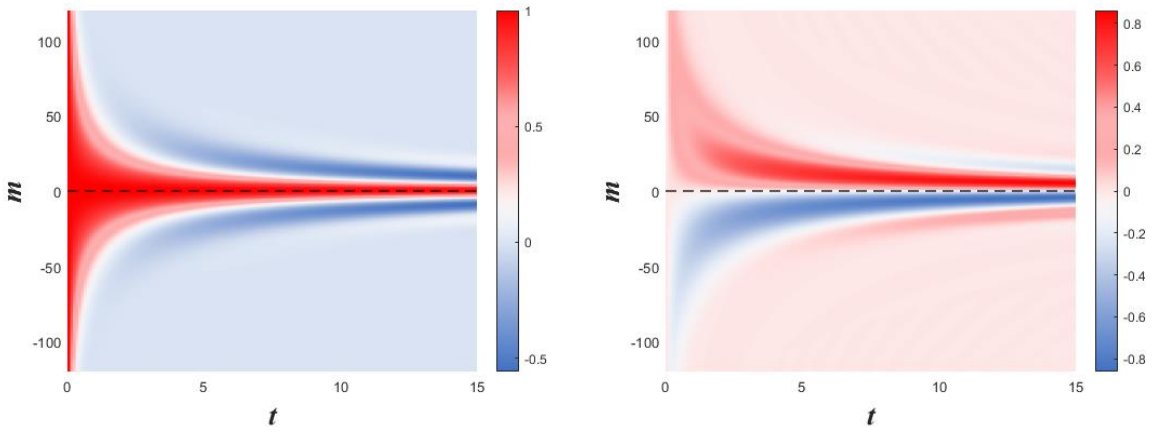

(a) (b)

Figure 4-6 (a) The real part of SCF and (b) The imaginary part of SCF when $t \in [0,15]$. The black dotted line is drawn when $m = 0$

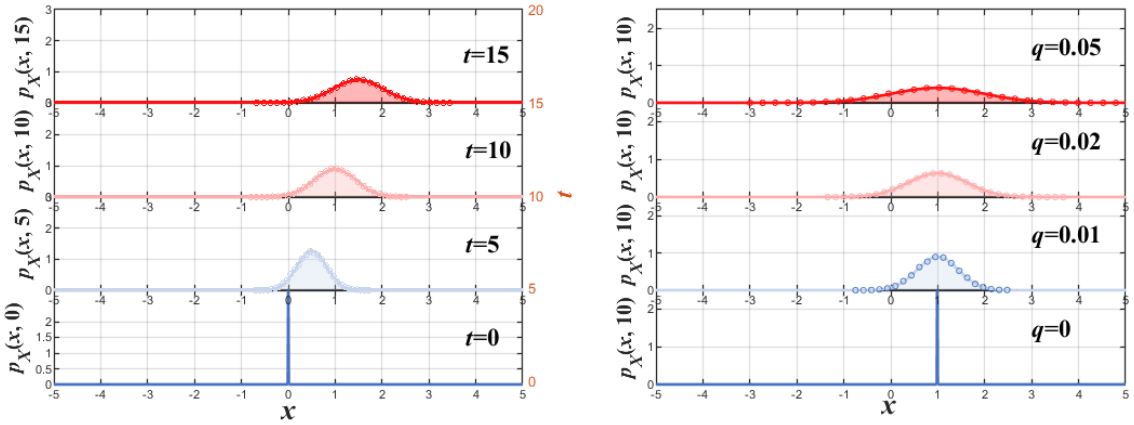

(a) (b)

Figure 4-7 (a) The reconstructed PDF when $t = 0,5,10,15$ and $q = 0.01$; (b) The reconstructed PDF when $q = 0, 0.01, 0.02, 0.05$ and $t = 10$. The line is the reconstructed PDF by SCF method, and the dotted is the results obtained by Monte Carlo simulation

Figure 4-6 exhibits the SCF when $\beta = 0$, where the Figure 4-6 (a) is the real part, and the Figure 4-6 (b) is the imaginary part. Figure 4-7 displays the PDF vary with time t and the intensity of noise q. According to the calculation process, the calculation time using the SCF method is within 1 second. Comparing to the Monte Carlo Simulation, the SCF method is both efficient and accurate in reconstructing the double-sided PDF. Especially, the results demonstrate that the SCF remains highly accurate for different time and noise intensities.

4.5. Comparison of SCF and CFM in Reconstructing the PDF of a Random Variable

Several studies have focused on reconstructing the PDF of RVs using a limited amount of information, primarily through complex fractional moments based on the Mellin transform.

This method has been applied to solve the FPK equation. In this section, a critical review of reconstruction of PDF by CFM and SCF methods is presented. The CFM method is based on the Mellin transform of the one-sided PDF, namely

$$\mathcal{M}\{p_X(x);\gamma\} = \int_0^\infty x^{\gamma-1} p_X(x)\mathrm{d}x = E\left[X^{\gamma-1}\right]; \quad \gamma = \rho + i\eta. \tag{4-45}$$

The MT exists if the real part of γ belongs to the FS of the Mellin transform, for a wider discussion or of the domain of existence of the MT. The Shift property in the Mellin domain is given by

$$\mathcal{M}\{x^\alpha p_X(x);\gamma\} = \mathcal{M}\{p_X(x);\gamma-\alpha\} \tag{4-46}$$

Provided ρ belongs to the FS, the inverse MT return the PDF in the form:

$$\mathcal{M}^{-1}\left\{E\left[X^{\gamma-1}\right];x\right\} = \frac{1}{2\pi}\int_{\eta=-\infty}^{\infty} E\left[X^{\gamma-1}\right]x^{-\gamma}\mathrm{d}\eta = p_X(x). \tag{4-47}$$

The discrete form of the Eq. (4-47) obtained by discretization of the η axis into small intervals of equal length $\Delta\eta$, is:

$$x^{\rho-1}p_X(x)\mathrm{d}x = \frac{1}{2b}\left[E\left[X^{\rho-1}\right] + 2\sum_{k=1}^{m}\left(A_p^{\mathcal{M}}(\gamma_k)\cos\left(\frac{k\pi y}{b}\right) + B_p^{\mathcal{M}}(\gamma_k)\sin\left(\frac{k\pi y}{b}\right)\right)\right]\mathrm{d}y, \tag{4-48}$$

where $b = \pi/\Delta\eta$, $A_p^{\mathcal{M}}(\gamma_k) = \mathrm{Re}\left(E\left[X^{\gamma_k-1}\right]\right)$, $B_p^{\mathcal{M}}(\gamma_k) = \mathrm{Im}\left(E\left[X^{\gamma_k-1}\right]\right)$, $\gamma_k = \rho + ik\pi/b$, and $y = \ln x$, $\mathrm{d}y = \mathrm{d}x/x$.

As in the SCF method at the r.h.s of Eq. (4-48), a Fourier series appear. The difference between the CFM and the Fourier series is that the trigonometric functions in the CFM method are represented on a logarithmic scale over the interval $[-b,b]$ in y axis. Additionally, in the CFM method for $\rho = 1$, corresponding to $\beta = 0$ in the SCF, the first term of the r.h.s of Eq. (4-48) is $1/2b$. In the discretized form at the r.h.s of Eq. (4-48), the integral has been approximated by truncating the Fourier series in the η domain, retaining m terms instead of ∞ terms $(m\Delta\eta = m\pi/b)$.

For the one sided PDF, the integration in $[0,b]$ at the r.h.s of Eq. (4-48) in y domain corresponds to an integration in $\left[e^{-b}, e^{b}\right]$ in x domain, and thus for $\rho = 1$, $\int_{e^{-b}}^{e^{b}} p_X(x)\mathrm{d}x \neq 1$, that is a measure of the error obtained by truncating the Fourier series given in Eq. (4-48) in the η domain. By selecting $\rho = 2$ in Eq. (4-45), the one sided PDF is reconstructed by considering the centroid of the PDF as the reference line in ρ domain, as in the classical definition of the probabilistic analysis, where the cumulants are referred to a central

line $\left(E\left[X-E\left[X\right]\right]\right)$, we will refer to $\rho=2$ in the MT and $\beta=1$ in LT as central CFM and central SCF, respectively. The case of double-sided PDF was addressed, where the problem is solved by writing

$$p_X(x)=u_X(x)+v_x(x)=\frac{1}{2}\left(p_X(x)+p_X(-x)\right)+\frac{1}{2}\left(p_X(x)-p_X(-x)\right), \tag{4-49}$$

namely the PDF is divided into a symmetric and antisymmetric parts, and the one sided MT is applied to both $u_X(x)$ and $v_X(x)$. However, reconstructing the PDF by using the Eq. (4-48), produces unsatisfactory results due to the singularity of the factor $x^{-\rho}\to\infty$ in zero. To address this issue, the double-sided MT is introduced with the aid of the aid of $u_X(x)$ and $v_X(x)$,

$$\begin{aligned}\bar{\mathcal{M}}\left\{u_X(x);\gamma\right\}&=\int_{-\infty}^{\infty}u_X(x)|x|^{\gamma-1}\,\mathrm{d}x,\\ \bar{\mathcal{M}}\left\{v_X(x);\gamma\right\}&=\int_{-\infty}^{\infty}\operatorname{sign}(x)v_X(x)|x|^{\gamma-1}\,\mathrm{d}x.\end{aligned} \tag{4-50}$$

Since $u_X(x)$ and $v_X(x)$ are symmetric and antisymmetric function, respectively, the inverse double-sided MT is expressed as:

$$p_X(x)=\frac{\mathcal{P}}{4\pi}\int_{\eta=-\infty}^{\infty}\bar{\mathcal{M}}\left\{u_X(x);\gamma\right\}|x|^{-\gamma}\,\mathrm{d}\eta+\frac{1}{4\pi}\int_{\eta=-\infty}^{\infty}\operatorname{sign}(x)\bar{\mathcal{M}}\left\{v_X(x);\gamma\right\}|x|^{-\gamma}\,\mathrm{d}\eta, \tag{4-51}$$

of which the discretized form is:

$$\begin{aligned}&p_X(x)\\&=\frac{1}{4b}\sum_{k=-m}^{m}\bar{\mathcal{M}}\left\{u_X(x);\gamma_k\right\}|x|^{-\gamma_k}\Big|_{p_X(0)=\left(p_X(\Delta x)+p_X(-\Delta x)\right)/2}+\frac{1}{4b}\sum_{k=-m}^{m}\operatorname{sign}(x)\bar{\mathcal{M}}\left\{v_X(x);\gamma_k\right\}|x|^{-\gamma_k}\\&=\frac{|x|^{-\rho}}{4b}\left[A_p^{\bar{\mathcal{M}}}(\gamma_0)+2\sum_{k=1}^{m}\left(A_p^{\bar{\mathcal{M}}}(\gamma_k)\cos\left(\frac{k\pi\ln\left(|x|\right)}{b}\right)+B_p^{\bar{\mathcal{M}}}(\gamma_k)\sin\left(\frac{k\pi\ln\left(|x|\right)}{b}\right)\right)\right]\Bigg|_{p_X(0)=\frac{p_X(\Delta x)+p_X(-\Delta x)}{2}}\end{aligned} \tag{4-52}$$

where $A_p^{\bar{\mathcal{M}}}(\gamma_k)=A_u^{\bar{\mathcal{M}}}(\gamma_k)+\operatorname{sign}(x)A_v^{\bar{\mathcal{M}}}(\gamma_k)$, $B_p^{\bar{\mathcal{M}}}(\gamma_k)=B_u^{\bar{\mathcal{M}}}(\gamma_k)+\operatorname{sign}(x)B_v^{\bar{\mathcal{M}}}(\gamma_k)$, $A_u^{\bar{\mathcal{M}}}(\gamma_k)$, $A_v^{\bar{\mathcal{M}}}(\gamma_k)$ and $B_u^{\bar{\mathcal{M}}}(\gamma_k)$, $B_v^{\bar{\mathcal{M}}}(\gamma_k)$ are the real part and imaginary part of $\bar{\mathcal{M}}\left\{u_X(x);\gamma_k\right\}$ and $\bar{\mathcal{M}}\left\{v_X(x);\gamma_k\right\}$, Δx is the unit step in x axis. The presence of the Cauchy Principle Value (PV) is essential for overcoming the singularity at zero. In this way, the problem of the singular kernel in the symmetric part of the PDF in $x=0$ disappear when the principle value is taken into account, and the translated function along real axis is introduced. In Figure 4-7 and 4-8, the asymmetric Gaussian distribution is reconstructed using $\bar{\mathcal{L}}\left\{p_X(x);s\right\}$,

$\bar{\mathcal{M}}\{u_X(x);\gamma\}$ and $\bar{\mathcal{M}}\{v_X(x);\gamma\}$. For comparison purposes, the SCF is calculated with $\beta=1$, $\Delta\theta=0.1,0.12,0.24$, and for the CFM with $\rho=2$, $\Delta\eta=0.2,0.4,0.6$. The selection of n (in Laplace) and m (in Mellin) is shown below:

In the asymmetric case, we choose the Gaussian distribution with μ_X the mean value and σ_X^2 the standard deviation, namely

$$p_X(x)=\frac{1}{\sqrt{2\pi}\sigma_X}e^{-\frac{(x-\mu_X)^2}{\sigma_X^2}};\ -\infty<x<\infty, \tag{4-53}$$

Thus we have

$$\begin{aligned}\bar{\mathcal{L}}\{p_X(x);s\}=&\frac{e^{-\mu_X(\beta-i\theta)+\frac{1}{4}\sigma_X^2(\beta-i\theta)^2}}{2\sqrt{2}}\operatorname{Erfc}\left(\frac{(\beta-i\theta)\sigma_X^2-2\mu_X}{2\sigma_X}\right)\\&+\frac{e^{\mu_X(\beta+i\theta)+\frac{1}{4}\sigma_X^2(\beta+i\theta)^2}}{2\sqrt{2}}\operatorname{Erfc}\left(\frac{(\beta+i\theta)\sigma_X^2+2\mu_X}{2\sigma_X}\right),\end{aligned} \tag{4-54}$$

$$\bar{\mathcal{M}}\{u_X(x);\gamma\}=\frac{1}{\sqrt{2\pi}}\sigma_X^{\gamma-1}\Gamma\left(\frac{\gamma}{2}\right){}_1F_1\left(\frac{1-\gamma}{2},\frac{1}{2},-\frac{\mu_X^2}{\sigma_X^2}\right), \tag{4-55}$$

$$\bar{\mathcal{M}}\{v_X(x);\gamma\}=\frac{\sqrt{2}\mu_X}{\sqrt{\pi}}\sigma_X^{\gamma-2}\Gamma\left(\frac{1+\gamma}{2}\right){}_1F_1\left(1-\frac{\gamma}{2},\frac{3}{2},-\frac{\mu_X^2}{\sigma_X^2}\right). \tag{4-56}$$

where $\operatorname{Erfc}(\bullet)$ represents the complementary error function, and ${}_1F_1(\bullet)$ represents the Kummer confluent hypergeometric function. Figure 4-8 and Figure 4-9 display the reconstructed PDF and the double-sided LT and double-sided MT of PDF for the case $\mu_X=1.5$ and $\sigma_X=1$. The results with and without PV is shown in Figure 4-9 (a).

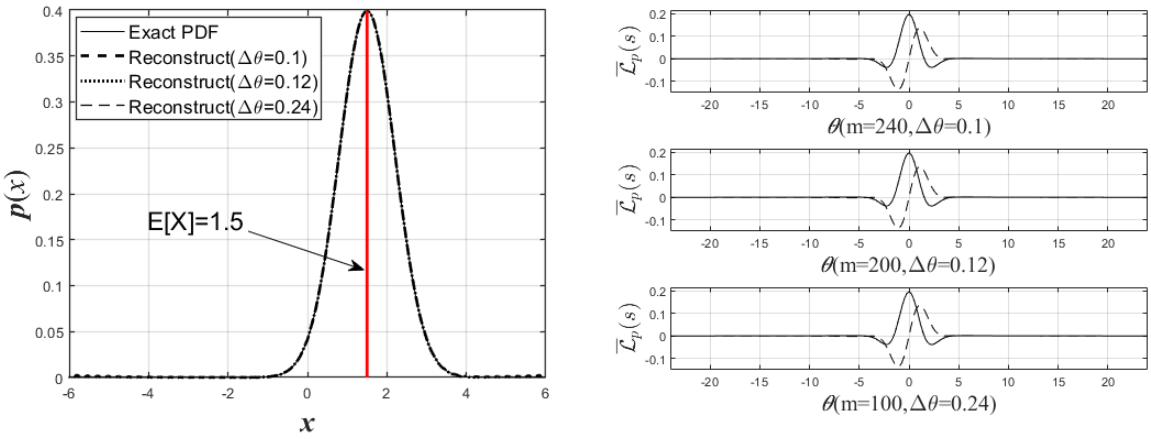

(a) (b)

Figure 4-8 $\beta=1$. Case 1 $\Delta\theta=0.1$, $n=240$; Case 2 $\Delta\theta=0.12$, $n=200$; Case 3 $\Delta\theta=0.24$. (a) Continuous line plot of exact PDF, dashed line and dotted line reconstruction of the PDF by SCF; (b) The

real part and imaginary part of $\bar{\mathcal{L}}_p\{p_X(x);s\}$

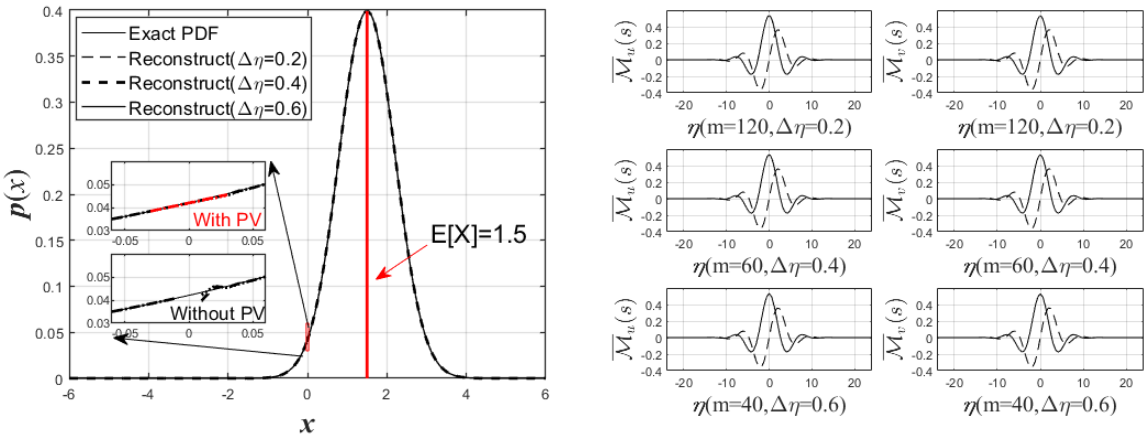

(a) (b)

Figure 4-9 $\rho=2$. Case 1: $\Delta\eta=0.2$, $m=120$; Case 2: $\Delta\eta=0.4$, $m=60$; Case 3: $\Delta\eta=0.6$, $m=40$. (a): Continuous line plot of exact PDF, dashed line and dotted line reconstruction of the PDF by CFM; (b): The real part and imaginary part of $\bar{\mathcal{M}}_u\{u_X(x);\gamma\}$ and $\bar{\mathcal{M}}_v\{v_X(x);\gamma\}$.

As concluding remark, both the double-sided LT and MT can be effectively used to reconstruct the PDF with a limited number of complex quantities, which can be easily evaluated from experimental data or from Monte Carlo Simulation. It is to be remarked that the selection of β in the SCF or ρ in CFM methods has to be selected properly ($0\le\beta\le1$ or $1\le\rho\le2$) in the two methods in order to avoid that MT or LT have high oscillatory trend in the corresponding imaginary axis.

At this stage, peoples may ask a question: since both Laplace and Mellin transform can be used to reconstruct the solution of linear fractional differential equations in deterministic setting with time dependent parameters, as well as the solution of the FPK equation, what of the two transforms is preferable? It is important to note that from the Itô equation, the nonlinear term $g(x)$ produces the drift term, and in the PDF space of $p_X(x(t))$, this corresponds to a linear differential equation of the form $\partial p_X(x,t)/\partial t=-\partial\left(g(x)\,p_X(x,t)\right)/\partial x$, which is linear with respect to $p_X(x,t)$, with $g(x)$ acting as the variable coefficient. It follows that if the nonlinear term in Eq. (4-39) is of exponential law, it is preferable working in Laplace domain. Because the shift property remain valid. By contrast if $g(x)$ follows a power law, then the shift property, namely $\mathcal{M}\{x^{\alpha}p_X(x);\gamma\}=\mathcal{M}\{p_X(x);\gamma+\alpha\}$ remain valid, and thus the solution of the FPK equation can be reconstruct in more easy way by using MT.

4.6. Conclusion

The Shifted Characteristic Function based on Laplace transform has been presented as a method for reconstructing the one-sided PDF of random variable using a limited number of

complex quantities, that is $E\left[\exp\left(-sX\right)\right]$ for $x>0$, $s=\beta+i\theta$. The extension to the case of double-sided distribution of the type $E\left[\exp\left(-\left(\beta-i\text{sign}\left(X\right)\theta\right)\left|X\right|\right)\right]$ has also been discussed, leading to a different formulation from those previously reported in the literature. The discretized form of both one-sided and double-sided inverse Laplace transform is performed along the imaginary axis to reconstructed the PDF. The SCF coincides with the Fourier transform for both one-sided and double-sided distribution when $\beta=0$. It is shown that the SCF method, in its discretized form, leads to a representation of the PDF in a classical Fourier series. Applications of these concepts to solve deterministic fractional differential equations with variable coefficients, as well as the FPK equation, have also been presented. Lastly, a comparison with Mellin transform, as proposed in the past studies [82, 84], working with complex moments of the form $E\left[X^{\gamma-1}\right]$ ($\gamma=\rho+i\eta$) has been revisited to address the singularity at zero in the reconstruction of PDFs using complex fractional moments.

In conclusion, we can assert that working in complex domain for constructing PDFs or solving the FPK equation in cases involving exponential-type non-linearities in the form $\sum_{j=1}^{n}c_j\exp\left(-\alpha_j x\right)$ is efficient, which requests minimal computational effort and avoids the problems associated with those using integer-order moments.

Chapter 5. Generalized complex fractional moments for the probabilistic characteristic of random vectors

5.1. Introduction

Dynamic systems in stochastic environments can experience fundamental changes in their intrinsic characteristics due to external disturbances. The probability density function is typically the most widely used tool to describe these characteristics. In practice, constructing a PDF for stochastic systems generally involves either collecting sample data through experiments or simulating system behavior using abstract models. However, achieving an optimal balance between accuracy and computational efficiency when directly obtaining probabilistic characteristics through these methods remains a significant challenge.

Moment statistics, as functions of sample data, can summarize overall information from samples without requiring knowledge of the underlying distribution parameters. The relationship between moments and probabilistic characteristics has been extensively researched. Moments have been used to reconstruct the probabilistic characteristics of random variables or processes, and fractional moments $E\left[X^a\right], a \in \mathbb{R}$ have been developed based on traditional integer moments $E\left[X^a\right], a \in \mathbb{Z}$ In 2012, the complex fractional moment $E\left[X^\gamma\right], \gamma = \rho + i\eta$ based on the Mellin transform was proposed. It established a direct equivalence with the PDF, and because its reconstruction process occurs along the imaginary axis, it can reconstruct probabilistic characteristics when higher-order moments of random variables, such as α-stable random variables, do not exist.

Since its introduction, the complex fractional moment method has been applied to reconstruct probabilistic characteristics across various scenarios, significantly enhancing computational efficiency. However, its use has been confined to one-dimensional positive real domains. In multi-degree-of-freedom dynamic systems, the stochastic averaging method must be employed to reduce dimensionality before applying the complex fractional moment approach. Analyzing the probabilistic evolution of multi-dimensional systems is crucial. While probabilistic density evolution methods and finite element methods can be used for such systems, the current complex fractional moment theory cannot address these challenges. Thus, expanding this theory to enable multi-dimensional probabilistic evolution analysis is of great importance.

This chapter proposes a multi-dimensional complex fractional moment theory based on the multivariable Mellin transform, establishing an equivalence between multi-dimensional complex fractional moments, multi-dimensional PDFs, and multi-dimensional characteristic functions. It also enables the reconstruction of marginal probabilistic characteristics using high-dimensional complex fractional moments. The research framework of this chapter is as follows:

Section 5.2 introduces the application background of complex fractional moments. Section 5.3 expands the complex fractional moment theory, establishing the equivalence of multi-dimensional complex fractional moments with multi-dimensional PDFs and multi-dimensional characteristic functions in the high-dimensional positive real domain, and extends this equivalence to the full real domain in Section 5.4. Section 5.5 proposes a method to solve marginal PDFs using high-dimensional complex fractional moments, followed by numerical validation of the above theory in Section 5.6. Section 5.7 provides a summary of this chapter.

5.2. Mellin transform and complex fractional moment

The Mellin integral transform (MT) of any real function $f(x)$ defined on the range $(0,\infty)$ is expressed as follows:

$$M_f(\gamma-1)=\mathcal{M}\{f(x);\gamma\}=\int_0^\infty f(x)x^{\gamma-1}\mathrm{d}x;\quad \gamma=\rho+i\eta, \tag{5-1}$$

where $\mathcal{M}\{\bullet\}$ represent the Mellin transform operator, $M_f(\gamma-1)$ is the function of the complex parameter γ, $\rho,\eta\in\mathbb{R}$. The existence of the MT is related to the trend at zero and infinity of $f(x)$. In more details, the existence of the MT is $-p<\rho<-q$, where p and q refer to the asymptotic behavior of $f(x)$ at $x=0$ and $x=\infty$, respectively, namely:

$$\lim_{x\to 0} f(x)=\mathcal{O}(x^p);\lim_{x\to\infty} f(x)=\mathcal{O}(x^q), \tag{5-2}$$

where $\mathcal{O}(\bullet)$ means the order of zero of the term in parenthesis. As an example, for $f(x)=1/(1+x^2)$, the corresponding domain of existence of the MT may be evaluated as:

$$\lim_{x\to 0} f(x)=1\to O(x^0);\lim_{x\to\infty} f(x)=x^{-2}\to O(x^{-2}), \tag{5-3}$$

thus, the existence domain in this case is $0<\rho<2$. The domain of existence of the MT is called Fundamental Strip (FS) of the Mellin transform. If $-q\le -p$, the FS doesn't exist and $f(x)$ is not Mellin transformable. Such an example $f(x)=x^n, n>0$ or $f(x)=e^{\alpha x}, \alpha>0$ are not Mellin transformable.

If the MT exists, then the inverse of MT exists and $f(x)$ is given as:

$$f(x)=\mathcal{M}^{-1}\{M_f(\gamma-1);x\}=\frac{1}{2\pi i}\int_{\rho-i\infty}^{\rho+i\infty} M_f(\gamma-1)x^{-\gamma}\mathrm{d}\gamma. \tag{5-4}$$

The integral in Eq. (5-4) may be evaluated by a discretization of the η axis into small steps of equal amplitude $\Delta\eta$. Since both the real and imaginary part of $M_f(\gamma-1)$ readily turns to zero for η large enough, the discretized form of Eq. (5-4) may be written as:

$$f(x) \cong \frac{\Delta\eta}{2\pi}\sum_{k=-m}^{m} M_f(\gamma_k - 1)x^{-\gamma_k} = \frac{x^{-\rho}}{2b}\left(M_f(\rho-1) + 2\mathrm{Re}\left(\sum_{k=1}^{m} M_f(\gamma_k - 1)x^{-i\eta_k}\right)\right), \quad (5\text{-}5)$$

where $b = \pi/\Delta\eta$, $\gamma_k = \rho + ik\pi/b$, $M_f(\gamma_k - 1) = M_f^*(\gamma_{-k} - 1)$ (where the * means complex conjugate), $\mathrm{Re}(\bullet)$ means the real part, and m is the cut-off value. In case that $f(x)$ is the Probability Density Function (PDF) defined in the positive domain, the MT of the PDF denoted as $p(x)$ is for sure Mellin transformable (including the case of $\alpha-$stable Random variables for which $0 < \rho < \alpha - 1$). The MT of $p(x)$ can be expressed as follows:

$$M_p(\gamma - 1) = \mathcal{M}\{p(x);\gamma\} = \int_0^\infty p_X(x)x^{\gamma-1}\mathrm{d}x = E\left[X^{\gamma-1}\right], \quad (5\text{-}6)$$

where $E[\bullet]$ means the mean value of the random variable in parenthesis and has been defined as complex fractional moment (CFM), these CFMs are related to the MT of $p(x)$ as well as the Riesz fractional integral of $p(x)$ evaluated in 0,

$$2v_c(\gamma)\left[\mathrm{I}^\gamma p_X(x)\right]_{x=0} = \left[\int_0^\infty |x-\xi|^{\gamma-1} p_X(\xi)d\xi\right]_{x=0} = E\left[X^{\gamma-1}\right]; \rho > 0, \rho \neq 1, 2, ..., \quad (5\text{-}7)$$

where $\mathrm{I}^\gamma(\bullet)$ is the Riesz fractional integral operator, $v_c(\gamma) = \Gamma(\gamma)\cos(\gamma\pi/2)$, and $\Gamma(\gamma)$ is the Euler Gamma function. According to Eq.(5-5), we realize that with $m+1$ finite information, namely, the CFM, the PDF $p(x)$ of a random variables can also be entirely reconstructed by setting $f(x)$ as $p(x)$ in Eq. (5-5)and then $M_f(\gamma-1) = E\left[X^{\gamma-1}\right]$.

$$p_X(x) = \frac{1}{2b}E\left[X^{\rho-1}\right]x^{-\rho} + \frac{1}{b}\mathrm{Re}\left(\sum_{k=1}^{m} E\left[X^{\gamma_k-1}\right]x^{-\gamma_k}\right); x > 0. \quad (5\text{-}8)$$

Extension to the case in which the PDF is symmetric $\left(p(x) = p(-x)\right)$ is straightforward making the MT of $p(x)U(x)$ and finding the CFM of this function $M_{p/2}(\gamma) = E\left[X^{\gamma-1}\right]/2$. Extension to the case of non-symmetric PDF can be found in the previous work [84, 94].

CFM method can be applied to solving FPK equation. Such an example expressed as follow:

$$\frac{\partial p_X(x,t)}{\partial t} = -\frac{\partial\left[m(x)p_X(x,t)\right]}{\partial x} + \frac{1}{2}\frac{\partial^2\left[\sigma^2(x)p_X(x,t)\right]}{\partial x^2}. \quad (5\text{-}9)$$

Substituting Eq.(5-6) into Eq. (5-9), the related CFM equation shown below:

$$\frac{\partial M_p(\gamma-1,t)}{\partial t}=-\left[m(x)x^{\gamma-1}p_X(x,t)\right]\Big|_0^\infty+(\gamma-1)\int_0^\infty x^{\gamma-2}m(x)p_X(x,t)\mathrm{d}x$$
$$+\frac{1}{2}\frac{\partial}{\partial x}\left[\sigma^2(x)p_X(x,t)x^{\gamma-1}\right]\Big|_0^\infty-\frac{1}{2}(\gamma-1)\sigma^2(x)p_X(x,t)x^{\gamma-2}\Big|_0^\infty \quad (5\text{-}10)$$
$$+\frac{1}{2}(\gamma-1)(\gamma-2)\int_0^\infty x^{\gamma-3}\sigma^2(x)p_X(x,t)\mathrm{d}x.$$

Based on the initial conditions and boundary conditions of Eq.(5-9), Eq. (5-10) can be transformed into a set of ODEs, and the transient PDF of Eq. (5-8) can be reconstructed. At this stage, some comments are necessary.

1) By knowing the CFM, the entire PDF may be reconstructed including the trend of the PDF at infinity;
2) In Eq.(5-4), the integration is performed along to the imaginary axis while ρ remain constant. This is particularly advantageous because if the real part of γ, namely ρ, is selected into the FS, $E\left[X^{\gamma-1}\right]$ exist;
3) The usual Taylor expansion of the CF or the ln(CF) giving classical integer moments or cumulants, respectively, requires that moments or cumulants exist and this happens rarely, and in any case, produces unsatisfactory trend of the PDF at infinity. Moreover, for some distributions, like the PDF of $\alpha-$stable $(0<\alpha<2)$ random variables, moments and cumulants of high order do not exist, unless the case $\alpha=2$ that is the Gaussian distribution.

5.3. Extension of CFM in the multi-dimensional positive space

Mellin transform was introduced in 1896 [144], then the multi-dimensional Mellin transform (MMT) was defined in 1921 [145]. The condition of existence of the MMT was proofed by Antipova [146] in 2007. Let $\boldsymbol{M}_F(\boldsymbol{\gamma}-\mathbf{1})=\boldsymbol{\mathcal{M}}\{F(\boldsymbol{x});\boldsymbol{\gamma}\}$ denote the MMT of a multi-variable real function, denoted as $F(\boldsymbol{x})$, which can be expressed as follows:

$$\boldsymbol{M}_F(\boldsymbol{\gamma}-\mathbf{1})=\boldsymbol{\mathcal{M}}\{F(\boldsymbol{x});\boldsymbol{\gamma}\}=\int_{\mathbb{R}_+^n}F(\boldsymbol{x})\boldsymbol{x}^{\boldsymbol{\gamma}-\mathbf{1}}\mathrm{d}\boldsymbol{x}, \quad (5\text{-}11)$$

where $\boldsymbol{\mathcal{M}}\{\bullet\}$ is the multi-dimensional Mellin transform operator, $\boldsymbol{M}_F(\boldsymbol{\gamma}-\mathbf{1})$ is a complex scalar function of the complex vector $\boldsymbol{\gamma}$, where $\boldsymbol{\gamma}=\boldsymbol{\rho}+i\boldsymbol{\eta}=[\gamma_1,\gamma_2,...,\gamma_n]$ $=[\rho_1+i\eta_1,\rho_2+i\eta_2,...,\rho_n+i\eta_n]$, and $\boldsymbol{x}^{\boldsymbol{\gamma}-1}=\left[x_1^{\gamma_1-1},x_2^{\gamma_2-1},...,x_n^{\gamma_n-1}\right]$. The inverse of Eq. (5-11) can be expressed as:

$$F(\boldsymbol{x})=\boldsymbol{\mathcal{M}}^{-1}\{\boldsymbol{M}_F(\boldsymbol{\gamma}-\mathbf{1});\boldsymbol{x}\}=\frac{1}{(2\pi i)^n}\int_{\boldsymbol{\rho}+i\mathbb{R}^n}\boldsymbol{M}_F(\boldsymbol{\gamma}-\mathbf{1})\boldsymbol{x}^{-\boldsymbol{\gamma}}\mathrm{d}\boldsymbol{\gamma}. \quad (5\text{-}12)$$

Eq. (5-11) and Eq. (5-12) holds when $F(\boldsymbol{x})$ and $\boldsymbol{M}_F(\boldsymbol{\gamma}-\mathbf{1})$ satisfy the following transformable condition [146].

Theorem 1. If

$$F(\boldsymbol{x}) \in V_{\Theta}^{U}, \tag{5-13}$$

where V_{Θ}^{U} is a vector space. $F(\boldsymbol{x})$ holomorphic in $S_{k\Theta} = \left\{ x \in \mathbb{R}_{+}^{n} \times \mathbb{R}^{n} : \arg x \in k\Theta \right\}$, $k > 1$, and satisfying

$$\left| F(\boldsymbol{x}) \right| \le C(a) \left| x^{-a} \right|, x \in S_{k\Theta}, a \in U, \tag{5-14}$$

where $U \subset \mathbb{R}^n$ is a convex domain, and $C(a)$ is an coefficient, $\Theta \subset \mathbb{R}^n$ is a bounded domain and $0 \in \Theta$, then

$$\boldsymbol{\mathcal{M}}^{-1}\boldsymbol{\mathcal{M}}(F) = F. \tag{5-15}$$

Theorem 2. If

$$\boldsymbol{M}_F(\boldsymbol{\gamma}-\mathbf{1}) \in V_{U}^{\Theta}, \tag{5-16}$$

where V_{U}^{Θ} is a vector space, and $\Theta \in \mathbb{R}^n$. $\boldsymbol{M}_F(\boldsymbol{\gamma}-\mathbf{1})$ holomorphic in the tube domain $U + i\mathbb{R}^n$, and satisfies that

$$\left| \boldsymbol{M}_F(\boldsymbol{\rho} + i\boldsymbol{\eta} - \mathbf{1}) \right| \le K(\boldsymbol{\rho}) e^{-kH_{\Theta}(\boldsymbol{\eta})}, k > 1, \boldsymbol{\gamma} = \boldsymbol{\rho} + i\boldsymbol{\eta}, \tag{5-17}$$

where $H_{\Theta}(\boldsymbol{\eta})$ is a support function of Θ, then

$$\boldsymbol{\mathcal{M}}\boldsymbol{\mathcal{M}}^{-1}(\boldsymbol{M}_F) = \boldsymbol{M}_F. \tag{5-18}$$

Usually, Eq. (5-12) can also be expressed as：

$$F(\boldsymbol{x}) = \boldsymbol{M}_F^{-1}\left\{ \boldsymbol{M}_F(\boldsymbol{\gamma}-\mathbf{1}); \boldsymbol{x} \right\} = \frac{1}{(2\pi)^n} \int_{\mathbb{R}^n} \boldsymbol{M}_F(\boldsymbol{\gamma}-\mathbf{1}) \boldsymbol{x}^{-\boldsymbol{\gamma}} \mathrm{d}\boldsymbol{\eta}. \tag{5-19}$$

The discretized form of Eq. (5-19) can be expressed as：

$$\begin{aligned} F(\boldsymbol{x}) &= \frac{1}{(2\pi)^n} \sum_{\boldsymbol{k}=-\boldsymbol{m}}^{\boldsymbol{m}} \boldsymbol{M}_F(\boldsymbol{\gamma}_{\boldsymbol{k}} - 1) \boldsymbol{x}^{-\boldsymbol{\gamma}_{\boldsymbol{k}}} \Delta\boldsymbol{\eta} = \frac{1}{2^n B} \sum_{\boldsymbol{k}=-\boldsymbol{m}}^{\boldsymbol{m}} \boldsymbol{M}_F(\boldsymbol{\gamma}_{\boldsymbol{k}} - 1) \boldsymbol{x}^{-\boldsymbol{\gamma}_{\boldsymbol{k}}} \\ &= \frac{1}{2^n B} \sum_{k_1=-m_1}^{m_1} \cdots \sum_{k_n=-m_n}^{m_m} \boldsymbol{M}_F(\gamma_{k_1} - 1, ..., \gamma_{k_n} - 1) x_1^{-\gamma_{k_1}} \cdots x_n^{-\gamma_{k_n}}, \end{aligned} \tag{5-20}$$

where $\boldsymbol{\gamma}_{\boldsymbol{k}} = \boldsymbol{\rho} + i\boldsymbol{k}\Delta\boldsymbol{\eta} = [\rho_1 + ik_1\Delta\eta_1, .., \rho_n + ik_n\Delta\eta_n,]$, $\boldsymbol{m} = [m_1, .., m_n]$, $\boldsymbol{k} = [k_1, .., k_n]$, $B = \pi^n / \prod_{i=1}^{n} \Delta\eta_i$, and $m_i \times \Delta\eta_i$ is the cut-off value of *i*-th dimension.

Moreover, the definition of multi-dimensional Riesz fractional integral can be expressed as follows [147]:

$$\begin{aligned}&\left(I_R^{\boldsymbol{\gamma}}F\right)\left(x_1,x_2,...,x_n\right)\\&=\frac{1}{2^n\prod_{j=1}^{n}\nu_c\left(\gamma_j\right)}\int_0^{\infty}\cdots\int_0^{\infty}\left|x_1-\xi_1\right|^{\gamma_1-1}\cdots\left|x_n-\xi_n\right|^{\gamma_n-1}f\left(\xi_1,\ldots,\xi_n\right)\mathrm{d}\xi_1\cdots\mathrm{d}\xi_n.\end{aligned}\tag{5-21}$$

The multi-dimensional Riemann-Liouville(RL) fractional integral [83], which is denoted as $\left(I_{\pm\ldots\pm}^{\boldsymbol{\gamma}}F\right)\left(\boldsymbol{x}\right)$ is given in the form:

$$\begin{aligned}&\left(I_{\pm\ldots\pm}^{\boldsymbol{\gamma}}F\right)\left(x_1,x_2,...,x_n\right)\\&=\frac{1}{\prod_{j=1}^{n}\Gamma\left(\gamma_j\right)}\int_0^{\infty}\cdots\int_0^{\infty}\xi_1^{\gamma_1-1}\ldots\xi_n^{\gamma_n-1}F\left(x_1\mp\xi_1,\ldots,x_n\mp\xi_n\right)\mathrm{d}\xi_1\ldots\mathrm{d}\xi_n.\end{aligned}\tag{5-22}$$

According to Eqs. (5-21)-(5-22), MMT can be denoted as follows:

$$2^n\prod_{j=1}^{n}\nu_c\left(\gamma_j\right)\left(I_R^{\boldsymbol{\gamma}}F\right)\left(0\right)=\boldsymbol{M}_F\left(\boldsymbol{\gamma}-\mathbf{1}\right),\tag{5-23}$$

$$\prod_{j=1}^{n}\Gamma\left(\gamma_j\right)\left(I_{\pm\ldots\pm}^{\boldsymbol{\gamma}}F\right)\left(0\right)=\boldsymbol{M}_{F^{\mp\ldots\mp}}\left(\boldsymbol{\gamma}-\mathbf{1}\right).\tag{5-24}$$

According to the property of fractional integral, we introduce the Fourier transform to build the connection between the Fourier transformable function $F\left(\boldsymbol{x}\right)$ and $\boldsymbol{M}_F\left(\boldsymbol{\gamma}-\mathbf{1}\right)$ in the sense of Fourier transform. Let $F\left(\boldsymbol{x}\right)\in\mathbb{R}^n$ be the multi-dimensional Fourier transformable function, and denote $\boldsymbol{\mathcal{F}}\left\{\bullet\right\}$ the multi-dimensional Fourier transform (MFT) operator, $\Phi\left(\boldsymbol{\theta}\right)=\boldsymbol{\mathcal{F}}\left\{F\left(\boldsymbol{x}\right);\boldsymbol{\theta}\right\}$ is a function respect to the vector of parameters $\boldsymbol{\theta}$, then we have

$$\Phi\left(\boldsymbol{\theta}\right)=\boldsymbol{\mathcal{F}}\left\{F\left(\boldsymbol{x}\right);\boldsymbol{\theta}\right\}=\int_{\mathbb{R}^n}F\left(\boldsymbol{x}\right)e^{-i\boldsymbol{\theta}\boldsymbol{x}}\mathrm{d}\boldsymbol{x},\tag{5-25}$$

$$F\left(\boldsymbol{x}\right)=\boldsymbol{\mathcal{F}}^{-1}\left\{\Phi\left(\boldsymbol{\theta}\right);\boldsymbol{x}\right\}=\frac{1}{\left(2\pi\right)^n}\int_{\mathbb{R}^n}\Phi\left(\boldsymbol{\theta}\right)e^{i\boldsymbol{\theta}\boldsymbol{x}}\mathrm{d}\boldsymbol{\theta},\tag{5-26}$$

where $\boldsymbol{\theta}=\left[\theta_1,\theta_2,...,\theta_n\right]^{\mathrm{T}}$ denotes n-dimensional random vectors. Moreover, the MFT and the inverse MFT of Riesz fractional integral is given as [148, 149]:

$$\boldsymbol{\mathcal{F}}\left\{\left(I_R^{\boldsymbol{\gamma}}F\right)\left(\boldsymbol{x}\right);\boldsymbol{\theta}\right\}=\left|\boldsymbol{\theta}\right|^{-\boldsymbol{\gamma}}\boldsymbol{\mathcal{F}}\left\{F\left(\boldsymbol{x}\right);\boldsymbol{\theta}\right\},\tag{5-27}$$

$$\left(I_R^{\boldsymbol{\gamma}}F\right)\left(\boldsymbol{x}\right)=\boldsymbol{\mathcal{F}}^{-1}\left\{\left|\boldsymbol{\theta}\right|^{-\boldsymbol{\gamma}}\boldsymbol{\mathcal{F}}\left\{F\left(\boldsymbol{x}\right);\boldsymbol{\theta}\right\};\boldsymbol{x}\right\}.\tag{5-28}$$

Also, the MFT and the inverse MFT of RL fractional integral

$$\mathcal{F}\left\{\left(I^{\gamma}_{\pm\ldots\pm}F\right)(\boldsymbol{x});\boldsymbol{\theta}\right\}=(\mp i\boldsymbol{\theta})^{-\boldsymbol{\gamma}}\,\mathcal{F}\left\{F(\boldsymbol{x});\boldsymbol{\theta}\right\}, \tag{5-29}$$

$$\left(I^{\gamma}_{\pm\ldots\pm}F\right)(\boldsymbol{x})=\mathcal{F}^{-1}\left\{(\mp i\boldsymbol{\theta})^{-\boldsymbol{\gamma}}\,\mathcal{F}\left\{F(\boldsymbol{x});\boldsymbol{\theta}\right\};\boldsymbol{x}\right\}. \tag{5-30}$$

Based on the abovementioned transform, considering the multi-variable function $F(\boldsymbol{x})$ in probability set, and representing $F(\boldsymbol{x})$ as joint PDF, donated as $p(\boldsymbol{x})$. According to the definition, the MMT of $p(\boldsymbol{x})$, namely $\boldsymbol{M}_p(\boldsymbol{\gamma}-\mathbf{1})$, can also be expressed as $E\left[\boldsymbol{X}^{\boldsymbol{\gamma}-1}\right]$, which is named as *Generalized Complex Fractional Moment* (GCFM). In this case, Eqs. (5-28) and (5-30) in terms of the PDF is the multi-dimensional Characteristic function terms $\Phi(\boldsymbol{\theta})$:

$$\left(I^{\gamma}_{R}p\right)(\boldsymbol{x})=\mathcal{F}^{-1}\left\{|\boldsymbol{\theta}|^{-\boldsymbol{\gamma}}\,\Phi(\boldsymbol{\theta});\boldsymbol{x}\right\}, \tag{5-31}$$

$$\left(I^{\gamma}_{\pm\ldots\pm}p\right)(\boldsymbol{x})=\mathcal{F}^{-1}\left\{(\mp i\boldsymbol{\theta})^{-\boldsymbol{\gamma}}\,\Phi(\boldsymbol{\theta});\boldsymbol{x}\right\}. \tag{5-32}$$

According to Eqs.(5-23)-(5-24), we have

$$2^n\prod_{j=1}^{n}\nu_c(\gamma_j)\,\mathcal{F}^{-1}\left\{|\boldsymbol{\theta}|^{-\boldsymbol{\gamma}}\,\Phi(\boldsymbol{\theta});\boldsymbol{x}\right\}\Big|_{\boldsymbol{x}=0}=2^n\prod_{j=1}^{n}\nu_c(\gamma_j)\left(I^{\gamma}_{R}p\right)(0)=\boldsymbol{M}_p(\boldsymbol{\gamma}-\mathbf{1}), \tag{5-33}$$

$$\prod_{j=1}^{n}\Gamma(\gamma_j)\,\mathcal{F}^{-1}\left\{(\mp i\boldsymbol{\theta})^{-\boldsymbol{\gamma}}\,\Phi(\boldsymbol{\theta});\boldsymbol{x}\right\}\Big|_{\boldsymbol{x}=0}=\prod_{j=1}^{n}\Gamma(\gamma_j)\left(I^{\gamma}_{\pm\ldots\pm}p\right)(0)=\boldsymbol{M}_{p^{\mp\ldots\mp}}(\boldsymbol{\gamma}-\mathbf{1}), \tag{5-34}$$

where

$$(\mp i\theta_i)^{-\gamma_i}=\left[\cos\left(\frac{\pi\gamma_i}{2}\right)\pm i\,\mathrm{sgn}(\theta_i)\sin\left(\frac{\pi\gamma_i}{2}\right)\right]|\theta_i|^{-\gamma_i}. \tag{5-35}$$

Eqs. (5-33) and (5-34) provide the method to construct the $\boldsymbol{M}_p(\boldsymbol{\gamma}-\mathbf{1})$ by the characteristic function. According to Eq. (5-20), the MPDF can be reconstructed by the following expression:

$$p_{\boldsymbol{X}}(\boldsymbol{x})=\frac{1}{(2\pi)^n}\int_{\mathbb{R}^n}E\left[\boldsymbol{X}^{\boldsymbol{\gamma}-1}\right]\boldsymbol{x}^{-\boldsymbol{\gamma}}\mathrm{d}\boldsymbol{\eta}=\frac{1}{(2\pi)^n}\int_{\mathbb{R}^n}\boldsymbol{M}_p(\boldsymbol{\gamma}-\mathbf{1})\,\boldsymbol{x}^{-\boldsymbol{\gamma}}\mathrm{d}\boldsymbol{\eta}, \tag{5-36}$$

and the MPDF can be reconstructed by the following expression:

$$p_{\boldsymbol{X}}(\boldsymbol{x})=\frac{1}{2^nB}\sum_{\boldsymbol{k}=-\boldsymbol{m}}^{\boldsymbol{m}}E\left[\boldsymbol{X}^{\boldsymbol{\gamma}-1}\right]\boldsymbol{x}^{-\boldsymbol{\gamma}_{\boldsymbol{k}}}=\frac{1}{2^nB}\sum_{\boldsymbol{k}=-\boldsymbol{m}}^{\boldsymbol{m}}\boldsymbol{M}_p(\boldsymbol{\gamma}-\mathbf{1})\,\boldsymbol{x}^{-\boldsymbol{\gamma}_{\boldsymbol{k}}}. \tag{5-37}$$

Eq. (5-37) can also be expressed as:

$$p_{\boldsymbol{X}}(\boldsymbol{x})=\frac{\prod_{k=1}^{n}\Delta\eta_k}{(2\pi)^n}E\left[X_1^{\gamma_1-1}\otimes X_2^{\gamma_2-1}\otimes\ldots\otimes X_n^{\gamma_n-1}\right]^{\mathrm{T}}\left(x_1^{-\gamma_1}\otimes x_2^{-\gamma_2}\otimes\ldots\otimes x_n^{\gamma_n}\right). \tag{5-38}$$

Where $X_j^{\gamma_j-1}=\left[X_j^{\gamma_j^{-m}-1},X_j^{\gamma_j^{-m+1}-1},...,X_j^{\gamma_j^{m}-1}\right]^{\mathrm{T}}$, $x_j^{-\gamma_j}=\left[x_j^{-\gamma_j^{-m}},x_j^{-\gamma_j^{-m+1}},...,x_j^{-\gamma_j^{m}}\right]^{\mathrm{T}}$, and the symbol $\otimes$ represent the Kronecker product.

5.4. Extension of CFM in the multi-dimensional real space

In the previous section, the GCFM is defined based on MMT which defined on the positive domain in the multi-dimensional space, that means only the positive part of the function in multi-dimensional space can be reconstructed. Here, we introduce a method to reconstruct the function in all multi-dimensional real space.

Considering the function $p(\boldsymbol{x})$ in multi-dimensional space, and dividing $p(\boldsymbol{x})$ as follows:

$$p_X(\boldsymbol{x})=\begin{cases}p_1(\boldsymbol{x}),x_1,...,x_n>0,\\ p_2(\boldsymbol{x}),x_1\le 0,x_2..,x_n>0,\\ p_3(\boldsymbol{x}),x_2\le 0,x_1,x_3..,x_n>0,\\ \vdots\\ p_{2^n}(\boldsymbol{x}),x_1,...,x_n\le 0,\end{cases} \tag{5-39}$$

where $p_i(\boldsymbol{x}),i=1,2,...,2^n$ is a part of $p(\boldsymbol{x})$ in i-th domain. Denoting $p_i(\boldsymbol{x})$ by $p_i(\boldsymbol{x}_P,\boldsymbol{x}_N)$, where $\boldsymbol{x}_P$ is the set of $\boldsymbol{x}$ over the positive real domain, and $\boldsymbol{x}_N$ is the set of $\boldsymbol{x}$ over the negative real domain, thus the integral of $p_i(\boldsymbol{x}_P,\boldsymbol{x}_N)$ in the sense of MMT is defined as:

$$\boldsymbol{M}_{p_i}(\boldsymbol{\gamma}_P-1,\boldsymbol{\gamma}_N-1)=\int_{\mathbb{R}_P^+}\int_{\mathbb{R}_N^-}p_i(\boldsymbol{x}_P,\boldsymbol{x}_N)\boldsymbol{x}_P^{\boldsymbol{\gamma}_P-1}\boldsymbol{x}_N^{\boldsymbol{\gamma}_N-1}\mathrm{d}\boldsymbol{x}_P\mathrm{d}\boldsymbol{x}_N. \tag{5-40}$$

Assuming that $p_i(\boldsymbol{x}_P,\boldsymbol{x}_N)\subset\mathbb{R}_P^+\times\mathbb{R}_N^-$, Eq.(5-40) can be expressed as:

$$\begin{aligned}\boldsymbol{M}_{p_i}(\boldsymbol{\gamma}_P-1,\boldsymbol{\gamma}_N-1)&=\int_{\mathbb{R}_P^+}\int_{\mathbb{R}_N^-}p_i(\boldsymbol{x}_P,-\boldsymbol{x}_N)\boldsymbol{x}_P^{\boldsymbol{\gamma}_P-1}(-\boldsymbol{x}_N)^{\boldsymbol{\gamma}_N-1}\mathrm{d}\boldsymbol{x}_P\mathrm{d}(-\boldsymbol{x}_N)\\&=(-1)^{\boldsymbol{\gamma}_N-1}\int_{\mathbb{R}_P^+}\int_{\mathbb{R}_N^+}p_i(\boldsymbol{x}_P,-\boldsymbol{x}_N)\boldsymbol{x}_P^{\boldsymbol{\gamma}_P-1}\boldsymbol{x}_N^{\boldsymbol{\gamma}_N-1}\mathrm{d}\boldsymbol{x}_P\mathrm{d}\boldsymbol{x}_N,\end{aligned} \tag{5-41}$$

where

$$\int_{\mathbb{R}_P^+}\int_{\mathbb{R}_N^+}p_i(\boldsymbol{x}_P,-\boldsymbol{x}_N)\boldsymbol{x}_P^{\boldsymbol{\gamma}_P-1}\boldsymbol{x}_N^{\boldsymbol{\gamma}_N-1}\mathrm{d}\boldsymbol{x}_P\mathrm{d}\boldsymbol{x}_N=\boldsymbol{\mathcal{M}}_{p_i}\{p_i;\boldsymbol{\gamma}_P-1,\boldsymbol{\gamma}_N-1\}=E\left[\boldsymbol{X}_P{}^{\boldsymbol{\gamma}-1},\boldsymbol{X}_N{}^{\boldsymbol{\gamma}-1}\right] \tag{5-42}$$

is the MMT of $p_i(\boldsymbol{x}_P,-\boldsymbol{x}_N)$, and satisfies:

$$\boldsymbol{\mathcal{M}}_{p_i}\{p_i;\boldsymbol{\gamma}_P-1,\boldsymbol{\gamma}_N-1\}=(-1)^{1-\boldsymbol{\gamma}_N}\boldsymbol{M}_{p_i}(\boldsymbol{\gamma}_P-1,\boldsymbol{\gamma}_N-1). \tag{5-43}$$

Moreover, if $\Phi(\boldsymbol{\theta})$ is the characteristic function of Eq. (5-39), and it can be divided as

follows:

$$\Phi(\boldsymbol{\theta})=\begin{cases}\Phi_1(\boldsymbol{\theta}),\theta_1,...,\theta_n>0;\\ \Phi_2(\boldsymbol{\theta}),\theta_1\le 0,\theta_2..,\theta_n>0;\\ \Phi_3(\boldsymbol{\theta}),\theta_2\le 0,\theta_1,\theta_3..,\theta_n>0;\\ \vdots\\ \Phi_{2^n}(\boldsymbol{\theta}),\theta_1,...,\theta_n\le 0.\end{cases} \tag{5-44}$$

According to Eq. (5-34)

$$\begin{aligned}\boldsymbol{M}_{p_i}(\boldsymbol{\gamma}_P-1,\boldsymbol{\gamma}_N-1)&=\Gamma(\gamma_1)\cdots\Gamma(\gamma_n)\left(I_+^{\boldsymbol{\gamma}_P}I_-^{\boldsymbol{\gamma}_N}p\right)(0)\\&=\Gamma(\gamma_1)\cdots\Gamma(\gamma_n)\boldsymbol{\mathcal{F}}^{-1}\left\{(i\boldsymbol{\theta}_P)^{-\boldsymbol{\gamma}_P}(-i\boldsymbol{\theta}_N)^{-\boldsymbol{\gamma}_N}\Phi_i(\boldsymbol{\theta})\right\},\end{aligned} \tag{5-45}$$

and then,

$$p_i(\boldsymbol{x}_P,-\boldsymbol{x}_N)=\frac{1}{(2\pi i)^n}\int_{\boldsymbol{\rho}+i\boldsymbol{\eta}}(-1)^{1-\boldsymbol{\gamma}_N}\boldsymbol{M}_{p_i}(\boldsymbol{\gamma}_P-1,\boldsymbol{\gamma}_N-1)\boldsymbol{x}^{-\boldsymbol{\gamma}}\mathrm{d}\boldsymbol{\gamma}. \tag{5-46}$$

Eq. (5-46) can also be expressed as:

$$p_i(\boldsymbol{x}_P,\boldsymbol{x}_N)=\frac{1}{(2\pi i)^n}\int_{\boldsymbol{\rho}+i\boldsymbol{\eta}}(-1)^{1-\boldsymbol{\gamma}_N}\boldsymbol{M}_{p_i}(\boldsymbol{\gamma}_P-1,\boldsymbol{\gamma}_N-1)\boldsymbol{x}_P^{-\boldsymbol{\gamma}_P}(-\boldsymbol{x})_N^{-\boldsymbol{\gamma}_N}\,\mathrm{d}\boldsymbol{\gamma}, \tag{5-47}$$

which can be simplified as:

$$p_i(\boldsymbol{x}_P,\boldsymbol{x}_N)=\frac{1}{(2\pi)^n}\int_{\mathbb{R}^n}(-1)^{1-\boldsymbol{\gamma}_N}\boldsymbol{M}_{p_i}(\boldsymbol{\gamma}_P-1,\boldsymbol{\gamma}_N-1)\boldsymbol{x}_P^{-\boldsymbol{\gamma}_P}(-\boldsymbol{x})_N^{-\boldsymbol{\gamma}_N}\,\mathrm{d}\boldsymbol{\eta}. \tag{5-48}$$

The discrete expression of Eq. (5-48) is shown below:

$$p_i(\boldsymbol{x}_P,\boldsymbol{x}_N)=\frac{\Delta\boldsymbol{\eta}}{(2\pi)^n}\sum_{\boldsymbol{k}=-\boldsymbol{m}}^{\boldsymbol{m}}(-1)^{1-\boldsymbol{\gamma}_N^{\boldsymbol{k}}}\boldsymbol{M}_{p_i}^{\boldsymbol{k}}(\boldsymbol{\gamma}_P^{\boldsymbol{k}}-1,\boldsymbol{\gamma}_N^{\boldsymbol{k}}-1)\boldsymbol{x}_P^{-\boldsymbol{\gamma}_P^{\boldsymbol{k}}}(-\boldsymbol{x})_N^{-\boldsymbol{\gamma}_N^{\boldsymbol{k}}}. \tag{5-49}$$

5.5. Constructing the marginal probability distribution by GCFM

In section 5.3 and 5.4, the definition of GCFM and extend the GCFM to multi-dimensional real domain have been proposed. In this section, we will establish the method to construct the marginal distribution by GCFM.

5.5.1 Symmetric distribution

According to Eq.(5-36), the MPDF can be constructed by multi-dimensional GCFM, which is:

$$p_X(\boldsymbol{x})=\frac{1}{(2\pi)^n}\int_{\mathbb{R}^n}\boldsymbol{M}_p(\boldsymbol{\gamma}-1)\boldsymbol{x}^{-\boldsymbol{\gamma}}\mathrm{d}\boldsymbol{\eta}, \tag{5-50}$$

the marginal distribution function of Eq. (5-50) can be expressed as:

$$p_X\left(\boldsymbol{x}_{mar}\right)=\int_{\mathbb{R}_{nmar}} p_X\left(\boldsymbol{x}\right)\mathrm{d}\boldsymbol{x}_{nmar}=\frac{1}{\left(2\pi\right)^n}\int_{\mathbb{R}_{nmar}}\int_{\mathbb{R}^n}\boldsymbol{M}_p\left(\gamma-1\right)\boldsymbol{x}^{-\gamma}\mathrm{d}\boldsymbol{\eta}\mathrm{d}\boldsymbol{x}_{nmar}, \tag{5-51}$$

where $\boldsymbol{x}_{mar}$ is the set of marginal variable, and $*_{nmar}$ is the set of nonmarginal variables. Eq. (5-51) can be simplified as:

$$\begin{aligned} p_X\left(\boldsymbol{x}_{mar}\right)&=\frac{1}{\left(2\pi\right)^n}\int_{\mathbb{R}^n}\boldsymbol{M}_p\left(\gamma-1\right)\int_{\mathbb{R}_{nmar}}\boldsymbol{x}^{-\gamma}\mathrm{d}\boldsymbol{x}_{nmar}\mathrm{d}\boldsymbol{\eta}\\ &=\frac{1}{\left(2\pi\right)^n}\int_{\mathbb{R}^n}\boldsymbol{M}_p\left(\gamma-1\right)\left(\frac{\boldsymbol{x}_{nmar}^{1-\gamma}}{1-\gamma_{nmar}}\bigg|_{\mathbb{R}_{nmar}}\right)\mathrm{d}\boldsymbol{\eta}. \end{aligned} \tag{5-52}$$

5.5.2 Asymmetric distribution

Since the domain of definition of asymmetrical distribution is divided into the positive real field and the negative real field, according to Eq.(5-46), the distribution can be expressed as follows:

$$p_i\left(\boldsymbol{x}_P,-\boldsymbol{x}_N\right)=\frac{1}{\left(2\pi i\right)^n}\int_{\mathbb{R}_{nmar}+i\mathbb{R}_{nmar}}\left(-1\right)^{1-\gamma_N}\boldsymbol{M}_{p_i}\left(\gamma_P-1,\gamma_N-1\right)\boldsymbol{x}^{-\gamma}\mathrm{d}\gamma, \tag{5-53}$$

and the marginal distribution can be expressed as:

$$\begin{aligned} p_i\left(\boldsymbol{x}_{P_{mar}},-\boldsymbol{x}_{N_{mar}}\right)&=\int_{\mathbb{R}_{nmar}}p_i\left(\boldsymbol{x}_P,-\boldsymbol{x}_N\right)\mathrm{d}\boldsymbol{x}_{nmar}\\ &=\frac{1}{\left(2\pi i\right)^n}\int_{\mathbb{R}_{nmar}+i\mathbb{R}_{nmar}}\left(-1\right)^{1-\gamma_N}\boldsymbol{M}_{p_i}\left(\gamma_P-1,\gamma_N-1\right)\int_{\mathbb{R}nmar}\boldsymbol{x}^{-\gamma}\mathrm{d}\boldsymbol{x}_{nmar}\mathrm{d}\gamma, \end{aligned} \tag{5-54}$$

Eq. (5-54) can be simplified as:

$$\begin{aligned} p_i\left(\boldsymbol{x}_{mar}\right)&=\frac{1}{\left(2\pi i\right)^n}\int_{\mathbb{R}_{nmar}+i\mathbb{R}_{nmar}}\left(-1\right)^{1-\gamma_N}\boldsymbol{M}_{p_i}\left(\gamma_P-1,\gamma_N-1\right)\left(\frac{1}{1-\gamma_{nmar}}\boldsymbol{x}^{1-\gamma}\bigg|_{\mathbb{R}_{nmar}}\right)\mathrm{d}\gamma\\ &=\frac{1}{\left(2\pi\right)^n}\int_{\mathbb{R}_{nmar}}\left(-1\right)^{1-\gamma_N}\boldsymbol{M}_{p_i}\left(\gamma_P-1,\gamma_N-1\right)\left(\frac{1}{1-\gamma_{nmar}}\boldsymbol{x}^{1-\gamma}\bigg|_{\mathbb{R}_{nmar}}\right)\mathrm{d}\boldsymbol{\eta}. \end{aligned} \tag{5-55}$$

5.6. Numerical simulation

In this part, we select the α-stable distribution as the example. The characteristic function of the α-stable random variables when $0<\alpha\le 2$ can be expressed as follows:

$$\varphi_\alpha\left(\Theta\right)=\begin{cases} e^{-\int_{S_d}\left|\left(\Theta,s\right)\right|^\alpha\left(1-i\,\mathrm{sgn}\left(\left(\Theta,s\right)\right)\tan\left(\frac{\pi\alpha}{2}\right)\right)L\left(\mathrm{d}s\right)+i\left(\Theta,\mu\right)}, & \alpha\neq 1.\\ e^{-\int_{S_d}\left|\left(\Theta,s\right)\right|^\alpha\left(1-i\frac{2}{\pi}\mathrm{sgn}\left(\left(\Theta,s\right)\right)\ln\left|\left(\Theta,s\right)\right|\right)L\left(\mathrm{d}s\right)+i\left(\Theta,\mu\right)}, & \alpha=1. \end{cases} \tag{5-56}$$

The FS for symmetric α-stable RVs is $0<\rho<1+\alpha$, where $L(\bullet)$ is finite measure, and S_d is unit sphere of $\mathbb{R}^n$. Currently, the α-stable random variable has the expression for its PDF only in $\alpha=1/2$ (Lévy distribution), $\alpha=1$ (Cauchy distribution), $\alpha=2$ (Gaussian distribution). Here, we consider the 2-dimensional distribution when $\alpha=2$, thus, Eq.(5-56) can be rewritten as follows:

$$\Phi(\theta_1,\theta_2)=e^{-i(\mu_1\theta_1+\mu_2\theta_2)-\frac{1}{2}\left(\sigma_1^2|\theta_1|^2+\sigma_2^2|\theta_2|^2\right)}, \tag{5-57}$$

and the PDF denoted as $p(x,y)$ of Eq. (5-57)can be expressed as:

$$p_{XY}(x,y)=\frac{1}{2\pi\sqrt{|\Sigma|}}e^{-\frac{1}{2}\left([x-\mu_1,y-\mu_2]\Sigma^{-1}[x-\mu_1,y-\mu_2]^{\mathrm{T}}\right)}. \tag{5-58}$$

Some other cases are given in **Appendix. E.**

Considering Eq. (5-58), where

$$\Sigma=\begin{bmatrix}\sigma_1^2 & 0\\ 0 & \sigma_2^2\end{bmatrix},\Sigma^{-1}=\begin{bmatrix}1/\sigma_1^2 & 0\\ 0 & 1/\sigma_2^2\end{bmatrix}, \tag{5-59}$$

then we divide $p(x,y)$ as follows:

$$p_{XY}(x,y)=\begin{cases}p_1(x,y), x>0, y>0;\\ p_2(x,y), x\le 0, y>0;\\ p_3(x,y), x>0, y\le 0;\\ p_4(x,y), x\le 0, y\le 0.\end{cases} \tag{5-60}$$

According to Eq. (5-40):

$$\boldsymbol{M}_p(\gamma_1-1,\gamma_2-1)=\begin{cases}\boldsymbol{M}_{p_{++}}(\gamma_1-1,\gamma_2-1)=\int_0^\infty\int_0^\infty p_1(x,y)x^{\gamma_1-1}y^{\gamma_2-1}\mathrm{d}x\mathrm{d}y, x>0, y>0;\\ \boldsymbol{M}_{p_{-+}}(\gamma_1-1,\gamma_2-1)=\int_0^\infty\int_0^\infty p_2(-x,y)x^{\gamma_1-1}y^{\gamma_2-1}\mathrm{d}x\mathrm{d}y, x\le 0, y>0;\\ \boldsymbol{M}_{p_{+-}}(\gamma_1-1,\gamma_2-1)=\int_0^\infty\int_0^\infty p_3(x,-y)x^{\gamma_1-1}y^{\gamma_2-1}\mathrm{d}x\mathrm{d}y, x>0, y\le 0;\\ \boldsymbol{M}_{p_{--}}(\gamma_1-1,\gamma_2-1)=\int_0^\infty\int_0^\infty p_4(-x,-y)x^{\gamma_1-1}y^{\gamma_2-1}\mathrm{d}x\mathrm{d}y, x\le 0, y\le 0.\end{cases}$$

(5-61)

Also, $\boldsymbol{M}_p(\gamma_1-1,\gamma_2-1)$ can be constructed by the characteristic function $\Phi(\theta_1,\theta_2)$, according to Eq.(5-34), namely:

$$\boldsymbol{M}_{p^{\pm\pm}}(\gamma_1-1,\gamma_2-1)=\frac{\Gamma(\gamma_1)\Gamma(\gamma_2)}{(2\pi)^2}\int_{-\infty}^{\infty}\int_{-\infty}^{\infty}(\pm i\theta_1)^{-\gamma_1}(\pm i\theta_2)^{-\gamma_2}\Phi(\theta_1,\theta_2)\mathrm{d}\theta_1\mathrm{d}\theta_2, \tag{5-62}$$

where

$$\left(\mp i\theta_i\right)^{-\gamma_i}=\left[\cos\left(\frac{\pi\gamma_i}{2}\right)\pm i\,\mathrm{sgn}\left(\theta_i\right)\sin\left(\frac{\pi\gamma_i}{2}\right)\right]\left|\theta_i\right|^{-\gamma_i},i=1,2. \tag{5-63}$$

By inserting Eq.(5-57) into Eq. (5-62), then we have

$$\begin{aligned}&\boldsymbol{M}_{p^{\pm_1\pm_2}}\left(\gamma_1-1,\gamma_2-1\right)\\&=\frac{\Gamma\left(\gamma_1\right)\Gamma\left(\gamma_2\right)}{\left(2\pi\right)^2}\int_{-\infty}^{\infty}\int_{-\infty}^{\infty}\left(\pm_1 i\theta_1\right)^{-\gamma_1}\left(\pm_2 i\theta_2\right)^{-\gamma_2}e^{i\left(\mu_1\theta_1+\mu_2\theta_2\right)-\frac{1}{2}\left(\sigma_1^2\theta_1^2+\sigma_2^2\theta_2^2\right)}\mathrm{d}\theta_1\mathrm{d}\theta_2.\end{aligned} \tag{5-64}$$

According to Eq. (5-34), $p\left(x,y\right)$ can be reconstructed as:

$$p_{XY}\left(x,y\right)=\begin{cases}\dfrac{1}{\left(2\pi\right)^2}\displaystyle\int_{-\infty}^{\infty}\int_{-\infty}^{\infty}\boldsymbol{M}_{p_{--}}\left(\gamma_1-1,\gamma_2-1\right)x^{-\gamma_1}y^{-\gamma_2}\mathrm{d}\eta_1\mathrm{d}\eta_2,x>0,y>0;\\ \dfrac{1}{\left(2\pi\right)^2}\displaystyle\int_{-\infty}^{\infty}\int_{-\infty}^{\infty}\left(-1\right)^{1-\gamma_1}\boldsymbol{M}_{p_{+-}}\left(\gamma_1-1,\gamma_2-1\right)\left(-x\right)^{-\gamma_1}y^{-\gamma_2}\mathrm{d}\eta_1\mathrm{d}\eta_2,x\le 0,y>0;\\ \dfrac{1}{\left(2\pi\right)^2}\displaystyle\int_{-\infty}^{\infty}\int_{-\infty}^{\infty}\left(-1\right)^{1-\gamma_2}\boldsymbol{M}_{p_{-+}}\left(\gamma_1-1,\gamma_2-1\right)x^{-\gamma_1}\left(-y\right)^{-\gamma_2}\mathrm{d}\eta_1\mathrm{d}\eta_2,x>0,y\le 0;\\ \dfrac{1}{\left(2\pi\right)^2}\displaystyle\int_{-\infty}^{\infty}\int_{-\infty}^{\infty}\left(-1\right)^{2-\gamma_1-\gamma_2}\boldsymbol{M}_{p_{++}}\left(\gamma_1-1,\gamma_2-1\right)\left(-x\right)^{-\gamma_1}\left(-y\right)^{-\gamma_2}\mathrm{d}\eta_1\mathrm{d}\eta_2,x\le 0,y\le 0.\end{cases} \tag{5-65}$$

Based on Eq. (5-58), assuming that $\mu_1,\mu_2\neq 0$, the PDF can be expressed as:

$$p_{XY}\left(x,y\right)=\frac{1}{2\pi\sigma_1\sigma_2}e^{-\frac{1}{2}\left(\frac{\left(x-\mu_1\right)^2}{\sigma_1^2}+\frac{\left(y-\mu_2\right)^2}{\sigma_2^2}\right)}. \tag{5-66}$$

The CF of Eq. (5-66) is:

$$\Phi\left(\theta_1,\theta_2\right)=e^{-i\left(\mu_1\theta_1+\mu_2\theta_2\right)-\frac{1}{2}\left(\sigma_1^2\theta_1^2+\sigma_2^2\theta_2^2\right)}. \tag{5-67}$$

According to Eq. (5-62), we can obtain:

$$\boldsymbol{M}_{p^{\pm_1\pm_2}}\left(\gamma_1-1,\gamma_2-1\right)=\frac{1}{\pi^2}2^{-2-\frac{\gamma_1}{2}-\frac{\gamma_2}{2}}\sigma_1^{\gamma_1-3}\sigma_2^{\gamma_2-2}\Gamma\left(\gamma_1\right)\Gamma\left(\gamma_2\right)\left(S_1\pm_1 S_2\right)\left(S_3\pm_2 S_4\right), \tag{5-68}$$

where

$$
\begin{aligned}
S_1 &= \sqrt{2}\sigma_1^2 \cos\left(\frac{\pi\gamma_1}{2}\right)\Gamma\left(\frac{1-\gamma_1}{2}\right){}_1F_1\left(\frac{1-\gamma_1}{2},\frac{1}{2},-\frac{\mu_1^2}{2\sigma_1^2}\right),\\
S_2 &= \gamma_1\mu_1\sigma_1 \sin\left(\frac{\pi\gamma_1}{2}\right)\Gamma\left(-\frac{\gamma_1}{2}\right){}_1F_1\left(1-\frac{\gamma_1}{2},\frac{3}{2},-\frac{\mu_1^2}{2\sigma_1^2}\right),\\
S_3 &= \sqrt{2}\sigma_2 \cos\left(\frac{\pi\gamma_2}{2}\right)\Gamma\left(\frac{1-\gamma_2}{2}\right){}_1F_1\left(\frac{1-\gamma_2}{2},\frac{1}{2},-\frac{\mu_2^2}{2\sigma_2^2}\right),\\
S_4 &= \gamma_2\mu_2 \sin\left(\frac{\pi\gamma_2}{2}\right)\Gamma\left(-\frac{\gamma_2}{2}\right){}_1F_1\left(1-\frac{\gamma_2}{2},\frac{3}{2},-\frac{\mu_2^2}{2\sigma_2^2}\right),
\end{aligned}
\tag{5-69}
$$

where ${}_1F_1(\bullet)$ is Kummer confluent hypergeometric function. Considering first quadrant in 2-dimentional space,

$$
F(\boldsymbol{x}) = p_{XY}(x,y) = \frac{1}{2\pi\sigma_1\sigma_2} e^{-\frac{1}{2}\left(\frac{(x-\mu_1)^2}{\sigma_1^2}+\frac{(y-\mu_2)^2}{\sigma_2^2}\right)}, \tag{5-70}
$$

$$
C(\boldsymbol{a})\boldsymbol{x}^{-\boldsymbol{a}} = e^{-\langle \boldsymbol{a},\ln x\rangle+\ln(C(\boldsymbol{a}))} = e^{-(a_1\ln x+a_2\ln y)+C_1(a_1)+C_2(a_2)}, \tag{5-71}
$$

where $\boldsymbol{a}=[a_1,a_2]$, and $\boldsymbol{x}=[x,y]$. Since $\mu_1,\mu_2,\sigma_1,\sigma_2$ are constant, it is obviously that there exist $\boldsymbol{a}\subset\mathbb{R}^2$, and proper function $C_1(a_1), C_2(a_2)$ satisfy:

$$
\begin{aligned}
a_1\ln x - C_1(a_1) &< \frac{(x-\mu_1)^2}{2\sigma_1^2} - \ln\frac{1}{\sqrt{2\pi}\sigma_1},\\
a_2\ln y - C_2(a_2) &< \frac{(y-\mu_2)^2}{2\sigma_2^2} - \ln\frac{1}{\sqrt{2\pi}\sigma_2}.
\end{aligned}
\tag{5-72}
$$

Hence

$$
p_{XY}(x,y) < C(\boldsymbol{a})\boldsymbol{x}^{-\boldsymbol{a}}, \tag{5-73}
$$

which means the normal distribution satisfy **Theorem 1**.

Moreover, since $\left|\boldsymbol{M}_{p^{\pm1\pm2}}(\gamma_1-1,\gamma_2-1)\right|$ is finite at a tube domain except 0 and infinity, it is clear that we can found a function $K(\boldsymbol{\rho})$ of $\boldsymbol{\rho}$, and $H_\Theta(\boldsymbol{\eta})$ of $\boldsymbol{\eta}$, as well as a real number $k>1$ satisfy:

$$
\left|\boldsymbol{M}_{p^{\pm1\pm2}}(\gamma_1-1,\gamma_2-1)\right| \le K(\boldsymbol{\rho})e^{-kH_\Theta(\boldsymbol{\eta})},\ k>1,\ \boldsymbol{\gamma}=\boldsymbol{\rho}+i\boldsymbol{\eta}, \tag{5-74}
$$

which means $\boldsymbol{M}_{p^{\pm1\pm2}}(\gamma_1-1,\gamma_2-1)$ satisfy **Theorem 2**.

The more generalized Gaussian distribution can be expressed as follows:

$$p_{XY}(x,y)=\frac{1}{2\pi\sigma_1\sigma_2\sqrt{1-\zeta^2}}e^{-\frac{1}{2(1-\zeta^2)}\left[\left(\frac{x-\mu_1}{\sigma_1}\right)^2-2\zeta\left(\frac{x-\mu_1}{\sigma_1}\right)\left(\frac{y-\mu_2}{\sigma_2}\right)+\left(\frac{y-\mu_2}{\sigma_2}\right)^2\right]},\tag{5-75}$$

where ζ is the correlation coefficient, the numerical solution of 2D-GCFM is given at the **Appendix D.**

5.6.1 Symmetric case ($\mu_1=\mu_2=0$)

In this case, S_2 and S_4 in Eq. (5-69) are 0, then Eq. (5-68) can be expressed as follows:

$$\boldsymbol{M}_p(\gamma_1-1,\gamma_2-1)=\frac{\sigma_1^{\gamma_1-1}\sigma_2^{\gamma_2-1}}{\pi^2 2^{\frac{\gamma_1}{2}+\frac{\gamma_2}{2}+1}}\Gamma(\gamma_1)\Gamma(\gamma_2)\cos\left(\frac{\pi\gamma_1}{2}\right)\cos\left(\frac{\pi\gamma_2}{2}\right)\Gamma\left(\frac{1-\gamma_1}{2}\right)\Gamma\left(\frac{1-\gamma_2}{2}\right).\tag{5-76}$$

In addition, the expression of MMT of $p(x,y)$ by Eq. (5-11) and Eq.(5-66) is:

$$\boldsymbol{M}_p(\gamma_1-1,\gamma_2-1)=\frac{1}{\pi}2^{\frac{\gamma_1}{2}+\frac{\gamma_2}{2}-3}\sigma_1^{\gamma_1-1}\sigma_2^{\gamma_2-1}\Gamma\left(\frac{\gamma_1}{2}\right)\Gamma\left(\frac{\gamma_2}{2}\right),\tag{5-77}$$

according to the formula

$$\Gamma(1-z)\Gamma(z)=\frac{\pi}{\sin(\pi z)},\tag{5-78}$$

and

$$\Gamma(z)\Gamma\left(z+\frac{1}{2}\right)=2^{1-2z}\sqrt{\pi}\Gamma(2z),\tag{5-79}$$

Eq. (5-76) and (5-77) can be translated each other.

In the symmetric case, $p(x,y)$ can be constructed by:

$$p_{XY}(x,y)=\frac{1}{(2\pi)^2}\int_{-\infty}^{\infty}\int_{-\infty}^{\infty}\boldsymbol{M}_p(\gamma_1-1,\gamma_2-1)|x|^{-\gamma_1}|y|^{-\gamma_2}\,\mathrm{d}\eta_1\mathrm{d}\eta_2,\tag{5-80}$$

and the discrete expression of Eq. (5-80) can be expressed as:

$$p_{XY}(x,y)\cong\frac{1}{4\pi^2}\sum_{k_2=-m_2}^{m_2}\sum_{k_1=-m_1}^{m_1}\boldsymbol{M}_p(\gamma_1^{k_1}-1,\gamma_2^{k_2}-1)|x|^{-\gamma_1^{k_1}}|y|^{-\gamma_2^{k_2}}\Delta\eta_1\Delta\eta_2.\tag{5-81}$$

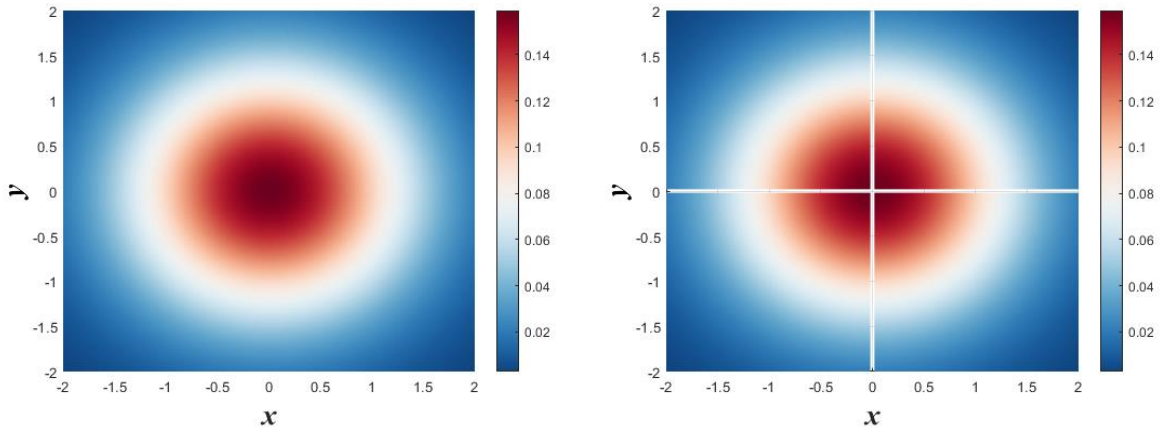

(a) (b)

Figure 5-1 (a) The original normal distribution; (b) The normal distribution reconstructed by 2D-GCFM. Where $\sigma_1 = 1, \sigma_2 = 1$

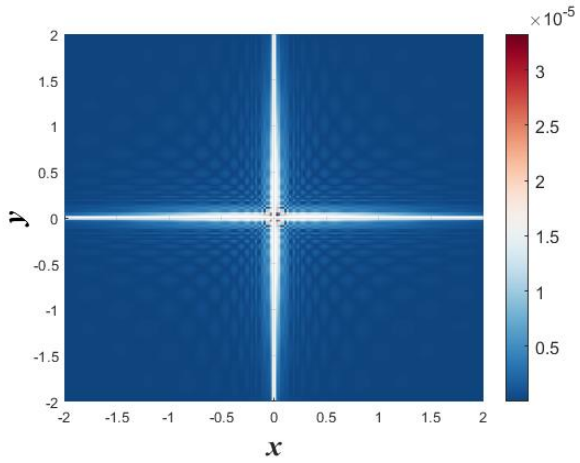

Figure 5-2 The absolute error of original normal distribution and reconstructed normal distribution

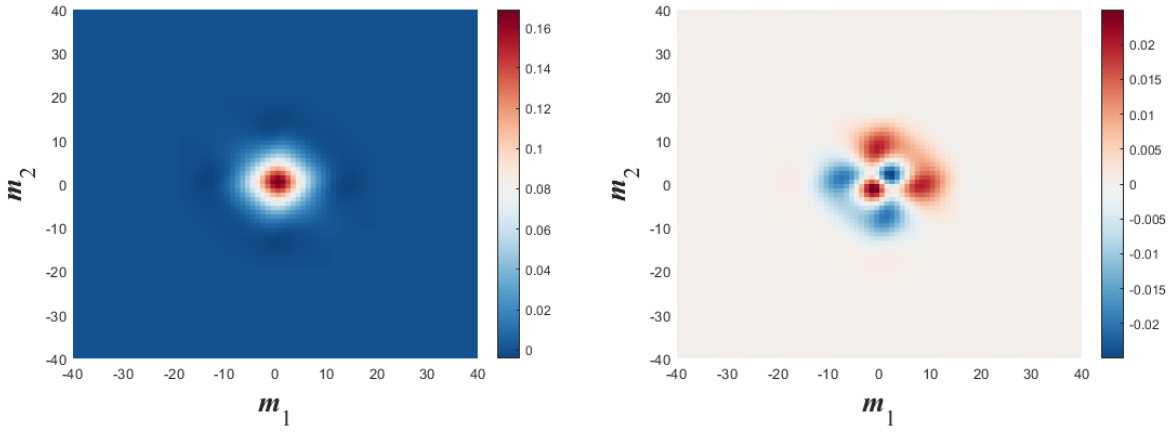

(a) (b)

Figure 5-3 (a) The real part of 2D-GCFM. (b) The imaginary part of 2D-GCFM. $m_1 = m_2 = 40$

In this example, we choose the standard deviation as $\sigma_1 = 1$, $\sigma_2 = 1$, the calculation parameters of GCFM method is selected as $\rho_1 = 1.5$, $\rho_2 = 1.5$, $\Delta\eta_1 = 0.4$, $\Delta\eta_2 = 0.4$, and $x, y \in [-2, 2]$, $\Delta x = \Delta y = 0.02$. The exact normal distribution is shown in Figure 5-1 (a). Figure

5-1(b) displays the reconstructed normal distribution when $m_1 = m_2 = 40$. Figure 5-2 exhibits the absolute error between Figure 5-1 (a) and Figure 5-1 (b), which illustrate the accuracy of GCFM method.

It is worth noticing that there exists two lines in Figure 5-1 (b) when $x = 0$ and $y = 0$, which are generated for the reason that the singularity of Mellin transform when $x = 0$, and also the singularity in $\boldsymbol{x} = \mathbf{0}$ of MMT.

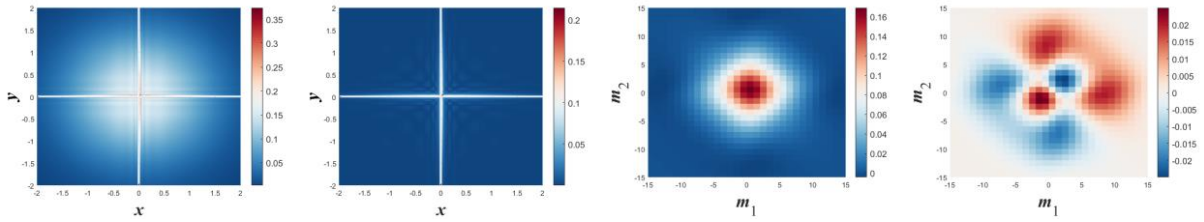

(a) (b) (c) (d)

Figure 5-4 (a) The normal distribution reconstructed by 2D-GCFM. (b) The absolute error of original normal distribution and reconstructed normal distribution. (c) The real part of 2D-GCFM. (d) The imaginary part of 2D-GCFM. $m_1 = m_2 = 15$

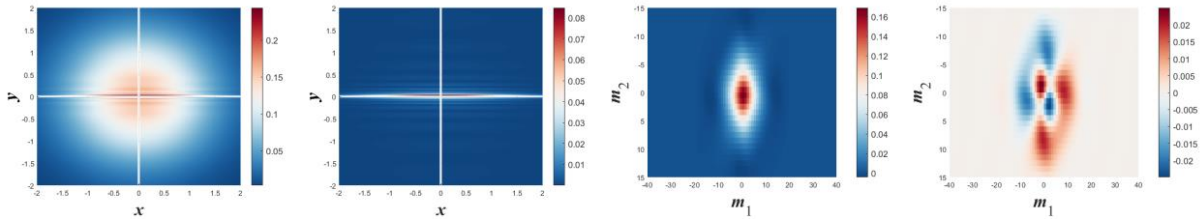

(a) (b) (c) (d)

Figure 5-5 (a) The normal distribution reconstructed by 2D-GCFM. (b) The absolute error of original normal distribution and reconstructed normal distribution. (c) The real part of 2D-GCFM. (d) The imaginary part of 2D-GCFM. $m_1 = 40$, $m_2 = 15$

Figure 5-4 (a) and Figure 5-5(a) display the Gauss distributions reconstructed by 2D-GCFM with different cutoff value $m_1 = m_2 = 15$ and $m_1 = 40, m_2 = 15$, respectively, where Figure 5-4(b-d) and Figure 5-5 (b-d) exhibit the absolute error, as well as the real and imaginary part of 2D-GCFM. According to the results, it is obviously that the accuracy of 2D-GCFM method increase with the cutoff value.

Another example is shown in Figure 5-6 when $\sigma_1 = 2$, $\sigma_2 = 0.5$, where Figure 5-6 (a) and (b) are the exact normal distribution and reconstructed normal distribution when $m_1 = m_2 = 40$, Figure 5-6(c-e) are the absolute error as well as the real and imaginary part of 2D-GCFM, which also verified the accuracy of GCFM method.

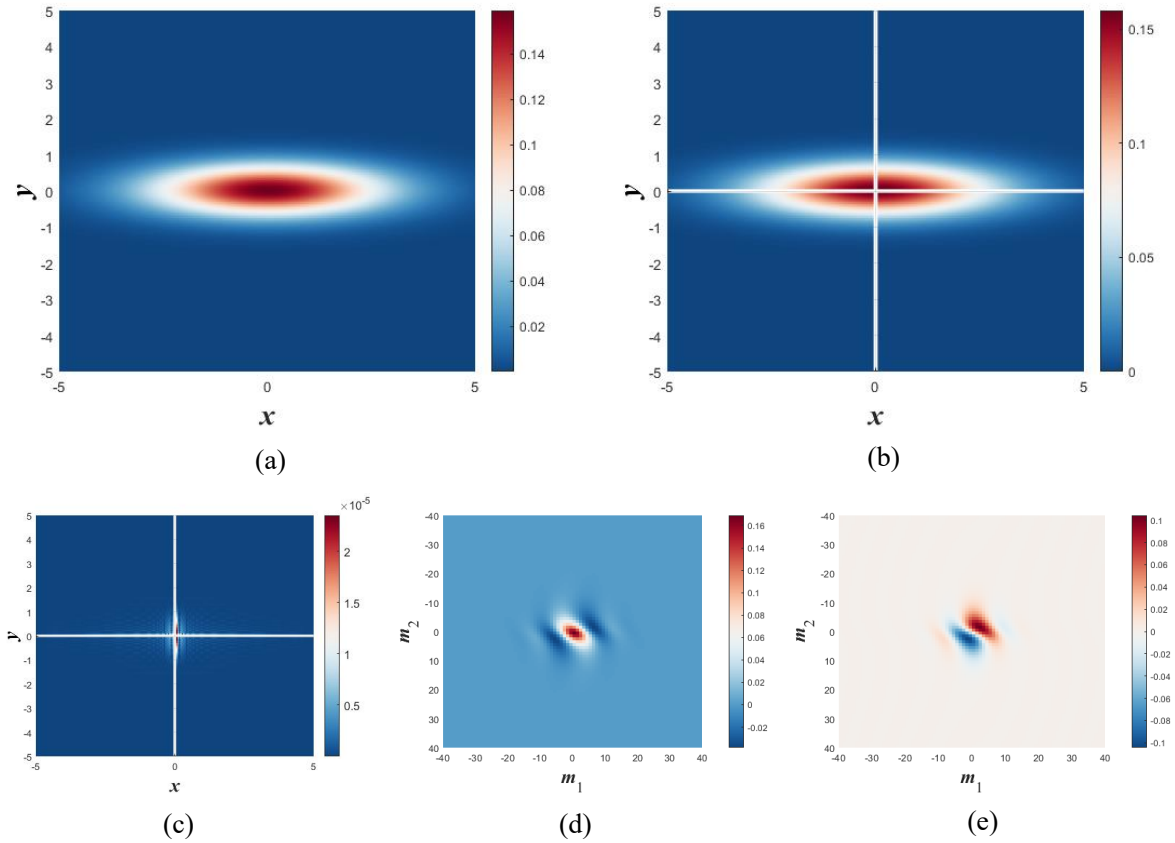

Figure 5-6 (a) The exact normal distribution. (b) The reconstructed normal distribution by 2D-GCFM. (c) The absolute error. (d) The real part of 2D-GCFM. (e) The imaginary part of 2D-GCFM. $m_1 = m_2 = 40$, $\sigma_1 = 2$, $\sigma_2 = 0.5$

5.6.2 Asymmetric case ($\mu_1 \neq 0, \mu_2 \neq 0$)

In this part, we verify the accuracy of the generalized CFM in asymmetric case. According to Eqs. (5-65)-(5-69), the asymmetric distribution (5-66) can be reconstructed.

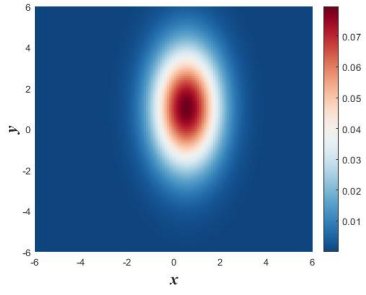

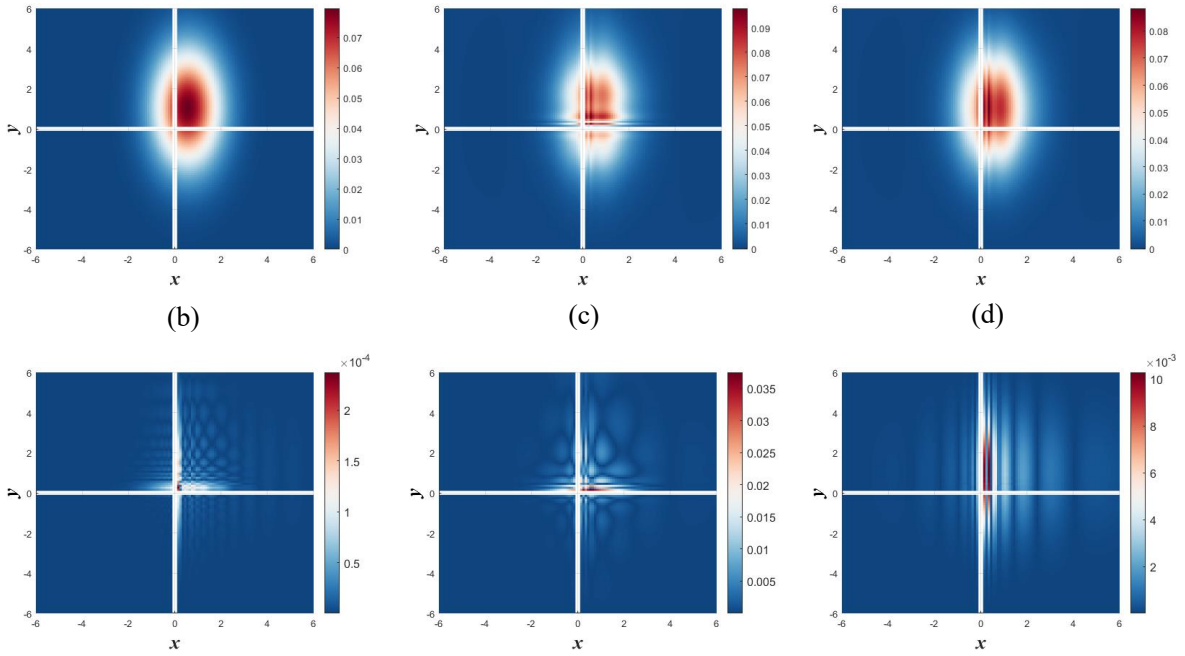

Figure 5-7 (a) The exact normal distribution; (b-d) The normal distribution reconstructed by 2D-GCFM, and (e-g) the absolute error. (Case 1 $m_1 = m_2 = 40$; Case 2 $m_1 = m_2 = 15$; Case 2 $m_1 = 15, m_2 = 40$). $\rho_1 = \rho_2 = 1.5, \Delta\eta_1 = \Delta\eta_2 = 0.3$

Assuming that $\mu_1 = 0.5, \mu_2 = 1, \sigma_1 = 1, \sigma_2 = 2$, Figure 5-7 displays the original normal distribution and the normal distribution reconstructed by 2D-GCFM with different m_1 and m_2. According to the results, the GCFM can also reconstructed the asymmetric distribution when m_1 and m_2 is large enough. Figure 5-8 to Figure 5-10 exhibit the real part and imaginary part of 2D-GCFM in the first quadrant to fourth quadrant with different m_1 and m_2. Compared with Figure 5-8 to Figure 5-10, it can be seen from the results that the increase of the truncation value retains more information of the GCFM.

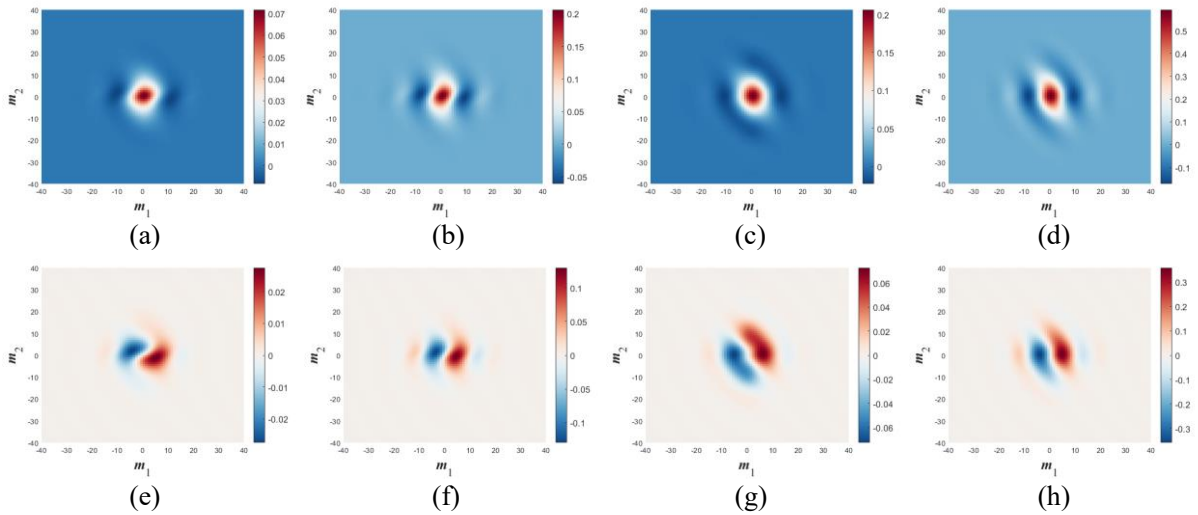

Figure 5-8 (a-d) the real part of 2D-GCFM in first quadrant to fourth quadrant; (e-h) the imaginary part of 2D-GCFM in first quadrant to fourth quadrant. $m_1 = 40, m_2 = 40$

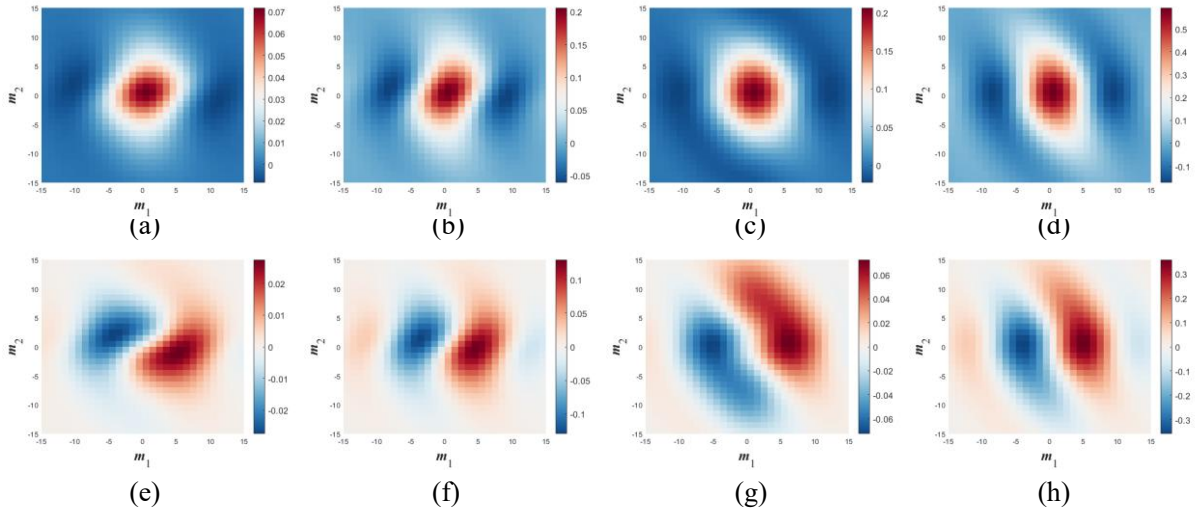

Figure 5-9 (a-d) the real part of 2D-GCFM in first quadrant to fourth quadrant; (e-h) the imaginary part of 2D-GCFM in first quadrant to fourth quadrant. $m_1 = 15, m_2 = 15$

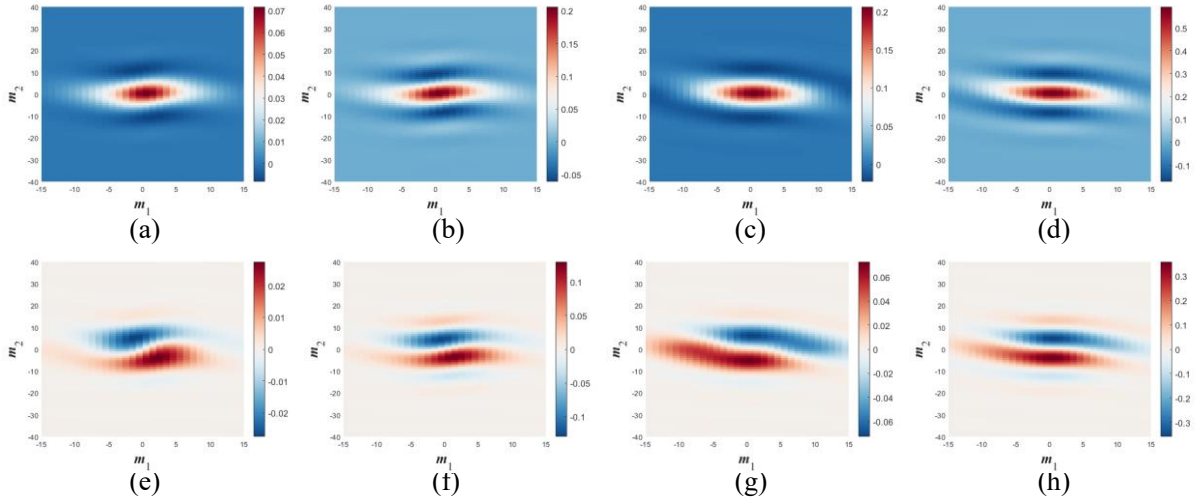

Figure 5-10 (a-d) the real part of 2D-GCFM in first quadrant to fourth quadrant; (e-h) the imaginary part of 2D-GCFM in first quadrant to fourth quadrant. $m_1 = 15, m_2 = 40$

The following conclusions can be drawn from the analysis:

1) For multidimensional probability distributions, limited GCFM is sufficient for the reconstruction of the probability distribution, and this reconstruction is effective for both symmetric and non-symmetric distributions.

2) The size of the truncation value and step size determines the amount of preserved information in the GCFM, and more GCFM information leads to a more precise reconstruction of the probability distribution.

3) From the results, the probability distribution is reconstructed at $\boldsymbol{x} \neq 0$, where there are no values when $\boldsymbol{x} = 0$, which is caused by the singularity of the Mellin transform at $\boldsymbol{x} = 0$.

5.6.3 Marginal probability distribution

Considering the asymmetric distribution in Eq. (5-66), for the $p_i(x,y), i = 1,...,4$, the PDF can be reconstructed by the following expression:

$$p_i(x,y) = \frac{1}{(2\pi)^2}\int_{-\infty}^{\infty}\int_{-\infty}^{\infty} \boldsymbol{M}_{p_i}(\gamma_1 - 1, \gamma_2 - 1)\, x^{-\gamma_1} y^{-\gamma_2} \mathrm{d}\eta_1 \mathrm{d}\eta_2, \quad x > 0, y > 0. \tag{5-82}$$

Integrating Eq. (5-82) by x, we can obtain the expression of $p_i(y)$ as follows:

$$p_i(y) = \frac{1}{(2\pi)^2}\int_{-\infty}^{\infty}\int_{-\infty}^{\infty} \boldsymbol{M}_{p_i}(\gamma_1 - 1, \gamma_2 - 1)\left(\frac{1}{1-\gamma_1} x^{1-\gamma_1}\Big|_{\Omega}\right) y^{-\gamma_2} \mathrm{d}\eta_1 \mathrm{d}\eta_2, x > 0, y > 0. \tag{5-83}$$

Utilizing Eq. (5-83), the marginal distribution can be obtained by 2D-GCFM. The discrete expression of Eq. (5-83)can be expressed as follows:

$$p_i(y) = \frac{1}{(2\pi)^2}\sum_{k_2=-m_2}^{m_2}\left(\sum_{k_1=-m_1}^{m_1} \boldsymbol{M}_{p_i}(\gamma_1^{k_1} - 1, \gamma_2^{k_2} - 1)\left(\frac{1}{1-\gamma_1^{k_1}} x^{1-\gamma_1^{k_1}}\Big|_{\Omega}\right)\Delta\eta_1\right) y^{-\gamma_2^{k_2}}\Delta\eta_2, \tag{5-84}$$

where Ω usually represent the domain of integration.

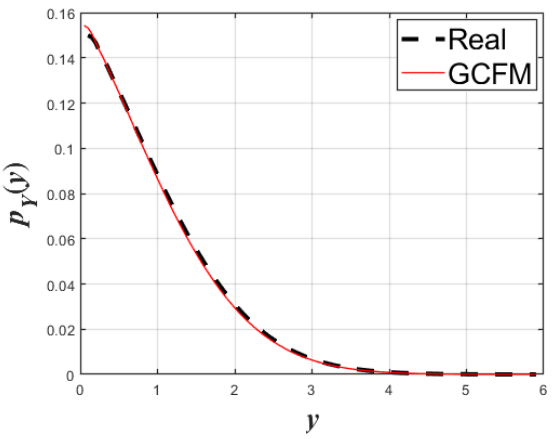

(a)

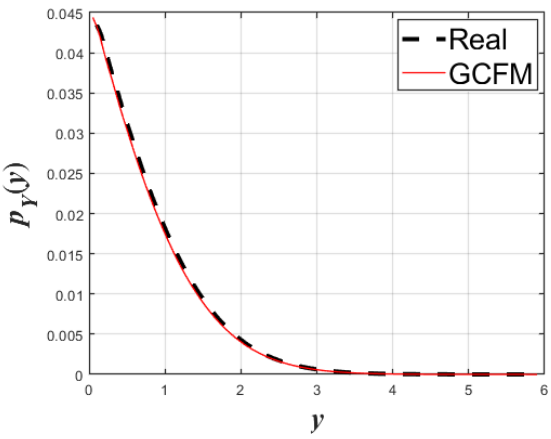

(b)

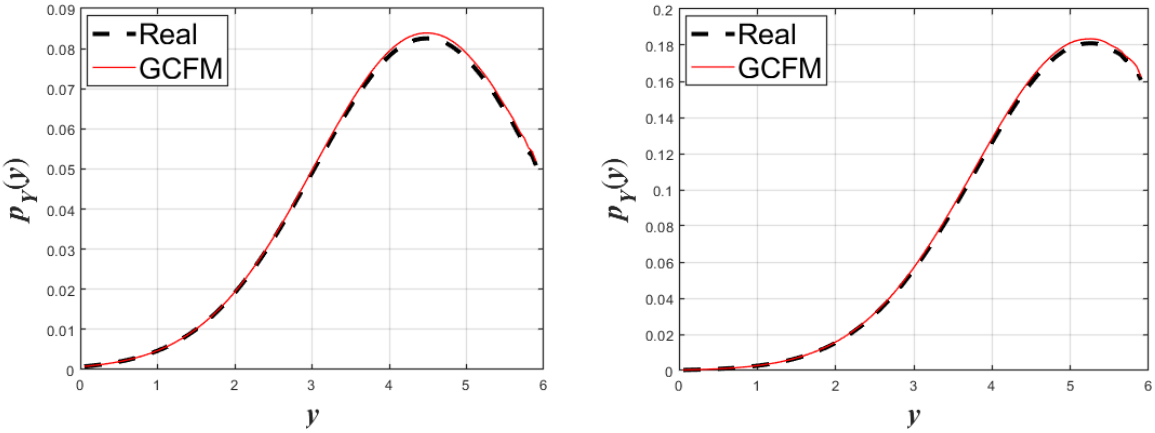

Figure 5-11 The marginal distribution $p_Y(y)$ in (a) first quadrant; (b) second quadrant; (c) third quadrant; (d) fourth quadrant

Figure 5-11 exhibits the marginal distribution in four quadrant that obtained by Eq. (5-84), where the scatter is the results obtained by the original distribution function, and the line is obtained by 2D-GCFM. According to the results, the low marginal distribution can be obtained directly by using high-dimensional CFM, which means that the high dimensional CFM contains complete information in each lower dimension.

5.6.4 GCFM method for stochastic dynamic system

In the previous study, the CFM method is utilized to reconstruct the transient PDF of stochastic dynamic system efficiently. In this part, the GCFM method is applied to obtained the transient joint PDF of 2-dimensional stochastic dynamic system. A sample second order stochastic dynamic system expressed as follows:

$$\ddot{X}(t)+kX(t)=\sigma\xi(t), \tag{5-85}$$

Eq. (5-85) can be translated into the 2-dimensional differential equation form as follows:

$$\begin{aligned} \mathrm{d}X(t)&=Y(t)\mathrm{d}t,\\ \mathrm{d}Y(t)&=-kX(t)\mathrm{d}t+\sigma\mathrm{d}W(t), \end{aligned} \tag{5-86}$$

where $\xi(t)$ represents the Gaussian white noise, $W(t)$ is wiener process. The FPK equation ruling the joint PDF $p_{XY}(x,y,t)$ can be written as:

$$\frac{\partial p_{XY}(x,y,t)}{\partial t}=-\frac{\partial\left[yp_{XY}(x,y,t)\right]}{\partial x}+k\frac{\partial\left[xp_{XY}(x,y,t)\right]}{\partial y}+\frac{1}{2}\sigma^2\frac{\partial^2\left[p_{XY}(x,y,t)\right]}{\partial y^2}. \tag{5-87}$$

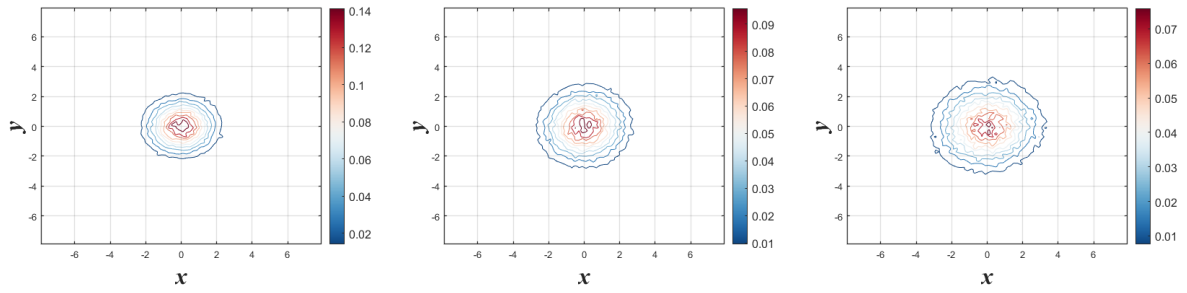

(a) (b) (c)

Figure 5-12 The distribution of systems when (a) $t=10$; (b) $t=15$; (a) $t=20$. $k=1, \sigma=0.1$

Figure 5-12 displays the distribution of system (5-86) when $t=10,15,20$. Assuming that $\left[\left(X_1(t),Y_1(t)\right),\left(X_2(t),Y_2(t)\right),...,\left(X_N(t),Y_N(t)\right)\right]$ are realizations of the random valuable at time t, the 2D-GCFM of this case in any quadrant can be obtained from the following equation:

$$E\left[\left|X(t)\right|^{\gamma_1-1}\left|Y(t)\right|^{\gamma_2-1}\right]=\frac{1}{N}\sum_{k=1}^{N}\left|X_k(t)\right|^{\gamma_1-1}\left|Y_k(t)\right|^{\gamma_2-1}. \tag{5-88}$$

The transient marginal PDFs are shown in Figure 5-13, where Figure 5-13(a-c) are the results of $p(x,t)$, Figure 5-13(d-f) are the results of $p(y,t)$.The dashed line and real line represent the results obtained from Monte Carlo Simulation and GCFM method, respectively. Here, we select $\rho_1=\rho_2=1.5, m_1=m_2=80, \Delta\eta_1=\Delta\eta_2=0.5$. Comparing the results, GCFM method displays the high accuracy in the reconstruction of the transient PDF of stochastic dynamic system. The transient joint PDFs constructed by MCS and GCFM method when $t=10,15,20$ is shown in Figure 5-14(a-c) and Figure 5-14 (d-f).

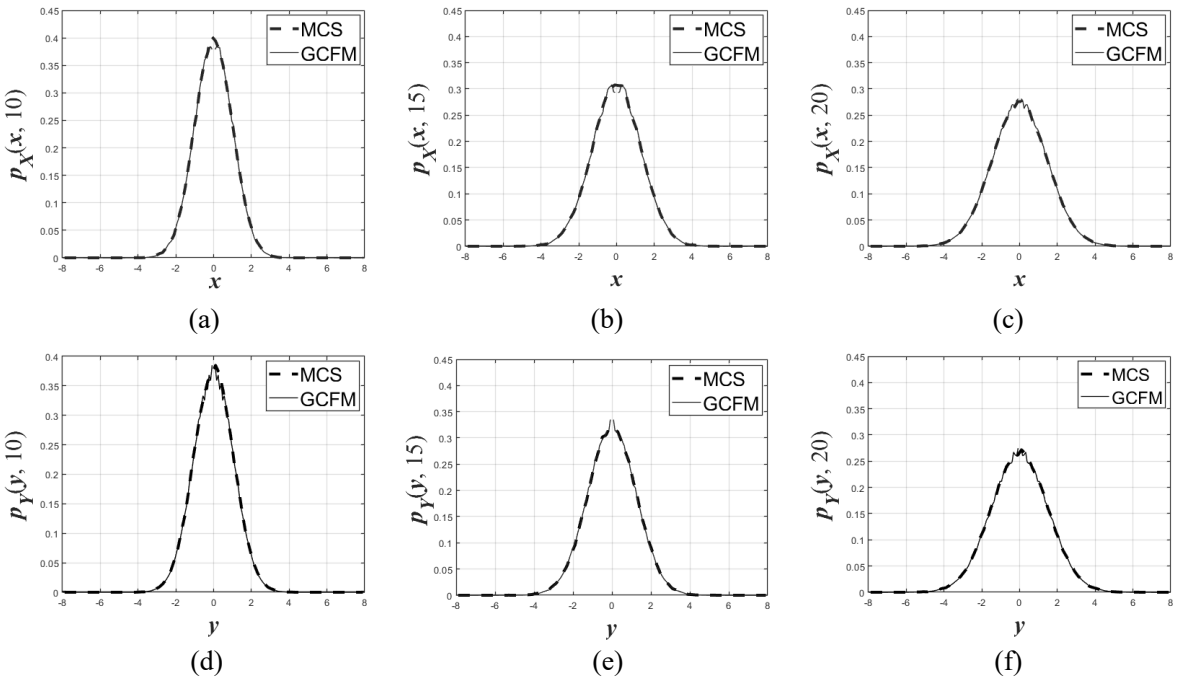

Figure 5-13 Transient marginal PDF of system. (a) $p_X(x,10)$; (b) $p_X(x,15)$; (c) $p_X(x,20)$; (d) $p_Y(y,10)$; (e) $p_Y(y,15)$; (f) $p_Y(y,20)$

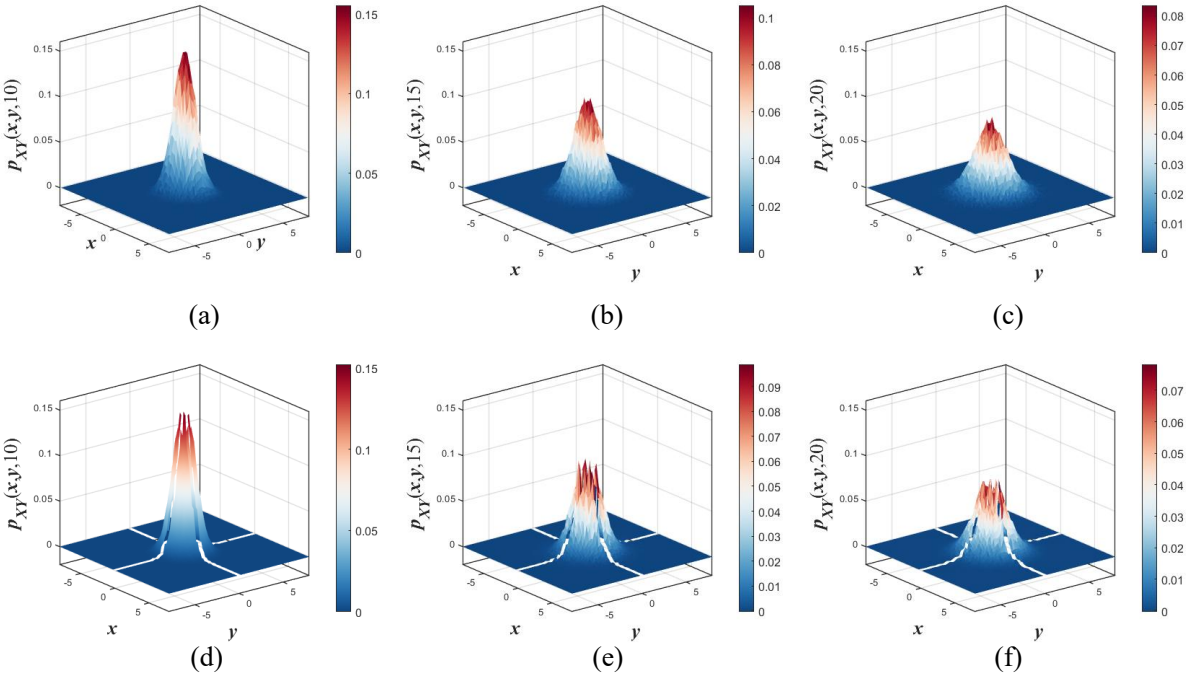

Figure 5-14 Transient joint PDF of system constructed by MCS when (a) $t=10$; (b) $t=15$; (c) $t=20$. GCFM when (d) $t=10$; (e) $t=15$; (f) $t=20$

5.7. Conclusion

This chapter introduces the concept of generalized complex fractional moments using the multi-dimensional Mellin integral transform, extending the theory to multi-dimensional scenarios. The equivalence between multi-dimensional probability density functions, multi-dimensional characteristic functions, and generalized complex fractional moments are established. This equivalence is further extended to the multi-dimensional real domain through function partitioning. Additionally, a method to construct marginal probability density functions using high-dimensional complex fractional moments is proposed, which is validated through a two-dimensional Gaussian distribution. Results indicate that in its integral form, the generalized complex fractional moment is fully equivalent to multi-dimensional probability density functions, while in its discrete form, increasing the truncation value significantly enhances computational accuracy. However, due to the singularity of Mellin transform at $x=0$, singularities in reconstructing the probability distribution at $x=0$ remain in multi-dimensional cases. A simple two-dimensional stochastic dynamic system is also used to verify the applicability of generalized complex fractional moments in engineering.

Chapter 6. Maximum entropy principle handled by using complex fractional moments

6.1. Introduction

Probability distributions are essential tools for quantifying the characteristics of random variables or stochastic processes. In dynamic systems, the presence of external or internal random factors makes constructing transient PDFs highly important for analyzing system behavior under stochastic perturbations. The transient PDF offers valuable insights into how the system evolves over time in response to randomness, helping to understand its probabilistic state at any given moment. However, deriving these PDFs, especially during the transient phase, remains a challenging problem in stochastic dynamics.

Traditional methods, such as Monte Carlo simulations, path integral methods [17, 134, 150, 151], Wiener path integral methods [19, 20, 152], finite element methods [24, 67], and finite difference methods [153], can be employed to solve the transient PDF of stochastic dynamic systems. These approaches typically allow for numerical or semi-analytical solutions. However, these methods often involve significant computational costs, especially for complex systems, and may require considerable resources to achieve high accuracy. Other methods, such as, probability evolution equation methods [77, 154-156], neural network methods [27, 157], provides a new perspective for obtaining transient probability of the system.

Since its inception, the CFM method has been proven to efficiently and accurately reconstruct probability density functions [84]. The theoretical framework has continually expanded [158] and been applied in various fields [91, 95, 96, 102, 106, 159-161]. For transient PDF reconstruction problems, the CFM method involves applying the Mellin transform to the FPK equation, and deriving the corresponding CFM equation. Traditionally, the CFM method reconstructs transient PDFs based on inverse Mellin transforms and sufficient CFM information. However, reconstructing PDFs with insufficient CFM data remains challenge.

The Maximum Entropy Principle [158] is widely applied in fields such as information theory [159], statistical mechanics [160], and probability theory [161]. Its key concept is deriving the most unbiased probability distribution under known constraints. By incorporating these constraints into the entropy function and optimizing it using the Lagrange multiplier method, the MEP produces an optimal probability distribution. While MEP with traditional integer or fractional moments constraints has been established, however, applying it to PDF reconstruction under CFM constraints has yet to be explored.

In this chapter, a new MEP method with CFM constraints is proposed, which can be applied for constructing the most unbiased probability distribution with few known CFM constraints. The MEP method is introduced in Section 6.2, and review the conception as well as the application of CFM in Section 6.3. In Section 6.4, the MEP with CFM constraints has been

established, which has been verified with numerical simulation, and compared with traditional CFM method, which has been applied for stochastic dynamic system for the reconstruction of transient PDFs in Section 6.5.

6.2. Maximum entropy principle

The Maximum Entropy Principle is a method used to infer the most unbiased probability distribution given limited information [162]. It is grounded in the concept of maximizing the Shannon entropy, subject to constraints provided by known data.

According to the MEP, for a stochastic process, its associated transient probability density function is represented as $p_X(x,t)$ is determined by the maximization of entropy functional. The entropy of this distribution can be expressed in the following form:

$$H\left(p_X(x,t)\right) = -\int p_X(x,t)\ln p_X(x,t)\,\mathrm{d}x. \tag{6-1}$$

Eq. (6-1) quantifies the uncertainty or randomness of the probability distribution $p_X(x,t)$ over time t, which under some assigned constraints. The normalization condition of $p_X(x,t)$ is

$$\int p_X(x,t)\,\mathrm{d}x = 1. \tag{6-2}$$

When maximizing the entropy function $H\left(p_X(x,t)\right)$, certain constraints must be satisfied. Typically, these constraints can be expressed in the form of the following integral equations:

$$\int F_k(x)\,p_X(x,t)\,\mathrm{d}x = \varphi_k(t), \quad k = 1,2,...,n \tag{6-3}$$

where $F_k(x)$ represents the functions characterizing the stochastic process. These constraints ensure that the reconstructed probability density function reflects the known properties of the stochastic process.

Noticing the constraints in Eq. (6-3) is time-varying, in this case, we consider the constraints of Eq. (6-1) at each fixed time t. Denoting $\lambda_k(t), k = 0,1,...,n$ as the Lagrange multipliers, and considering the entropy functional Eq. (6-1) and constraints (6-3), we may construct the extended entropy functional given as follows:

$$\begin{aligned}\tilde{H}\left(p_X(x,t),\lambda_0,\lambda_1,...,\lambda_m\right) = &-\int p_X(x,t)\ln p_X(x,t)\,\mathrm{d}x \\ &-\sum_{k=0}^{n}\lambda_k(t)\left[\int F_k(x)\,p_X(x,t)\,\mathrm{d}x - \varphi_k(t)\right].\end{aligned} \tag{6-4}$$

Based on the concave properties of the entropy functional, we can use differential operations to find its extremum points. By performing the variation with respect to $p_X(x,t)$, namely, $\partial\tilde{H}\left(p_X(x,t),\lambda_0,\lambda_1,...,\lambda_m\right)/\partial p = 0$, we can obtain

$$-\ln p_X(x,t)-1-\sum_{k=0}^{n}\lambda_k(t)F_k(x)=0, \tag{6-5}$$

namely,

$$p_X(x,t)=C(t)\exp\left(-\sum_{k=1}^{n}\lambda_k(t)F_k(x)\right). \tag{6-6}$$

By expressing

$$p_X(x,t)=C(t)\,p_X^{(1)}(x,t), \tag{6-7}$$

where

$$p_X^{(1)}(x,t)=\exp\left(-\sum_{k=1}^{n}\lambda_k(t)F_k(x)\right), \tag{6-8}$$

then we may find,

$$\int\exp\left(-\sum_{k=1}^{n}\lambda_k(t)F_k(x)\right)\mathrm{d}x=C^{-1}(t), \tag{6-9}$$

and

$$\int F_k(x)\,p_X^{(1)}(x,t)\,\mathrm{d}x=C^{-1}(t)\varphi_k(t), \tag{6-10}$$

where $C(t)$ is the normalization coefficient given as $C(t)=\exp\left(-\lambda_0(t)-1\right)$.

If the moments are available, then the function $F_k(x)$ can be expressed as x^k, and $\varphi_k(t)=m_k(t)=E\left[X^k(t)\right]$. Substituting Eq. (6-6) into Eq.(6-3), we have:

$$C(t)\int_{-\infty}^{\infty}p_X^{(1)}(x,t)\,x^k\mathrm{d}x=m_k(t)=E\left[X^k(t)\right],k=1,2,...,n, \tag{6-11}$$

The MEP may be applied under some limitations:

1) The integer moments must be constrained up to a certain order n. It follows that for $\alpha-$stable random variables $(0<\alpha<2)$ in which the moments of higher order than 2 do not exist, as a consequence, the MEP may not be applied for $\alpha-$stable distribution.
2) By solving the set of nonlinear algebraic Eq. (6-11) in the unknown $\lambda_k(t)$, in some case, the MEP with classical constraints involving integer moment could be invalid.

6.3. The complex fractional moment

In this section, the concept of CFM based on the Mellin transform is briefly introduced, an example is given to explain the existence condition.

6.3.1 The concept of complex fractional moment

Based on the Mellin transform, the complex fractional moments (CFMs) is defined in the positive domain as $E\left[X^{\gamma-1}\right]$, $\gamma=\rho+i\eta$, i represents the imaginary unit. Supposing $p_X(x,t)$ is defined in the range $x\geq 0$, then the Mellin transform of $p_X(x,t)$ is defined as:

$$M(\gamma-1,t)=\mathcal{M}\{p_X(x,t);\gamma-1\}=\int_0^{\infty}p_X(x,t)x^{\gamma-1}\mathrm{d}x=E\left[X^{\gamma-1}\right], \tag{6-12}$$

where $\mathcal{M}\{\bullet\}$ represents the Mellin transform operator. The Mellin transform of the PDF exist provided ρ belong to the so called Fundamental Strip (FS) of the Mellin transform. Usually, the FS, namely the existence of the Mellin transform is defined as $-p<\rho<-q$, where p and q depend on the order of $p_X(x,t)$ at $x=0$ and $x=\infty$, namely,

$$\lim_{x\to 0}p_X(x)=\mathcal{O}\left(x^{p}\right);\quad \lim_{x\to\infty}p_X(x)=\mathcal{O}\left(x^{q}\right). \tag{6-13}$$

Where $\mathcal{O}(\bullet)$ means of the order of the term in parenthesis. The existence of the FS is guarantee from the fact that $p_X(x)\geq 0$ and it is a finite quantity (for symmetric distribution and for every distribution defined in $0\leq x<\infty$). Such an example for the stable symmetric Cauchy distribution, of which the PDF is:

$$p_X(x)=\frac{\sigma}{\pi\left(x^2+\sigma^2\right)}, \tag{6-14}$$

with σ represents the scale factor. The FS is $p=0, q=-2$, it follows that the FS is $0<\rho<2$. This means that the moment more than second order of the Cauchy distribution does not exists.

If ρ belongs to the FS, then $p_X(x,t)$ can be reconstructed by using inverse Mellin transform, which can be expressed as follows:

$$p_X(x)=\mathcal{M}^{-1}\{M(\gamma-1);x\}=\frac{1}{2\pi i}\int_{\rho-i\infty}^{\rho+i\infty}E\left[X^{\gamma-1}\right]x^{-\gamma}\mathrm{d}\gamma. \tag{6-15}$$

Eq. (6-15) can also be written as:

$$p_X(x)=\frac{1}{2\pi}\int_{-\infty}^{\infty}E\left[X^{\gamma-1}\right]x^{-\gamma}\mathrm{d}\eta. \tag{6-16}$$

The discretized form of Eq. (6-16) can be written as:

$$p_X(x)=\frac{\Delta\eta}{2\pi}\sum_{k=-m}^{m}E\left[X^{\gamma_k-1}\right]x^{-\gamma_k}$$
$$=\frac{x^{-\rho}}{2b}\left(E\left[X^{\rho-1}\right]+2\sum_{k=1}^{m}\left(\mathrm{Re}\left(E\left[X^{\gamma_k-1}\right]\right)\cos\left(\eta_k\ln x\right)+\mathrm{Im}\left(E\left[X^{\gamma_k-1}\right]\right)\sin\left(\eta_k\ln x\right)\right)\right) \tag{6-17}$$

Where $b=\pi/\Delta\eta$, $\mathrm{Re}(\bullet)$ and $\mathrm{Im}(\bullet)$ represent the real part and imaginary part of the term on parenthesis, respectively.

6.3.2 The application of complex fractional moment

The CFM method can be applied to obtain the probability density function (PDF) of the stochastic dynamic system. For a stochastic dynamic system, which is expressed as follow:

$$\ddot{X}(t)+f\left(X(t),\dot{X}(t)\right)=\sum_{i=1}^{n}g_i(x,\dot{x})W_i(t), \tag{6-18}$$

where $W_i(t)$ are uncorrelated zero-mean normal white noise, of which the correlation function is:

$$\begin{aligned}&\mathrm{R}_{w_iw_i}(t_1,t_2)=E\left[W_i(t_1)W_i(t_2)\right]=q\delta(t_2-t_1),\\&\mathrm{R}_{w_iw_j}(t_1,t_2)=E\left[W_i(t_1)W_j(t_2)\right]=0,\end{aligned} \tag{6-19}$$

and $f\left(X(t),\dot{X}(t)\right)$ is a nonlinear function $X(t)$. Applying the stochastic averaging method, the FPK equation ruling the evolution of the amplitude PDF is given as:

$$\begin{cases}\dfrac{\partial}{\partial t}p_A(a,t)=-\dfrac{\partial}{\partial x}\left[\bar{m}(a)\,p_A(a,t)\right]+\dfrac{1}{2}\dfrac{\partial^2\left[\bar{\sigma}^2(a)\,p_A(a,t)\right]}{\partial a^2},\\ p_A(a,0)=p_{A_0}(a),\end{cases} \tag{6-20}$$

where $\bar{m}(a)$ and $\bar{\sigma}^2(a)$ represent the drift and diffusion term, respectively, and the boundary conditions are expressed as follows:

$$\lim_{a\to0}p_A(a,t)\to0;\quad\lim_{a\to\infty}p_A(a,t)\to0;\quad\lim_{a\to\infty}\frac{\partial}{\partial a}p_A(a,t)\to0. \tag{6-21}$$

Multiplying the both sides of Eq. (6-20) by $x^{\gamma-1}$, and integrating in the range $(0,\infty)$, we can obtain:

$$\begin{aligned}\frac{\mathrm{d}M_p(\gamma-1,t)}{\mathrm{d}t} &= -\left[\bar{m}(a)a^{\gamma-1}p_A(a,t)\right]\Big|_0^\infty + (\gamma-1)\int_0^\infty a^{\gamma-2}p_A(a,t)\mathrm{d}a \\ &+ \frac{1}{2}\left[\frac{\partial\left[\bar{\sigma}^2(a)\,p_A(a,t)\right]}{\partial a}a^{\gamma-1}\right]\Big|_0^\infty \\ &- \frac{1}{2}\left[(\gamma-1)a^{\gamma-2}\bar{\sigma}^2(a)\,p_A(a,t)\right]\Big|_0^\infty \\ &+ \frac{1}{2}(\gamma-1)(\gamma-2)\int_0^\infty a^{\gamma-3}\bar{\sigma}^2(a)\,p_A(a,t)\mathrm{d}a.\end{aligned} \tag{6-22}$$

Considering the boundary conditions, and vanishing the first, third, and fourth term of the right side of Eq. (6-22), we can obtain the complex fractional moments equation as follows:

$$\frac{\mathrm{d}M_p(\gamma-1,t)}{\mathrm{d}t} = (\gamma-1)\int_0^\infty a^{\gamma-2}p_A(a,t)\mathrm{d}a + \frac{1}{2}(\gamma-1)(\gamma-2)\int_0^\infty a^{\gamma-3}\bar{\sigma}^2(a)\,p_A(a,t)\mathrm{d}a. \tag{6-23}$$

With the normalized conditions, Eq. (6-23) can be solved directly.

At this stage, some comments may be drawn:

1) With limited number of CFMs, the PDF of the random variables, or random process may be reconstructed, including the case of $\alpha-$stable distribution.
2) The CFM method can be applied for reconstructing the PDF by deriving the CFM equation using the FPK equation.
3) By solving the ODEs governing the CFM, a set of $2m+1$ CFMs can be obtained at any time t.

6.4. MEP handled by CFM

Let us assume that the enlarged functional $\tilde{H}\left(p_X(x,t),\lambda_{-m},...,\lambda_0,...,\lambda_m\right)$ is constructed by the unconstrained functional $H\left(p_X(x,t)\right)$, according to the Lagrange multiplier method with the constraints (known quantities) are the CFM instead of the integer moments, in this case:

$$\begin{aligned}&\tilde{H}\left(p_X(x,t),\lambda_{-m},...,\lambda_0,...,\lambda_m\right) \\ &= -\int_0^\infty p_X(x,t)\ln p_X(x,t)\mathrm{d}x - \sum_{k=-m}^{m}\lambda_k\left[\int_0^\infty p_X(x,t)x^{\gamma_k-1}\mathrm{d}x - E\left[X^{\gamma_k-1}\right]\right] \\ &= \max_{p_X(x,t),\lambda_{-m},...,\lambda_0,...,\lambda_m},\end{aligned} \tag{6-24}$$

where $\lambda_{-m},...,\lambda_m$ are complex Lagrange multiplier.

By noting that $p_X(x,t)\in\mathbb{R}^+$ and reconstruct the complex term as following:

$$E\left[X^{\gamma_k-1}\right] = A_{p_X}^{\mathcal{M}}(\gamma_k) + iB_{p_X}^{\mathcal{M}}(\gamma_k), \quad x^{\gamma_k-1} = x^{\rho-1}\left(\cos(\eta_k\ln x) + i\sin(\eta_k\ln x)\right), \tag{6-25}$$

the enlarged function may be rewritten as

$$\begin{aligned}
&\tilde{H}\left(p_X(x,t),\lambda_0,\lambda_1...,\lambda_m\right)\\
&=-\int_0^\infty p_X(x,t)\ln p_X(x,t)\,\mathrm{d}x\\
&\quad-\sum_{k=-m}^{m}\lambda_k\left[\int_0^\infty p_X(x,t)\,x^{\rho-1}\cos\left(\eta_k\ln x\right)\mathrm{d}x-A_{p_X}^{\mathcal{M}}(\gamma_k)\right]\\
&\quad-i\sum_{k=-m}^{m}\lambda_k\left[\int_0^\infty p_X(x,t)\,x^{\rho-1}\sin\left(\eta_k\ln x\right)\mathrm{d}x-B_{p_X}^{\mathcal{M}}(\gamma_k)\right]\\
&=\max_{p_X(x,t),\lambda_{-m},...,\lambda_0,...,\lambda_m}
\end{aligned}\tag{6-26}$$

By performing derivatives to $p_X(x,t)$, we get the approximate PDF of $p_X(x,t)$ as follow, which is denoted as $\hat{p}_X(x,t)$:

$$\hat{p}_X(x,t)=\exp\left\{-\lambda_e-\sum_{k=-m}^{m}x^{\rho-1}\left[\lambda_k^R\cos\left(\eta_k\ln x\right)-\lambda_k^I\sin\left(\eta_k\ln x\right)\right]\right\},\tag{6-27}$$

where λ_e is a normalized coefficient, λ_k^R and λ_k^I are the real part and imaginary part of λ_k, which satisfy:

$$\lambda_k^R=\lambda_{-k}^R;\quad \lambda_k^I=-\lambda_{-k}^I;\quad \lambda_0^I=0.\tag{6-28}$$

Thus, Eq.(6-27) can also be rewritten as:

$$\hat{p}_X(x,t)=\exp\left\{-\lambda_e-\lambda_0^R x^{\rho-1}-2\sum_{k=1}^{m}x^{\rho-1}\left[\lambda_k^R\cos\left(\eta_k\ln x\right)-\lambda_k^I\sin\left(\eta_j\ln x\right)\right]\right\}.\tag{6-29}$$

With m CFMs of $X(t)$, the optimization value of $\left[\lambda_e,\lambda_0^R,\lambda_1^R,...,\lambda_m^R,\lambda_1^I,...,\lambda_m^I\right]$ may be found by following constrained equations:

$$\begin{cases}
\text{Minimize}:\sum_j {}_R E_j^2+{}_I E_j^2\\
\text{subject to}:\ {}_R E_j=A\left(\rho,\eta_j\right)-\int_0^\infty \hat{p}_X(x,t)\,x^{\rho-1}\cos\left(\eta_j\ln x\right)\mathrm{d}x,\\
\qquad\qquad {}_I E_j=B\left(\rho,\eta_j\right)-\int_0^\infty \hat{p}_X(x,t)\,x^{\rho-1}\sin\left(\eta_j\ln x\right)\mathrm{d}x,\\
\qquad\qquad \int_0^\infty \hat{p}_X(x,t)\,\mathrm{d}x=1,
\end{cases}\tag{6-30}$$

It is worth noticing to observe that m is the number of the multiplier that depend on the number of the constraints that we impose in the enlarged functional.

In order to quantify the discrepancy of the $\hat{p}_X(x,t)$ from $p_X(x,t)$, we introduce the L_2 norm as follow:

$$L_2\left(\hat{p},p\right)=\left\{\int_\Omega\left[\hat{p}(x,t)-p(x,t)\right]^2\mathrm{d}x\right\}^{\frac{1}{2}}.\tag{6-31}$$

and also the Kullback-Leibler (KL) measure of the discrepancy [163], denoted as:

$$KL\left(\hat{p},p\right)=\int_{\Omega}\hat{p}\left(x,t\right)\log\left(\frac{\hat{p}\left(x,t\right)}{p\left(x,t\right)}\right)\mathrm{d}x. \tag{6-32}$$

6.5. Numerical simulations

In this section, we validate the accuracy of proposed method in last section with two kinds of distribution, and the discrepancy is quantified by using L_2 norm and KL measure.

6.5.1 Example 1

Firstly, we discuss the feasibility of MEP method with CFM constraint in Gaussian distribution, of which the value is not zero at $x=0$. The Gaussian distribution is expressed as follow:

$$p_X\left(x\right)=\frac{1}{\sqrt{2\pi}\sigma}e^{-\frac{\left(x-\mu\right)^2}{2\sigma^2}}, \tag{6-33}$$

and the CFM expression of Eq. (6-33) is written as following:

$$M\left(\gamma-1\right)=\frac{1}{\sqrt{2\pi}}2^{\frac{\gamma}{2}-1}\sigma^{\gamma-1}\left(\Gamma\left(\frac{\gamma}{2}\right){}_1F_1\left(\frac{1-\gamma}{2},\frac{1}{2},-\frac{\mu^2}{2\sigma^2}\right)+\frac{\sqrt{2}\mu}{\sigma}\Gamma\left(\frac{1+\gamma}{2}\right){}_1F_1\left(1-\frac{\gamma}{2},\frac{3}{2},-\frac{\mu^2}{2\sigma^2}\right)\right), \tag{6-34}$$

According to the objective function and constraint equations expressed in Eq. (6-30), we can obtain the optimal value of λ_k. Table 6-1 exhibits the optimal parameters in Eq. (6-29), Table 6-2 displays the discrepancy of MEP method and classical CFM with 2,4,6 CFM values. Figure 6-1 exhibits the reconstructed distribution with classical CFM method and MEP method.

Table 6-1 Optimal parameters with different m and discrepancy when $\mu=0$, $\sigma=1$

Parameter	$m=2$	$m=4$	$m=6$
λ_e	2.0884	2.1042	1.7536
λ_0	0.3894	0.1921	1.1195
λ_1	0.1271 - 3.8911i	0.1014 - 3.8831i	0.0152 - 3.0048i
λ_2	-0.6750 + 1.2470i	0.2384 + 1.4459i	-0.0496 - 0.0150i
λ_3	--	-0.5365 - 0.4444i	-1.7425 + 0.5340i
λ_4	--	0.2308 + 0.2635i	1.4332 + 0.4230i
λ_5	--	--	-0.4557 - 0.3842i
λ_6	--	--	0.0738 + 0.0852i

Table 6-2 L_2 norm and KL discrepancy $\mu=0$, $\sigma=1$

	Divergence	$m=2$	$m=4$	$m=6$
MEP	$L_2(\hat{p},p)$	0.0195	0.0091	0.0032
	$KL(\hat{p},p)$	0.0187	0.0086	0.0024
CFM	$L_2(\hat{p},p)$	1.8167	1.1378	0.2184
	$KL(\hat{p},p)$	1.8551	0.8549	0.1898

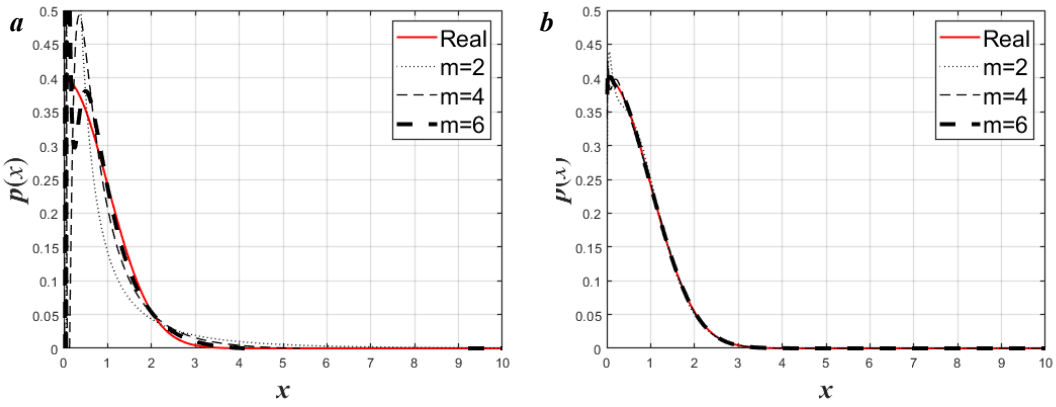

Figure 6-1 The exact PDF and the PDF reconstructed with (a) CFM method; (b) MEP method

Table 6-3 displays the optimal parameters when $\sigma=1.5$, and Table 6-4 exhibits the related discrepancy of MEP and classical CFM method. Figure 6-2 show the reconstructed distribution using CFM method and MEP method when $m=2,4,6$.

Table 6-3 Optimal parameters with different m and discrepancy when $\mu=0$, $\sigma=1.5$

Parameter	$m=2$	$m=4$	$m=6$
λ_e	2.5233	4.3466	2.0008
λ_0	-0.5194	-2.1599	0.0868
λ_1	0.0292 - 3.0640i	2.2019 -12.2869i	0.2665 - 2.1503i
λ_2	-0.2724 + 1.1067i	-5.6055 + 8.0799i	-0.4851 + 0.3483i
λ_3	--	4.1561 - 1.8729i	-0.3724 + 0.3543i
λ_4	--	-1.0852 - 0.0464i	0.3734 - 0.0013i
λ_5	--	--	-0.0266 - 0.0349i
λ_6	--	--	-0.0269 - 0.0206i

Table 6-4 L_2 norm and KL discrepancy $\mu=0$, $\sigma=1.5$

	Divergence	$m=2$	$m=4$	$m=6$
MEP	$L_2(\hat{p},p)$	0.0169	0.0111	0.0045
	$KL(\hat{p},p)$	0.0204	0.0143	0.0025
CFM	$L_2(\hat{p},p)$	0.2831	1.3762	0.731
	$KL(\hat{p},p)$	1.4489	0.9866	0.463

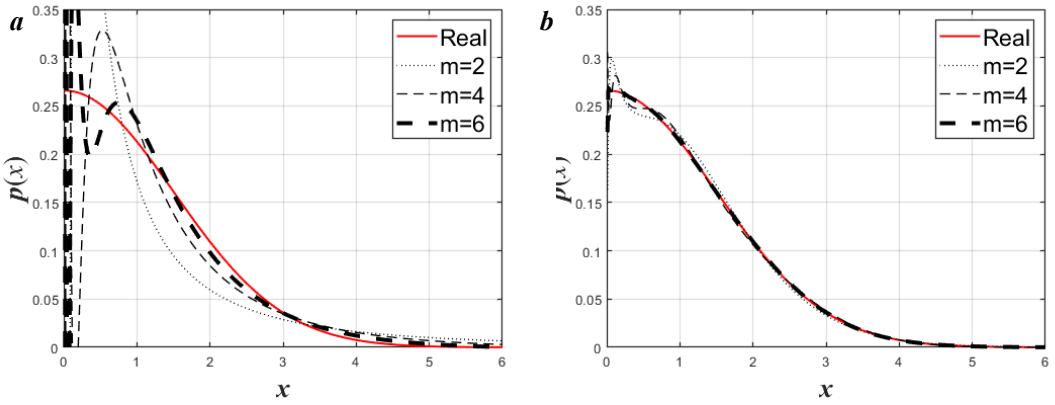

Figure 6-2 The exact PDF and the PDF reconstructed with (a) CFM method; (b) MEP method

6.5.2 Example 2

Due to the MEP method based on the exponential-type function, namely $\exp(\bullet)$, of which the value is not zero when $x=0$. Here, we discuss the feasibility of MEP method with exponential distribution, which expressed as follows:

$$p_X(x)=xe^{-\nu x}, \tag{6-35}$$

of which the CFM is:

$$M(\gamma-1)=\nu^{-1-\gamma}\Gamma(\gamma+1), \tag{6-36}$$

where $\Gamma(\bullet)$ represents the Euler Gamma function.

According to the objective function and constraint equations expressed in Eq.(6-30), we can obtain the optimal value of λ_k. Table 6-5 and Table 6-6 displays the parameters and the divergence of MEP method and CFM method when $\nu=1$, and Table 6-7 and Table 6-8 displays the parameters and the divergence of MEP method and CFM method when $\nu=1.5$. Figure 6-3 and Figure 6-4 display the exact and reconstructed PDF by using CFM method and MEP method.

Table 6-5 Optimal parameters with different m and discrepancy when $\nu = 1$

Parameter	$m = 2$	$m = 4$	$m = 6$
λ_e	4.683	2.746	3.89
λ_0	4.663	2.776	3.8236
λ_1	-4.826+2.283i	-1.436+1.93i	-3.245+2.97i
λ_2	0.65-1.21i	-1.526-0.525i	-0.484-1.878i
λ_3	--	0.789-0.68i	0.315+0.358i
λ_4	--	-0.085+0.305i	0.093-0.293i
λ_5	--	--	-0.0054+0.282i
λ_6	--	--	-0.0345-0.09i

Table 6-6 L_2 norm and KL discrepancy $\nu = 1$

	Divergence	$m = 2$	$m = 4$	$m = 6$
MEP	$L_2(\hat{p}, p)$	0.0214	0.0073	0.0028
	$KL(\hat{p}, p)$	0.0434	0.0145	0.0057
CFM	$L_2(\hat{p}, p)$	0.2306	0.0826	0.0275
	$KL(\hat{p}, p)$	0.5732	0.159	0.05

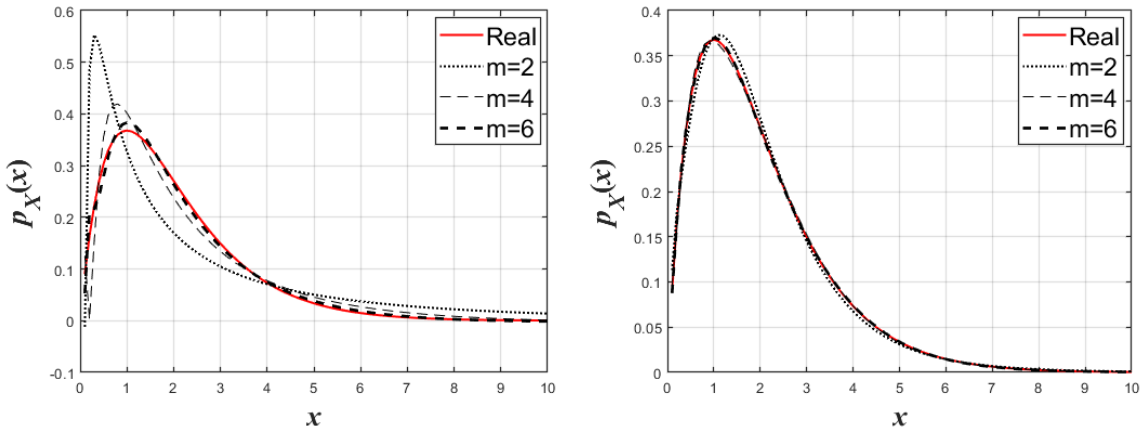

Figure 6-3 The exact PDF and the PDF reconstructed with (a) CFM method; (b) MEP method

Table 6-7 Optimal parameters with different m and discrepancy when $\nu = 1.5$

Parameter	$m=2$	$m=4$	$m=6$
λ_e	5.1332	3.02	3.5375
λ_0	4.9614	2.920.3	3.5375
λ_1	-4.5067-3.2742i	-1.0714-1.99i	-0.27+0.038i
λ_2	0.1883+1.4088i	-1.4977-0.35i	0.71+0.073i
λ_3	--	0.1566+1.143i	-0.61-0.091i
λ_4	--	0.1995-0.3057i	0.38-0.494i
λ_5	--	--	-0.65-0.098i
λ_6	--	--	-2.46+1.8i

Table 6-8 L_2 norm and KL discrepancy $\nu = 1.5$

	Divergence	$m=2$	$m=4$	$m=6$
MEP	$L_2(\hat{p}, p)$	0.0115	0.0073	0.0044
	$KL(\hat{p}, p)$	0.0193	0.0145	0.0063
CFM	$L_2(\hat{p}, p)$	0.1245	0.0478	0.0152
	$KL(\hat{p}, p)$	0.349	0.0964	0.0362

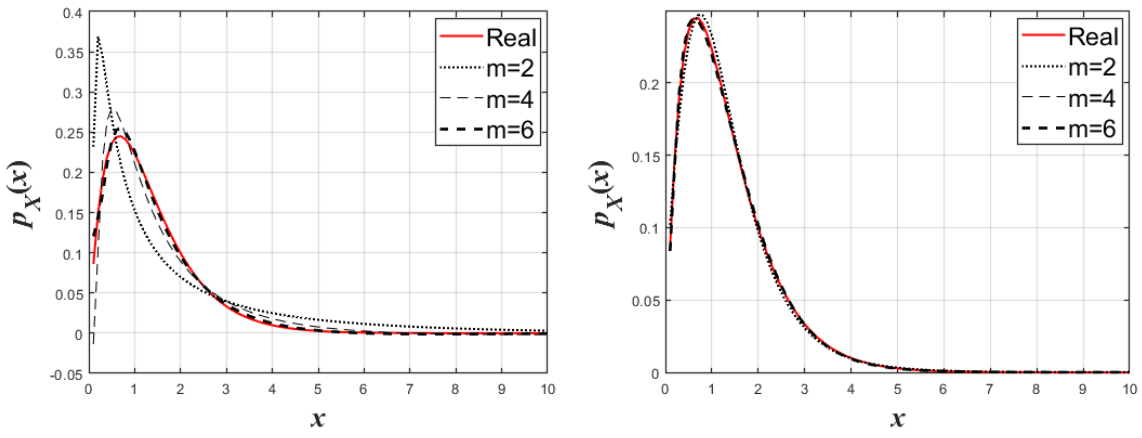

(a) (b)

Figure 6-4 The exact PDF and the PDF reconstructed with (a) CFM method; (b) MEP method

According to the results, some comments can be drawn:

1. The MEP with CFM constrains can also reconstruct the PDF by finding the optimal parameters;
2. Compared with the reconstruction by CFM method directly, the MEP with CFM constrains method can reconstruct the PDF with less complex quantities and with more accuracy;
3. With any certain complex quantities, the MEP with CFM constraints can reconstruct the

probability distribution, which means if we obtain the CFM by the CFM equations (Eq. (6-23)), the PDF can also be reconstructed, this provide a possible to construct the transient PDF of a stochastic dynamic systems. That will be discussed in the next section.

6.6. Solution of the FPK equation by MEP with CFM constraints

In the previous sections, we explored the MEP with CFM constraints, demonstrating that this approach can reconstruct the PDF with fewer complex parameters and higher accuracy. In this section, we will extend the application of MEP with CFM constraints to derive the transient PDF of stochastic dynamic systems, examining its effectiveness in capturing the evolving probabilistic behavior over time in such systems.

Considering a system as follows [85]:

$$\ddot{X}+\left(c_1+c_2X^2\right)\dot{X}+\omega^2X=\left(e_1+e_2X\right)W\left(t\right), \tag{6-37}$$

where c_1 and c_2 represents the coefficients of linear and nonlinear damping, $W\left(t\right)$ is the Gaussian white noise of whose intensity of noise is $2D$. Appling the stochastic averaging method, we can obtain the FPK equation governing the transient PDF, and introducing the Mellin transform, we can derive the ODEs governing the CFM as follows:

$$\begin{aligned}\frac{\mathrm{d}M_{p_X}\left(\gamma_s-1,t\right)}{\mathrm{d}t}=&\left(-\frac{c_1}{2}\left(\gamma_s-1\right)+\frac{e_2^2D}{8\omega^2}\left(\gamma_s-1\right)\left(\gamma_s+1\right)\right)M_{p_X}\left(\gamma_s-1,t\right)\\&-\frac{c_2}{8}\left(\gamma_s-1\right)M_{p_X}\left(\gamma_s+1,t\right)+2\frac{e_1^2D}{8\omega^2}\left(\gamma_s-1\right)^2M_{p_X}\left(\gamma_s-3,t\right),\end{aligned} \tag{6-38}$$

here $s=-m,...,-1,0,1,...,m$. Eq. (6-38) can be solved by using the following normalization conditions:

$$M_{p_X}\left(\gamma_s-1+\Delta\rho,t\right)=\frac{1}{2b}\sum_{k=-m}^{m}M_{p_X}\left(\gamma_s-1,t\right)c_{ks}\left(-\Delta\rho\right). \tag{6-39}$$

Based on Eq. (6-38) and (6-39), we can obtain the CFMs at any time t, and applying the MEP method mentioned in the previous section, the PDF can be reconstructed. The parameters selected in this section as follows:

Table 6-9 Parameters

Parameter	Values	Parameter	Values
c_1	0.01	c_2	0.01
e_1	1	e_2	1
D	0.01	ω	1
ρ	2.1	$\Delta\eta$	0.5
m	50		

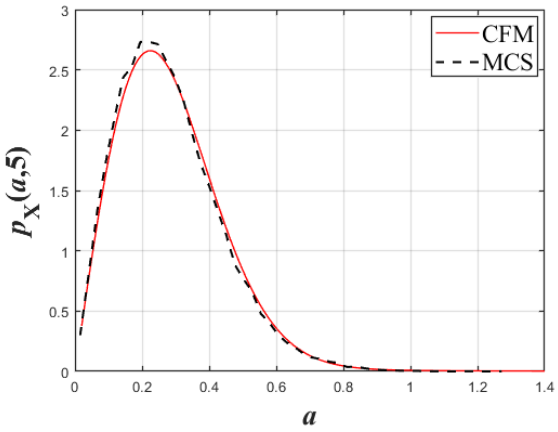

Figure 6-5 The transient PDF reconstructed by CFM method and MCS method when $t=5$, $m=50$

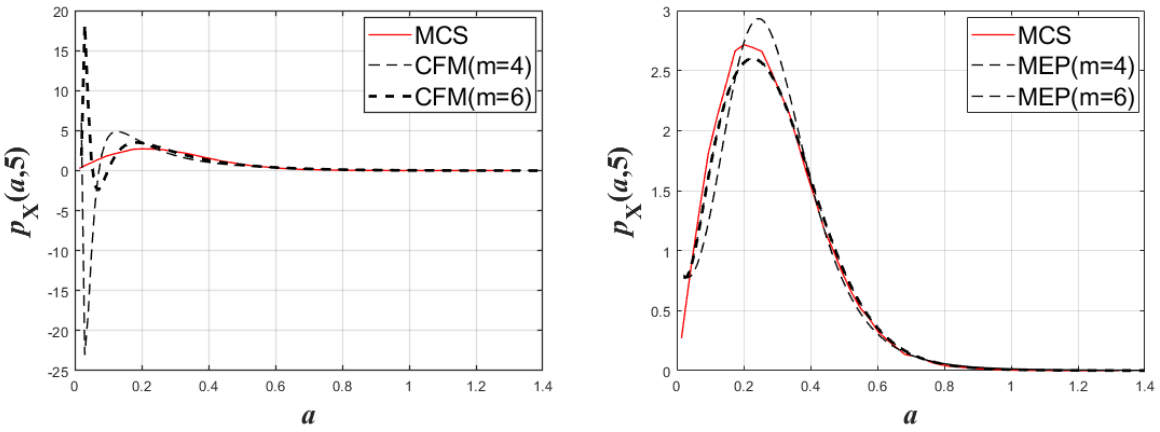

(a) (b)

Figure 6-6 Reconstruction of transient PDF by (a) CFM method, (b) MEP method when $t=5$

Figure 6-5 presents the transient PDF of system (6-37) obtained using the Monte Carlo Simulation, alongside the results from the CFM method with a truncation parameter of $m = 50$, $\Delta\eta = 0.5$. Figure 6-6 illustrates the transient PDFs computed using the CFM and MEP methods for truncation parameters $m = 4$ and 6. The results indicate that while the traditional CFM method effectively reconstructs the transient PDF with a large truncation parameter, its accuracy diminishes with smaller values of m. In contrast, the MEP method constrained by CFM demonstrates superior performance in reconstructing the transient PDF under reduced truncation conditions. Table 6-10 displays the value of Lagrange multipliers λ_i when $m = 4$ and 6.

Table 6-10 Optimal parameters with different m

Parameter	$m=4$	$m=6$
λ_e	0.1827	0.204
λ_0	0.2245	0.2452
λ_1	0.1873-0.8204i	0.1418-1.6597i
λ_2	0.0639-1.2113i	0.1777-1.4225i
λ_3	0.5417-0.5258i	0.8517+0.0466i
λ_4	1.1006+0.848i	0.8449+0.7436i
λ_5	--	-0.3419+0.3377i
λ_6	--	0.4371-0.5413i

Figure 6-7 presents the computational results for noise intensity D = 0.1 at different truncation parameters m = 4 and m = 6, when t = 10. Figure 6-7(a) and Figure 6-7(b) show the transient PDF obtained using the CFM method and the MEP method, respectively. The results indicate that, under high noise intensity, the traditional CFM method exhibits significant errors with small truncation values. In contrast, the MEP method, constrained by fewer CFMs, proves more effective for reconstructing the system's transient PDF. Table 6-11 displays the value of Lagrange multipliers λ_i when m = 4 and 6.

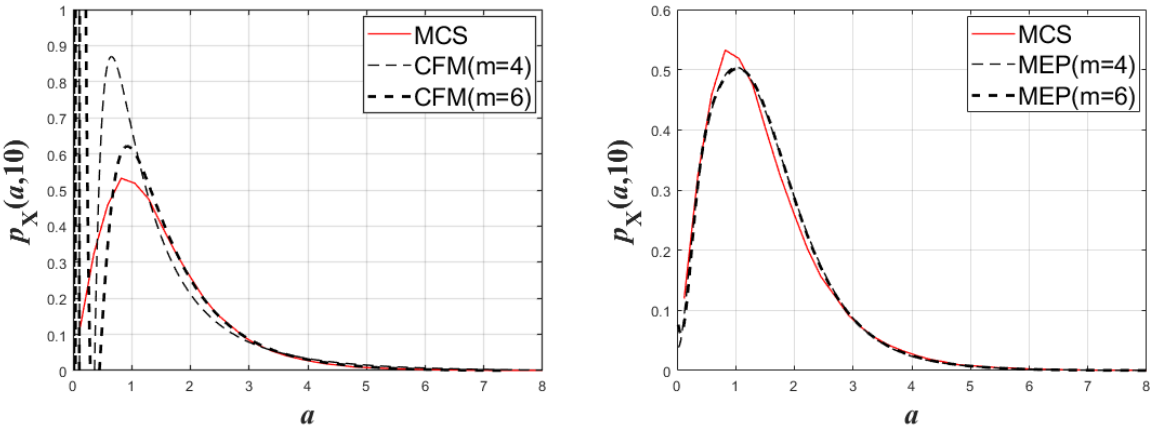

(a) (b)

Figure 6-7 Reconstruction of transient PDF by (a) CFM method; (b) MEP method when $D=0.1$

Table 6-11 Optimal parameters with different m

Parameter	$m=4$	$m=6$
λ_e	3.1909	2.5758
λ_0	-1.4162	-0.3136
λ_1	-0.31-1.8696i	-0.41-0.1447i
λ_2	-1.9345-0.0048i	-0.6883-0.2909i
λ_3	2.2818-1.0247i	-0.1788-0.5131i
λ_4	-0.582+0.574i	0.2604-0.5815i
λ_5	--	0.4957+0.5076i
λ_6	--	-0.2752+0.0013i

6.6. Conclusion

In this chapter, a novel Maximum Entropy Principle method constrained by CFMs is introduced. By incorporating CFM constraints, the PDF approximation is derived using complex Lagrange multipliers. The method decomposes the CFMs into their real and imaginary components, establishing constraints for the complex Lagrange multipliers and deriving an entropy constraint equation in complex form. Numerical examples show that this approach achieves higher accuracy than traditional CFM methods, even with limited moment information. Furthermore, the method is applied to transient PDFs in stochastic dynamic systems, demonstrating its effectiveness in scenarios with minimal moment data.

Chapter 7. Conclusions and outlooks

7.1. Conclusions

Nonlinear dynamic systems are essential mathematical models for describing activities based on mechanical principles. When combined with randomness, these systems reveal deeper insights into the physical world. However, due to the inherent unpredictable of stochastic dynamic systems, traditional trajectory-based methods are limited. In contrast, probability analysis based on statistical characteristics is advantageous. The Mellin integral transform maps probability density functions to complex fractional moments, establishing equivalence between these moments and probability characteristics within the framework of integral transforms and fractional calculus. This equivalence is efficient for reconstructing probability characteristics from discrete sequences, while avoiding periodic fluctuations caused by traditional transforms.

This thesis combined probability theory and integral transform theory to develop and refine the theory of complex fractional moments. The theory is applied to the transient analysis of stochastic dynamic systems under different theoretical frameworks. The main contributions and conclusions are as follows:

1. A method for conducting transient analysis of complex fractional moments in stochastic Hamiltonian systems is proposed. By using stochastic averaging of generalized displacement and momentum equations under Gaussian white noise, the FPK equation governing the probability density of the Hamiltonian function is derived. A polynomial approximation for implicit drift terms and applied the Mellin transform to derive associated non-homogeneous linear ODEs. Numerical simulations demonstrated the method's accuracy and efficiency. The results show that increasing the polynomial parameters reduces system divergence, while increases in external and internal noise, along with higher initial values, amplify divergence.

2. The application of complex fractional moments to reconstruct the probability evolution function of stochastic dynamic systems with Caputo-type fractional derivatives under random excitation is explored. Normalized differential equations for probability evolution reconstruction are formulated, along with advanced methods for stochastic reliability analysis using complex fractional moments. The effects of parameters on probability evolution and reliability are examined by analyzing the probability density function, first passage time, and reliability functions. For nonlinear stochastic dynamic systems with internal and external Gaussian noise, our method, using a discrete parameter $m=120$, achieved an average error below 0.01, satisfying precision requirements across different parameters. Increased noise intensity D_1 and D_2 heightened system divergence, while changes in the fractional order α had minimal effects. The effects of inherent and disturbance parameters on system bifurcation evolution are also studied, noting that increased polynomial parameter β and external noise strength D_1 accelerated bifurcation, while increased fractional parameter μ delayed the

final state. From a reliability perspective, changes in μ and D_1 significantly affected the reliability function and first passage time.

3. In the Laplace context, the concept of exponential configuration of complex fractional moments, or shifted characteristic functions is introduced, and a theoretical framework for probability reconstruction is established. Utilizing the orthogonality of complex exponential functions, shifted characteristic function switch equations is established. The double-sided Laplace transform is defined to extend these theories to the full real domain, and relevant methods for transient probability analysis are developed. Results demonstrate that, within the probability space, shifted characteristic functions and double-sided Laplace transforms are equivalent to probability density functions, avoiding singularity at the origin in power-type complex fractional moments. In discrete terms, a negative correlation between period and step size can lead to false signal issues, which can be mitigated by selecting an appropriate step size. The feasibility of this theory was validated through its application in reconstructing probabilities for differential equations and FPK equations. Comparative analysis revealed that shifted characteristic functions and complex fractional moments are respectively preferable for exponential and power-type drift term FPK equation probability reconstructions.

4. The framework of complex fractional moments was extended to multidimensional spaces, establishing a data-driven method for probability evolution analysis of multidimensional stochastic dynamic systems. Through the introduction of multidimensional integral transforms and fractional calculus in probability space, generalized complex fractional moments are defined on the positive real domain, and their equivalence to multidimensional probability characteristics is established. This equivalence is further extended to multidimensional real spaces through spatial partitioning. Marginal integrals confirmed the equivalence between generalized complex fractional moments and marginal probability densities. The results show that in discrete states, generalized complex fractional moments in multidimensional spaces accurately construct symmetric, asymmetric, and marginal probability densities. Additionally, a method using generalized complex fractional moments for data-driven probability reconstruction of multidimensional stochastic dynamic systems is proposed. Numerical experiments demonstrated that this method approximates the evolution probability analysis of multidimensional stochastic dynamic systems in the time field using a limited number of generalized complex fractional moments.

5. A novel MEP method based on CFM constraints is introduced. The approach derives approximate PDFs by incorporating complex Lagrange multipliers. By decomposing the CFMs into real and imaginary components, constraints for the multipliers are established, leading to a complex entropy equation. Numerical results show that this method surpasses traditional CFM methods in accuracy when CFMs are limited. Its application to transient PDFs in stochastic dynamic systems highlights its effectiveness with minimal moment data.

7.2. Outlooks

The theory of complex fractional moments and its application to the transient analysis of stochastic dynamic systems have demonstrated excellent performance and significant research potential. However, the study of complex fractional moments is still in its early stages, and the theoretical framework remains incomplete. This thesis extends the theory of complex fractional moments and investigates transient analysis problems of stochastic dynamic systems within this extended framework, offering a new perspective for probabilistic evolution analysis in stochastic dynamics. Nevertheless, several issues require further exploration:

1. Algorithm design for complex fractional moments. The distribution of information in the real and imaginary parts of complex fractional moments is concentrated near the origin and exhibits fluctuating patterns, as shown in Figures 2-4. Currently, the fixed-step rectangle formula algorithm used for probability reconstruction with complex fractional moments can be inefficient. Larger steps near the origin lead to increased errors due to high information fluctuation, while smaller steps away from the origin waste computational resources. Developing variable-step or adaptive-step algorithms based on the characteristics of complex fractional moments is essential for improving computational efficiency, especially when reconstructing the evolution probability of stochastic dynamic systems in high-dimensional spaces.

2. Expansion of the theoretical framework. Currently, the framework primarily focuses on transient response probability analysis. However, as a moment statistic, it bridges integral transform theory and fractional calculus, offering significant potential for constructing statistical data characteristics. Future research directions include applying complex fractional moments to contemporary issues such as data-driven artificial intelligence and so on.

3. Expansion to high-dimensional transient analysis. This thesis introduces a generalized framework for complex fractional moments in high-dimensional spaces and proposes a data-driven method for transient probability reconstruction. Future research should focus on reconstructing the evolution probability of multidimensional systems, developing real-axis switching equations for generalized complex fractional moments in high-dimensional scenarios and their normalization.

4. Theoretical expansion and application of shifted characteristic functions. This thesis introduces the concept and theory of shifted characteristic functions and develops methods for solving FPK equations with exponential drift terms based on these functions. This provides a new perspective for the theory of complex fractional moments. The next step is to expand the application scenarios of shifted characteristic functions, refine the related theoretical framework, and apply it to physical problems.

Bibliography

[1] Y. Zhang and G. Luo, "Detecting unstable periodic orbits and unstable quasiperiodic orbits in vibro-impact systems," *International Journal of Non-Linear Mechanics,* vol. 96, pp. 12-21, 2017, doi: 10.1016/j.ijnonlinmec.2017.07.011.

[2] G. Luo, J. Xie, and S. Guo, "Periodic motions and global bifurcations of a two-degree-of-freedom system with plastic vibro-impact," *Journal of sound and vibration,* vol. 240, no. 5, pp. 837-858, 2001, doi: 10.1006/jsvi.2000.3259.

[3] J. Jiang, W. Xu, P. Han, and L. Niu, "Most probable transition paths in eutrophicated lake ecosystem under Gaussian white noise and periodic force," *Chinese Physics B,* vol. 31, no. 6, p. 060203, 2022/05/01 2022, doi: 10.1088/1674-1056/ac5616.

[4] W. Zhang, W. Xu, L. Niu, and Y. Tang, "Bifurcations analysis of a multiple attractors energy harvesting system with fractional derivative damping under random excitation," *Communications in Nonlinear Science and Numerical Simulation,* vol. 118, p. 107069, 2023/04/01/ 2023, doi: 10.1016/j.cnsns.2022.107069.

[5] Q. He, W. Xu, H. Rong, and T. Fang, "Stochastic bifurcation in Duffing–Van der Pol oscillators," *Physica A: Statistical Mechanics and its Applications,* vol. 338, no. 3, pp. 319-334, 2004, doi: 10.1016/j.physa.2004.01.067.

[6] M. Su, W. Xu, and Y. Zhang, "Theoretical analysis of piezoelectric energy harvesting system with impact under random excitation - ScienceDirect," *International Journal of Non-Linear Mechanics,* vol. 119, 2020, doi: 10.1016/j.ijnonlinmec.2019.103322.

[7] M. Su, W. Xu, Y. Zhang, and G. Yang, "Response of a vibro-impact energy harvesting system with bilateral rigid stoppers under Gaussian white noise," *Applied Mathematical Modelling,* vol. 89, 08/01 2020, doi: 10.1016/j.apm.2020.07.022.

[8] Y. Qiao *et al.*, "Frequency unlocking-based MEMS bifurcation sensors," *Microsystems & Nanoengineering,* vol. 9, 05/16 2023, doi: 10.1038/s41378-023-00522-2.

[9] Y. Qiao, M. s. Arab, W. Xu, H. Zhang, and E. Abdel-Rahman, "The impact of thermal-noise on bifurcation MEMS sensors," *Mechanical Systems and Signal Processing,* vol. 161, p. 107941, 12/01 2021, doi: 10.1016/j.ymssp.2021.107941.

[10] Y. Qiao, Y. Jiao, and W. Xu, "Stabilization of electrostatic MEMS resonators using a stochastic optimal control," *Chaos, Solitons & Fractals,* vol. 154, p. 111702, 01/01 2022, doi: 10.1016/j.chaos.2021.111702.

[11] Y. Song and W. Xu, "Asymmetric lévy noise changed stability in a gene transcriptional regulatory system," *Chaos, Solitons & Fractals,* vol. 151, p. 111211, 2021, doi: 10.1016/j.chaos.2021.111211.

[12] Y. Song, W. Xu, and L. Niu, "Multiplicative Lévy noise-induced transitions in gene

expression," *Science China Technological Sciences,* vol. 65, no. 8, pp. 1700-1709, 2022/08/01 2022, doi: 10.1007/s11431-021-2020-3.

[13] Y. Song, W. Xu, W. Wei, and L. Niu, "Dynamical transition of phenotypic states in breast cancer system with Lévy noise," *Physica A: Statistical Mechanics and its Applications,* vol. 627, p. 129122, 2023/10/01/ 2023, doi: 10.1016/j.physa.2023.129122.

[14] Y. Song, W. Xu, W. Wei, and L. Niu, "Switch dynamics in a genetic toggle network driven by Lévy noise," *Nonlinear Dynamics,* vol. 110, no. 4, pp. 3779-3790, 2022/12/01 2022, doi: 10.1007/s11071-022-07781-0.

[15] P. Han, W. Xu, H. Zhang, and L. Wang, "Most probable trajectories in the delayed tumor growth model excited by a multiplicative non-Gaussian noise," *Chaos, Solitons & Fractals,* vol. 156, p. 111801, 03/01 2022, doi: 10.1016/j.chaos.2022.111801.

[16] N. Kar and N. Ozalp, "A fractional mathematical model approach on glioblastoma growth: tumor visibility timing and patient survival," *Mathematical Modelling and Numerical Simulation with Applications,* vol. 4, pp. 66-85, 03/29 2024, doi: 10.53391/mmnsa.1438916.

[17] A. Di Matteo, M. Di Paola, and A. Pirrotta, "Path integral solution for nonlinear systems under parametric Poissonian white noise input," *Probabilistic Engineering Mechanics,* vol. 44, pp. 89-98, 2016, doi: 10.1016/j.probengmech.2015.09.020.

[18] P. Kumar and S. Narayanan, "Modified path integral solution of Fokker–Planck equation: Response and bifurcation of nonlinear systems," vol. 5, pp. 1-12, 2010, doi: 10.1115/1.4000312.

[19] I. Kougioumtzoglou and P. Spanos, "An analytical Wiener path integral technique for non-stationary response determination of nonlinear oscillators," *Probabilistic Engineering Mechanics,* vol. 28, pp. 125-131, 2012, doi: 10.1016/j.probengmech.2011.08.022.

[20] I. A. Kougioumtzoglou and P. D. Spanos, "Nonstationary stochastic response determination of nonlinear systems: A Wiener path integral formalism," *Journal of Engineering Mechanics,* vol. 140, no. 9, p. 04014064, 2014, doi: 10.1061/(ASCE)EM.1943-7889.0000780.

[21] J.-B. Chen and M.-Z. Lyu, "Probabilistic response determination of high-dimensional nonlinear dynamical systems enforced by parametric multiple Poisson white noises," *Nonlinear Dynamics,* vol. 112, pp. 1-16, 05/20 2024, doi: 10.1007/s11071-024-09592-x.

[22] M.-Z. Lyu, D.-C. Feng, X.-Y. Cao, and M. Beer, "A full-probabilistic cloud analysis for structural seismic fragility via decoupled M-PDEM," *Earthquake Engineering & Structural Dynamics,* vol. 53, 01/21 2024, doi: 10.1002/eqe.4093.

[23] J. Dunne and M. Ghanbari, "Extreme-value prediction for non-linear stochastic oscillators via numerical solutions of the stationary FPK equation," *Journal of Sound and Vibration,* vol. 206, no. 5, pp. 697-724, 1997, doi: 10.1006/jsvi.1997.1148.

[24] S. Le-Chung and W. Teng-Yuan, "A finite-element method for analysis of a non-linear system under stochastic parametric and external excitation," *International journal of non-linear mechanics,* vol. 31, no. 2, pp. 193-201, 1996, doi: 10.1016/0020-7462(95)00049-6.

[25] J. Chen and P. Lin, "Dimension-reduction of FPK equation via equivalent drift coefficient," *Theoretical and Applied Mechanics Letters,* vol. 4, no. 1, p. 013002, 2014, doi: 10.1063/2.1401302.

[26] J. Sun and B. Song, "Solutions of the FPK equation for time-delayed dynamical systems with the continuous time approximation method," *Probabilistic engineering mechanics,* vol. 27, no. 1, pp. 69-74, 2012, doi: 10.1016/j.probengmech.2011.05.009.

[27] J. Qian, L. Chen, and J.-Q. Sun, "Transient response prediction of randomly excited vibro-impact systems via RBF neural networks," *Journal of Sound and Vibration,* vol. 546, p. 117456, 2023, doi: 10.1016/j.jsv.2022.117456.

[28] S. M. Stigler, *The history of statistics*. Harvard University Press, 1990.

[29] S. E. Fienberg, "A brief history of statistics in three and one-half chapters: A review essay," ed: JSTOR, 1992.

[30] J. Graunt, "Natural and political observations mentioned in a following index, and made upon the bills of mortality," *Mathematical demography,* vol. 6, pp. 11-20, 1977, doi: 10.1007/978-3-642-35858-6_2.

[31] I. Schneider, "Jakob Bernoulli, Ars Conjectandi (1713)," in *Landmark Writings in Western Mathematics 1640-1940*: Elsevier, 2005, pp. 88-104.

[32] C. F. Gauss, *Theory of the motion of the heavenly bodies moving about the sun in conic sections: a translation of Gauss's" Theoria Motus." with an appendix*. Little, Brown, 1857.

[33] F. Galton, *Natural inheritance*. Macmillan, 1889.

[34] J. M. Stanton, "Galton, Pearson, and the peas: A brief history of linear regression for statistics instructors," *Journal of Statistics Education,* vol. 9, no. 3, 2001, doi: 10.1080/10691898.2001.11910537.

[35] K. Pearson, "X. On the criterion that a given system of deviations from the probable in the case of a correlated system of variables is such that it can be reasonably supposed to have arisen from random sampling," *The London, Edinburgh, and Dublin Philosophical Magazine and Journal of Science,* vol. 50, no. 302, pp. 157-175, 1900/07/01 1900, doi: 10.1080/14786440009463897.

[36] R. A. Fisher, "Two new properties of mathematical likelihood," *Proceedings of the Royal Society of London. Series A, Containing Papers of a Mathematical and Physical Character,* vol. 144, no. 852, pp. 285-307, 1934, doi: jstor.org/stable/2935559.

[37] R. A. Fisher, "On the mathematical foundations of theoretical statistics," *Philosophical transactions of the Royal Society of London. Series A, containing papers of a*

mathematical or physical character, vol. 222, no. 594-604, pp. 309-368, 1922, doi: 10.1098/rsta.1922.0009.

[38] J. Neyman and E. S. Pearson, "On the use and interpretation of certain test criteria for purposes of statistical inference: Part I," *Biometrika,* pp. 175-240, 1928.

[39] J. Neyman and E. S. Pearson, "IX. On the problem of the most efficient tests of statistical hypotheses," *Philosophical Transactions of the Royal Society of London. Series A, Containing Papers of a Mathematical or Physical Character,* vol. 231, no. 694-706, pp. 289-337, 1933, doi: 10.1098/rsta.1933.0009.

[40] F. Wilcoxon, "Individual comparisons by ranking methods," in *Breakthroughs in statistics: Methodology and distribution*: Springer, 1992, pp. 196-202.

[41] F. Wilcoxon, "Probability tables for individual comparisons by ranking methods," *Biometrics,* vol. 3, no. 3, pp. 119-122, 1947.

[42] S. H. Strogatz, "Exploring complex networks," *nature,* vol. 410, no. 6825, pp. 268-276, 2001, doi: 10.1038/35065725.

[43] S. Boccaletti, V. Latora, Y. Moreno, M. Chavez, and D.-U. Hwang, "Complex networks: Structure and dynamics," *Physics reports,* vol. 424, no. 4-5, pp. 175-308, 2006, doi: 10.1016/j.physrep.2005.10.009.

[44] C. M. Bishop, "Neural networks and their applications," *Review of scientific instruments,* vol. 65, no. 6, pp. 1803-1832, 1994, doi: 10.1063/1.1144830.

[45] M. Rheinfurth and L. W. Howell, "Probability and statistics in aerospace engineering," 1998.

[46] G. K. Karagiannidis, "Moments-based approach to the performance analysis of equal gain diversity in Nakagami-m fading," *IEEE Transactions on Communications,* vol. 52, no. 5, pp. 685-690, 2004, doi: 10.1109/TCOMM.2004.826255.

[47] A. Daoui, H. Karmouni, M. Sayyouri, and H. Qjidaa, "Efficient methods for signal processing using Charlier moments and artificial bee Colony algorithm," *Circuits, Systems, and Signal Processing,* vol. 41, no. 1, pp. 166-195, 2022, doi: 10.1007/s00034-021-01764-z.

[48] D. Bielińska-Wąż, "Graphical and numerical representations of DNA sequences: statistical aspects of similarity," *Journal of mathematical chemistry,* vol. 49, pp. 2345-2407, 2011, doi: 10.1007/s10910-011-9890-8.

[49] C. H. Beentjes, R. Perez-Carrasco, and R. Grima, "Exact solution of stochastic gene expression models with bursting, cell cycle and replication dynamics," *Physical Review E,* vol. 101, no. 3, p. 032403, 2020, doi: 10.1103/PhysRevE.101.032403.

[50] M. Soltani and A. Singh, "Using higher-order statistics to infer random forces driving a nano sensor."

[51] H. Neubert, "Uncertainty-Based Design Optimization of MEMS/NEMS," in *Bio and Nano Packaging Techniques for Electron Devices: Advances in Electronic Device*

Packaging: Springer, 2012, pp. 119-137.

[52] L. Tomy, C. Chesneau, and A. K. Madhav, "Statistical Techniques for Environmental Sciences: A Review," *Mathematical and Computational Applications,* vol. 26, no. 4, p. 74, 2021, doi: 10.1007/978-3-642-28522-6_6.

[53] M. Panella and R. Altilio, "A smartphone-based application using machine learning for gesture recognition: Using feature extraction and template matching via Hu image moments to recognize gestures," *IEEE consumer electronics magazine,* vol. 8, no. 1, pp. 25-29, 2018, doi: 10.1109/MCE.2018.2868109.

[54] T. A. M. Elhassan, M. S. M. Rahim, T. T. Swee, S. Z. M. Hashim, and M. Aljurf, "Feature extraction of white blood cells using CMYK-moment localization and deep learning in acute myeloid leukemia blood smear microscopic images," *IEEE Access,* vol. 10, pp. 16577-16591, 2022, doi: 10.1109/ACCESS.2022.3149637.

[55] J. Yao, S. Zheng, and Z. Bai, "Sample covariance matrices and high-dimensional data analysis," *Cambridge UP, New York,* 2015.

[56] H. Gzyl and A. Tagliani, "Hausdorff moment problem and fractional moments," *Applied Mathematics and Computation,* vol. 216, no. 11, pp. 3319-3328, 2010, doi: 10.1016/j.amc.2010.04.059.

[57] G. Talenti, "Recovering a function from a finite number of moments," *Inverse problems,* vol. 3, no. 3, p. 501, 1987, doi: 10.1088/0266-5611/3/3/016.

[58] P. L. Butzer and U. Westphal, "An introduction to fractional calculus," in *Applications of fractional calculus in physics*: World Scientific, 2000, pp. 1-85.

[59] J. T. Machado, V. Kiryakova, and F. Mainardi, "Recent history of fractional calculus," *Communications in nonlinear science and numerical simulation,* vol. 16, no. 3, pp. 1140-1153, 2011, doi: 10.1016/j.cnsns.2010.05.027.

[60] H. Sun, Y. Zhang, D. Baleanu, W. Chen, and Y. Chen, "A new collection of real world applications of fractional calculus in science and engineering," *Communications in Nonlinear Science and Numerical Simulation,* vol. 64, pp. 213-231, 2018, doi: 10.1016/j.cnsns.2018.04.019.

[61] L. Debnath, "Recent applications of fractional calculus to science and engineering," *International Journal of Mathematics and Mathematical Sciences,* vol. 2003, no. 54, pp. 3413-3442, 2003, doi: 10.1155/S0161171203301486.

[62] O. Naifar and A. B. Makhlouf, *Fractional Order Systems--Control Theory and Applications*. Springer, 2022.

[63] R. L. Magin, "Fractional calculus models of complex dynamics in biological tissues," *Computers & Mathematics with Applications,* vol. 59, no. 5, pp. 1586-1593, 2010, doi: 10.1016/j.camwa.2009.08.039.

[64] R. Magin, "Fractional calculus in bioengineering, part 1," *Critical Reviews™ in Biomedical Engineering,* vol. 32, no. 1, 2004, doi:

10.1615/CritRevBiomedEng.v32.i1.10.

[65] Y. Zhang, H. Sun, H. H. Stowell, M. Zayernouri, and S. E. Hansen, "A review of applications of fractional calculus in Earth system dynamics," *Chaos, Solitons & Fractals,* vol. 102, pp. 29-46, 2017, doi: 10.1016/j.chaos.2017.03.051.

[66] D. Mondal and P. Debnath, "An application of fractional calculus to geophysics: Effect of a strike-slip fault on displacement, stresses and strains in a fractional order Maxwell type visco-elastic half space," *International Journal of Applied Mathematics,* vol. 34, no. 5, p. 873, 2021, doi: 10.12732/ijam.v34i5.2.

[67] R. G. Ghanem and P. D. Spanos, *Stochastic finite elements: a spectral approach*. Springer-Verlag, 1991.

[68] J. B. Roberts and P. D. Spanos, *Random Vibration and Statistical Linearization*. Random Vibration and Statistical Linearization, 2003.

[69] P. D. S. R. Ghanem, "A stochastic Galerkin expansion for nonlinear random vibration analysis," *Probabilistic Engineering Mechanics,* vol. 8, no. 3-4, pp. 255-264, 1993, doi: 10.1016/0266-8920(93)90019-R.

[70] X. Chen, X. Jin, and Z. Huang, "Stability and reliability analysis of nonlinear stochastic system using data-driven dimensional analysis method," *Mechanical Systems and Signal Processing,* vol. 212, p. 111299, 2024/04/15/ 2024, doi: doi.org/10.1016/j.ymssp.2024.111299.

[71] X. Chen, X. Jin, and Z. Huang, "Reliability control of nonlinear stochastic dynamical system based on discrete data," *JVC/Journal of Vibration and Control,* Article 2024, doi: 10.1177/10775463241248979.

[72] X. Chen, X. Jin, and Z. Huang, "Data-driven identification for approximate analytical solution of first-passage problem," *Probabilistic Engineering Mechanics,* Article vol. 73, 2023, Art no. 103467, doi: 10.1016/j.probengmech.2023.103467.

[73] J. Qian, L. Chen, and J. Q. Sun, "Non-stationary stochastic response determination of vibro-impact system under combination harmonic and Gaussian white noise excitations," *Engineering Structures,* Article vol. 304, 2024, Art no. 117677, doi: 10.1016/j.engstruct.2024.117677.

[74] F. Yang, L. Chen, Z. Yuan, and J. Q. Sun, "Transient response of energy harvesting systems with multi-well potential under Poisson white noise excitations," *International Journal of Non-Linear Mechanics,* Article vol. 155, 2023, Art no. 104463, doi: 10.1016/j.ijnonlinmec.2023.104463.

[75] J. Qian, L. Chen, and J. Q. Sun, "A candidate method for prediction of the non-stationary response of strongly nonlinear systems under wide-band noise excitation," *International Journal of Non-Linear Mechanics,* Article vol. 159, 2024, Art no. 104621, doi: 10.1016/j.ijnonlinmec.2023.104621.

[76] J. B. Chen and M. Z. Lyu, "Globally-evolving-based generalized density evolution

equation for nonlinear systems involving randomness from both system parameters and excitations," *Proceedings of the Royal Society A: Mathematical, Physical and Engineering Sciences,* Article vol. 478, no. 2264, 2022, Art no. 20220356, doi: 10.1098/rspa.2022.0356.

[77] J. Li and J. B. Chen, "The probability density evolution method for dynamic response analysis of non-linear stochastic structures," *International Journal for Numerical Methods in Engineering,* vol. 65, no. 6, pp. 882-903, 2006, doi: 10.1002/nme.1479.

[78] C. Soize, "Transient responses of dynamical systems with random uncertainties," *Probabilistic Engineering Mechanics,* vol. 16, no. 4, pp. 363-372, 2001/10/01/ 2001, doi: 10.1016/S0266-8920(01)00026-1.

[79] Z. H. Liu, J. H. Geng, and W. Q. Zhu, "Transient stochastic response of quasi non-integerable Hamiltonian system," *Probabilistic Engineering Mechanics,* vol. 43, pp. 148-155, 2016/01/01/ 2016, doi: 10.1016/j.probengmech.2015.09.009.

[80] X. Yue, W. Xu, L. Wang, and B. Zhou, "Transient and steady-state responses in a self-sustained oscillator with harmonic and bounded noise excitations," *Probabilistic Engineering Mechanics,* vol. 30, pp. 70-76, 2012/10/01/ 2012, doi: 10.1016/j.probengmech.2012.06.001.

[81] X. Yue, Y. Wang, Q. Han, Y. Xu, and W. Xu, "Transient responses of nonlinear dynamical systems under colored noise," *Europhysics Letters,* vol. 127, no. 2, p. 24004, 2019, doi: 10.1209/0295-5075/127/24004.

[82] G. Cottone and M. Di Paola, "On the use of fractional calculus for the probabilistic characterization of random variables," *Probabilistic Engineering Mechanics,* vol. 24, no. 3, pp. 321-330, 2009.

[83] G. Cottone, M. Di Paola, and R. Metzler, "Fractional calculus approach to the statistical characterization of random variables and vectors," *Physica A: Statistical Mechanics and its Applications,* vol. 389, no. 5, pp. 909-920, 2010.

[84] M. Di Paola and F. P. Pinnola, "Riesz fractional integrals and complex fractional moments for the probabilistic characterization of random variables," *Probabilistic Engineering Mechanics,* Article vol. 29, pp. 149-156, 2012, doi: 10.1016/j.probengmech.2011.11.003.

[85] X. Jin, Y. Wang, Z. Huang, and M. Di Paola, "Constructing transient response probability density of non-linear system through complex fractional moments," *International Journal of Non-Linear Mechanics,* Article vol. 65, pp. 253-259, 2014, doi: 10.1016/j.ijnonlinmec.2014.06.004.

[86] M. Di Paola, "Fokker Planck equation solved in terms of complex fractional moments," *Probabil Engineering Mechanics,* vol. 38, pp. 70-76, 2014.

[87] X. Xiufeng, L. Junlin, L. Di, and G. Rong, "Transient response of nonlinear vibro-impact system under Gaussian white noise excitation through complex fractional moments," *Acta Mechanica,* vol. 228, no. 3, pp. 1-11, 2016.

[88] A. Di Matteo, M. Di Paola, and A. Pirrotta, "Poisson white noise parametric input and response by using complex fractional moments," *Probabil Engineering Mechanics,* vol. 38, pp. 119-126, 2014.

[89] A. Di Matteo, M. Di Paola, and A. Pirrotta, "Probabilistic characterization of nonlinear systems under Poisson white noise via complex fractional moments," *Nonlinear Dynamics,* Article vol. 77, no. 3, pp. 729-738, 2014, doi: 10.1007/s11071-014-1333-1.

[90] G. Alotta and M. D. Paola, "Einstein-Smoluchowsky equation handled by complex fractional moments," in *ICFDA 14*, 2014.

[91] G. Alotta and M. Di Paola, "Probabilistic characterization of nonlinear systems under α-stable white noise via complex fractional moments," *Physica A: Statistical Mechanics and its Applications,* Article vol. 420, pp. 265-276, 2015, doi: 10.1016/j.physa.2014.10.091.

[92] S. Butera and M. Di Paola, "Fractional differential equations solved by using Mellin transform," *Communications in Nonlinear Science and Numerical Simulation,* Article vol. 19, no. 7, pp. 2220-2227, 2014, doi: 10.1016/j.cnsns.2013.11.022.

[93] M. Di Paola, A. Pirrotta, G. Alotta, A. Di Matteo, and F. P. Pinnola, "Complex fractional moments for the characterization of the probabilistic response of non-linear systems subjected to white noises," in *Topics in Nonlinear Mechanics and Physics: Selected Papers from CSNDD 2018*, 2019: Springer, pp. 203-227, doi: 10.1007/978-981-13-9463-8_11.

[94] H. Dai, Z. Ma, and L. Li, "An improved complex fractional moment-based approach for the probabilistic characterization of random variables," *Probabilistic Engineering Mechanics,* Article vol. 53, pp. 52-58, 2018, doi: 10.1016/j.probengmech.2018.05.005.

[95] L. Niu, W. Xu, and Q. Guo, "Transient response of the time-delay system excited by Gaussian noise based on complex fractional moments," *Chaos,* Article vol. 31, no. 5, 2021, Art no. 053111, doi: 10.1063/5.0033593.

[96] L. Niu, Y. Song, and W. Xu, "Application of Complex Fractional Moment in nonlinear system with Gaussian colored noise," *International Journal of Non-Linear Mechanics,* Article vol. 141, 2022, Art no. 103945, doi: 10.1016/j.ijnonlinmec.2022.103945.

[97] D. Itoh, T. Tsuchida, and K. Kimura, "An analysis of a nonlinear system excited by combined Gaussian and Poisson white noises using complex fractional moments," *Theoretical and Applied Mechanics Japan,* vol. 64, pp. 103-114, 2018, doi: 10.11345/nctam.64.103.

[98] D. Itoh and T. Tsuchida, "Transient response analysis of a system with nonlinear stiffness and nonlinear damping excited by Gaussian white noise based on complex fractional moments," *Acta Mechanica,* vol. 233, pp. 1-16, 07/01 2022, doi: 10.1007/s00707-022-03264-w.

[99] T. Tsuchida, D. Itoh, and T. Eguchi, "Transient response analysis of nonlinear oscillators with fractional derivative elements under Gaussian white noise using complex fractional

moments," *ASME Open Journal of Engineering,* vol. 3, 2024, doi: 10.1115/1.4065126.

[100] E. H. Vanmarcke, "Properties of spectral moments with applications to random vibration," *Journal of the Engineering Mechanics Division,* vol. 98, no. 2, pp. 425-446, 1972, doi: 10.1061/JMCEA3.0001593.

[101] M. Di Paola, "Transient spectral moments of linear systems," *SM archives,* Article vol. 10, no. 3, pp. 225-243, 1985.

[102] G. Cottone and M. D. Paola, "A new representation of power spectral density and correlation function by means of fractional spectral moments," *Probabilistic Engineering Mechanics,* vol. 25, no. 3, pp. 348-353, 2010, doi: 10.1016/j.probengmech.2010.04.003.

[103] G. Cottone, M. Di Paola, and R. Santoro, "A novel exact representation of stationary colored Gaussian processes (fractional differential approach)," *Journal of Physics A: Mathematical and Theoretical,* vol. 43, no. 8, p. 085002, 2010, doi: 10.1088/1751-8113/43/8/085002.

[104] G. Cottone and M. Di Paola, "Fractional spectral moments for digital simulation of multivariate wind velocity fields," *Journal of Wind Engineering and Industrial Aerodynamics,* vol. 99, no. 6-7, pp. 741-747, 2011, doi: 10.1016/j.jweia.2011.03.006.

[105] K. Runtemund, G. Cottone, and G. Müller, "Treatment of arbitrarily autocorrelated load functions in the scope of parameter identification," *Computers and Structures,* Article vol. 126, no. 1, pp. 29-40, 2013, doi: 10.1016/j.compstruc.2012.11.021.

[106] F. P. Pinnola, "Statistical correlation of fractional oscillator response by complex spectral moments and state variable expansion," *Communications in Nonlinear Science and Numerical Simulation,* vol. 39, pp. 343-359, 2016, doi: 10.1016/j.cnsns.2016.03.013.

[107] G. Alotta, M. Di Paola, and G. Failla, "A Mellin transform approach to wavelet analysis," *Communications in Nonlinear Science and Numerical Simulation,* Article vol. 28, no. 1-3, pp. 175-193, 2015, doi: 10.1016/j.cnsns.2015.04.001.

[108] M. Di Paola, "Complex Fractional Moments and Their Use in Earthquake Engineering," in *Encyclopedia of Earthquake Engineering*, M. Beer, I. A. Kougioumtzoglou, E. Patelli, and S.-K. Au Eds. Berlin, Heidelberg: Springer Berlin Heidelberg, 2015, pp. 446-461.

[109] G. Alotta, M. Di Paola, and F. P. Pinnola, "Cross-correlation and cross-power spectral density representation by complex spectral moments," *International Journal of Non-Linear Mechanics,* Article vol. 94, pp. 20-27, 2017, doi: 10.1016/j.ijnonlinmec.2017.02.001.

[110] M. Hitsuda, "Representation of Gaussian processes equivalent to Wiener process," 1968.

[111] J. L. Doob, "What is a stochastic process?," *The American Mathematical Monthly,* vol. 49, no. 10, pp. 648-653, 1942.

[112] Z.-x. Xu, D.-y. Zhou, and Z.-c. Deng, "Numerical method based on Hamilton system

and symplectic algorithm to differential games," *Applied Mathematics and Mechanics,* vol. 27, no. 3, pp. 341-346, 2006/03/01 2006, doi: 10.1007/s10483-006-0309-y.

[113] J. Candy and W. Rozmus, "A symplectic integration algorithm for separable Hamiltonian functions," *Journal of Computational Physics,* vol. 92, no. 1, pp. 230-256, 1991, doi: 10.1016/0021-9991(91)90299-Z.

[114] E. Luo, W.-J. Huang, and F.-H. Jiang, "Hamilton System and Symplectic Algorithm for Dynamic Analysis of Honeycomb Sandwich Plates," *Acta Aeronautica et Astronautica Sinica,* vol. 27, no. 2, pp. 236-240, 2006.

[115] H. Öz and E. Adigüzel, "Hamilton's law of varying action: Part I: Assumed-time-modes method," *Journal of Sound and Vibration,* vol. 179, no. 4, pp. 697-710, 1995/01/26/ 1995, doi: 10.1006/jsvi.1995.0045.

[116] H. Öz and A. Raffie, "Inverse response problem (control) of dynamic systems via Hamilton's law," *Computer Methods in Applied Mechanics and Engineering,* vol. 62, no. 1, pp. 17-26, 1987/05/01/ 1987, doi: 10.1016/0045-7825(87)90087-9.

[117] W. Zhu, "Stochastic averaging of quasi-Hamiltonian systems," *SCIENCE IN CHINA SERIES A-MATHEMATICS PHYSICS ASTRONOMY,* vol. 39, no. 1, pp. 97-107, 1996.

[118] W. Jia, W. Zhu, and Y. Xu, "Stochastic averaging of quasi-non-integrable Hamiltonian systems under combined Gaussian and Poisson white noise excitations," *International Journal of Non-Linear Mechanics,* vol. 51, pp. 45-53, 2013/05/01/ 2013, doi: 10.1016/j.ijnonlinmec.2012.12.003.

[119] M. L. Deng and W. Q. Zhu, "Stochastic averaging of quasi-non-integrable Hamiltonian systems under fractional Gaussian noise excitation," *Nonlinear Dynamics,* vol. 83, no. 1, pp. 1015-1027, 2016/01/01 2016, doi: 10.1007/s11071-015-2384-7.

[120] C. B. Gan and W. Q. Zhu, "First-passage failure of quasi-non-integrable-Hamiltonian systems," *International Journal of Non-Linear Mechanics,* vol. 36, no. 2, pp. 209-220, 2001/03/01/ 2001, doi: 10.1016/S0020-7462(00)00006-8.

[121] M. Di Paola, "Fokker Planck equation solved in terms of complex fractional moments," *Probabilistic Engineering Mechanics,* Article vol. 38, pp. 70-76, 2014, doi: 10.1016/j.probengmech.2014.09.003.

[122] K. B. Oldham, "Fractional differential equations in electrochemistry," *Advances in Engineering software,* vol. 41, no. 1, pp. 9-12, 2010.

[123] H. W. Zhou and S. Yang, "Fractional derivative approach to non-Darcian flow in porous media," *Journal of Hydrology,* vol. 566, pp. 910-918, 2018/11/01/ 2018, doi: 10.1016/j.jhydrol.2018.09.039.

[124] W. Chen, "A speculative study of 2/3-order fractional Laplacian modeling of turbulence: Some thoughts and conjectures," *Chaos: An Interdisciplinary Journal of Nonlinear Science,* vol. 16, no. 2, 2006.

[125] D. T. Spasic, N. I. Kovincic, and D. V. Dankuc, "A new material identification pattern

for the fractional Kelvin-Zener model describing biomaterials and human tissues," *Communications in Nonlinear Science and Numerical Simulation,* Article vol. 37, pp. 193-199, 2016, doi: 10.1016/j.cnsns.2016.01.004.

[126] Y. Yang, W. Xu, and G. Yang, "Bifurcation analysis of a noisy vibro-impact oscillator with two kinds of fractional derivative elements," *Chaos: An Interdisciplinary Journal of Nonlinear Science,* vol. 28, no. 4, 2018.

[127] Y.-G. Yang, W. Xu, Y.-H. Sun, and X.-D. Gu, "Stochastic response of van der Pol oscillator with two kinds of fractional derivatives under Gaussian white noise excitation," *Chinese Physics B,* vol. 25, no. 2, p. 020201, 2015.

[128] L. Chen, W. Wang, Z. Li, and W. Zhu, "Stationary response of Duffing oscillator with hardening stiffness and fractional derivative," *International Journal of Non-Linear Mechanics,* vol. 48, pp. 44-50, 2013/01/01/ 2013, doi: 10.1016/j.ijnonlinmec.2012.08.001.

[129] L. Chen, F. Hu, and W. Zhu, "Stochastic dynamics and fractional optimal control of quasi integrable Hamiltonian systems with fractional derivative damping," *Fractional Calculus and Applied Analysis,* vol. 16, no. 1, pp. 189-225, 2013/03/01 2013, doi: 10.2478/s13540-013-0013-z.

[130] Y.-H. Sun, Y.-G. Yang, and W. Xu, "Stochastic P-bifurcations of a noisy nonlinear system with fractional derivative element," *Acta Mechanica Sinica,* vol. 37, no. 3, pp. 507-515, 2021/03/01 2021, doi: 10.1007/s10409-020-01020-8.

[131] A. Navarro-Quiles, "Probabilistic solution of a homogeneous linear second-order differential equation with randomized complex coefficients," *Probabilistic Engineering Mechanics,* vol. 68, p. 103232, 2022/04/01/ 2022, doi: 10.1016/j.probengmech.2022.103232.

[132] M. C. Casabán, J. C. Cortés, J. V. Romero, and M. D. Roselló, "Solving Random Homogeneous Linear Second-Order Differential Equations: A Full Probabilistic Description," *Mediterranean Journal of Mathematics,* vol. 13, no. 6, pp. 3817-3836, 2016/12/01 2016, doi: 10.1007/s00009-016-0716-6.

[133] M. F. Wehner and W. Wolfer, "Numerical evaluation of path-integral solutions to Fokker-Planck equations," *Physical Review A,* vol. 27, no. 5, p. 2663, 1983.

[134] M. Di Paola and R. Santoro, "Path integral solution for non-linear system enforced by Poisson white noise," *Probabilistic Engineering Mechanics,* vol. 23, no. 2-3, pp. 164-169, 2008.

[135] A. Naess and V. Moe, "Efficient path integration methods for nonlinear dynamic systems," *Probabilistic engineering mechanics,* vol. 15, no. 2, pp. 221-231, 2000.

[136] J.-B. Chen and M.-Z. Lyu, "Probabilistic response determination of high-dimensional nonlinear dynamical systems enforced by parametric multiple Poisson white noises," *Nonlinear Dynamics,* pp. 1-16, 2024.

[137] Y. Bai, W. Xu, and W. Zhang, "Reliability analysis of iced transmission lines under Poisson white noise excitation via path integration method," *Nonlinear Dynamics,* 2024/05/09 2024, doi: 10.1007/s11071-024-09662-0.

[138] S. Takenaka, "Stable Non-Gaussian Random Processes - Stochastic Models with Infinite Variance - G. Samorodnitsky; M. S. Taqqu," 1996.

[139] M. Grigoriu, *Applied non-Gaussian processes. Examples, theory, simulation, linear random vibration, and MATLAB solutions (3 1/2 disk)*. Applied non-Gaussian processes. Examples, theory, simulation, linear random vibration, and MATLAB solutions (3 1/2 disk). 1995.

[140] S. Guiasu and A. Shenitzer, "The principle of maximum entropy," *The mathematical intelligencer,* vol. 7, pp. 42-48, 1985.

[141] W. Boomsma, J. Ferkinghoff-Borg, and K. Lindorff-Larsen, "Combining experiments and simulations using the maximum entropy principle," *PLoS computational biology,* vol. 10, no. 2, p. e1003406, 2014.

[142] W. R. Le Page, *Complex variables and the Laplace transform for engineers*. Courier Corporation, 1980.

[143] R. Bracewell and P. B. Kahn, "The Fourier transform and its applications," *American Journal of Physics,* vol. 34, no. 8, pp. 712-712, 1966.

[144] H. Mellin, *Über die fundamentale Wichtigkeit des Satzes von Cauchy für die Theorien der Gamma-und der hypergeometrischen Functionen*. Societatis litterariae fennicae, 1896.

[145] H. Mellin, "Résolution de l'équation algébrique généralea l'aide de la fonction gamma," vol. 172, pp. 658-661, 1921.

[146] I. Antipova, "Inversion of many-dimensional Meilin transforms and solutions of algebraic equations," *Sbornik Mathematics,* Article vol. 198, no. 3-4, pp. 447-463, 2007, doi: 10.1070/SM2007v198n04ABEH003844.

[147] S. Samko, "Fractional integration and differentiation of variable order: An overview," *Nonlinear Dynamics,* Review vol. 71, no. 4, pp. 653-662, 2013, doi: 10.1007/s11071-012-0485-0.

[148] M. Cai and C. Li, "On Riesz derivative," *Fractional Calculus and Applied Analysis,* vol. 22, no. 2, pp. 287-301, 2019, doi: doi:10.1515/fca-2019-0019.

[149] C. Li and J. Beaudin, "On the Generalized Riesz Derivative," *Mathematics,* vol. 8, p. 1089, 07/03 2020, doi: 10.3390/math8071089.

[150] U. Alibrandi, M. Di Paola, and G. Ricciardi, *Path Integral Solution solved by the kernel density maximum entropy approach*. 2007.

[151] P. C. Bressloff and J. M. Newby, "Path integrals and large deviations in stochastic hybrid systems," *Physical Review E,* vol. 89, no. 4, p. 042701, 04/01/ 2014, doi: 10.1103/PhysRevE.89.042701.

[152] A. Di Matteo, I. A. Kougioumtzoglou, A. Pirrotta, P. D. Spanos, and M. Di Paola, "Stochastic response determination of nonlinear oscillators with fractional derivatives elements via the Wiener path integral," *Probabilistic Engineering Mechanics,* vol. 38, pp. 127-135, 2014.

[153] Y. Zhang, "A finite difference method for fractional partial differential equation," *Applied Mathematics and Computation,* vol. 215, no. 2, pp. 524-529, 2009.

[154] Y. Luo, M.-Z. Lyu, J.-B. Chen, and P. Spanos, "Equation governing the probability density evolution of multi-dimensional linear fractional differential systems subject to Gaussian white noise," *Theoretical and Applied Mechanics Letters,* vol. 13, p. 100436, 02/01 2023, doi: 10.1016/j.taml.2023.100436.

[155] M.-Z. Lyu, J.-B. Chen, and J. Shen, "Refined probabilistic response and seismic reliability evaluation of high-rise reinforced concrete structures via physically driven dimension-reduced probability density evolution equation," *Acta Mechanica,* vol. 235, pp. 1-27, 08/18 2023, doi: 10.1007/s00707-023-03666-4.

[156] M.-Z. Lyu, D.-C. Feng, J.-B. Chen, and J. Li, "A decoupled approach for determination of the joint probability density function of a high-dimensional nonlinear stochastic dynamical system via the probability density evolution method," *Computer Methods in Applied Mechanics and Engineering,* vol. 418, p. 116443, 01/01 2024, doi: 10.1016/j.cma.2023.116443.

[157] Y. Guan, W. Li, D. Huang, and N. Gubeljak, "A new LBFNN algorithm to solve FPK equations for stochastic dynamical systems under Gaussian or Non-Gaussian excitation," *Chaos, Solitons & Fractals,* vol. 173, p. 113641, 2023/08/01/ 2023, doi: doi.org/10.1016/j.chaos.2023.113641.

[158] E. T. Jaynes, "Information theory and statistical mechanics," *Physical review,* vol. 106, no. 4, p. 620, 1957.

[159] A. Golan, "Information and entropy econometrics—A review and synthesis," *Foundations and trends® in econometrics,* vol. 2, no. 1–2, pp. 1-145, 2008.

[160] A. Berger, S. A. Della Pietra, and V. J. Della Pietra, "A maximum entropy approach to natural language processing," *Computational linguistics,* vol. 22, no. 1, pp. 39-71, 1996.

[161] X. Zhang and M. D. Pandey, "Structural reliability analysis based on the concepts of entropy, fractional moment and dimensional reduction method," *Structural Safety,* vol. 43, pp. 28-40, 2013/07/01/ 2013, doi: 10.1016/j.strusafe.2013.03.001.

[162] J. Trębicki and K. Sobczyk, "Maximum entropy principle and non-stationary distributions of stochastic systems," *Probabilistic Engineering Mechanics,* vol. 11, no. 3, pp. 169-178, 1996/07/01/ 1996, doi: doi.org/10.1016/0266-8920(96)00008-2.

[163] K. Sobezyk and J. Trębicki, "Maximum entropy principle in stochastic dynamics," *Probabilistic Engineering Mechanics,* vol. 5, no. 3, pp. 102-110, 1990.

Appendix

Appendix. A

1) Classical one-order differential equation

Starting with the one-order differential equation:

$$\begin{cases} \dot{X}(t)+\nu X(t)=f(t), \nu>0; \\ X(0)=0. \end{cases} \tag{A-1}$$

By making LT of this equation, we get

$$s\mathcal{L}_X(s)+\nu\mathcal{L}_X(s)=\mathcal{L}_f(s), s=\beta-i\theta, \tag{A-2}$$

namely

$$\mathcal{L}_X(s)=\frac{1}{s+\nu}\mathcal{L}_f(s). \tag{A-3}$$

Putting

$$f^{\mathcal{L}}(s)=A_f^{\mathcal{L}}(s)+iB_f^{\mathcal{L}}(s),\ \ x^{\mathcal{L}}(s)=A_x^{\mathcal{L}}(s)+iB_x^{\mathcal{L}}(s), \tag{A-4}$$

the inverse LT of $f(t)$ and $x(t)$ are given as

$$f(t)=\frac{e^{\beta t}}{2b}\left[A_f^{\mathcal{L}}(\beta)+2\sum_{k=1}^{m}\left(A_f^{\mathcal{L}}(s_k)\cos\left(\frac{k\pi t}{b}\right)+B_f^{\mathcal{L}}(s_k)\sin\left(\frac{k\pi t}{b}\right)\right)\right], \tag{A-5}$$

$$x(t)=\frac{e^{\beta t}}{2b}\left[A_x^{\mathcal{L}}(\beta)+2\sum_{k=1}^{m}\left(A_x^{\mathcal{L}}(s_k)\cos\left(\frac{k\pi t}{b}\right)+B_x^{\mathcal{L}}(s_k)\sin\left(\frac{k\pi t}{b}\right)\right)\right], \tag{A-6}$$

where $s_k=\beta+ik\pi/b$. Substituting Eq. (A-4) into Eq. (A-2), we can obtain:

$$A_X^{\mathcal{L}}(\beta)=\frac{A_x^{\mathcal{L}}(\beta)}{\beta+\nu}; A_X^{\mathcal{L}}(s_k)=\frac{(\beta+\nu)A_f^{\mathcal{L}}(s_k)+\theta_k B_f^{\mathcal{L}}(s_k)}{(\beta+\nu)^2+\theta_k^2}; B_X^{\mathcal{L}}(s_k)=\frac{(\beta+\nu)B_f^{\mathcal{L}}(s_k)-\theta_k A_f^{\mathcal{L}}(s_k)}{(\beta+\nu)^2+\theta_k^2}; \tag{A-7}$$

Such an example when $f(t)=\cos(t)$ to verify the accuracy.

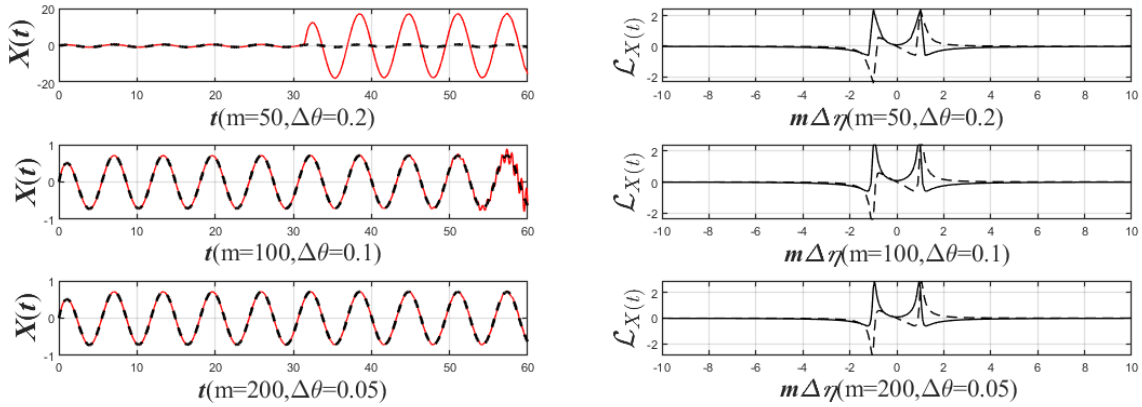

(a) (b)

Figure A-1 (a) The black dashed line is the exact $X(t)$, and the red real line is the reconstruct $X(t)$. (b) The real line is the $A_x^{\mathcal{L}}(s_k)$, and the dashed line is the imaginary part $B_x^{\mathcal{L}}(s_k)$. $\nu = 1$

2) Fractional differential equation

Now, let us consider the fractional differential equations with expressed as:

$$\begin{cases} {}^{C}D^{\alpha}X(t) + \nu X(t) = f(t), \\ X(0) = 0. \end{cases} \tag{A-8}$$

By making the LT of both members of Eq. (A-8), we get

$$\left(s^{\alpha} + \nu\right)\mathcal{L}_X(s) = \mathcal{L}_f(s), s = \beta - i\theta, \tag{A-9}$$

Namely:

$$\mathcal{L}_X(s) = \frac{1}{s^{\alpha} + \nu}\mathcal{L}_f(s), s = \beta - i\theta. \tag{A-10}$$

If $\beta = 0$, namely we work in terms of FT, we recall that

$$\left(\mp i\theta\right)^{\alpha} = \left(\cos\left(\frac{\alpha\pi}{2}\right) \pm i\,\mathrm{sign}(\theta)\sin\left(\frac{\alpha\pi}{2}\right)\right)|\theta|^{-\alpha}. \tag{A-11}$$

Thus we have

$$A_X^{\mathcal{L}}\left(-i\theta_k\right)=\frac{\left(\cos\left(\frac{\alpha\pi}{2}\right)\left|\theta_k\right|^{-\alpha}+\nu\right)A_f^{\mathcal{L}}\left(-i\theta_k\right)+\operatorname{sign}\left(\theta_k\right)\sin\left(\frac{\alpha\pi}{2}\right)\left|\theta_k\right|^{-\alpha}B_f^{\mathcal{L}}\left(-i\theta_k\right)}{\left(\cos\left(\frac{\alpha\pi}{2}\right)\left|\theta_k\right|^{-\alpha}+\nu\right)^2+\left(\sin\left(\frac{\alpha\pi}{2}\right)\left|\theta_k\right|^{-\alpha}\right)^2},$$

$$B_X^{\mathcal{L}}\left(-i\theta_k\right)=\frac{\left(\cos\left(\frac{\alpha\pi}{2}\right)\left|\theta_k\right|^{-\alpha}+\nu\right)B_f^{\mathcal{L}}\left(-i\theta_k\right)-\operatorname{sign}\left(\theta_k\right)\sin\left(\frac{\alpha\pi}{2}\right)\left|\theta_k\right|^{-\alpha}A_f^{\mathcal{L}}\left(-i\theta_k\right)}{\left(\cos\left(\frac{\alpha\pi}{2}\right)\left|\theta_k\right|^{-\alpha}+\nu\right)^2+\left(\sin\left(\frac{\alpha\pi}{2}\right)\left|\theta_k\right|^{-\alpha}\right)^2}.$$

(A-12)

The example is shown in Figure A-2 when $f\left(t\right)=\cos\left(t\right)$.

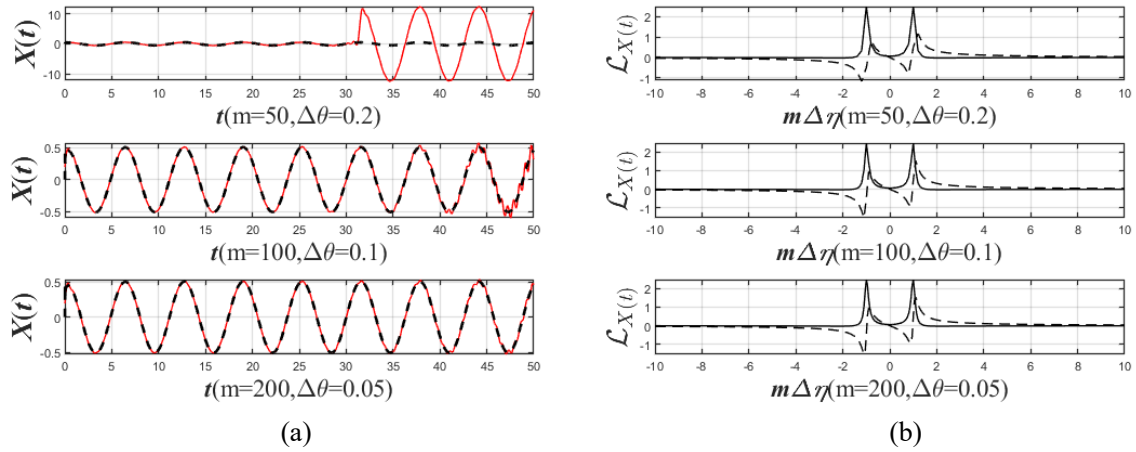

Figure A-2 (a) The black dashed line is the exact $X\left(t\right)$, and the red real line is the reconstruct $X\left(t\right)$. (b) The real line is the $A_X^{\mathcal{L}}\left(s_k\right)$, and the dashed line is the imaginary part $B_X^{\mathcal{L}}\left(s_k\right)$. $\alpha=0.2$, $\nu=1$

3) Fractional differential equation of variable coefficient

Now, let us consider the fractional differential equations with exponential time-dependent coefficient expressed as:

$$\begin{cases}{}^{C}D^{\alpha}X\left(t\right)+ce^{-\nu t}X\left(t\right)=f\left(t\right),\\ X\left(0\right)=0.\end{cases}\tag{A-13}$$

By making the LT of both members of Eq. (A-13), and according to the exponential property, we get:

$$s^{\alpha}\mathcal{L}_X\left(s\right)+c\mathcal{L}_X\left(s+\nu\right)=\mathcal{L}_f\left(s\right),\tag{A-14}$$

Now, we set $s^{\alpha}=A_{\alpha}^{\mathcal{L}}\left(s\right)+iB_{\alpha}^{\mathcal{L}}\left(s\right)$, according to Eq. (4-11)-(4-14), then Eq. (A-14) can be transferred into:

$$A_X^{\mathcal{L}}(s_J)A_\alpha^{\mathcal{L}}(s_J)-B_X^{\mathcal{L}}(s_J)B_\alpha^{\mathcal{L}}(s_J)+c\left\{\frac{1}{2b}A_X^{\mathcal{L}}(\beta)a_{0J}+\frac{1}{b}\sum_{k=1}^{m}\left[A_X^{\mathcal{L}}(s_k)a_{Jk}+B_X^{\mathcal{L}}(s_k)c_{Jk}\right]\right\}=A_f^{\mathcal{L}}(s_J),$$
$$A_X^{\mathcal{L}}(s_J)B_\alpha^{\mathcal{L}}(s_J)+B_X^{\mathcal{L}}(s_J)A_\alpha^{\mathcal{L}}(s_J)+c\left\{\frac{1}{2b}A_X^{\mathcal{L}}(\beta)b_{0J}+\frac{1}{b}\sum_{k=1}^{m}\left[A_X^{\mathcal{L}}(s_k)c_{kJ}+B_X^{\mathcal{L}}(s_k)b_{Jk}\right]\right\}=B_f^{\mathcal{L}}(s_J).$$

(A-15)

Eq. (A-15) can also be written as the matrix form, which is

$$\mathbf{E}^{\mathcal{L}}\mathcal{L}_X(s_k)+c\frac{1}{2b}\mathbf{D}^{\mathcal{L}}\mathcal{L}_X(s_k)=\mathcal{L}_f(s_k), \tag{A-16}$$

where

$$\mathcal{L}_X(s_k)=\left[A_x^{\mathcal{L}}(\beta),\ \boldsymbol{A}_x^{\mathcal{L}}(s_k),\ \boldsymbol{B}_x^{\mathcal{L}}(s_k)\right]^{\mathrm{T}},\quad \mathcal{L}_f(s_k)=\left[A_f^{\mathcal{L}}(\beta),\ \boldsymbol{A}_f^{\mathcal{L}}(s_k),\ \boldsymbol{B}_f^{\mathcal{L}}(s_k)\right]^{\mathrm{T}},$$

(A-17)

And $\mathbf{E}$ is a matrix with $(2m+1)\times(2m+1)$ elements, where

$$\begin{aligned}&\mathbf{E}_{11}^{\mathcal{L}}=A_\alpha^{\mathcal{L}}(s_0);\\&\mathbf{E}_{kk}^{\mathcal{L}}=A_\alpha^{\mathcal{L}}(s_{k-1});\mathbf{E}_{k(k+m)}^{\mathcal{L}}=-B_\alpha^{\mathcal{L}}(s_{k-1});2\le k\le m+1,\\&\mathbf{E}_{k(k-m)}^{\mathcal{L}}=B_\alpha^{\mathcal{L}}(s_{k-m-1});\mathbf{E}_{kk}^{\mathcal{L}}=A_\alpha^{\mathcal{L}}(s_{k-m-1});m+2\le k\le 2m+1.\end{aligned} \tag{A-18}$$

Thus we have

$$\mathcal{L}_X(s_k)=\left(\mathbf{E}^{\mathcal{L}}+c\frac{1}{2b}\mathbf{D}^{\mathcal{L}}\right)^{-1}\mathcal{L}_f(s_k), \tag{A-19}$$

If $\beta=0$, namely we work in terms of FT, then

$$A_\alpha^{\mathcal{L}}(s_k)=\cos\left(\frac{\alpha\pi}{2}\right)|\theta_k|^{-\alpha},\ \ B_\alpha^{\mathcal{L}}(s_k)=\operatorname{sign}(\theta_k)\sin\left(\frac{\alpha\pi}{2}\right)|\theta_k|^{-\alpha}. \tag{A-20}$$

Then Eq. (A-19) can be expressed as:

$$\mathcal{L}_X(-i\theta_k)=\left(\mathbf{E}+c\frac{1}{2b}\mathbf{D}^{\mathcal{L}}\right)^{-1}\mathcal{L}_f(-i\theta_k). \tag{A-21}$$

Such an example when $f(t)=\cos(t)$ is shown in Figure A-3.

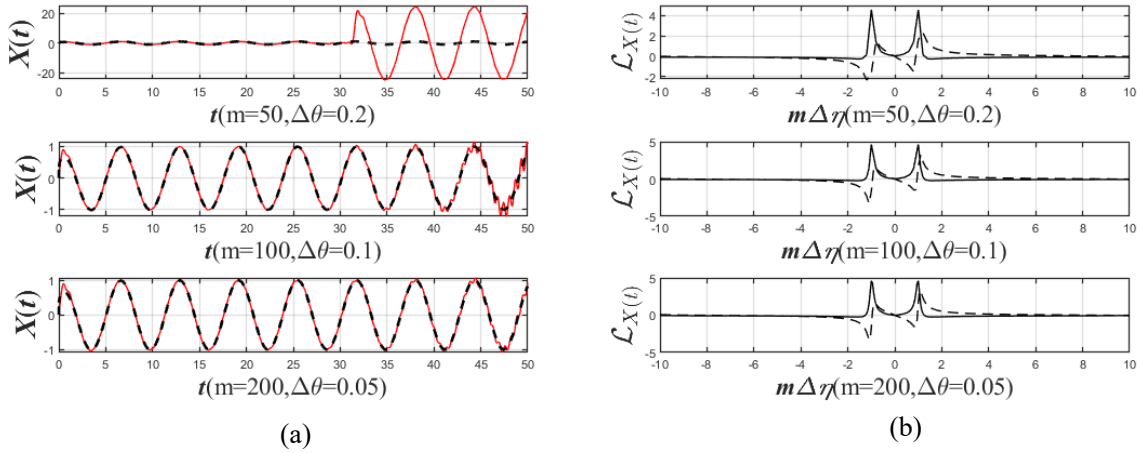

Figure A-3 (a) The black dashed line is the exact $X(t)$, and the red real line is the reconstruct $X(t)$. (b) The real line is the $A_X^{\mathcal{L}}(s_k)$, and the dashed line is the imaginary part $B_X^{\mathcal{L}}(s_k)$. $\alpha = 0.2$, $c = 0.5$, $\nu = 1$

Appendix. B

Since the double-sided PDF can be reconstructed with the double-sided SCF with the fixed real part of s, namely, β belongs to the FS. According to discretized form of inverse Laplace transform, the following equation holds:

$$\begin{aligned} p_X(x) &= \frac{e^{\beta|x|}}{2b}\left[A_p^{\bar{\mathcal{L}}}(\beta)+2\sum_{k=1}^{m}\left(A_p^{\bar{\mathcal{L}}}(s_k)\cos\left(\frac{k\pi}{b}x\right)+B_p^{\bar{\mathcal{L}}}(s_k)\sin\left(\frac{k\pi}{b}x\right)\right)\right] \\ &= \frac{e^{(\beta+\Delta\beta)|x|}}{2b}\left[A_p^{\bar{\mathcal{L}}}(\beta+\Delta\beta)+2\sum_{k=1}^{m}\left(A_p^{\bar{\mathcal{L}}}(s_k+\Delta\beta)\cos\left(\frac{k\pi}{b}x\right)+B_p^{\bar{\mathcal{L}}}(s_k+\Delta\beta)\sin\left(\frac{k\pi}{b}x\right)\right)\right], \end{aligned} \tag{B-1}$$

namely

$$\begin{aligned} &\left[A_p^{\bar{\mathcal{L}}}(\beta+\Delta\beta)+2\sum_{k=1}^{m}\left(A_p^{\bar{\mathcal{L}}}(s_k+\Delta\beta)\cos\left(\frac{k\pi}{b}x\right)+B_p^{\bar{\mathcal{L}}}(s_k+\Delta\beta)\sin\left(\frac{k\pi}{b}x\right)\right)\right] \\ &= e^{-\Delta\beta|x|}\left[A_p^{\bar{\mathcal{L}}}(\beta)+2\sum_{k=1}^{m}\left(A_p^{\bar{\mathcal{L}}}(s_k)\cos\left(\frac{k\pi}{b}x\right)+B_p^{\bar{\mathcal{L}}}(s_k)\sin\left(\frac{k\pi}{b}x\right)\right)\right]. \end{aligned} \tag{B-2}$$

Now, multiplying Eq. (B-2) with $\cos\left(\frac{J\pi}{b}x\right)$ and $\sin\left(\frac{J\pi}{b}x\right)$ respectively, integrating in the range $(-b,b)$, then we man have

$$\begin{aligned} A_{p_X}^{\bar{\mathcal{L}}}(s_J+\Delta\beta) &= \frac{1}{2b}A_{p_X}^{\bar{\mathcal{L}}}(\beta)a_{0,J}^{\bar{\mathcal{L}}}+\frac{1}{b}\sum_{k=1}^{m}\left[A_{p_X}^{\bar{\mathcal{L}}}(s_k)a_{Jk}^{\bar{\mathcal{L}}}+B_{p_X}^{\bar{\mathcal{L}}}(s_k)c_{Jk}^{\bar{\mathcal{L}}}\right], \\ B_{p_X}^{\bar{\mathcal{L}}}(s_J+\Delta\beta) &= \frac{1}{2b}A_{p_X}^{\bar{\mathcal{L}}}(\beta)b_{0,J}^{\bar{\mathcal{L}}}+\frac{1}{b}\sum_{k=1}^{m}\left[A_{p_X}^{\bar{\mathcal{L}}}(s_k)c_{kJ}^{\bar{\mathcal{L}}}+B_{p_X}^{\bar{\mathcal{L}}}(s_k)b_{Jk}^{\bar{\mathcal{L}}}\right]. \end{aligned} \tag{B-3}$$

where

$$
\begin{aligned}
a_{0,J}^{\bar{\mathcal{L}}} &= \int_{-b}^{b} e^{-\Delta\beta|x|}\cos\left(\frac{J\pi}{b}x\right)\mathrm{d}x = 2b^2\Delta\beta r_J,\\
b_{0,J}^{\bar{\mathcal{L}}} &= \int_{-b}^{b} e^{-\Delta\beta|x|}\sin\left(\frac{J\pi}{b}x\right)\mathrm{d}x = 0,\\
a_{Jk}^{\bar{\mathcal{L}}} &= \int_{-b}^{b} e^{-\Delta\beta|x|}\cos\left(\frac{J\pi}{b}x\right)\cos\left(\frac{k\pi}{b}x\right)\mathrm{d}x = b^2\Delta\beta\left(t_{Jk}+s_{Jk}\right),\\
b_{Jk}^{\bar{\mathcal{L}}} &= \int_{-b}^{b} e^{-\Delta\beta|x|}\sin\left(\frac{J\pi}{b}x\right)\sin\left(\frac{k\pi}{b}x\right)\mathrm{d}x = b^2\Delta\beta\left(t_{Jk}-s_{Jk}\right),\\
c_{Jk}^{\bar{\mathcal{L}}} &= \int_{-b}^{b} e^{-\Delta\beta|x|}\cos\left(\frac{J\pi}{b}x\right)\sin\left(\frac{k\pi}{b}x\right)\mathrm{d}x = 0,\\
t_{Jk} &= \frac{1-e^{-b\Delta\beta}\cos\left(\left(J-k\right)\pi\right)}{b^2\Delta\beta^2+\left(J-k\right)^2\pi^2},\\
s_{Jk} &= \frac{1-e^{-b\Delta\beta}\cos\left(\left(J+k\right)\pi\right)}{b^2\Delta\beta^2+\left(J+k\right)^2\pi^2},\\
r_J &= \frac{\left(1-e^{-b\Delta\beta}\cos\left(J\pi\right)\right)}{b^2\Delta\beta^2+J^2\pi^2}\\
J,k &= 1,2,...,m.\ \ \Delta\beta\neq 0
\end{aligned}
\tag{B-4}
$$

The matrix form can be rewritten as

$$
\mathbf{a}_p^{\bar{\mathcal{L}}}\left(s+\Delta\beta\right) = \frac{1}{2b}\mathbf{D}^{\bar{\mathcal{L}}}\mathbf{a}_p^{\bar{\mathcal{L}}}\left(s\right);\ \ s=\beta+i\theta,\ \ \Delta\beta\neq 0, \tag{B-5}
$$

$$
\mathbf{D}^{\bar{\mathcal{L}}} = \begin{pmatrix} a_{00} & \boldsymbol{a}_{0J}^{\mathrm{T}} & \mathbf{0} \\ \boldsymbol{a}_{0J} & \mathbf{2A} & \mathbf{0} \\ \mathbf{0} & \mathbf{0} & \mathbf{2B} \end{pmatrix};
\mathbf{a}_p^{\bar{\mathcal{L}}}\left(s\right) = \begin{pmatrix} A_{p_X}^{\bar{\mathcal{L}}}\left(\beta\right) \\ \boldsymbol{A}_{p_X}^{\bar{\mathcal{L}}}\left(s_k\right) \\ \boldsymbol{B}_{p_X}^{\bar{\mathcal{L}}}\left(s_k\right) \end{pmatrix};
\mathbf{a}_p^{\bar{\mathcal{L}}}\left(s+\Delta\beta\right) = \begin{pmatrix} A_{p_X}^{\bar{\mathcal{L}}}\left(\beta+\Delta\beta\right) \\ \boldsymbol{A}_{p_X}^{\bar{\mathcal{L}}}\left(s_k+\Delta\beta\right) \\ \boldsymbol{B}_{p_X}^{\bar{\mathcal{L}}}\left(s_k+\Delta\beta\right) \end{pmatrix}; \tag{B-6}
$$

where $\mathbf{A}$ is the matrix with the element of $a_{Jk}^{\bar{\mathcal{L}}}$, $\boldsymbol{a}_{0J}$ is a vector with the element of $a_{0,J}^{\bar{\mathcal{L}}}$, $\mathbf{B}$ is the matrix with the element of $b_{Jk}^{\bar{\mathcal{L}}}$. $\mathbf{D}^{\bar{\mathcal{L}}}$ is identity matrix multiplied by $2b$ when $\Delta\beta=0$. Figure B-1 verified the accuracy of above equation with the asymmetric distribution $p_X\left(x\right)=\frac{\nu}{2}\exp\left(-\nu\left|x-\mu\right|\right)$, where $\nu=0.5$ and $\mu=-2$.

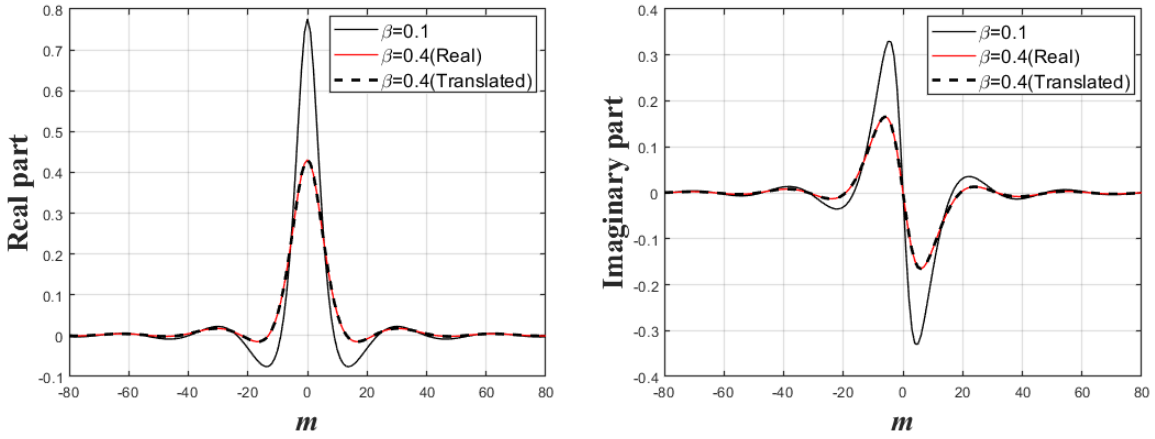

(a) (b)

Figure B-1 The translated double-sided SCF with the initial $\beta = 0.1$, and $\Delta\beta = 0.3$, the translated $\beta = 0.4$. (a) the real part; (b) The imaginary part

Appendix. C

Here, we propose the equation to translate the CFM along the real axis. Firstly, to avoid the singularity, we set $p_X(0)=\left(p_X(\Delta x)+p_X(-\Delta x)\right)/2$ for all the equation, the PDF can be reconstructed based on the double-sided CFM with fixed real part ρ when ρ belongs to the FS, namely:

$$p_X(x)=\frac{|x|^{-\rho}}{4b}\left[A_p^{\bar{M}}(\gamma_0)+2\sum_{k=1}^{m}\left(A_p^{\bar{M}}(\gamma_k)\cos\left(\frac{k\pi\ln(|x|)}{b}\right)+B_p^{\bar{M}}(\gamma_k)\sin\left(\frac{k\pi\ln(|x|)}{b}\right)\right)\right]$$
$$=\frac{|x|^{-(\rho+\Delta\rho)}}{4b}\left[A_p^{\bar{M}}(\gamma_0+\Delta\rho)+2\sum_{k=1}^{m}\left(A_p^{\bar{M}}(\gamma_k+\Delta\rho)\cos\left(\frac{k\pi\ln(|x|)}{b}\right)+B_p^{\bar{M}}(\gamma_k+\Delta\rho)\sin\left(\frac{k\pi\ln(|x|)}{b}\right)\right)\right] \tag{C-1}$$

Here, we set $y=\ln(|x|)$, thus the Eq. (C-1) can be rewritten as:

$$e^{-\Delta\rho y}\left[A_p^{\bar{M}}(\gamma_0+\Delta\rho)+2\sum_{k=1}^{m}\left(A_p^{\bar{M}}(\gamma_k+\Delta\rho)\cos\left(\frac{k\pi y}{b}\right)+B_p^{\bar{M}}(\gamma_k+\Delta\rho)\sin\left(\frac{k\pi y}{b}\right)\right)\right]$$
$$=\left[A_p^{\bar{M}}(\gamma_0)+2\sum_{k=1}^{m}\left(A_p^{\bar{M}}(\gamma_k)\cos\left(\frac{k\pi y}{b}\right)+B_p^{\bar{M}}(\gamma_k)\sin\left(\frac{k\pi y}{b}\right)\right)\right]. \tag{C-2}$$

Multiplying the Eq. (C-2) with $\cos\left(\frac{J\pi}{b}y\right)$ and $\sin\left(\frac{J\pi}{b}y\right)$ respectively, and integrate in the x range $\left(-e^{b},-e^{-b}\right)\cup\left(e^{-b},e^{b}\right)$, namely the y range $(-b,b)$, then we man have:

$$\begin{aligned}A_{p_X}^{\bar{M}}(\gamma_J)&=\frac{1}{2b}A_{p_X}^{\bar{M}}(\gamma_k+\Delta\rho)a_{0J}^{\bar{M}}+\frac{1}{b}\sum_{k=1}^{m}\left[A_{p_X}^{\bar{M}}(\gamma_k+\Delta\rho)a_{Jk}^{\bar{M}}+B_{p_X}^{\bar{M}}(\gamma_k+\Delta\rho)c_{Jk}^{\bar{M}}\right],\\ B_{p_X}^{\bar{M}}(\gamma_J)&=\frac{1}{2b}A_{p_X}^{\bar{M}}(\gamma_k+\Delta\rho)b_{0J}^{\bar{M}}+\frac{1}{b}\sum_{k=1}^{m}\left[A_{p_X}^{\bar{M}}(\gamma_k+\Delta\rho)c_{kJ}^{\bar{M}}+B_{p_X}^{\bar{M}}(\gamma_k+\Delta\rho)b_{Jk}^{\bar{M}}\right],\end{aligned} \tag{C-3}$$

where

$$
\begin{aligned}
a_{0,J}^{\bar{M}} &= \int_{-b}^{b} e^{-\Delta\rho y}\cos\left(\frac{J\pi}{b}y\right)\mathrm{d}y = 2b^2\Delta\rho r_J,\\
b_{0,J}^{\bar{M}} &= \int_{-b}^{b} e^{-\Delta\rho y}\sin\left(\frac{J\pi}{b}y\right)\mathrm{d}y = 2bJ\pi r_J,\\
a_{Jk}^{\bar{M}} &= \int_{-b}^{b} e^{-\Delta\rho y}\cos\left(\frac{J\pi}{b}y\right)\cos\left(\frac{k\pi}{b}y\right)\mathrm{d}y = b^2\left(b^2\Delta\rho^2+\left(k^2+J^2\right)\pi^2\right)\Delta\rho t_{Jk},\\
b_{Jk}^{\bar{M}} &= \int_{-b}^{b} e^{-\Delta\rho y}\sin\left(\frac{J\pi}{b}y\right)\sin\left(\frac{k\pi}{b}y\right)\mathrm{d}y = 2b^2kJ\pi^2\Delta\rho t_{Jk},\\
c_{Jk}^{\bar{M}} &= \int_{-b}^{b} e^{-\Delta\rho y}\cos\left(\frac{J\pi}{b}y\right)\sin\left(\frac{k\pi}{b}y\right)\mathrm{d}y = k\pi b\left(b^2\Delta\rho^2+\left(k^2-J^2\right)\pi^2\right)t_{Jk},\\
t_{Jk} &= \frac{e^{-b\Delta\rho}\cos\left(k\pi\right)\cos\left(J\pi\right)\left(e^{2b\Delta\rho}-1\right)}{\left(b^2\Delta\rho^2+\left(J-k\right)^2\pi^2\right)\left(b^2\Delta\rho^2+\left(J+k\right)^2\pi^2\right)},\\
r_J &= \frac{\cos\left(J\pi\right)\sinh\left(b\Delta\rho\right)}{b^2\Delta\rho^2+J^2\pi^2},\\
J,k &= 1,2,...,m,\quad \Delta\rho\neq 0.
\end{aligned}
\tag{C-4}
$$

In matrix form, Eq. (C-4) may be rewritten as:

$$
\mathbf{a}_p^{\bar{M}}\left(\gamma\right) = \frac{1}{2b}\mathbf{D}^{\bar{M}}\mathbf{a}_p^{\bar{M}}\left(\gamma+\Delta\rho\right);\quad \gamma=\rho+i\eta \tag{C-5}
$$

$$
\mathbf{D}^{\bar{M}} = \begin{pmatrix} a_{00} & \boldsymbol{a}_{0J}^{\mathrm{T}} & \boldsymbol{b}_{0J}^{\mathrm{T}} \\ \boldsymbol{a}_{0J} & \mathbf{2A} & \mathbf{2C}^{\mathrm{T}} \\ \boldsymbol{b}_{0J} & \mathbf{2C} & \mathbf{2B} \end{pmatrix};\mathbf{a}_p^{\bar{M}}\left(\gamma\right) = \begin{pmatrix} A_{p_x}^{\bar{M}}\left(\rho\right) \\ \boldsymbol{A}_{p_x}^{\bar{M}}\left(\gamma_k\right) \\ \boldsymbol{B}_{p_x}^{\bar{M}}\left(\gamma_k\right) \end{pmatrix};\mathbf{a}_p^{\bar{M}}\left(\gamma+\Delta\rho\right) = \begin{pmatrix} A_{p_x}^{\bar{M}}\left(\rho+\Delta\rho\right) \\ \boldsymbol{A}_{p_x}^{\bar{M}}\left(\gamma_k+\Delta\rho\right) \\ \boldsymbol{B}_{p_x}^{\bar{M}}\left(\gamma_k+\Delta\rho\right) \end{pmatrix}; \tag{C-6}
$$

where $\mathbf{A}$ is the matrix with the element of $a_{Jk}^{\bar{M}}$, $\boldsymbol{a}_{0J}$ is a vector with the element of $a_{0,J}^{\bar{M}}$, $\mathbf{B}$ is the matrix with the element of $b_{Jk}^{\bar{M}}$, $\mathbf{C}$ is the matrix with the element of $c_{Jk}^{\bar{M}}$. $\mathbf{D}^{\bar{M}}$ is an identity matrix multiplied by $2b$ when $\Delta\rho=0$. The example:

$$
p_X\left(x\right) = \frac{1}{\sqrt{2\pi}\sigma_X}e^{-\frac{\left(x-\mu_X\right)^2}{\sigma_X^2}};\quad -\infty<x<\infty, \tag{C-7}
$$

is applied to verify the accuracy of above equation with $\mu_X=1,\sigma_X=1.$

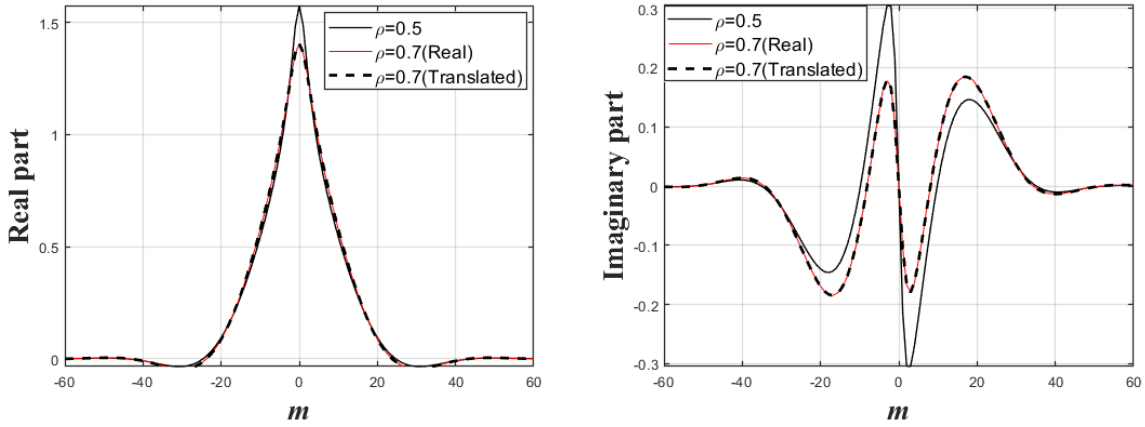

(a) (b)

Figure C-1 The translated double-sided SCF with the initial $\rho = 0.5$, and $\Delta\rho = -0.2$, the translated $\rho = 0.7$. (a) the real part; (b) The imaginary part.

Appendix. D

Considering the 2-D Gaussian distribution as follow:

$$p_{XY}(x,y)=\frac{1}{2\pi\sigma_1\sigma_2\sqrt{1-\zeta^2}}e^{-\frac{1}{2\left(1-\zeta^2\right)}\left[\left(\frac{x-\mu_1}{\sigma_1}\right)^2-2\zeta\left(\frac{x-\mu_1}{\sigma_1}\right)\left(\frac{y-\mu_2}{\sigma_2}\right)+\left(\frac{y-\mu_2}{\sigma_2}\right)^2\right]}, \tag{D-1}$$

According to the definition of GCFM, we can obtain:

$$\begin{cases}\boldsymbol{M}_{p_1}(\gamma_1-1,\gamma_2-1)\\ =\dfrac{1}{2\pi\sigma_1\sigma_2\sqrt{1-\zeta^2}}\displaystyle\int_0^\infty\int_0^\infty e^{-\frac{1}{2\left(1-\zeta^2\right)}\left[\left(\frac{x-\mu_1}{\sigma_1}\right)^2-2\zeta\left(\frac{x-\mu_1}{\sigma_1}\right)\left(\frac{y-\mu_2}{\sigma_2}\right)+\left(\frac{y-\mu_2}{\sigma_2}\right)^2\right]}x^{\gamma_1-1}y^{\gamma_2-1}\mathrm{d}x\mathrm{d}y,\\ \qquad\qquad x>0,y>0,\\ \boldsymbol{M}_{p_2}(\gamma_1-1,\gamma_2-1)\\ =\dfrac{1}{2\pi\sigma_1\sigma_2\sqrt{1-\zeta^2}}\displaystyle\int_0^\infty\int_0^\infty e^{-\frac{1}{2\left(1-\zeta^2\right)}\left[\left(\frac{-x-\mu_1}{\sigma_1}\right)^2-2\zeta\left(\frac{-x-\mu_1}{\sigma_1}\right)\left(\frac{y-\mu_2}{\sigma_2}\right)+\left(\frac{y-\mu_2}{\sigma_2}\right)^2\right]}x^{\gamma_1-1}y^{\gamma_2-1}\mathrm{d}x\mathrm{d}y,\\ \qquad\qquad x\le 0,y>0,\\ \boldsymbol{M}_{p_3}(\gamma_1-1,\gamma_2-1)\\ =\dfrac{1}{2\pi\sigma_1\sigma_2\sqrt{1-\zeta^2}}\displaystyle\int_0^\infty\int_0^\infty e^{-\frac{1}{2\left(1-\zeta^2\right)}\left[\left(\frac{x-\mu_1}{\sigma_1}\right)^2-2\zeta\left(\frac{x-\mu_1}{\sigma_1}\right)\left(\frac{-y-\mu_2}{\sigma_2}\right)+\left(\frac{-y-\mu_2}{\sigma_2}\right)^2\right]}x^{\gamma_1-1}y^{\gamma_2-1}\mathrm{d}x\mathrm{d}y,\\ \qquad\qquad x>0,y\le 0,\\ \boldsymbol{M}_{p_4}(\gamma_1-1,\gamma_2-1)\\ =\dfrac{1}{2\pi\sigma_1\sigma_2\sqrt{1-\zeta^2}}\displaystyle\int_0^\infty\int_0^\infty e^{-\frac{1}{2\left(1-\zeta^2\right)}\left[\left(\frac{-x-\mu_1}{\sigma_1}\right)^2-2\zeta\left(\frac{-x-\mu_1}{\sigma_1}\right)\left(\frac{-y-\mu_2}{\sigma_2}\right)+\left(\frac{-y-\mu_2}{\sigma_2}\right)^2\right]}x^{\gamma_1-1}y^{\gamma_2-1}\mathrm{d}x\mathrm{d}y,\\ \qquad\qquad x\le 0,y\le 0.\end{cases} \tag{D-2}$$

The discrete format of Eq. (D-2) is

$$
\begin{cases}
\boldsymbol{M}_{p_1}\left(\gamma_1-1,\gamma_2-1\right) \\
=\dfrac{\Delta x\Delta y}{2\pi\sigma_1\sigma_2\sqrt{1-\zeta^2}}\sum_{i=1}^{n_1}\sum_{j=1}^{n_2}e^{-\frac{1}{2\left(1-\zeta^2\right)}\left[\left(\frac{x_i-\mu_1}{\sigma_1}\right)^2-2\zeta\left(\frac{x_i-\mu_1}{\sigma_1}\right)\left(\frac{y_j-\mu_2}{\sigma_2}\right)+\left(\frac{y_j-\mu_2}{\sigma_2}\right)^2\right]}x_i^{\gamma_1-1}y_j^{\gamma_2-1}, \\
\qquad\qquad x_i>0,y_j>0, \\
\boldsymbol{M}_{p_2}\left(\gamma_1-1,\gamma_2-1\right) \\
=\dfrac{\Delta x\Delta y}{2\pi\sigma_1\sigma_2\sqrt{1-\zeta^2}}\sum_{i=1}^{n_1}\sum_{j=1}^{n_2}e^{-\frac{1}{2\left(1-\zeta^2\right)}\left[\left(\frac{-x_i-\mu_1}{\sigma_1}\right)^2-2\zeta\left(\frac{-x_i-\mu_1}{\sigma_1}\right)\left(\frac{y_j-\mu_2}{\sigma_2}\right)+\left(\frac{y_j-\mu_2}{\sigma_2}\right)^2\right]}x_i^{\gamma_1-1}y_j^{\gamma_2-1}, \\
\qquad\qquad x_i\le 0,y_j>0, \\
\boldsymbol{M}_{p_3}\left(\gamma_1-1,\gamma_2-1\right) \\
=\dfrac{\Delta x\Delta y}{2\pi\sigma_1\sigma_2\sqrt{1-\zeta^2}}\sum_{i=1}^{n_1}\sum_{j=1}^{n_2}e^{-\frac{1}{2\left(1-\zeta^2\right)}\left[\left(\frac{x_i-\mu_1}{\sigma_1}\right)^2-2\zeta\left(\frac{x_i-\mu_1}{\sigma_1}\right)\left(\frac{-y_j-\mu_2}{\sigma_2}\right)+\left(\frac{-y_j-\mu_2}{\sigma_2}\right)^2\right]}x_i^{\gamma_1-1}y_j^{\gamma_2-1}, \\
\qquad\qquad x_i>0,y_j\le 0, \\
\boldsymbol{M}_{p_4}\left(\gamma_1-1,\gamma_2-1\right) \\
=\dfrac{\Delta x\Delta y}{2\pi\sigma_1\sigma_2\sqrt{1-\zeta^2}}\sum_{i=1}^{n_1}\sum_{j=1}^{n_2}e^{-\frac{1}{2\left(1-\zeta^2\right)}\left[\left(\frac{-x_i-\mu_1}{\sigma_1}\right)^2-2\zeta\left(\frac{-x_i-\mu_1}{\sigma_1}\right)\left(\frac{-y_j-\mu_2}{\sigma_2}\right)+\left(\frac{-y_j-\mu_2}{\sigma_2}\right)^2\right]}x_i^{\gamma_1-1}y_j^{\gamma_2-1}, \\
\qquad\qquad x_i\le 0,y_j\le 0.
\end{cases}
\tag{D-3}
$$

Then, the PDF can be reconstructed by the following equation

$$
p_{XY}\left(x,y\right)=\begin{cases}
\dfrac{\Delta\eta_1\Delta\eta_2}{\left(2\pi\right)^2}\sum_{k_1=-m_1}^{m_1}\sum_{k_2=-m_2}^{m_2}\boldsymbol{M}_{p_1}\left(\gamma_1^{k_1}-1,\gamma_2^{k_2}-1\right)x^{-\gamma_1^{k_1}}y^{-\gamma_2^{k_2}}, \\
\qquad\qquad x>0,y>0, \\
\dfrac{\Delta\eta_1\Delta\eta_2}{\left(2\pi\right)^2}\sum_{k_1=-m_1}^{m_1}\sum_{k_2=-m_2}^{m_2}\left(-1\right)^{1-\gamma_1^{k_1}}\boldsymbol{M}_{p_2}\left(\gamma_1^{k_1}-1,\gamma_2^{k_2}-1\right)\left(-x\right)^{-\gamma_1^{k_1}}y^{-\gamma_2^{k_2}}, \\
\qquad\qquad x\le 0,y>0, \\
\dfrac{\Delta\eta_1\Delta\eta_2}{\left(2\pi\right)^2}\sum_{k_1=-m_1}^{m_1}\sum_{k_2=-m_2}^{m_2}\left(-1\right)^{1-\gamma_2^{k_2}}\boldsymbol{M}_{p_3}\left(\gamma_1^{k_1}-1,\gamma_2^{k_2}-1\right)x^{-\gamma_1^{k_1}}\left(-y\right)^{-\gamma_2^{k_2}}, \\
\qquad\qquad x>0,y\le 0, \\
\dfrac{\Delta\eta_1\Delta\eta_2}{\left(2\pi\right)^2}\sum_{k_1=-m_1}^{m_1}\sum_{k_2=-m_2}^{m_2}\left(-1\right)^{2-\gamma_1^{k_1}-\gamma_2^{k_2}}\boldsymbol{M}_{p_4}\left(\gamma_1^{k_1}-1,\gamma_2^{k_2}-1\right)\left(-x\right)^{-\gamma_1^{k_1}}\left(-y\right)^{-\gamma_2^{k_2}}, \\
\qquad\qquad x\le 0,y\le 0.
\end{cases}
\tag{D-4}
$$

The parameters are selected as $\mu_1=0.5$, $\mu_2=-1$, $\sigma_1=1$, $\sigma_2=1.5$, $\zeta=0.5$.

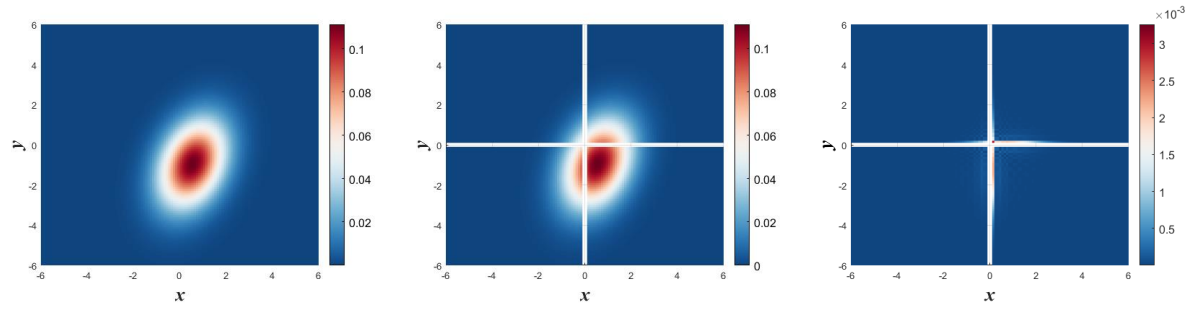

(a) (b) (c)

Figure D-1 (a) The exact normal distribution; (b) The reconstructed normal distribution by 2D-GCFM; (c) The absolute error between (a) and (b). $m_1 = m_2 = 40$, $\rho_1 = \rho_2 = 1.5$, $\Delta\eta_1 = \Delta\eta_2 = 0.4$

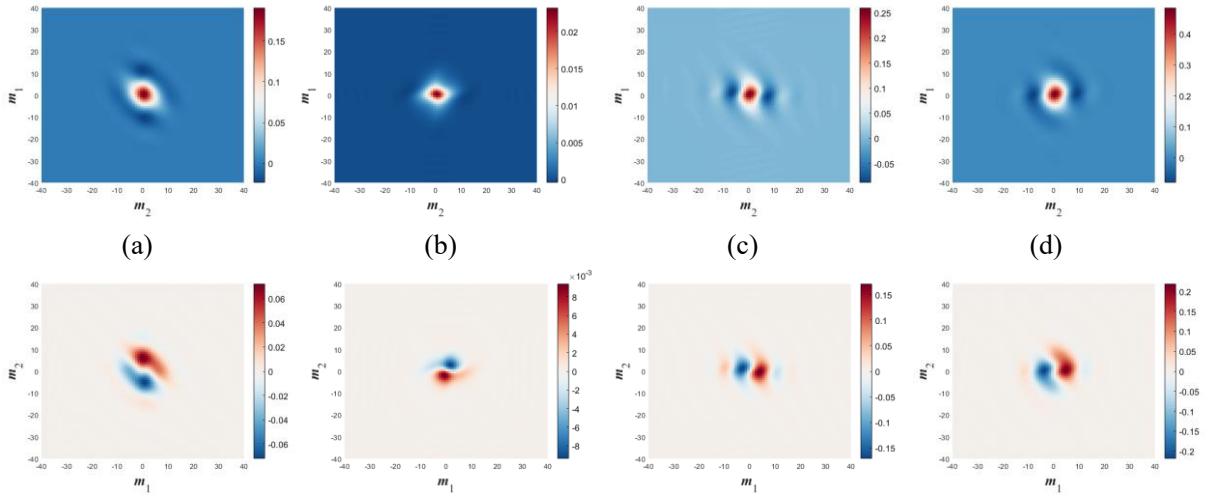

(a) (b) (c) (d)

(e) (f) (g) (h)

Figure D-2 (a-d) The real part of 2D-GCFM in first quadrant to fourth quadrant; (e-h) The imaginary part of 2D-GCFM in first quadrant to fourth quadrant

Appendix. E

Here, we give two kinds of distribution and their GCFM.

2-D exponential distribution

$$p(x,y)=\lambda\mu e^{-(\lambda x+\mu y)},\ \ x>0,y>0 \tag{E-1}$$

$$\boldsymbol{M}_p(\gamma_1-1,\gamma_2-1)=\lambda^{1-\gamma_1}\mu^{1-\gamma_2}\Gamma(\gamma_1)\Gamma(\gamma_2). \tag{E-2}$$

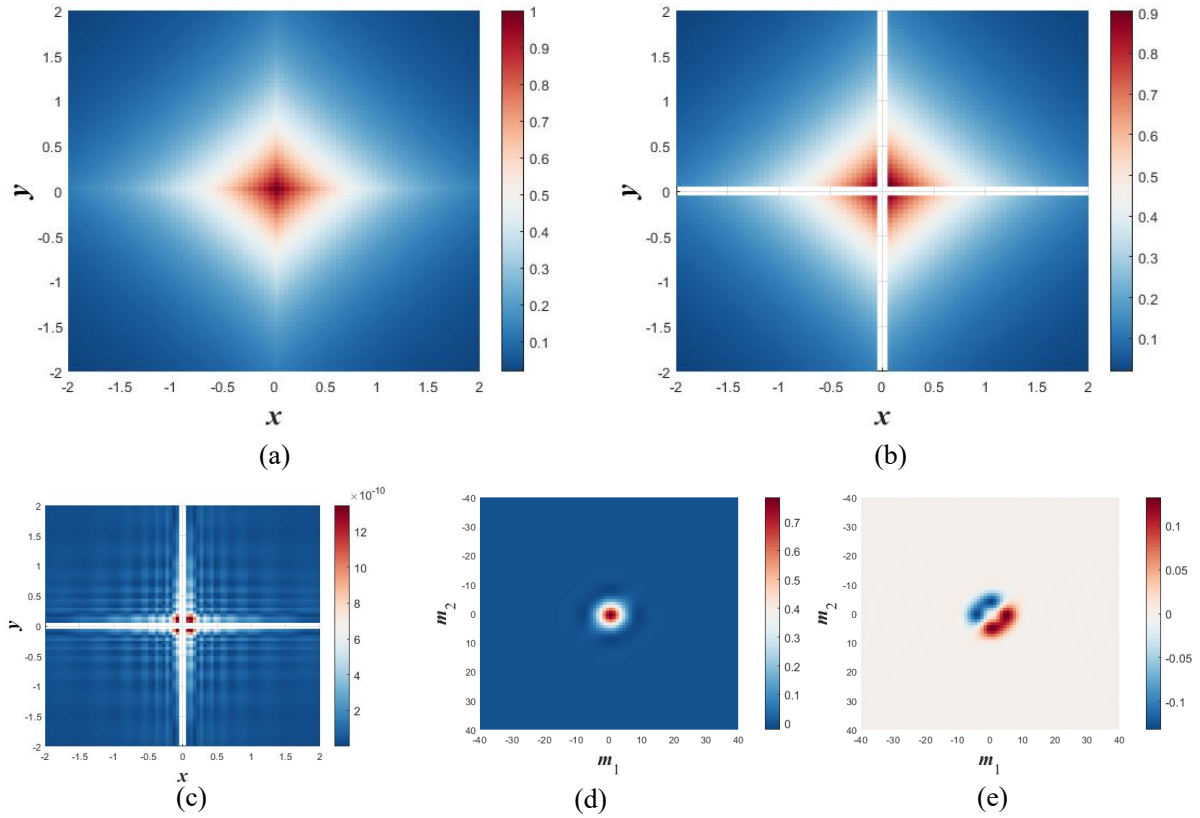

Figure E-1 (a) The exact exponential distribution. (b) The reconstructed exponential distribution by 2D-GCFM. (c) The absolute error. (d) The real part of 2D-GCFM. (e) The imaginary part of 2D-GCFM. $m_1=m_2=40$, $\rho_1=\rho_2=0.5$, $\Delta\eta_1=\Delta\eta_2=0.4$, $\lambda=\mu=1$

2-D standard Cauchy distribution

$$p(x,y)=\frac{1}{2\pi\left[1+x^2+y^2\right]^{3/2}}. \tag{E-3}$$

$$\Phi_{XY}(\theta_1,\theta_2)=e^{-\left(\theta_1^2+\theta_2^2\right)^{\frac{1}{2}}}. \tag{E-4}$$

$$\boldsymbol{M}_p\left(\gamma_1-1,\gamma_2-1\right)=\frac{\pi^{\frac{2}{3}}}{4}\Gamma\left[\frac{\gamma_1}{2}\right]\Gamma\left[\frac{\gamma_1}{2}\right]\Gamma\left[\frac{3-\gamma_1-\gamma_2}{2}\right]. \tag{E-5}$$

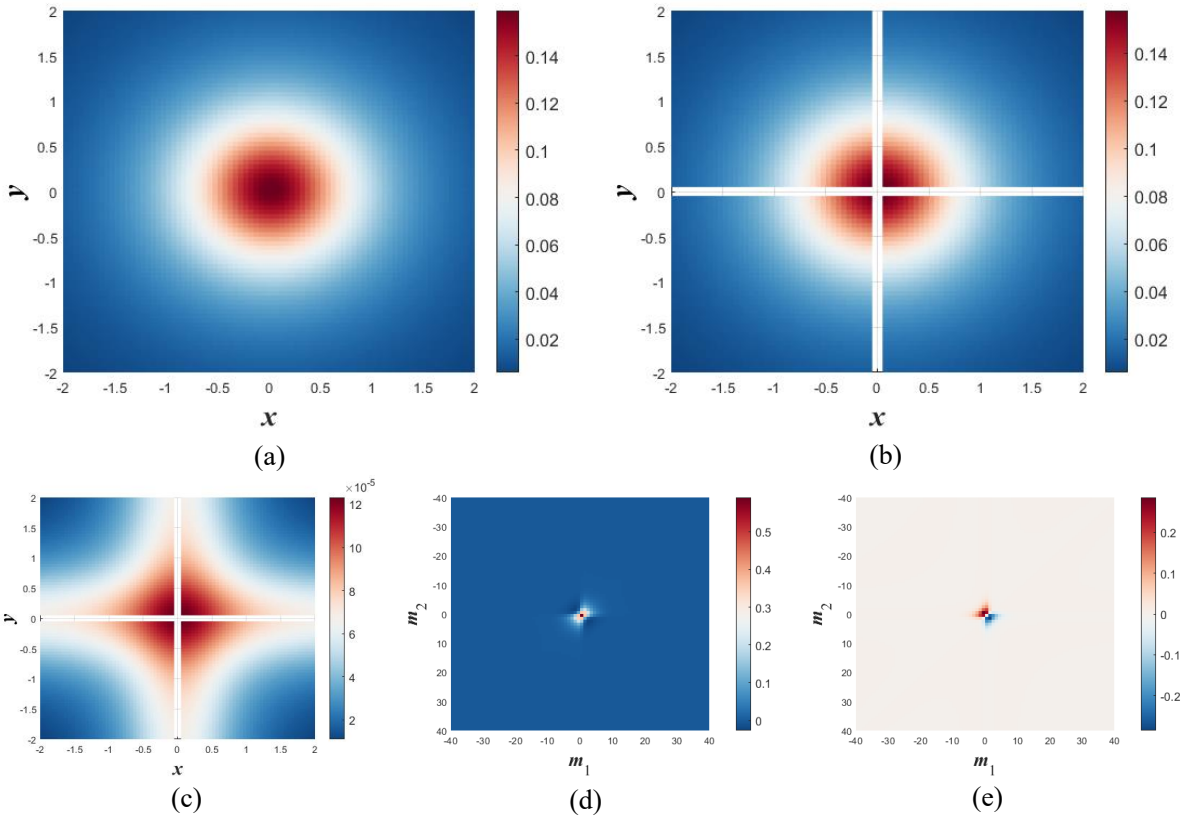

Figure E-2 (a) The exact Cauchy distribution. (b) The reconstructed Cauchy distribution by 2D-GCFM. (c) The absolute error. (d) The real part of 2D-GCFM. (e) The imaginary part of 2D-GCFM. $m_1=m_2=40$, $\rho_1=\rho_2=0.5$, $\Delta\eta_1=\Delta\eta_2=0.4$

Acknowledgements

First and foremost, my sincere gratitude to my Tutor Prof. Mario Di Paola and Prof. Antonina Pirrotta in university of Palermo, also Prof. Wei Xu in Northwestern Polytechnical University, for their enthusiastic guidance, professional suggestions of science and human nature. Their patience, encouragement, invaluable insights and constructive feedback have been instrumental in shaping the direction and quality of this work as well as my perception to research.

I would like to profoundly thank Prof. Salvatore Russotto and Prof. Chiara Masnata in university of Palermo, for their great assistance during my permanence in university of Palermo.

Special thanks to my colleagues and friends Salvatore Orlando, Salvatore Dario Di Trapani and Adam Leonardo Di Nardo in the Experimental Dynamic Laboratory, for the collaboration and hospitality. The camaraderie and support from everyone in the lab have made this journey enjoyable and memorable.

My heartfelt thanks go to my parents for their unwavering love, patience, and encouragement, which kept me going through the tough times.

I would like to acknowledge all the authors whose works have inspired and informed my research. Your contributions to the field have been a guiding light for this study.

Lastly, I am also grateful to the reviewers for their professional comments to improve the thesis a lot.

Thank you all for your support and encouragement.